

Fate of Microplastic Particles in Standing Waters and Lakes

DISSERTATION

Zur Erlangung des akademischen Grades eines Doktors
der Naturwissenschaften (Dr. rer. nat.)
in der Bayreuther Graduiertenschule für Mathematik und Naturwissenschaften
der Universität Bayreuth

vorgelegt von

Pouyan Ahmadi

aus Kermanshah, Iran

Bayreuth, 2023

Die vorliegende Arbeit wurde in der Zeit von October/2019 bis November/2023 in Leipzig am Helmholtz-Zentrum für Umweltforschung unter Betreuung von Herrn Professor Dr. Jan H. Fleckenstein angefertigt.

Vollständiger Abdruck der von der Bayreuther Graduiertenschule für Mathematik und Naturwissenschaften (BayNAT) der Universität Bayreuth genehmigten Dissertation zur Erlangung des akademischen Grades eines Doktors der Naturwissenschaften (Dr. rer. nat.).

Form der Dissertation: Kumulative Dissertation

Dissertation eingereicht am: 10.11.2023

Zulassung durch das Leitungsgremium: 27.11.2023

Wissenschaftliches Kolloquium: 19.11.2024

Amtierender Direktor: Prof. Dr. Jürgen Köhler

Prüfungsausschuss:

Prof. Dr. Jan Fleckenstein (Gutachter)

Prof. Dr. Stephan Gekle (Gutachter)

Prof. Dr. Vadym Aizinger (Vorsitz)

Prof. Dr. Efstathios Diamantopoulos

" The search for truth is on one hand painful, on the other simple. It is evident that no single individual can grasp it perfectly, but not everybody fails completely either. However, as each contributes something about nature that individually may be null or minimal, when all the contributions are compounded, a finite progress is made. "

Aristotle, Book I, Chapter VII

Acknowledgments

You know, writing this section of the dissertation feels as tough as saying goodbye to the people you really care about. But, you see, time is rolling like a river to the sea, and it brings those moments you'd rather not think about right at your doorstep, and well, I'm no exception to that either.

Going from ground zero to where I am now in my PhD journey was quite a ride, and it wouldn't have been possible without the rock-solid support of my supervisors, colleagues, friends, and, of course, my lovely family.

I will forever hold deep gratitude for Jan Fleckenstein's unshakable trust in me, his relentless support, and his guidance that set my feet in the right direction. He's not just a supervisor; he's been an amazing friend, helping me see broader horizons of life beyond research lens. I also thank my other supervisors at UFZ, Christian Schmidt, and at the University of Bayreuth, Benjamin Gilfedder, for their outstanding support and assistance throughout my PhD journey.

Franz Dichgans, my friend, and colleague, I'm so glad that our paths crossed, and we embarked on our PhD journeys together. You've been a great source of incredibly helpful advice, support, and friendship. I've loved every single day of the past four years working alongside you.

I would like to extend my thanks to my other co-authors in the University of Bayreuth, Hassan Elagami, Jan Pascal Boos, Lisa Jagau, Sven Frei, Vadym Aizinger, Stefan Peifer, Seema Agarwal, and Martin Obst, for their roles in shaping the content of this dissertation. I would also like to acknowledge the Collaborative Research Centre (CRC) 1357 Microplastic for funding my research and the Department of Hydrogeology at UFZ for hosting me.

Pia Ebeling, Franz Dichgans, Sarah Haug, my fellow office mates at room 353 over these four years, I appreciate how you've made this journey smoother with your help through productive scientific discussions, enjoyable diversions, and the friendships we've built. Also, I want to give a big shout-out to my PhD fellows, Mansi Nagpal, Maria Jose Cardenas Espinosa, Arianna Borriero, and Guilherme Nogueira. I really thank you for being there and helping me take more confident and solid steps on my PhD journey.

Last but not least, in Persian, to my beloved family:

از اینکه به اینجا رسیده ام خوشحالم، اما از اینکه عزیزانی داشتم که به من کمک کردند که به این مرحله از زندگی برسم، خوشحالترم. بدون شک اگر یاری خانواده عزیزم و خاله گرامی ام نبود، نمی توانستم حتی رویا و خیال جایگاه فعلی ام را در سرپرورانم. برای تمام کمک کردن ها و همراهی کردن هایتان سپاسگزارم.

Table of Contents

Abstract	1
Zusammenfassung	3
1. Introduction	5
1.1. Current understanding and perspectives	5
1.1.1. Plastics lifecycle: production, recycling, and disposal.....	5
1.1.2. Microplastic particle pollution in lake system	6
1.2. How to explore the role of MP particles and lakes physical factors in shaping MP particle fate?	7
1.2.1. MP particle physical characteristics.....	7
1.2.2. Lake hydrodynamics	8
2. Research objectives	9
2.1. Work package 1	9
2.2. Work package 2	9
3. Methodology and designed scenarios	11
3.1. Methods used in work package 1	11
3.1.1. Designed scenarios in study 1 and study 2.....	12
3.1.1.1. Hydrophobicity of the MP particles' surfaces (study 1 and study 2).....	12
3.1.1.2. Shape characteristics (study1).....	12
3.1.1.3. Surface area to volume ratio (study 1)	13
3.1.1.4. Density and volume of MP particles (study 1).....	13
3.1.1.5. Water temperature effect (study 1)	14
3.1.1.6. Effect of biofilm formation on TSV of MP particle (study 2)	14
3.2. Methods used in work package 2.....	14
3.2.1. Designed scenarios in study 3.....	16
3.2.1.1. Lake depth and bathymetry.....	16
3.2.1.2. MP particle size.....	16
3.2.1.3. Wind condition.....	16
3.2.1.4. Location and timing of MP particles release.....	16
3.2.2. Calculating D _{50%} and T _{50%} for the conducted scenarios	17
4. General results and discussion	18

4.1. Work package 1	18
4.1.1. Validation of CFD results against experiments and semi-empirical relationship	18
4.1.2. The relative importance of the different parameters affecting TSV of MP particles.....	18
4.1.2.1. Density and volume of MP particles.....	18
4.1.2.2. Surface area to volume ratio	20
4.1.2.3. Roundness and water temperature	21
4.1.2.4. Biofilm coated MP particles	21
4.2. Work package 2	21
4.2.1. The relative importance of the different parameters affecting spatiotemporal patterns of MP particles in lakes.....	21
4.2.1.1. Lake depth and MP particle size	23
4.2.1.2. Lake bathymetry	23
4.2.1.3. Release location, wind, and release time	24
4.2.2. Instability in water layering during fall.....	24
4.2.3. The joint impact of interconnected physical factors on the behavior of MP particles	25
5. Summary and conclusions.....	26
5.1. Work package 1	26
5.2. Work package 2	27
6. Outlook	29
Study 1: Systematic evaluation of physical parameters affecting the terminal settling velocity of microplastic particles in lakes using CFD.....	33
Study 2: Measurement of microplastic settling velocities and implications for residence time in thermally stratified lakes.....	59
Study 3: Systematic CFD-based evaluation of physical factors influencing the spatiotemporal distribution of MP particles in lakes	80
List of publications	102
Publications included in this thesis	102
Publications not included in this thesis	102
(Eidesstattliche) Versicherungen und Erklärungen	103

Abstract

Lake ecosystems are essential for aquatic life and freshwater resources, contributing to water quality, biodiversity, and human well-being. The emergence of microplastic (MP) pollution in these ecosystems necessitates studying the fate of MP particles in lakes.

This research represents a significant step forward in revealing the complex fate of MP particles within lake ecosystems. It adopted a comprehensive approach, examining the impact of physical factors on MP particle fate from two different perspectives, MP particles themselves and the characteristics of the lake environment, using a combination of Computational Fluid Dynamics (CFD) and experiments. Work package 1 (studies 1 and 2) explored how inherent physical characteristics of MP particles affect their Terminal Settling Velocities (TSVs). The investigated factors encompassed MP particle density, volume, roundness, surface area to volume ratios (SA:V), surface hydrophobicity and also biofilm formation and water temperature. Work package 2 (study 3) focused on how the physical conditions within lakes influence MP particle transport. The investigated factors included lake depth (shallow and deep lakes), bathymetry (uniform and non-uniform), MP particle size (10, 20 and 50 μ m), wind conditions (constant and variable wind), as well as the location and timing of MP particle release.

The investigations conducted in work package 1, study 1 and study 2, have shed light on critical factors influencing the TSV of MP particles within lake ecosystems. Foremost among the examined factors is particle density, which exerts a predominant influence. An increase in particle density amplifies the gravitational force acting on the particles, consequently elevating their TSV. Altering the volume of MP particles also impacts their TSV by increasing weight, albeit to a lesser degree, as it concurrently affects buoyancy and drag forces, exerting opposing effects. As a result, changes in particle volume exert a secondary, significant impact on TSV compared to the alterations in MP particle density. Furthermore, when comparing the influence of MP particle volume and SA:V variations on TSV, volume alterations prove to have a greater influence. Hydrophobicity and water temperature, although not as dominant as MP particle density, volume, and SA:V, are positioned below these factors in terms of their influence on TSV. Hydrophobic MP particles tend to accumulate air bubbles on their surfaces, boosting buoyant forces. This phenomenon is predominantly observed in biodegradable particles, although non-biodegradable particles also exhibit this effect, albeit less prominently. Alterations in water temperature during the time that lakes are thermally stratified, affect water density and kinematic viscosity, accelerating MP particle TSV in the upper water layers of a lake. Lastly, the formation of biofilms on MP particles, a common occurrence in lake ecosystems, exhibited the least significant impact on TSV values, with almost no difference in TSVs of MP particles before and after a prolonged incubation.

Work package 2 (study 3) offers essential insights into the spatiotemporal distribution patterns of MP particles in lake ecosystems, uncovering the significance level of critical controlling physical factors.

One of the principal findings of this study highlights the predominant influence of lake depth and particle size on the settling time of MP particles. A tenfold reduction in lake depth led to a substantial, sixteen-fold decrease in their settling times and highlights the critical role that travel distance plays in determining the fate of these particles. Furthermore, particle size, which influences settling velocity, emerged also as a primary controlling factor. 50 μ m MP particles displayed concentrated deposition patterns, which became more dispersed as the MP particle size decreased to 20 and 10 μ m. The most responsive reactions to changes in lake hydrodynamics and lake physical factors were observed for 10 μ m MP particles. Bathymetry, considered a second-order control factor, was found to significantly impact particle distribution patterns. Changing bathymetry from uniform to non-uniform facilitated faster settling of particles in shallow lake regions. Wind conditions, release location, and release time had relatively minor effects on MP particle behavior, but their significance increased as particle size decreased. Releasing 10 μ m MP particles in the deeper lakes with uniform bathymetry during summer thermal stratification led to a phase in the fall, lasting almost a month, during which both settling and rising of particles occurred concurrently. This phenomenon resulted from convective heat and water transport as the thermal stratification of the lake dissipated during this period. In these scenarios, approximately 2.6% to 5.5% of the initially released MP particles were either held in or returned to the lake water layers closer to the lake surface. Study 3 emphasizes that, besides lake depth and particle size being the most important factors controlling MP particle settling, it is ultimately the particular combination of different physical factors and their interactions that define the spatiotemporal distribution patterns of MP particles in a lake.

The findings of this research highlight the complexity of MP transportation within lake ecosystems, with numerous interconnected physical, biological, and hydrodynamic processes influencing their fate in the lake's water column.

Zusammenfassung

Seenökosysteme sind für das Leben im Wasser und die Süßwasserressourcen von wesentlicher Bedeutung und tragen zur Wasserqualität, zur biologischen Vielfalt und zum menschlichen Wohlergehen bei. Die zunehmende Verschmutzung durch Mikroplastik (MP) in diesen Ökosystemen macht es erforderlich, den Verbleib von MP-Partikeln in Seen zu untersuchen.

Diese Forschungsarbeit stellt einen bedeutenden Fortschritt in der Erforschung des komplexen Verbleibs von MP-Partikeln (MPP) in Seeökosystemen dar. Es wurde ein umfassender Ansatz gewählt, bei dem die Auswirkungen physikalischer Faktoren auf den Verbleib von MPP aus zwei verschiedenen Perspektiven untersucht wurden: zum Einen die Merkmale der MPP selbst und zum Anderen die Merkmale der Seen, wobei eine Kombination aus numerischer Strömungsmechanik (CFD) und Experimenten verwendet wurde. Arbeitspaket 1 (Studien 1 und 2) untersuchte, wie inhärente physikalische Eigenschaften der MPP ihre Endabsetzgeschwindigkeit (Terminal Settling Velocity; TSV) beeinflussen. Diese Faktoren umfassten die Dichte, das Volumen, die Rundheit, das Verhältnis von Oberfläche zu Volumen (Surface Area to Volume; SA:V), die Oberflächenhydrophobie sowie die Biofilmbildung und die Wassertemperatur. Arbeitspaket 2 (Studie 3) konzentrierte sich darauf, wie die physikalischen Bedingungen in Seen den Transport von MPP beeinflussen. Zu den untersuchten Faktoren gehörten die Seetiefe (flache und tiefe Seen), die Bathymetrie (gleichmäßig und ungleichmäßig), die Größe der MPP (10, 20 und 50 μm), die Windbedingungen (konstanter und variabler Wind) sowie der Ort und der Zeitpunkt der Freisetzung der MPP.

Die in Arbeitspaket 1, Studie 1 und Studie 2, durchgeführten Untersuchungen haben Aufschluss über kritische Faktoren gegeben, die die TSV von MPP in Seeökosystemen beeinflussen. An erster Stelle der untersuchten Faktoren steht die Partikeldichte, die den größten Einfluss ausübt. Eine Erhöhung der Partikeldichte verstärkt die auf die Partikel wirkende Gravitationskraft und erhöht somit deren TSV. Eine Änderung des Volumens der MPP wirkt sich ebenfalls auf die TSV aus, wenn auch in geringerem Maße, da sie sich gleichzeitig auf die Auftriebs- und die Widerstandskraft auswirkt und somit entgegengesetzte Effekte hervorruft. Infolgedessen wirken sich Änderungen des Partikelvolumens im Vergleich zu Änderungen der MPP-Dichte nur sekundär auf die TSV aus. Beim Vergleich des Einflusses des Volumens der MPP und der SA:V-Variationen auf die TSV erweisen sich die Volumenänderungen zudem als einflussreicher. Hydrophobie und Wassertemperatur sind zwar nicht so dominant wie MPP-Dichte, -Volumen und SA:V, und liegen damit hinsichtlich ihres Einflusses auf die TSV unterhalb dieser Faktoren. Hydrophobe MPP neigen dazu, Luftblasen auf ihrer Oberfläche anzusammeln, wodurch die Auftriebskräfte verstärkt werden. Dieses Phänomen ist vor allem bei biologisch abbaubaren Partikeln zu beobachten, wobei auch nicht biologisch abbaubare Partikel diesen Effekt aufweisen, wenn auch weniger ausgeprägt. Änderungen der Wassertemperatur während der Zeit, in der Seen thermisch geschichtet sind, wirken sich auf die Wasserdichte und die kinematische

Viskosität aus und beschleunigen den TSV von MPP in den oberen Wasserschichten eines Sees. Die Bildung von Biofilmen auf MP-Partikeln, die in Seenökosystemen häufig vorkommt, hatte in unseren Untersuchungen die geringsten Auswirkungen auf die TSV, da die ermittelten TSV vor und nach einer Inkubation sich nicht wesentlich unterschieden.

Arbeitspaket 2 (Studie 3) bietet wesentliche Einblicke in die raum-zeitlichen Verteilungsmuster von MPP in Seenökosystemen und deckt die Bedeutung kritischer physikalischer Einflussfaktoren auf. Eines der wichtigsten Ergebnisse dieser Studie zeigt den vorherrschenden Einfluss der Seetiefe und der Partikelgröße auf die Absetzzeit von MPP. Eine zehnfache Verringerung der Seetiefe führte zu einer beachtlichen Verringerung der Absetzzeiten um das Sechzehnfache und verdeutlicht die entscheidende Rolle, die die Transportdistanz bei der Bestimmung des Verbleibs dieser Partikel spielt. Darüber hinaus erwies sich auch die Partikelgröße, die die Absetzgeschwindigkeit beeinflusst, als ein wichtiger Kontrollfaktor. 50- μm -MPP zeigten konzentrierte Ablagerungsmuster, die sich ausdehnten, wenn die MPP-Größe auf 20 und 10 μm sank. Am stärksten reagierten die 10- μm -MPP auf Veränderungen der Hydrodynamik und der physikalischen Faktoren des Sees. Es wurde festgestellt, dass die Bathymetrie, die als Kontrollfaktor zweiter Ordnung angesehen wird, die Partikelverteilungsmuster erheblich beeinflusst. Eine Änderung der Bathymetrie von gleichförmig zu ungleichförmig beförderte ein schnelleres Absetzen von Partikeln in flachen Bereichen des Sees. Die Windverhältnisse, der Ort der Freisetzung und die Freisetzungszeit hatten relativ geringe Auswirkungen auf das Verhalten der MPP, aber ihre Bedeutung nahm mit abnehmender Partikelgröße zu. Die Freisetzung von 10- μm -MPP in den tieferen Seen mit gleichförmiger Bathymetrie während der sommerlichen thermischen Schichtung führte im Herbst zu einer fast einen Monat andauernden Phase, in der sowohl das Absetzen als auch das Aufsteigen der Partikel gleichzeitig stattfand. Dieses Phänomen ist auf konvektiven Wärme- und Wassertransport zurückzuführen, da sich die thermische Schichtung des Sees in diesem Zeitraum auflöste. In diesen Szenarien wurden etwa 2,6 % bis 5,4 % der ursprünglich freigesetzten MPP entweder in den oberflächennahen Wasserschichten des Sees gehalten oder kehrten dorthin zurück. Studie 3 unterstreicht, dass nicht nur die Seetiefe und die Partikelgröße wichtige Faktoren für die Ablagerung von MPP sind, sondern dass es letztlich die spezifische Kombination verschiedener Faktoren und ihre Wechselwirkungen sind, die die räumlich-zeitlichen Verteilungsmuster von MPP in einem See bestimmen.

Die Ergebnisse dieser Forschung verdeutlichen die Komplexität des Transports von MP in Seeökosystemen, wobei zahlreiche miteinander verbundene physikalische, biologische und hydrodynamische Prozesse den Verbleib dieser Stoffe in der Wassersäule des Sees beeinflussen.

1. Introduction

1.1. Current understanding and perspectives

1.1.1. Plastics lifecycle: production, recycling, and disposal

The emergence of synthetic polymers, commonly referred to as plastics, can be traced back to the 19th century when vulcanized rubber and polystyrene were discovered (Andrady and Neal, 2009). The commencement of large-scale production and distribution of synthetic polymers only occurred during the mid-20th century. Since then, the production volume of synthetic polymers has witnessed a dramatic surge, surpassing 359 million metric tons per year as of 2018, marking a more than 240-fold increase (Figure 1) (Banerjee et al.). Despite the wide array of polymer options available, a small selection of plastics, namely Polyethylene (PE), Polypropylene (PP), Polystyrene (PS), Polyethylene terephthalate (PET), Polyvinyl chloride (PVC), and Polyurethane (PU), dominate over 75% of the total plastic demand (Facts, 2019).

Plastics have undeniably revolutionized human society, bringing forth numerous advantages and enhancing convenience in daily life (Andrady and Neal, 2009). Plastics, known for their remarkable versatility, lightweight nature, and ability to withstand mechanical, chemical, and biological stresses, have found extensive applications in various industries, with the construction and disposable packaging sectors being the primary areas of use (Derraik, 2002; Facts, 2019; North and Halden, 2013). In addition to their contributions to everyday life, plastics have played a vital role in driving technological advancements. However, the extensive utilization of plastics has resulted in a substantial volume of plastic waste, which, if not managed properly, can inflict significant harm on the natural environments including terrestrial and aquatic ecosystems and atmosphere (Barnes et al., 2009; Claessens et al., 2011; de Souza Machado et al., 2018; Derraik, 2002; Frias and Nash, 2019; Liao and Chen, 2021; Rochman, 2018). Also, a considerable amount of plastic waste is typically designed for single use, and after use, it should be recycled and re-enter the production stream. However, life cycle studies show that only a small portion of the plastic produced is recycled, while the majority of the plastic waste is either incinerated or accumulated in landfills and the environment (Xanthos and Walker, 2017).

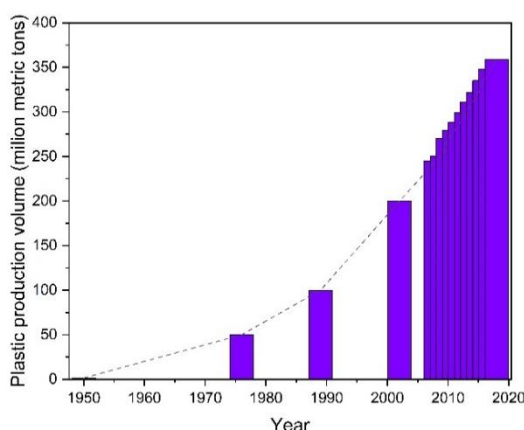


Figure 1: Worldwide plastic production from 1950 to 2018 (Banerjee et al.).

1.1.2. Microplastic particle pollution in lake system

The spectrum of plastic debris encompasses a range of sizes, extending from nano to mesoscale. Within this continuum of plastic debris sizes, particles smaller than 5mm are commonly referred to as microplastics (MP) (Falconieri et al., 2018; Lambert and Wagner, 2018). These MP particles can originate from two distinct sources: primary MP particles and secondary MP particles. Primary MP particles are micron-sized plastic particles intentionally manufactured for inclusion in various products like cosmetics and cleaners. In contrast, secondary MP particles result from degradation and fragmentation of larger plastic debris due to chemical breakdown, wave dynamics, and exposure to UV radiation (Browne et al., 2011; Williams and Simmons, 1996; Wright et al., 2020). Due to the slow decomposition of plastic products in natural environments, MP particles can persist in the environment and travel considerable distances, moving from land to large water bodies such as oceans, seas, and lakes. The introduction of MP particles into lakes can occur through direct, diffuse sources such as atmospheric deposition or indirect, concentrated sources via inflowing streams (Boos et al., 2021; Free et al., 2014; Nematollahi et al., 2020; Schmidt et al., 2017). Once in the lake, depending on MP particle characteristics, they can be distributed on the water surface or start settling in the lake water column. They may ultimately be either deposited onto the lake bed layer or flushed out of lake systems through various natural processes and human activities. Consequently, lakes could become a temporary or permanent sink for MP particles (An et al., 2020; Deleersnijder et al., 2006; Elagami et al., 2023).

MP particles present a considerable threat to the ecosystem of lakes due to the various negative impacts that they can have when found in different depths of a lake water column. The small size and irregular shape of MP particles make them easy for aquatic organisms to ingest, leading to the bioaccumulation of toxic chemicals and additives that they bring with themselves before entering the lakes (Castro-Castellon et al., 2022; Collard et al., 2019; Leiser et al., 2021b; Leiser et al., 2020; Wang et al., 2020). Moreover, MP particles with densities similar to that of lake water display a slow settling velocity, allowing them to remain suspended in the lake water column for extended periods, ranging from several months to even years. Nevertheless, the permanent or temporary status of lakes as sinks for MP particles can vary based on the lake's inlet and outlet locations and how they influence MP particle flushing rates. MP particles could eventually become buried within the lake sediment, yet they retain the potential for resuspension even after being deposited (Free et al., 2014; Klein et al., 2018; Lambert and Wagner, 2018; Zhang et al., 2023; Zhang et al., 2020).

Given that lakes serve diverse functions such as providing drinking water, supporting fisheries, enabling recreational activities, and mitigating flood risks, the existence of MP particles within these aquatic environments represents a substantial hazard to both the ecosystem and in turn human well-being (Zhang et al., 2020). With the acknowledged consequences of MP particles on lake environments and human health, it becomes imperative to explore the factors shaping the behavior of these particles in aquatic settings and to understand the evolving interdependencies between them and lakes during the settling process. This exploration is critical for advancing our understanding and in turn developing efficient strategies to counteract their negative consequences and safeguard these sensitive freshwater resources and preserve

aquatic biodiversity. Hence, this research takes the first step to explore the relative importance of the physical factors that influence the fate of MP particles in lake systems. It takes both the intrinsic characteristics of MP particles that influence their terminal settling velocity (TSV) and the effects stemming from hydrodynamic complexities within lake systems into account, allowing for the generalization of results and their corresponding conclusions to a wide range of MP particles and lakes.

1.2. How to explore the role of MP particles and lakes physical factors in shaping MP particle fate?

1.2.1. MP particle physical characteristics

The TSV of MP particles in a lake is predominantly governed by their physical characteristics (Khatmullina and Isachenko, 2017; Waldschläger and Schüttrumpf, 2019), although it can also be influenced by ecological (Chen et al., 2019; Kaiser et al., 2017; Leiser et al., 2020; Liao and Chen, 2021; Ziccardi et al., 2016) and chemical processes (Leiser et al., 2021a; Leiser et al., 2020) unique to each lake. Experimental research has mainly concentrated on the physical factors controlling the TSV of MP particles (Khatmullina and Isachenko, 2017; Waldschläger and Schüttrumpf, 2019). These investigations have resulted in the development of semi-empirical relationships that enable the estimation of TSV based on the physical characteristics of the MP particles. These semi-empirical relationships are usually derived as a function of MP particle size, their density, sphericity, and flatness. Nonetheless, the effectiveness of these semi-empirical relationships is constrained by the limited range of datasets utilized in the studies, thereby limiting their suitability for exploring the relative importance of physical factors affecting the TSV of MP particles. On the other hand, experimental approaches face challenges in obtaining particles with specific characteristics, which are essential for this type of investigation. Therefore, more flexible methods that allow to evaluate a larger range of necessary scenarios are needed to develop a comprehensive understanding of MP particle behavior in lake systems.

The use of modeling tools has become increasingly important for investigating the behavior of MP particles in aquatic environments including standing waters and lakes (Guerrini et al., 2021; Jérémy et al., 2020). Computational fluid dynamics (CFD) methods have been widely used for this purpose (Jérémy et al., 2020; Zhang, 2017) and can provide detailed information about the complex fluid dynamics around individual MP particles as well as high numbers of them. One of the advantages of these modeling tools is their ability to simulate the direct forces acting on particles, including the drag, buoyancy and gravity forces that control their behavior in the water (Jérémy et al., 2020). This information can be used to better understand the factors that influence the settling behavior of MP particles, such as their size, shape, and density. Moreover, these models can account for arbitrary particle shapes and properties, which is crucial given the variety of shapes and compositions that MP particles can take (Arora et al., 2010; Corey, 1949; Khatmullina and Isachenko, 2017).

1.2.2. Lake hydrodynamics

Lakes are dynamic ecosystems characterized by varying levels of hydrodynamics complexities that change both spatially and temporally (Boehrer and Schultze, 2008; Herschy, 2012). These changes in a lake's hydrodynamics are influenced by factors such as meteorological conditions, their location, seasonality, and the lake's geometry (Boehrer and Schultze, 2008; O'Sullivan and Reynolds, 2008). MP contamination is a widespread issue in lakes, and the impact of their presence varies depending on the lake's specific hydrodynamic complexities. Therefore, the spatiotemporal distribution patterns of MP particles are influenced not only by the inherent properties of the particles themselves but also by the hydrodynamics of the lakes (Anderson et al., 2017; Ballent et al., 2016; Rochman, 2018; Vaughan et al., 2017).

Based on a lake's geometry, solar radiation, and wind energy input, a lake can undergo thermal stratification during the summer season (Boehrer and Schultze, 2008). This leads to the formation of distinct density layers within the lake, with the surface water being less dense than the deeper layers. As air temperatures begin to cool down in the fall, this stratification gradually dissipates, and the water layers close to the lake surface become denser than the deeper layers, resulting in a heterogeneous density pattern across the lake. Lakes undergo different heat transfer mechanisms throughout the annual cycle, commencing with conductive heat transfer during thermal stratification development, progressing to the phase of greatest stratification, and ultimately shifting to convective heat transport when water moves in response to the reversed temperature gradient in the fall (Boehrer and Schultze, 2008). During and after lakes being thermally stratified, MP particles are likely affected differently by the associated hydrodynamic complexities across a lake (Elagami et al., 2023).

One approach to studying the distribution of MP particles within a lake is through sampling. However, sampling MP particles from various locations of a lake might not offer a complete comprehension of how these particles are distributed in the water column and the resulting deposition patterns. Furthermore, this approach can be resource-intensive and time-consuming (Cable et al., 2017). This is where modeling-based research becomes invaluable, as it enables us to simulate and assess the behavior of MP particles under diverse lake-specific circumstances, offering valuable insights into their destiny within the lake ecosystem. Furthermore, employing modeling-based studies enables us to explore a diverse array of scenarios, manipulating variables within the actual range of their fluctuations in natural environments. These scenarios could involve factors like lake geometry, the number of particles released, the location and timing of their release, and shifting in meteorological conditions. Implementing such scenarios in actual lake systems can be quite complex and, at times, impractical.

2. Research objectives

The existing research on MP particles has mostly focused on specific sets of particles, making it challenging to generalize the outcomes to a broader range of MP particles from different polymer types. Furthermore, the understanding of how hydrodynamics in lake systems influence MP particles remains limited, with few studies focusing on individual lakes that exhibit unique behavior based on their specific shape and meteorological conditions. In order to address these limitations, this research employed CFD-based approaches, which offer flexibility in designing scenarios that explore the impact of altering physical factors of MP particles and lakes within the actual range observed in the environment. To this end, the following work packages were designed and conducted:

2.1. Work package 1

The objectives of the first work package were to examine the impact of various physical factors of MP particles on their TSV. Work package 1 was divided into two studies: study 1 utilized numerical modeling approaches to simulate the behavior of individual MP particles, and study 2 focused on measuring the TSV of individual MP particles in the laboratory. The scenarios evaluated in study 1 and study 2 were formulated to investigate the following research questions:

- How do shape characteristics, including roundness, and surface area to volume ratio (SA:V), affect the TSV of MP particles?
- How do the density and volume of MP particles influence their TSV?
- What is the effect of the temperature of the water surrounding MP particles on their TSV?
- To what extent does the formation of biofilms on MP particles bodies alter their TSV?

2.2. Work package 2

In work package 2, the spatiotemporal patterns of MP particles in large-scale (i.e. lake) simulations was investigated. Due to the large number of MP particles involved in this phase and the associated computational costs and time constraints, it was impractical to consider all the complex details about MP particles that were investigated in work package 1. Therefore, the utilized modeling approach relied solely on the settling velocity value of the particles as input for the particle tracking model, representing the combined effects of all inherent MP characteristics. The specified quantity of MP particles was released into elliptical lakes, which are commonly found in natural settings, from various release locations (RLs). The selection of lake shape was deliberate to ensure that the findings encompass a significant portion of the lakes shape found in natural settings. This allowed for an investigation into the following questions:

- What role do lake depth and bathymetry play in shaping the spatiotemporal distribution patterns and settling time scales of MP particles within lakes?

-
- How does the size of MP particles influence their distribution patterns within lakes?
 - What impact do wind conditions have on the distribution patterns of MP particles in lakes?
 - Do the timing and location of MP particle release significantly affect the spatiotemporal distribution patterns of MP particles?

3. Methodology and designed scenarios

3.1. Methods used in work package 1

The modeling setup in study 1 (Figure 2A) was constructed to imitate the experimental setup utilized in study 2 (Figure 2B) to simulate the experimental conditions under which the settling velocities of MP particles were measured in a glass column filled with water. Moreover, the simulations considered water kinematic viscosity and density at 20°C to be $1 \text{ mm}^2 \text{ s}^{-1}$ and 0.9982 g cm^{-3} , respectively, to mimic the experimental condition. The velocity of water at the stationary walls and water column bottom were set to 0, and the upper side of the water column was kept open and an air/water interfacial tension of " σ : 0.007 kg s^{-2} " was set for all simulations.

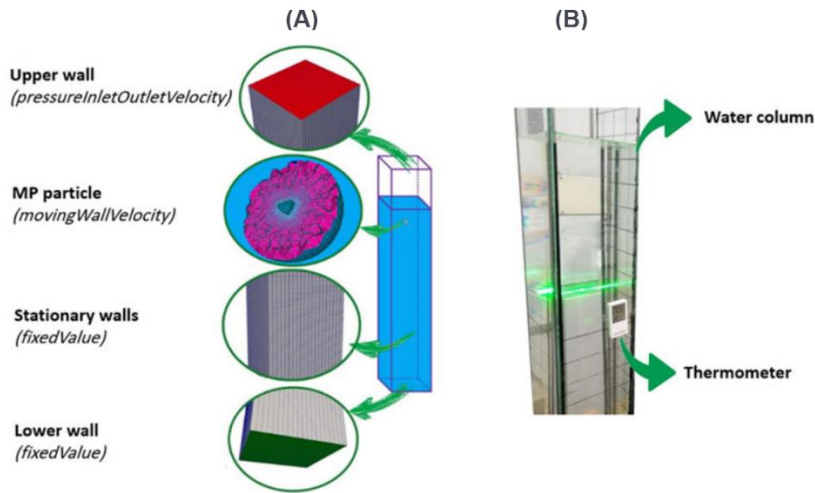


Figure 2: (A) the complete simulation setup and the specified velocity boundary conditions for each subset of the mesh domain, (B) the water column employed in the laboratory experiments, featuring a glass water container and a thermometer for monitoring water temperature during the experiments.

The solver `overInterDyMFoam` from the open-source C++ toolbox `OpenFOAM v1812` was used to simulate individual MP particles. The overset method was utilized to model MP settling in a deep-water column. The simulation involved two mesh domains, one for the water column (background mesh) and the other for the MP particle and its immediate surroundings (Figure 2A). The overset mesh cells serve as the link between the background mesh and the designed MP particle, facilitating the exchange of the resulting velocity fields between the water and the particle body in both directions without the need for any mesh deformation.

In study 2, a two-dimensional particle image velocimetry (PIV) system `iLa 5150` was used to measure the settling velocity for each particle. A reference particle was used to test for accuracy and precision by measuring it seven times under identical conditions. The laboratory was air-conditioned at $20 \pm 1^\circ\text{C}$, and the experimental setup consisted of a water-filled glass column with a filter mesh at the bottom to collect and retrieve individual particles after each settling experiment.

3.1.1. Designed scenarios in study 1 and study 2

In study 1, the first step involved simulating 110 irregular MP particles (size range from 0.5 to 2.5mm) made of seven different polymers of Polystyrene (PS), Polyamide 66 (PA66), Polycaprolactone (PCL), Polylactic acid (PLA), Poly (L-lactic) acid (PLLA), Polybutylenadipate terephthalate (PBAT), Polyvinyl chloride (PVC), which are commonly found in the lake environment (Rocha-Santos and Duarte, 2015; Webb et al., 2013; Wright et al., 2013). The simulation results were then compared to the results obtained from laboratory experiments in study 2 for corresponding MP particles. In the second step, simulated TSV were compared to corresponding TSVs estimated based on the developed semi-empirical relationships for the particles with regular and irregular shapes (Dietrich, 1982; Waldschläger and Schüttrumpf, 2019). Following the validation of simulation results, the additional scenarios, that were impractical or expensive/resource-intensive to test in the experimental setup of study 2, were explored through study 1, as described in the following sections. However, the impact of biofilm formation was only experimentally investigated in study 2, since its simulation would have required detailed information on the characteristics of the biofilm and its hydraulic effects, which were not obtainable with the available experimental methods.

3.1.1.1. Hydrophobicity of the MP particles' surfaces (study 1 and study 2)

After validating the TSVs obtained from simulations against experiments, a slight inconsistency was observed for some of the simulated MP particles when compared to the TSVs resulting from the experiments in study 2. This corroborated the hypothesis that the hydrophobicity of the surfaces of pristine MP particles could influence their settling behavior (Al Harraq and Bharti, 2021). Consequently, a set of additional experiments was designed using one biodegradable (PLA) and one non-biodegradable (PS) polymer. In these experiments, the surfactant “Tween 20” was applied to the particle surfaces, and their TSVs were reevaluated and compared to the TSVs of the pristine MP particle.

3.1.1.2. Shape characteristics (study1)

As Figure 3 illustrates, regular polygons were utilized to systematically change the roundness level of virtual MP particles and check its influence on their TSVs. Increasing the number N of sides of a regular polygon leads to polygons with shorter sides and larger internal angles, which gradually approach a perfect circle as N approaches infinity. By revolving these regular polygons with identical areas around one of their symmetry axes, 3D shapes with equal volumes were generated (Figure 3A). Five series of regular polygons with the same areas as circles with diameters of 0.5, 1, 1.5, 2, and 2.5 mm were created. To reduce computational costs, simulations were only performed for virtual particles with a density of 1.38 g cm^{-3} (PVC), allowing us to demonstrate the general trend of the impact of roundness on the TSV of MP particles.

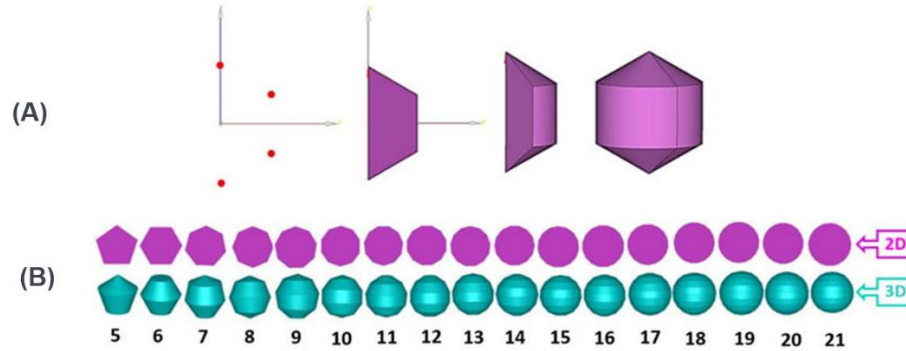


Figure 3: (A) The process of creating a 3D regular hexagon. Initially, half of a regular polygon is defined based on its vertex coordinates. This half-polygon is then rotated around one of its symmetry axes to create a 3D, regular, axis-symmetric particle, (B) 2D regular polygons and their corresponding 3D regular particles, with side numbers ranging from 5 to 21.

3.1.1.3. Surface area to volume ratio (study 1)

Numerical mesh computations were employed to calculate the surface area and volume of the simulated MP particles which had been designed based on the real MP particles used in study 2. A total of 75 irregular MP particles were included in the analysis. Their SA:V values were then compared to their respective TSV values in order to examine their relationship and detect any noticeable trends as SA:V varied.

3.1.1.4. Density and volume of MP particles (study 1)

The polygons used in section 3.1.1.2, which exhibited significant changes in TSV values as the roundness level increased (i.e. polygons with 5, 6, 7, 8, 12 sides, and a sphere), were selected to investigate how particle density and volume influenced the TSVs of MP particles. This enabled the monitoring of how the roundness level influenced the changes in TSV resulting from alterations in the density and volume of MP particles. The selected polygons had volumes equivalent to a sphere with a 1 mm diameter and a density of $\rho_{\text{PVC}} = 1.1 \text{ g cm}^{-3}$. By choosing this initial size and density, the newly generated particles stayed within the density and size range of the MP definition (Barnes et al., 2009).

To assess the impact of particle volume, the volumes of the chosen polygons (those with 5, 6, 7, 8, 12 sides, and a sphere) were increased by 10, 20, 50, and 100%. Likewise, to examine the influence of density, the initial particle densities were increased by 10, 20, 50, and 100%, resulting in particle densities of 1.21, 1.32, 1.65, and 2.2 g cm^{-3} , respectively. The highest density obtained through this procedure was comparable to very heavy polymers, such as polytetrafluoroethylene, which are found less frequently in the environment. However, for the purpose of a systematic evaluation of density effects, this choice was deemed acceptable.

In addition to the regular particles, 10 irregular MP particles were also selected, with an equivalent diameter range of 1 to 2mm, a Powers scale of roundness (Powers, 1953) of 4, and a Corey Shape Factor (Corey et al., 1949) ranging from 0.7 to 0.85. These particles were used to examine the impact of an increase in size and density on TSVs. The initial density of the particles was assumed to be 1.1 g cm^{-3} , and the same scenarios with respect to increasing volume and density as performed for regular particles (polygons) were repeated for the irregular ones as well.

3.1.1.5. Water temperature effect (study 1)

During summer, thermal stratification in lakes causes changes in water density that impact the TSV of MP particles as they move from warmer to colder lake water layers. To understand the effects of temperature changes on TSV, simulations were conducted for each of the three temperature regimes found in temperate climates. These regimes have characteristic temperatures of 18-24°C, 18-7.5°C, and 7.5-4°C for the epilimnion, metalimnion, and hypolimnion, respectively (Boehrer and Schultze, 2008; Gregory, 1983; Singh et al., 2019). The simulations involved 30 irregular PVC particles, and their TSVs were simulated at 20, 10, and 4°C as characteristic temperatures for the epilimnion, metalimnion and hypolimnion, respectively.

3.1.1.6. Effect of biofilm formation on TSV of MP particle (study 2)

To investigate the effects of biofilm formation on the settling behavior of MP particles, particles made of different types of plastic with sizes ranging from 300 to 2200 µm were incubated in a pond for 6, 8, 10, and 30 weeks. The particles were sealed in glass tubes with stainless steel screens of a mesh size of 51 µm, which allowed microorganisms to colonize the particles without allowing them to escape. Confocal laser scanning microscopy was then used to characterize the colonization of MP particle surfaces by biofilm-building microorganisms. The particles were incubated in a staining solution to visualize microbial cells and extracellular polymeric substances. The settling velocity of each incubated particle was then evaluated by comparing it to the TSV of the pristine particle.

3.2. Methods used in work package 2

The simulation of transport of MP particles in lakes was performed using the Delft3D software, which is widely used for modeling hydrodynamics, particle transport, and water quality. Delft3D-FLOW, the hydrodynamic modeling module, solves the system of the 3D hydrostatic equations with free surface, and it couples with the Lagrangian particle tracker implemented in the Delft3D-PART module to predict the fate of MP particles in aquatic environments. The simulations were set up for elliptical lake shapes, inferred from the shape of the shoreline of the Steinhuder Meer (52.47 N, 9.33 E) (Figure 4A) close to Hannover, Germany. Hydrodynamic computations in Delft3D used a structured mesh (80m × 80m) that horizontally covers the lake water surface (Figure 4B). In the vertical direction, lake water column was discretized using 10 to 15 sigma layers. A higher resolution of these layers was applied towards the lake water surface where the wind effect is more pronounced. A finer resolution of the sigma layers also utilized towards the lake bed layer in the lakes with more complex bathymetry shape (Figure 4 C3,C4).

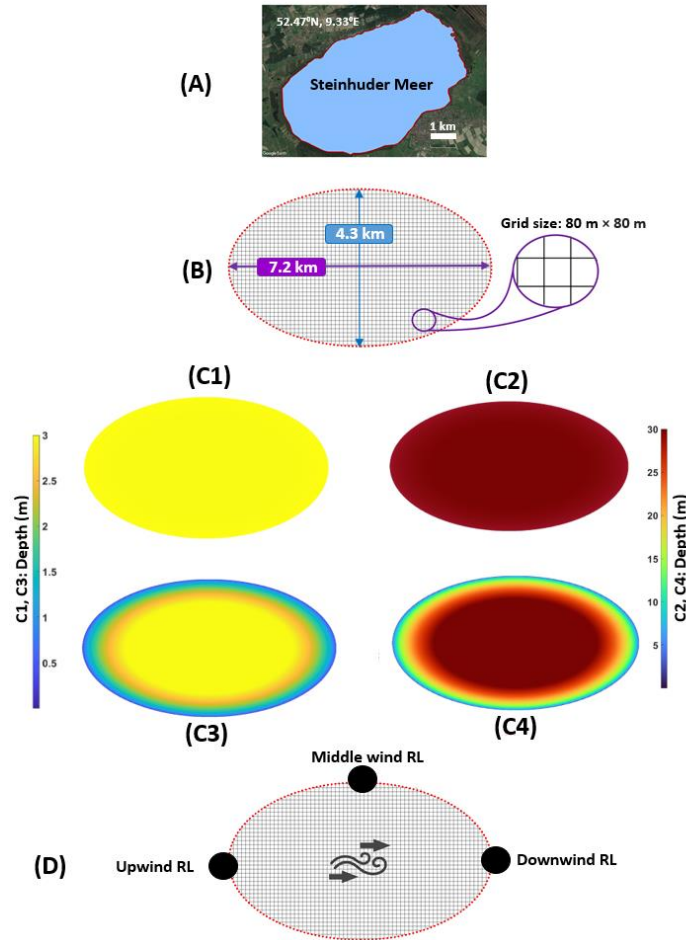


Figure 4: Steps taken to define particle tracking scenarios, (A) The map of Steinhuder Meer, (B) lake surface geometry and size of the used grid cells in the simulations, (C) The defined bathymetries ,C1 and C2 are the uniform bathymetries with constant depths of 3m (yellow color) and 30m (red color), C3 and C4 are the non-uniform bathymetries with the deepest points of 3m (center colored in yellow) and 30m (center colored in red), (D) the positioned RLs in the direction of the general western wind.

The $k-\epsilon$ turbulence model was used to model vertical eddy viscosity and turbulence-induced diffusivity in lake waters. The composite heat flux model was used to calculate the 3D temperature profiles across the lake water. This heat flux model calculates the latent and sensible heat fluxes, which are added to the effect of forced convection as long as air and water temperatures permit free convection (Deltares, 2013; Raimundo et al., 2020; Stuparu et al., 2015). Given that temperature profile's substantial influence on the vertical temperature profile in the water, the daily average air temperature data for the entire Germany was calculated and included. This step aimed to ensure that the resulting vertical temperature profile in the water represents the vertical temperature profile in the majority of lakes throughout Germany.

Throughout all the designed scenarios in study 3, the lake water surface geometry and the mentioned hydrodynamic configurations were kept constant. The following section describes the scenarios that were systematically designed to investigate the impacts of lake depth and bathymetry, MP particle size, wind conditions, and the release location (RL) and release time of MP particles.

3.2.1. Designed scenarios in study 3

3.2.1.1. Lake depth and bathymetry

To investigate the impact of lake depth on the formation of MP particle patterns in lakes, two depths of 3m and 30m were selected. These depth values were determined based on the deepest points in two reference lakes: the shallow Steinhuder Meer (maximum depth: 3m) and the relatively deep and quasi-elliptical lake "Großer Brombachsee" (maximum depth: 30m) located in Middle Franconia, Germany (52.47° N, 9.33° E). For each lake depth, two different bathymetry shapes were chosen: uniform and non-uniform bathymetry: (1) Uniform Bathymetry, indicating uniform water depths across the lake, with two scenarios at depths of 3m and 30m (Figure 4, C1, C2), and (2) Non-Uniform Bathymetry, representing a lakebed sloping from the shorelines to the center, forming a concave shape, intersected by a horizontal plane at depths of 3m (shallow lake scenarios, Figure 4, C3) and 30m (deep lake scenarios, Figure 4, C4).

3.2.1.2. MP particle size

In this study, the settling velocity associated with MP particles with sizes of 10, 20, and 50 μm were calculated based on Stokes' law using the density of Polystyrene (1030 kg m⁻³). Larger particles were not considered as their test runs did not reveal significant changes in the observed transport patterns within the investigated timeframe. Table 1 provides the detail about MP particle size and deposition time correspond to the chosen settling velocities calculated based on Stokes equations.

Table 1: MP particle sizes used in the scenarios in study 3 and corresponding settling velocities calculated based on Stokes equations.

Particle size (μm)	Settling velocity (m d ⁻¹)	Deposition time (d)	
		3m deep lake	30m deep lake
10	0.14	22	213
20	0.56	6	54
50	3.52	<1	8.5

3.2.1.3. Wind condition

Two wind conditions were applied to each of the four lake geometry scenarios (Figure 4,C1 to C4): once time series data of wind magnitudes and directions (variable wind), and once constant wind having an average wind magnitude (3.2 m s⁻¹) and direction (216°) calculated based on the data used in the variable wind scenario.

3.2.1.4. Location and timing of MP particles release

RLs of MP particles were deployed at the ends and middle of the upper arc of the elliptical shoreline in each hydrodynamic scenario. The RLs were named based on the direction of the western wind and

constantly referred to as: upwind RL, middle RL, and downwind RL (Figure 4D). A total of 30,000 particles were instantaneously released per RL, resulting in 90,000 particles released in each scenario.

The particle scenarios implemented through PART module were repeated for two different particle release times: the beginning of the year (1st of January) and the start of the second half of the year (1st of July). This approach allowed for the examination of particle release during a non-stratified period (winter) and a typical time of thermal stratification (summer). Table 2 provides an overview of the 48 scenarios conducted in the work package 2.

Table 2: Overview of the investigated physical factors throughout the 48 scenarios in study 3.

Bathymetry shape	Depth/deepest point (m)	Injection time	Wind state	Particle size (μm)	Number of scenarios
Uniform bathymetry	3, 30	January, July	Constant wind, Variable wind	10, 20, 50	24
Non-uniform bathymetry	3, 30	January, July	Constant wind, Variable wind	10, 20, 50	24

3.2.2. Calculating $D_{50\%}$ and $T_{50\%}$ for the conducted scenarios

Depending on the particle settling velocities, the achievement of 100% particle deposition demands time-consuming simulations and consequently results in excessive numerical costs. The analysis of 50% of the released particles was found to be sufficient for describing the impact of the examined variables. Therefore, the simulations were allowed to run until either all particles were settled within a reasonable period of simulation time (approximately 1 month for 50 μm particles) or a quasi-steady state was reached, with more than 75% of the MP particles deposited (approximately 18 months for 10 μm particles and 12 months for 20 μm particles). After reaching the quasi-steady state of particle deposition, $D_{50\%}$ (i.e., the median of the particle travel distance values from the injection point) was defined to represent the distance from the release point over which the first 50% of the deposited particles were found. This calculation was performed using cumulative frequency curves by counting deposited particles in equal distance intervals. Additionally, the time $T_{50\%}$ (the median settling time) taken for the first half of the released particles to settle in all scenarios was extracted. The distributions of MP particles for all scenarios were then compared to elucidate how these variables influenced $D_{50\%}$ and $T_{50\%}$.

4. General results and discussion

In this section, the physical factors investigated within each work package are presented and discussed in the order of their identified relative importance when compared to the other physical factors within the same work package.

4.1. Work package 1

4.1.1. Validation of CFD results against experiments and semi-empirical relationship

As shown in Figure 5A, comparing the TSVs obtained from the CFD simulations and the Dietrich semi-empirical relationship showed a strong correlation, with coefficients of determination (R^2) around 0.91 with a slope of approximately 0.95. Comparing the results from CFDs and Dietrich semi-empirical relationships with experiments (Figure 5B) demonstrated the TSVs scattered around 1:1 line with a slope of 1.059 and R^2 of 0.82, indicating a good agreement between the simulated TSVs and the experimental measurements. However, an overestimation in TSVs was observed in both CFD simulations and the Dietrich semi-empirical equation, particularly for biodegradable polymers including PCL, PLA, and PLLA, and to a lesser extent for the non-biodegradable polymer PS. It was hypothesized that this deviation was caused by air bubbles attaching to the hydrophobic, relatively coarse particle surfaces of the biodegradable polymers. This observation and hypothesis aligns with previous research findings regarding the effect of hydrophobicity on the settling behavior of MP particles of biodegradable polymers (Al Harraq and Bharti, 2021; Kwon et al., 2017). In order to further investigate the impact of hydrophobicity on TSV, additional settling experiments were conducted for PLA and PS particles. The experiments were conducted for untreated particles and particles treated with a surfactant (Tween 20) to reduce the hydrophobicity of the particle surfaces. The results, as shown in Figure 5C, reveal that the untreated particles exhibit significantly slower experimental TSVs compared to the TSVs obtained from the CFD model. However, this deviation between simulated and experimental TSVs is substantially reduced for the treated particles. This finding highlights the significant influence of surface properties of MP particles, particularly in relation to the polymer type, on their settling behavior.

4.1.2. The relative importance of the different parameters affecting TSV of MP particles

4.1.2.1. Density and volume of MP particles

The density of MP particles was found to be the most influential parameter in determining the TSV, as it directly affects the particle weight and the gravitational force governing the settling process. Doubling the density resulted in TSV increases over 400% (Figure 6A,C, Y-axes). On the other hand, the volume of MP particles emerged as the second-most influential factor controlling the TSV. While increasing the particle volume leads to gains in weight, the buoyancy and drag forces acting on the larger MP particle surfaces partly counteract the impact of the increased mass. Consequently, the TSV increases associated with changes in particle volume are smaller compared to the impact of density changes, ranging from 100% to 200% (Figure 6B,D, Y-axes).

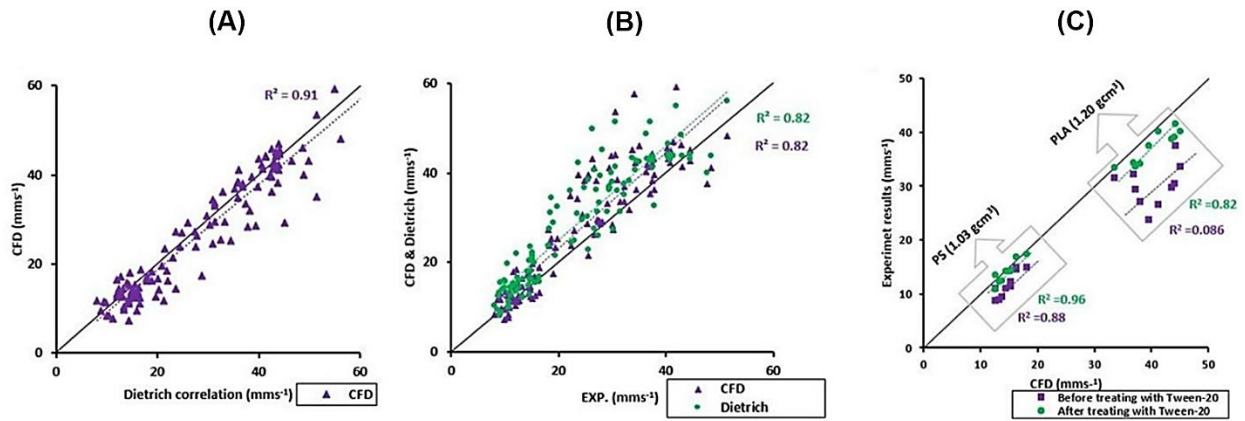


Figure 5: (A) CFD-simulated TSVs for 120 irregular MP particles plotted against TSVs estimated based on the Dietrich relationship, (B) CFD-based TSVs and TSVs estimated with the Dietrich relationship plotted against experimental results, (C) TSV changes due to particles' surface treatment using Tween-20 for two sets of MP particles (PS and PLA both in the range from 1 to 2 mm), the purple squares illustrate the TSVs before treatment with Tween-20 and the green circles represent their TSVs from the re-run experiments after the treatment with Tween-20.

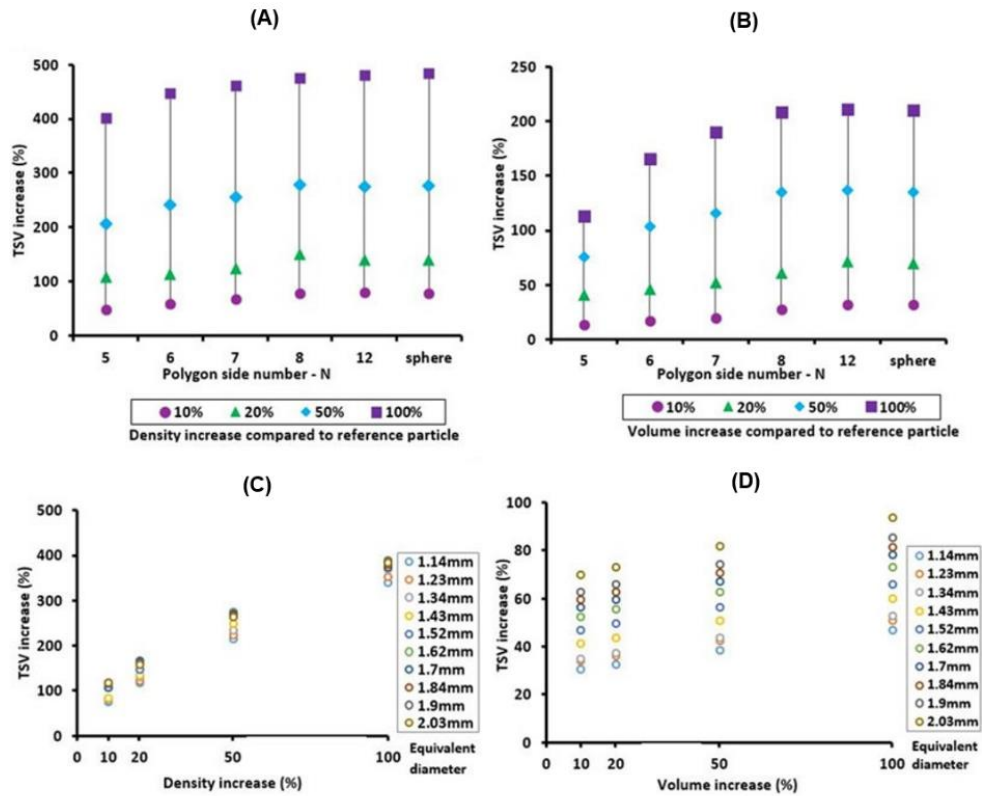


Figure 6: (A) Effects on TSV due to increasing the initial particle density (1.1 gcm³) by 10,20, 50, and 100% for particles with shapes derived from polygons with side numbers of 5,6,7,8,12 (see Figure 3) and a sphere with diameter of 1 mm (i.e., the level of roundness increases from left to right), (B) Effects on TSV due to increasing the initial particle volume (volume of a sphere with diameter of 1 mm) by 10, 20, 50, and 100% for the same particles as in A, (C) Effects of a density gain by 10, 20, 50, and 100% on TSVs for 10 randomly selected irregular particles (initial density = 1.1 g cm⁻³), (D) Impact of volume increase by 10, 20, 50, and 100% for the same 10 irregular MP particles as in (C).

4.1.2.2. Surface area to volume ratio

SA:V plays a significant role in determining the distribution of drag forces over the particle's surface and how these forces interact with gravitational forces to influence the particle's TSV. However, the effect of SA:V ratio was found to be less influential than the increase in MP particle volume. As Figure 7A depicts, the TSVs were sorted in ascending order for each polymer type, revealing descending trends for the SA:V ratios. This inverse relationship indicates that lower SA:V ratios generally lead to faster TSVs. However, there was considerable scatter in this trend, especially for lighter polymers like PS. Spearman rank correlations were conducted for each polymer class, assessing the relationship between SA:V and TSV. The results revealed mild correlations, ranging from 0.31 to 0.9. In contrast, the Spearman rank correlations between particle volumes and TSV showed stronger associations, with values ranging from 0.58 to 0.99. This suggests that the variability in TSV values for the irregular particles was primarily driven by changes in particle volume (i.e., weight), with the influence of SA:V variability being of secondary importance.

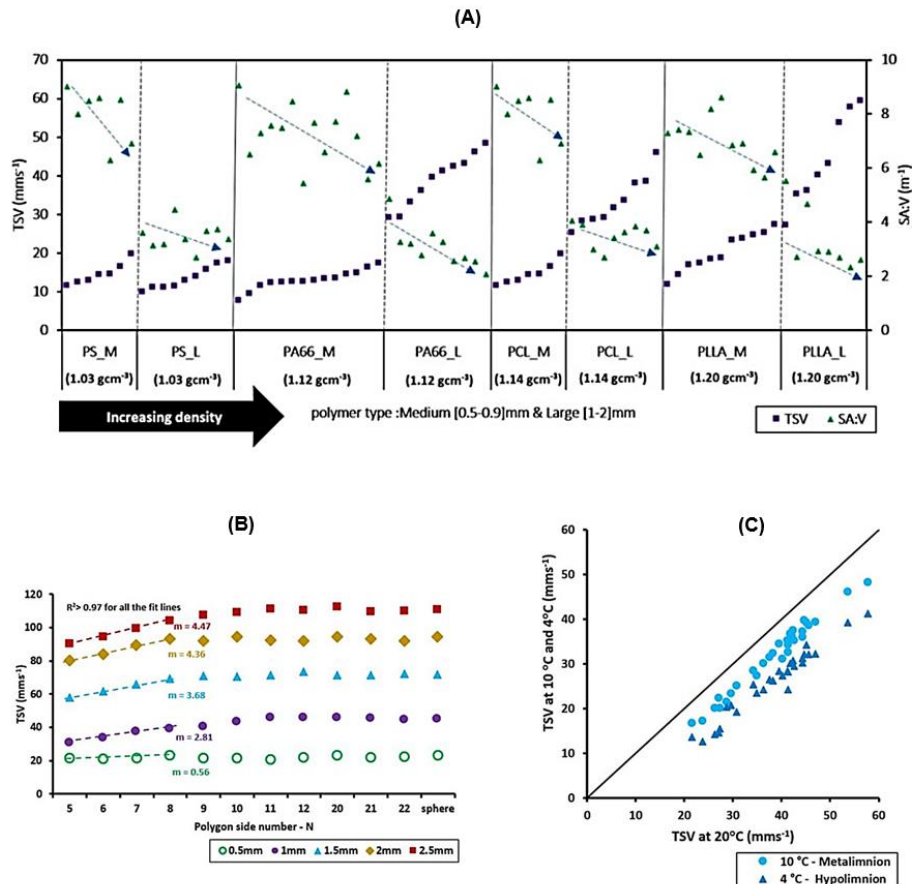


Figure 7: (A) Simulated TSVs (left axis) and calculated SA:V (right axis) for the 75 irregular MP particles. The different polymers are arranged in the order of increasing density along the x-axis with their equivalent diameters being grouped into intervals of 0.5–0.9 mm (Medium, e.g., PS-M) and 1–2 mm (Large, PS-L). The TSVs in each subset of particles of a particular polymer (e.g., PS_M or PS_L) were arranged in increasing order from left to right. The blue dashed arrows indicate the general direction of the trend in SA:V over an increasing TSV, (B) Effects of increasing roundness on TSV of MP particles for five different particle sizes. The different symbols depict the different diameters of the equivalent perfect spheres, which have the same volumes as the respective virtual particles derived from the polygons. Particles in all simulations have a density of 1.38 g cm⁻³, (C) Effects of water temperature changes in a stratified lake assuming a temperature of 20°C in the epilimnion, 10°C in the metalimnion and 4°C in the hypolimnion on the settling velocity of 30 irregular MP particles with a density of 1.38 g cm⁻³.

4.1.2.3. Roundness and water temperature

An increase in the roundness level of MP particles leads to a decrease in the SA:V ratio, resulting in reduced drag forces on their bodies and faster TSV. For particles with a diameter smaller than 1mm, in addition to their lower weight, the SA:V ratio increases significantly. Therefore, the changes in SA:V due to varying roundness levels are not sufficient to alter the TSV of these smaller particles, causing their TSVs to remain almost unaffected by changes in roundness level. However, the effect of changing roundness level became more pronounced as the diameter of MP particles increased over 1 mm (Figure 7B).

Changes in temperature from the epilimnion to metalimnion and hypolimnion affect the density and kinematic viscosity of water, which in turn impacts the drag force exerted on the particles. This effect became more pronounced as the MP particle size decreased (the more scattered TSVs around the 1:1 line in Figure 7C). The roundness level and water temperature had nearly equal levels of significance in influencing the TSV values, leading to a maximum of 45% TSV change due to altering the particle roundness and 47% TSV change due to the water temperature drop. This places them at a comparable level of importance after the effects of particle density, volume, and SA:V.

4.1.2.4. Biofilm coated MP particles

Biofilm formation had little impact on the density, shape, or roundness of MP particles, even after a 30-week incubation period. However, after 10 weeks of incubation, varying amounts of biofilms were observed on the particle surface using confocal laser scanning microscope images. These biofilms primarily consisted of microbial cells and extra polymeric substances, partially covering the particle surface and forming dense spots. The results also revealed that biofilm formation increased the tendency for MP aggregation and acted as an adhesive, binding particles together. Nevertheless, no significant differences in TSV values were observed between pristine and incubated MP particles after 6, 8, 10, and 30 weeks of incubation.

4.2. Work package 2

4.2.1. The relative importance of the different parameters affecting spatiotemporal patterns of MP particles in lakes

To analyze MP deposition patterns in the investigated lakes at the end of all simulations, the 48 scenarios were grouped into four categories based on MP release time (January / July) and wind condition (constant / variable). The comparison between the groups demonstrated that MP particle size, lake depth, and bathymetry consistently affect the deposition patterns. Figure 8 illustrates the MP particles deposition patterns for one of these groups with January as the release time and constant wind conditions. Figure 9 illustrates $D_{50\%}$ and $T_{50\%}$ for all 48 scenarios conducted in work package 2. Based on simulated MP deposition patterns (Figure 8) as well as the computed metrics (Figure 9), the following subsections will provide a comparative analysis of how the investigated physical factors impact particle distribution patterns in the investigated virtual lakes.

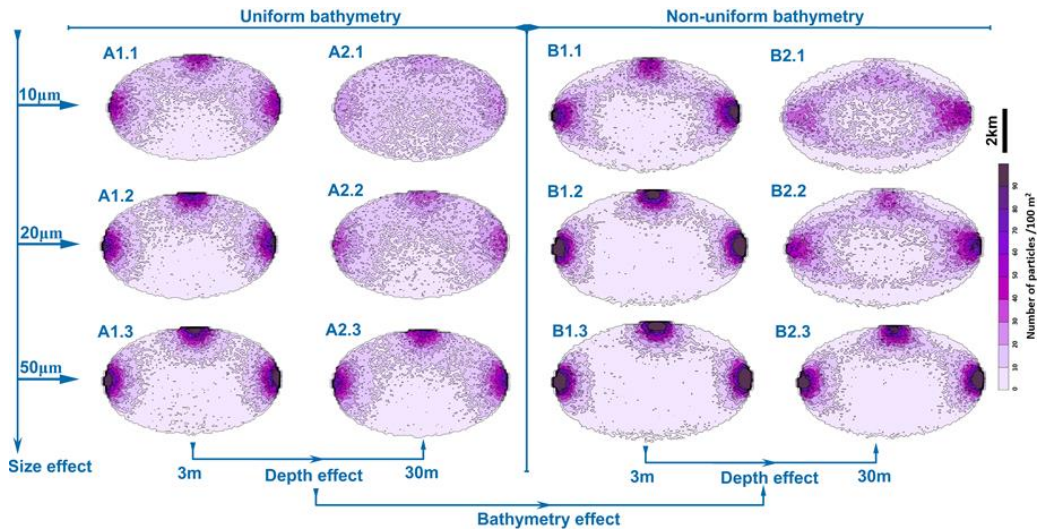


Figure 8: The deposition patterns of MP particles after reaching a quasi-steady state. The results are presented for two types of bathymetries: uniform (represented by "A") and non-uniform (represented by "B"). The table is organized into four columns: the first and third columns (indexed as 1.X) show the results for 3m-shallow lakes, with X:1,2 and 3 representing particle sizes of 10µm, 20µm, and 50µm, respectively. The second and fourth columns (indexed as 2.X) display the results for 30m-deep lakes, following the same order of particle sizes as for the 3m-shallow lakes. Wind speed was constant in this group of simulations.

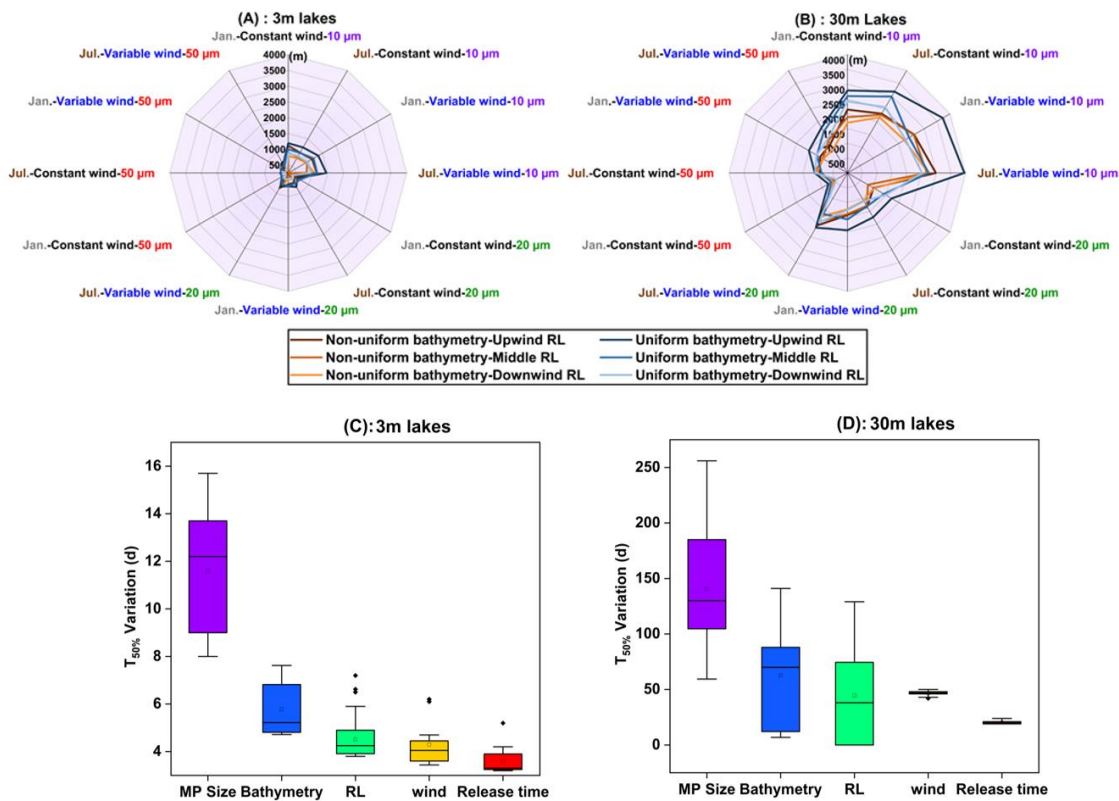


Figure 9: (A) The calculated $D_{50\%}$ at the end of the simulation for the 3m lakes, (B) and the 30m lakes; the injection time, wind condition, and MP particle sizes are labeled with different colors around each panel; Different blue and red color tones represent the $D_{50\%}$ separately sorted for RLs in the lakes with uniform and non-uniform bathymetries, (C) the $T_{50\%}$ variation in the lakes with 30m depth under the effect of investigated factors listed on the x-axis, (D) the same as panel A for the lakes with 3m depth.

4.2.1.1. Lake depth and MP particle size

According to the simulation results, the settling time scales of MP particles is primarily influenced by two factors: lake depth (travel distance) and particle size (settling velocity) (Figure 8, MP size and depth). Increasing lake depth from 3m to 30m, resulted in a substantial variation in the $D_{50\%}$ values, ranging from 678m to 2026m. Additionally, there was a notable increase in the variation of $T_{50\%}$ values (up to 16 times) with the change in lake depth from 3m to 30m (Figure 9C,D). The decrease in settling time was primarily attributed to shorter vertical travel distances and consistent mixing conditions in shallow lakes, resulting from the combined influence of wind on the upper water layers and bed layer roughness. Under these conditions shallow lakes slightly accelerated the settling of MP particles.

The simulation results provided $D_{50\%}$ values of 2909, 1678, and 998m for the 30m deep lake, and 986, 479, and 302m for the 3m deep lake, corresponding to 10, 20, and 50 μ m MP particles, respectively. Additionally, the $T_{50\%}$ values showed significant differences in the settling time scale when changing the MP particle size from 10 to 20 and 50 μ m in the 3m lakes (IQR: 9-13d) and 30m lakes (IQR: 102-178d) (Figure 9).

The settling velocities of the MP particles played a dominant role in determining the net settling timescales, overshadowing the influence of hydrodynamic processes and lake physical characteristics, and consequently, they had a significant impact on the deposition patterns. The 50 μ m MP particles consistently exhibited the most concentrated deposition patterns, regardless of changes in lake conditions. In contrast, altering the particle size to 20 μ m resulted in more dispersed deposition patterns. Among the different particle sizes studied, the 10 μ m MP particles were the most sensitive to changes in the lakes' hydrodynamics and other influential physical factors (Figure 8, MP size).

4.2.1.2. Lake bathymetry

The influence of lake bathymetry on the settling time and deposition patterns of MP particles was found to be less significant compared to the impact of lake depth and MP particle size, ranking it lower in importance (Figure 9). Altering the lake bathymetry from uniform to non-uniform shape resulted in a decrease in $D_{50\%}$ by up to 346m for the 3m deep lake and 834m for the 30m deep lake. Also, the change in bathymetry shape yielded the variations in $T_{50\%}$ values with an IQR of 11-89d for 30m lakes and 4.7-7d for 3m lakes. This variations in $D_{50\%}$ and $T_{50\%}$ values for each lake depth can be attributed to the specific geometry of the non-uniform bathymetry, which included shallow near-shore areas, facilitating faster particle settling.

The 30m deep lake scenarios with uniform bathymetry had more complex hydrodynamic processes, such as increased eddy density and mixing intensity typically found in deep lakes (Boehrer and Schultze, 2008; Woolway et al., 2020). These hydrodynamic complexities prolonged the floating duration of MP particles before their eventual settlement, which was particularly noticeable for smaller particles (i.e., 10 and 20 μ m MP particles) (Figure 9C, Bathymetry).

4.2.1.3. Release location, wind, and release time

The impact of altering the RL, wind condition, or shifting the release time on the deposition patterns and residence of MP particles was less significant compared to lake depth and particle size and bathymetry (Figure 9). For 50 μ m particles, these factors did not cause significant changes, but their influence increased as particle size decreased to 20 and 10 μ m.

Altering the RLs in both 3m and 30m deep lake scenarios resulted in slight changes in the deposition patterns for 50 μ m particles. These particles exhibited narrower deposition patterns around downwind RL, wider patterns around upwind RL, and remained relatively unaffected around the middle RLs under the influence of western winds. The same patterns were observed in the scenarios with 20 μ m MP particles. However, the 10 μ m MP particles did not show the patterns observed for the larger particles, as they were highly susceptible to the wind effect, causing them to stay in the upper water layers for an extended period and significantly changed the T_{50%} values among the RLs in 30m deep lakes (Figure 9D, RL).

4.2.2. Instability in water layering during fall

During the second half of the year in 30m lakes with uniform bathymetry, a reversal in the density gradient led to water layer instability and an increased likelihood of convective water transport. As illustrated in Figure 10, in these lakes, the settling velocity of 10 μ m MP particles was influenced by instability in water layering when released closer to the dissipation of thermal stratification (July release). This resulted in the particles remaining suspended in the water column for an extended period, increasing the likelihood of them being influenced by water movements caused by convective heat transport during this time of the year. Consequently, there was approximately a one-month period (Figure 10, Sep.) during which 2.6 and 5.5% of MP particles floating in the metalimnion were transported to the epilimnion in scenarios with constant and variable wind conditions, respectively.

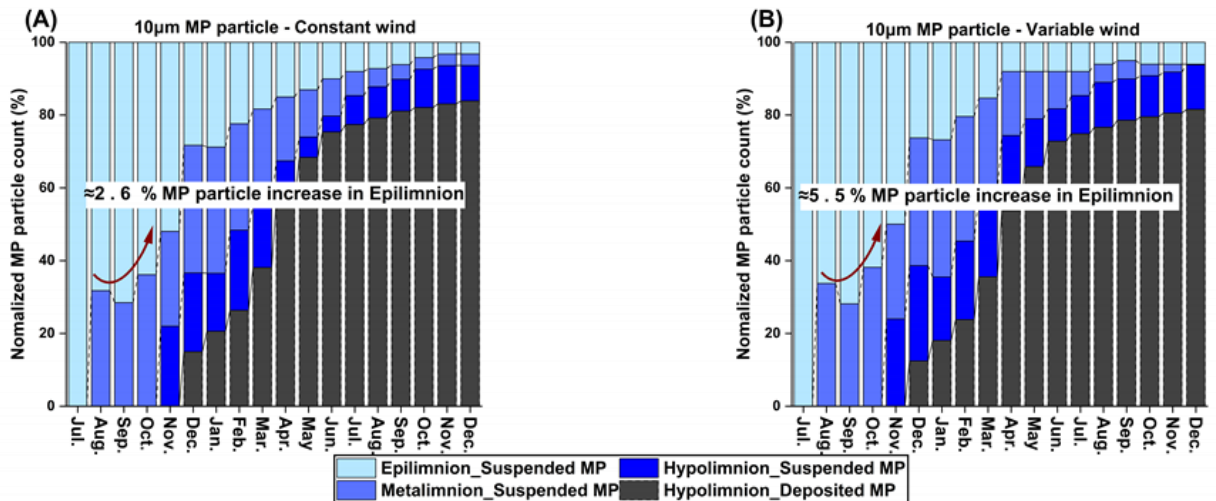


Figure 10: (A) MP particle counts for the suspended and deposited particles over 18 months of simulation for the lake with uniform bathymetry and 30m depth under constant wind, (B) same scenario as in panel A but under variable wind.

4.2.3. The joint impact of interconnected physical factors on the behavior of MP particles

Assessing the relative importance of each individual physical factor in shaping MP particle behavior is a challenging task due to their complex interplay and interdependencies. In certain instances, it is necessary to consider the simultaneous presence and active influence of multiple physical factors in order to observe their impact on MP particles. For instance, the RL influence on the behavior of 10 μ m particles became apparent when they were released near the lake turnover period. This specific timing enhances the likelihood of their presence in areas where they can be affected by convective heat transport and the resultant water movement within the lake. Furthermore, the importance of a single factor can be affected by the values and interactions of other factors simultaneously at work. For example, when the MP particle size decreases from 50 to 20 and 10 μ m, the impact of wind on the deposition times of MP particles became more evident. The reason for this effect is the prolonged time period during which smaller particles are affected by wind-induced currents, given their slow TSV.

5. Summary and conclusions

The objective of this research was to obtain a more comprehensive understanding of the fate of MP particles in lakes by focusing on the key physical factors controlling the behavior of individual particles as well as their spatiotemporal distributions in lakes. The importance of this research essentially lies in the fact that lakes provide fresh water that is consumed by humans as well as serving as habitats for various aquatic organisms, which depend on this ecosystem for survival and food. In work package 1, the primary objective was to explore the sensitivity of the TSV of MP particles to alteration of their physical properties, including density, volume, SA:V and roundness. In this work package also the impacts of surrounding water temperature as well as the formation of gas bubbles and biofilms on the body of MP particles, on the TSVs of MP particles were examined. This work package utilized a combination of CFD simulations (study 1) and experiments (study 2) to assess and prioritize the level of importance of the investigated factors. Work package 2 (study 3) focused on the investigation of MP particle behavior in an elliptical lake, a commonly found lake shape in natural environments. Study 3 examined the spatiotemporal distribution patterns of MP particles under the influence of various physical factors. These factors included lake geometry (depth and bathymetry), MP particle size, wind conditions, and the release time and location of the MP particles. The conclusions derived from the two work packages are outlined as follows:

5.1. Work package 1

- The magnitude of the TSV of MP particles is primarily influenced by their density. An increase in MP particle density results in a stronger gravitational force acting on the particles, which, in turn, enhances their TSV. Altering the volume of MP particles affects their weight/gravitational force, but it also influences buoyant and drag forces, which act in opposite direction. Consequently, changes in particle volume result in a secondary impact on TSV compared to the effect of MP particle density. Comparing the effects of MP particle volume and SA:V variations on the TSV of MP particles revealed that changes in volume have a greater influence on TSV values than alterations in SA:V. As a result, SA:V is ranked as the subsequent parameter in terms of importance after density and volume.
- The influences of hydrophobicity and water temperature on the TSV of MP particles were of comparable magnitude, positioning both factors after density, volume, and SA:V in terms of importance level. Hydrophobicity of and small irregularities in MP particle surfaces lead to the attachment of air bubbles on their surfaces, yielding an increase in the exerted buoyant force due to the attached air bubbles. This phenomenon is predominantly observed in biodegradable particles, while non-biodegradable particles also exhibit this effect, though to a lesser extent. A decrease in water temperature has an impact on water density and kinematic viscosity, affecting the TSV of MP particles. This causes the MP particles to sink with an accelerated TSV in the upper layers of a lake when it is thermally stratified compared to the mixing condition.

-
- The TSV of pristine MP particles remained almost unaffected after incubating them for more than seven months, indicating that the formation of biofilms on MP particles had the least impact on the TSV of MP particles. The biofilm structure on MP particles is non-uniform, tending to form dense patches. This spatial distribution could have implications for the aggregation and sinking behavior of MP particles over extended incubation periods. The hydrophobic nature of pristine MP particles enables rapid colonization by biofilms, making pristine MP particles rare in natural aquatic environments as they are typically covered by biofilms or adsorb other natural/toxic materials.

5.2. Work package 2

- The primary controlling factor over the spatiotemporal distribution of MP particles is lake depth, followed by the size of the MP particles. Increasing lake depth not only extends the settling time, but also results in more complex hydrodynamic processes. This, in turn, increases the likelihood of MP particles encountering interruptions during their sinking and strengthens the horizontal component of their velocity vector. Particle size is another critical factor that determines the settling time and the behavior of particles encountering different levels of lake hydrodynamic complexities. Increasing particle size and the resulting faster settling reduces susceptibility to lateral advective and dispersive transport, resulting in spatially more concentrated deposition patterns around their release locations.
- Bathymetry is another key-parameter following lake depth and particle size that controls the spatiotemporal distribution of MP particles. In lakes with non-uniform bathymetries, MP particles tend to settle faster compared to lakes with uniform bathymetry. In addition to lakes with non-uniform bathymetry being shallower close to the shoreline, they also exhibit less hydrodynamic complexities, providing simpler condition for the MP particles to settle. Deep lakes with uniform bathymetry, on the other hand, due to their larger water volume, require more time to readjust and thermally equilibrate in response to changing weather conditions in the lake area, when compared to lakes with non-uniform bathymetry. Accordingly, during the time that deep lakes are thermally stratified, the ones with uniform bathymetry exhibit a more pronounced vertical water temperature gradient compared to the lakes with non-uniform bathymetry. In contrast, the vertical water temperature gradient in shallow lakes remains very small, irrespective of the bathymetry type, because of a more rapid readjustment to the new weather conditions.
- The influence of altering wind conditions, release location, and release time on the spatiotemporal distribution patterns and residence time of MP particles in lakes is comparable, but less significant when compared to the other investigated factors including depth, MP particle size, and bathymetry. Generally, reducing the size of MP particles enhances the impact of wind-induced currents, facilitating their horizontal transport. Moreover, as the MP particle size decreases, the effect of altering the RL becomes more prominent, especially when particles are released around the time when the lake thermal stratification dissipates. During this period, due to the different levels of

hydrodynamic complexities across the lake, the MP particles are affected differently. The instability of lake water layering caused by convective heat transport is more prominent in areas near the center of the lake and in the lake regions down-wind of the dominant wind direction. During dissipation of the thermal stratification of the lake, the presence of small MP particles in the regions experiencing water movement due to convective heat transport increases the likelihood of these particles rising from the deeper parts of the lake (metalimnion) to shallower water layers close to the lake water surface (epilimnion).

- While individual factors have a substantial impact on the movement of MP particles in the studied lakes, it is the complex interplay among all factors that ultimately governs the transport and fate of the MP particles in lakes. For instance, the influence of wind conditions, release location, or release time becomes significant when they coincide with specific combinations of other factors, including lake depth, bathymetry, and particle size. Consequently, relying on the assessment of MP particle transport and fate in lakes based on evaluating isolated factors or a limited set of factors alone can lead to false conclusions. A comprehensive evaluation and analysis of all relevant factors and their interactions is essential to thoroughly understand the behavior of MP particles in lakes.

6. Outlook

While this dissertation provides a comprehensive investigation of MP particle fate in lake systems through various methodologies including numerical modelling and laboratory experiments, there are several crucial aspects that should be addressed in future studies:

Firstly, future studies should investigate the implications arising from the surface properties of MP particles, such as hydrophobic and hydrophilic properties as well as polymer surface charge, through the application of CFD and molecular dynamics (MD) simulations. These factors could have substantial influence on MP particle fate in lake systems through affecting their TSV and in turn residence times in the lake water column. Considering these factors in laboratory experiments and modeling-based research when dealing with MP particles composed of distinct polymers with individual surface characteristics can lead to results that are more accurate, dependable, and relevant to a wider range of MP particle variations.

Furthermore, the chemical composition of MP particles and their capacity to adsorb toxic substances from the environment, such as pesticides and heavy metals, add complexity to their behavior. These substances could enhance processes of aggregation, further influencing MP particle fate in lakes. Future research must investigate the presence and impact of these substances in lake ecosystems to better understand their role in MP particles' fate.

Additionally, the relatively short incubation periods of MP particles in ponds used in current studies may not fully represent their prolonged exposure to biofilm-building organisms in natural lake conditions. Addressing this, future studies should explore longer exposure periods in natural lake environments, considering seasonal variations and incubation depths. This research will offer valuable insights into how environmental variables affect MP particle behavior in real lake systems.

To achieve a more comprehensive understanding of MP particle fate in lakes, it is crucial for future studies to incorporate all factors influencing lake hydrodynamic complexities. This includes accounting for the effects of lake inlets and outlets. Furthermore, it is crucial to investigate how inflowing streams and rivers influence hydrodynamic complexities both before and after lake turnover, and how these factors impact this phenomenon and subsequently, the spatiotemporal distribution of MP particles.

By addressing these additional research questions and incorporating additional, relevant factors that influence MP particle transport in lakes in future work, we can take the findings of this dissertation yet another step further to achieve a deeper understanding of the complex interactions governing the fate of MP particles in lake ecosystems. This knowledge is crucial for developing sustainable solutions to manage MP pollution in lakes, preserving aquatic environments, and safeguarding human health. Continued research and improved simulations will play a crucial role in paving the way towards effective strategies for mitigating the impact of MP particles on our natural environment.

References

- Al Harraq, A. and Bharti, B. 2021. Microplastics through the Lens of Colloid Science. *ACS Environmental Au* 2(1), 3-10.
- An, L., Liu, Q., Deng, Y., Wu, W., Gao, Y. and Ling, W. 2020. Sources of microplastic in the environment. *Microplastics in terrestrial environments: Emerging contaminants and major challenges*, 143-159.
- Anderson, P.J., Warrack, S., Langen, V., Challis, J.K., Hanson, M.L. and Rennie, M.D. 2017. Microplastic contamination in lake Winnipeg, Canada. *Environmental pollution* 225, 223-231.
- Andrady, A.L. and Neal, M.A. 2009. Applications and societal benefits of plastics. *Philosophical Transactions of the Royal Society B: Biological Sciences* 364(1526), 1977-1984.
- Arora, C., Kumar, B.P. and Narayana, A. 2010. Influence of particle shape on drag coefficient for commonly occurring sandy particles in coastal areas. *The International Journal of Ocean and Climate Systems* 1(2), 99-112.
- Ballent, A., Corcoran, P.L., Madden, O., Helm, P.A. and Longstaffe, F.J. 2016. Sources and sinks of microplastics in Canadian Lake Ontario nearshore, tributary and beach sediments. *Marine pollution bulletin* 110(1), 383-395.
- Banerjee, V.K., Adhikary, P. and Pahari, U. *Circular Economy Advancements in Additive Manufacturing and Polymer Waste Recycling: Reshaping Sustainability*.
- Barnes, D.K., Galgani, F., Thompson, R.C. and Barlaz, M. 2009. Accumulation and fragmentation of plastic debris in global environments. *Philosophical transactions of the royal society B: biological sciences* 364(1526), 1985-1998.
- Boehrer, B. and Schultze, M. 2008. Stratification of lakes. *Reviews of Geophysics* 46(2).
- Boos, J.P., Gilfedder, B.S. and Frei, S. 2021. Tracking Microplastics Across the Streambed Interface: Using Laser-Induced-Fluorescence to Quantitatively Analyze Microplastic Transport in an Experimental Flume. *Water Resources Research* 57(12), e2021WR031064.
- Browne, M.A., Crump, P., Niven, S.J., Teuten, E., Tonkin, A., Galloway, T. and Thompson, R. 2011. Accumulation of microplastic on shorelines worldwide: sources and sinks. *Environmental science & technology* 45(21), 9175-9179.
- Cable, R.N., Beletsky, D., Beletsky, R., Wigginton, K., Locke, B.W. and Duhaime, M.B. 2017. Distribution and modeled transport of plastic pollution in the Great Lakes, the world's largest freshwater resource. *Frontiers in Environmental Science* 5, 45.
- Castro-Castellon, A.T., Horton, A.A., Hughes, J.M., Rampley, C., Jeffers, E.S., Bussi, G. and Whitehead, P. 2022. Ecotoxicity of microplastics to freshwater biota: Considering exposure and hazard across trophic levels. *Science of the Total Environment* 816, 151638.
- Chen, X., Xiong, X., Jiang, X., Shi, H. and Wu, C. 2019. Sinking of floating plastic debris caused by biofilm development in a freshwater lake. *Chemosphere* 222, 856-864.
- Claessens, M., De Meester, S., Van Landuyt, L., De Clerck, K. and Janssen, C.R. 2011. Occurrence and distribution of microplastics in marine sediments along the Belgian coast. *Marine pollution bulletin* 62(10), 2199-2204.
- Collard, F., Gasperi, J., Gabrielsen, G.W. and Tassin, B. 2019. Plastic particle ingestion by wild freshwater fish: a critical review. *Environmental Science & Technology* 53(22), 12974-12988.
- Corey, A.T. (1949) Influence of shape on the fall velocity of sand grains, Colorado A & M College.
- Corey, A.T., Albertson, M.L., Fults, J.L., Rollins, R.L., Gardner, R.A., Klinger, B. and Bock, R.O. 1949. Influence of shape on the fall velocity of sand grains.
- de Souza Machado, A.A., Kloas, W., Zarfl, C., Hempel, S. and Rillig, M.C. 2018. Microplastics as an emerging threat to terrestrial ecosystems. *Global change biology* 24(4), 1405-1416.
- Deleersnijder, E., Beckers, J.-M. and Delhez, E.J. 2006. The residence time of settling particles in the surface mixed layer. *Environmental Fluid Mechanics* 6, 25-42.
- Deltares, D. 2013. *Delft3D-FLOW user manual*. Deltares Delft, The Netherlands 330.

-
- Derraik, J.G. 2002. The pollution of the marine environment by plastic debris: a review. *Marine pollution bulletin* 44(9), 842-852.
- Dietrich, W.E. 1982. Settling velocity of natural particles. *Water resources research* 18(6), 1615-1626.
- Elagami, H., Frei, S., Boos, J.-P., Trommer, G. and Gilfedder, B.S. 2023. Quantifying microplastic residence times in lakes using mesocosm experiments and transport modelling. *Water Research* 229, 119463.
- Facts, P. 2019. An analysis of European plastics production, demand and waste data. *Plastics Europe*.
- Falconieri, M., Iannilli, V., Lecce, F., Pietrelli, L. and Sighicelli, M. 2018. Microplastic pollution in the surface waters of Italian Subalpine Lakes. *ENVIRONMENTAL POLLUTION* 236.
- Free, C.M., Jensen, O.P., Mason, S.A., Eriksen, M., Williamson, N.J. and Boldgiv, B. 2014. High-levels of microplastic pollution in a large, remote, mountain lake. *Marine pollution bulletin* 85(1), 156-163.
- Frias, J.P. and Nash, R. 2019. Microplastics: Finding a consensus on the definition. *Marine pollution bulletin* 138, 145-147.
- Gregory, M.R. 1983. Virgin plastic granules on some beaches of eastern Canada and Bermuda. *Marine Environmental Research* 10(2), 73-92.
- Guerrini, F., Mari, L. and Casagrandi, R. 2021. The dynamics of microplastics and associated contaminants: Data-driven Lagrangian and Eulerian modelling approaches in the Mediterranean Sea. *Science of the Total Environment* 777, 145944.
- Herschy, R.W. 2012. Ecological threat to lakes and reservoirs. *Encyclopedia of Lakes and Reservoirs*, 233-234.
- Jérémy, R., Gaston, L.P. and Valyrakis, M. 2020. Coupled CFD-DEM modelling to assess settlement velocity and drag coefficient of microplastics, p. 10049.
- Kaiser, D., Kowalski, N. and Waniek, J.J. 2017. Effects of biofouling on the sinking behavior of microplastics. *Environmental research letters* 12(12), 124003.
- Khatmullina, L. and Isachenko, I. 2017. Settling velocity of microplastic particles of regular shapes. *Marine pollution bulletin* 114(2), 871-880.
- Klein, S., Dimzon, I.K., Eubeler, J. and Knepper, T.P. 2018. Analysis, occurrence, and degradation of microplastics in the aqueous environment. *Freshwater microplastics: emerging environmental contaminants?*, 51-67.
- Kwon, J.H., Chang, S., Hong, S.H. and Shim, W.J. 2017. Microplastics as a vector of hydrophobic contaminants: Importance of hydrophobic additives. *Integrated environmental assessment and management* 13(3), 494-499.
- Lambert, S. and Wagner, M. (2018) *Microplastics are contaminants of emerging concern in freshwater environments: an overview*, Springer International Publishing.
- Leiser, R., Jongsma, R., Bakenhus, I., Möckel, R., Philipp, B., Neu, T.R. and Wendt-Potthoff, K. 2021a. Interaction of cyanobacteria with calcium facilitates the sedimentation of microplastics in a eutrophic reservoir. *Water Research* 189, 116582.
- Leiser, R., Schumann, M., Dadi, T. and Wendt-Potthoff, K. 2021b. Burial of microplastics in freshwater sediments facilitated by iron-organo floes. *Scientific Reports* 11(1), 1-12.
- Leiser, R., Wu, G.-M., Neu, T.R. and Wendt-Potthoff, K. 2020. Biofouling, metal sorption and aggregation are related to sinking of microplastics in a stratified reservoir. *Water research* 176, 115748.
- Liao, J. and Chen, Q. 2021. Biodegradable plastics in the air and soil environment: Low degradation rate and high microplastics formation. *Journal of hazardous materials* 418, 126329.
- Nematollahi, M.J., Moore, F., Keshavarzi, B., Vogt, R.D., Saravi, H.N. and Busquets, R. 2020. Microplastic particles in sediments and waters, south of Caspian Sea: frequency, distribution, characteristics, and chemical composition. *Ecotoxicology and Environmental Safety* 206, 111137.
- North, E.J. and Halden, R.U. 2013. Plastics and environmental health: the road ahead. *Reviews on environmental health* 28(1), 1-8.
- O'Sullivan, P. and Reynolds, C.S. (2008) *The lakes handbook, volume 1: limnology and limnetic ecology*, John Wiley & Sons.
-

-
- Powers, M.C. 1953. A new roundness scale for sedimentary particles. *Journal of Sedimentary Research* 23(2), 117-119.
- Raimundo, G.I., Sousa, M.C. and Dias, J.M. 2020. Numerical modelling of plastic debris transport and accumulation throughout Portuguese coast. *Journal of Coastal Research* 95(SI), 1252-1257.
- Rocha-Santos, T. and Duarte, A.C. 2015. A critical overview of the analytical approaches to the occurrence, the fate and the behavior of microplastics in the environment. *TrAC Trends in analytical chemistry* 65, 47-53.
- Rochman, C.M. 2018. Microplastics research—from sink to source. *Science* 360(6384), 28-29.
- Schmidt, C., Krauth, T. and Wagner, S. 2017. Export of Plastic Debris by Rivers into the Sea. *Environmental Science & Technology* 51(21), 12246-12253.
- Singh, P., Bagrania, J. and Haritash, A. 2019. Seasonal behaviour of thermal stratification and trophic status in a sub-tropical Palustrine water body. *Applied Water Science* 9(5), 1-6.
- Stuparu, D., van der Meulen, M., Kleissen, F., Vethaak, D. and El Serafy, G. 2015. Developing a transport model for plastic distribution in the North Sea.
- Vaughan, R., Turner, S.D. and Rose, N.L. 2017. Microplastics in the sediments of a UK urban lake. *Environmental Pollution* 229, 10-18.
- Waldschläger, K. and Schüttrumpf, H. 2019. Effects of particle properties on the settling and rise velocities of microplastics in freshwater under laboratory conditions. *Environmental science & technology* 53(4), 1958-1966.
- Wang, T., Yu, C., Chu, Q., Wang, F., Lan, T. and Wang, J. 2020. Adsorption behavior and mechanism of five pesticides on microplastics from agricultural polyethylene films. *Chemosphere* 244, 125491.
- Webb, H.K., Arnott, J., Crawford, R.J. and Ivanova, E.P. 2013. Plastic degradation and its environmental implications with special reference to poly (ethylene terephthalate). *Polymers* 5(1), 1-18.
- Williams, A. and Simmons, S. 1996. The degradation of plastic litter in rivers: implications for beaches. *Journal of Coastal Conservation* 2, 63-72.
- Woolway, R.I., Kraemer, B.M., Lenters, J.D., Merchant, C.J., O'Reilly, C.M. and Sharma, S. 2020. Global lake responses to climate change. *Nature Reviews Earth & Environment* 1(8), 388-403.
- Wright, S.L., Thompson, R.C. and Galloway, T.S. 2013. The physical impacts of microplastics on marine organisms: a review. *Environmental pollution* 178, 483-492.
- Wright, S.L., Ulke, J., Font, A., Chan, K.L.A. and Kelly, F.J. 2020. Atmospheric microplastic deposition in an urban environment and an evaluation of transport. *Environment international* 136, 105411.
- Xanthos, D. and Walker, T.R. 2017. International policies to reduce plastic marine pollution from single-use plastics (plastic bags and microbeads): A review. *Marine pollution bulletin* 118(1-2), 17-26.
- Zhang, H. 2017. Transport of microplastics in coastal seas. *Estuarine, Coastal and Shelf Science* 199, 74-86.
- Zhang, M., Xu, D., Liu, L., Wei, Y. and Gao, B. 2023. Vertical Differentiation of Microplastics Influenced by Thermal Stratification in a Deep Reservoir. *Environmental Science & Technology*.
- Zhang, Q., Xu, E.G., Li, J., Chen, Q., Ma, L., Zeng, E.Y. and Shi, H. 2020. A review of microplastics in table salt, drinking water, and air: direct human exposure. *Environmental Science & Technology* 54(7), 3740-3751.
- Ziccardi, L.M., Edgington, A., Hentz, K., Kulacki, K.J. and Kane Driscoll, S. 2016. Microplastics as vectors for bioaccumulation of hydrophobic organic chemicals in the marine environment: A state-of-the-science review. *Environmental toxicology and chemistry* 35(7), 1667-1676.
-

Study 1: Systematic evaluation of physical parameters affecting the terminal settling velocity of microplastic particles in lakes using CFD

Pouyan Ahmadi, Hassan Elagami, Franz Dichgans, Christian Schmidt, Benjamin S. Gilfedder, Sven Frei, Stefan Peiffer, Jan H. Fleckenstein

Corresponding Author: Pouyan Ahmadi

Published in *Frontiers in Environmental Science* in April 2022

<https://doi.org/10.3389/fenvs.2022.875220>

Own contribution:

- Concept and study design 70%
- Data acquisition 90%
- Data analyses 100%
- Figures 100%
- Discussion of results 80%
- Manuscript writing 80%

Author contribution statement:

PA set up the CFD modeling framework, conducted the CFD simulations, designing the additional experiments, data interpretation and writing the manuscript. HE performed the laboratory experiments, assisted in data interpretation and writing the manuscript. FD contributed to the initial set-up of the CFD modeling framework, to data interpretation and writing of the manuscript. CS assisted in data interpretation and writing the manuscript. BSG assisted in data interpretation and writing the manuscript. SF assisted in data interpretation and writing the manuscript. SP assisted in data interpretation and writing the manuscript. JHF conceived the project, assisted in data interpretation and contributed to writing and editing of the manuscript



Systematic Evaluation of Physical Parameters Affecting the Terminal Settling Velocity of Microplastic Particles in Lakes Using CFD

Pouyan Ahmadi^{1*}, Hassan Elagami^{2,3}, Franz Dichgans¹, Christian Schmidt^{1,4}, Benjamin S. Gilfedder^{2,3}, Sven Frei³, Stefan Peiffer³ and Jan H. Fleckenstein^{1,5*}

¹Department of Hydrogeology, Helmholtz-Centre for Environmental Research, UFZ, Leipzig, Germany, ²Limnological Research Station, Bayreuth Center of Ecology and Environmental Research, University of Bayreuth, Bayreuth, Germany, ³Department of Hydrology, Bayreuth Center of Ecology and Environmental Research (BayCEER), University of Bayreuth, Bayreuth, Germany, ⁴Department of Aquatic Systems Analysis and Management, Helmholtz-Centre for Environmental Research, UFZ, Leipzig, Germany, ⁵Hydrologic Modelling Unit, Bayreuth Center of Ecology and Environmental Research (BayCEER), University of Bayreuth, Bayreuth, Germany

OPEN ACCESS

Edited by:

Ping Wang,
Beijing Forestry University, China

Reviewed by:

Veerasingam S.,
Qatar University, Qatar
Qiqing Chen,
East China Normal University, China

*Correspondence:

Pouyan Ahmadi
pouyan.ahmadi@ufz.de
Jan H. Fleckenstein
jan.fleckenstein@ufz.de

Specialty section:

This article was submitted to
Freshwater Science,
a section of the journal
Frontiers in Environmental Science

Received: 13 February 2022

Accepted: 24 March 2022

Published: 13 April 2022

Citation:

Ahmadi P, Elagami H, Dichgans F,
Schmidt C, Gilfedder BS, Frei S,
Peiffer S and Fleckenstein JH (2022)
Systematic Evaluation of Physical
Parameters Affecting the Terminal
Settling Velocity of Microplastic
Particles in Lakes Using CFD.
Front. Environ. Sci. 10:875220.
doi: 10.3389/fenvs.2022.875220

Microplastic (MP) particles are commonly found in freshwater environments such as rivers and lakes, negatively affecting aquatic organisms and potentially causing water quality issues. Understanding the transport and fate of MP particles in these environments is a key prerequisite to mitigate the problem. For standing water bodies (lakes, ponds) the terminal settling velocity (TSV) is a key parameter, which determines particle residence times and exposure times of organisms to MP in lakes. Here we systematically investigate the effects of the physical parameters density, volume, shape and roundness, surface roughness and hydrophobicity and lake water temperature on the TSV of a large number of particles with regular and irregular shapes (equivalent diameters: 0.5–2.5 mm) and different polymer densities using computational fluid dynamics (CFD) simulations. Simulation results are compared to laboratory settling experiments and used to evaluate existing, semi-empirical relationships to estimate TSV. The semi-empirical relationships were generally found to be in reasonable agreement with the CFD simulations ($R^2 > 0.92$). Deviations were attributed to simplifications in their descriptions of particle shapes. Overall the CFD simulations also matched the TSVs from the experiments quite well, ($R^2 > 0.82$), but experimental TSVs were generally slower than model TSVs with the largest differences for the irregular particles made from biodegradable polymers. The deviations of up to 58% were found to be related to the attachment of air bubbles on irregularities in the particle surfaces caused by the hydrophobicity of the MP particles. Overall, density was the most decisive parameter for TSV with increases in TSV of up to 400% followed by volume (200%), water temperature (47%) and particle roundness (45%). Our simulation results provide a frame of reference for an improved evaluation of the relative effects of different particle characteristics on their TSV in lakes. This will in turn allow a more robust estimation of particle residence times and potential exposure times of organism to MP in the different compartments of a lake.

Keywords: CFD, Navier-Stokes equations, OpenFOAM, microplastic particles, terminal settling velocity

1 INTRODUCTION

Plastic products have a broad range of applications in all fields of daily life due to their useful properties such as durability and ductility (Derraik, 2002; North and Halden, 2013). Their widespread use, in turn, has led to large amounts of plastic waste, which, if mismanaged, may pose a threat to the environment (Derraik, 2002; Barnes et al., 2009; Claessens et al., 2011). Plastic debris, in a wide variety of sizes, can be found in the oceans, as well as in terrestrial freshwater systems and the atmosphere (Barnes et al., 2009; de Souza Machado et al., 2018; Rochman, 2018; Frias and Nash, 2019; Liao and Chen, 2021). A significant share of the plastic found in the terrestrial and marine environments belongs to the microplastic (MP) fraction (<5 mm - (Barnes et al., 2009)). These MP particles may enter the environment as primary MP via the release from cosmetic products and cleaners, via losses from production plants and during transport (Gregory, 1983; Gregory, 1996; Fendall and Sewell, 2009; Doyle et al., 2011) or as secondary MP resulting from the break-down and erosion of larger plastic debris in the environment (Williams and Simmons, 1996; Browne et al., 2011; Wright et al., 2020). Although different size ranges have been used to define MP (Claessens et al., 2011; Van Cauwenberghe et al., 2013), an upper size limit of 5,000 μm has been introduced as the definition of MP by the National Oceanic and Atmospheric Administration (Lambert and Wagner, 2018; Sighicelli et al., 2018) and is commonly accepted as the upper size limit in the literature. The lower size limit is not as clearly defined and may vary between different studies depending on their scope and questions (Khatmullina and Isachenko, 2017; Kaiser et al., 2019; Waldschlager and Schuttrumpf, 2019).

Freshwater lakes are amongst the main receptors of MP in the terrestrial environment (Zbyszewski et al., 2014; Ballent et al., 2016; Fischer et al., 2016; Anderson et al., 2017; Vaughan et al., 2017; Hendrickson et al., 2018; Sighicelli et al., 2018). MP particles can be taken up by organisms in different compartments of a lake with detrimental effects on the organisms as well as other organisms at higher trophic levels (Cole et al., 2013; Wright et al., 2013; Cole et al., 2016; Coppock et al., 2019). Transport vectors of MP particles determine their horizontal and vertical distribution patterns in a lake (Khatmullina and Isachenko, 2017; Kaiser et al., 2019; Waldschlager and Schuttrumpf, 2019; Isachenko, 2020) and in turn control residence times in the lake compartments as well as exposure of organisms to MP particles. It is therefore of particular importance to understand the physical controls of particle settling in lakes (Elagami et al., 2022). Vertical transport vectors are strongly controlled by physical parameters that define the force balance between downward gravitational forces, drag forces and upward buoyant forces acting on the body of an individual MP particle. A terminal settling velocity (TSV) is reached at the point where the summation of drag and buoyant forces is approximately equal to the weight force (Chubarenko et al., 2016; Khatmullina and Isachenko, 2017; Zhang, 2017).

Several experimental studies have investigated the TSV of MP particles primarily in marine systems (Arora et al., 2010; Wright

et al., 2013; Chubarenko et al., 2016; Kooi et al., 2016; Kowalski et al., 2016; Khatmullina and Isachenko, 2017; Zhang, 2017; Chubarenko et al., 2018; Akdogan and Guven, 2019; Kaiser et al., 2019), with studies explicitly addressing freshwater systems being rare (Khatmullina and Isachenko, 2017; Kaiser et al., 2019; Waldschlager and Schuttrumpf, 2019; Elagami et al., 2022). In some of these studies specific semi-empirical relationships have been developed to predict the TSV of MP particles in water considering particle size, density, and roundness as well as water density and kinematic viscosity (Dietrich, 1982; Khatmullina and Isachenko, 2017; Kaiser et al., 2019; Waldschlager and Schuttrumpf, 2019; Elagami et al., 2022). Comparisons with earlier, well established relationships developed for mineral particles (Dietrich, 1982) suggest that for certain MP characteristics adjustments to the known relationships are needed (Khatmullina and Isachenko, 2017; Waldschlager and Schuttrumpf, 2019). However, adjustments or new formulations on the basis of experiments only reflect the specific shapes of MP particles being used in the experiment and a more general, systematic assessment of the relative importance of different particle characteristics for TSV estimates would be useful. We take a first step in this direction.

Models are a useful tool for a systematic evaluation of particle transport in aquatic environments. Different types of models have been used to simulate the settling and transport of plastic debris, MP particles and individual MP particle in water bodies over a wide range of spatial scales. At global and regional scales studies have focused on MP transport in oceans using Eulerian circulation models for flow in combination with Lagrangian (Berlemont et al., 1990; Maximenko et al., 2012; Jalon-Rojas et al., 2019; Nooteboom et al., 2020; Guerrini et al., 2021) or Eulerian (advective dispersive) (Mountford and Morales Maqueda, 2019) transport formulations. These types of models rely on an adequate description of particle settling, which is typically obtained from semi-empirical relationships derived from experiments. At the smaller, process scale the direct forces acting on particles or sets of particles have been simulated using computational fluid dynamics (CFD) (Zhang, 2017; Jeremy et al., 2020) or Lattice Boltzmann methods (Trunk et al., 2021). While those approaches are computationally expensive they can account for arbitrary particle shapes and properties and provide valuable mechanistic insights into the dominant factors controlling particle settling. In turn they can also be used to validate and refine semi-empirical relationships from experiments. Following this argument, the main objective of this study is to systematically evaluate different factors, such as particle density, size (or volume) and shape, water temperature, and initial orientation of the particle, which control the settling behavior and in turn the TSV of MP particles. We further hypothesize that the hydrophobicity of the surfaces of pristine MP particles will significantly affect their settling behavior and TSV. Along those lines we quantify TSV of MP particle using CFD simulations of a large set of individual particles representing the following seven different polymers: Polystyrene (PS), Polyamide 66 (PA66), Polycaprolacton (PCL), Polylactic acid (PLA), Poly (L-lactic) acid (PLLA), Polybutylenadipate terephthalate (PBAT), Polyvinyl chloride (PVC), which are commonly found in the lake environment

(Webb et al., 2013; Wright et al., 2013; Rocha-Santos and Duarte, 2015) over a range of shapes, densities and sizes. First we verify our simulation approach against a set of laboratory experiments using physical conditions and particle parameters in our simulations, which are identical to those from the laboratory experiments of (Elagami et al., 2022). We then compare our simulation results to existing semi-empirical relationships developed for estimating the TSV of mineral (Dietrich, 1982) and MP particles (Waldschläger and Schüttrumpf, 2019) before conducting a systematic, model-based evaluation of the key parameters controlling TSV and their relative importance.

2 METHODS

Three methods were used to investigate the TSV of MP particles i) numerical simulations, ii) laboratory settling experiments, iii) semi-empirical settling relationships. For our analyses we used two general classes of particles in terms of their shapes: a) regular spherical particles and b) irregular particles with arbitrary shapes. Additionally we generated a set of virtual, axis-symmetrical (regular) particles derived from revolved polygons (see **Section 2.4.1**) for a systematic evaluation of the effects of particle roundness, which were only evaluated with the CFD model. The irregular MP particles were selected from larger sets of particles made from seven abundant polymers (PS, PA66, PCL, PLLA, PLA, PBAT, and PVC). These MP particles can be categorized into biodegradable (PCL, PLA and PLLA) versus non-biodegradable (PS, PA66, PBAT, PVC) polymers. Their size and density ranged from 500 to 2,200 μm and 1.03 to 1.38 kgm^{-3} , respectively (cf. **Supplementary Material S1, Supplementary Table S1**). All biodegradable and non-biodegradable particles were provided by the Department of Macromolecular Chemistry at the University of Bayreuth, Germany. MP particles with sizes smaller than 500 μm were intentionally not considered as the simulation of their settling would require very fine numerical meshes in the simulations and excessive numerical costs, in particular if many particles are to be simulated. Furthermore the settling of very small particles will increasingly be affected by their electro-chemical surface properties and less by their physical shapes and properties (Zhang et al., 2017), so that other tools and methods would be required for an assessment of their settling. The same holds true for very specific shapes like fibers (Wei et al., 2021). Our study specifically focuses on particle settling in standing freshwater (e.g., freshwater lakes), which is in line with the experimental data available for verification. However, it is generally possible to also apply our methodology to other environments such as saltwater lakes, simply by changing the properties of the water in the model. Numerical simulations form the core of this work, while the experiments and semi-empirical relationships are used to provide a reference for the simulations. In the following the three different methods are described in more detail.

2.1 Model Setup and Boundary Conditions

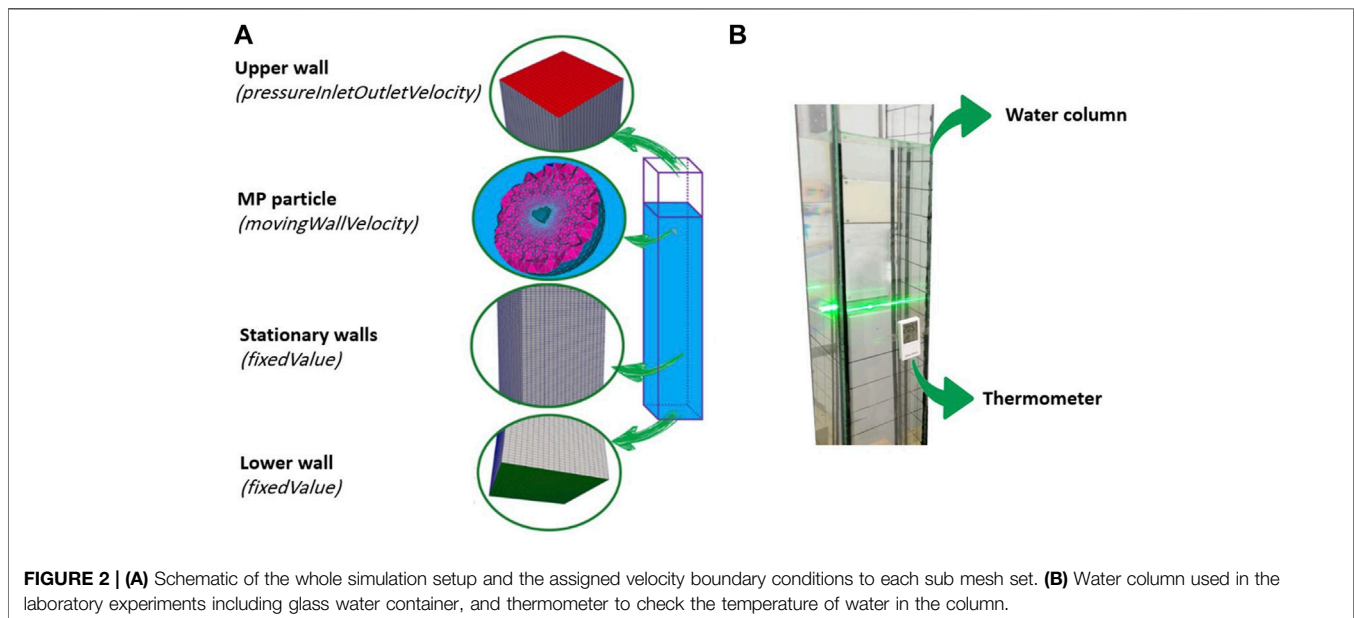
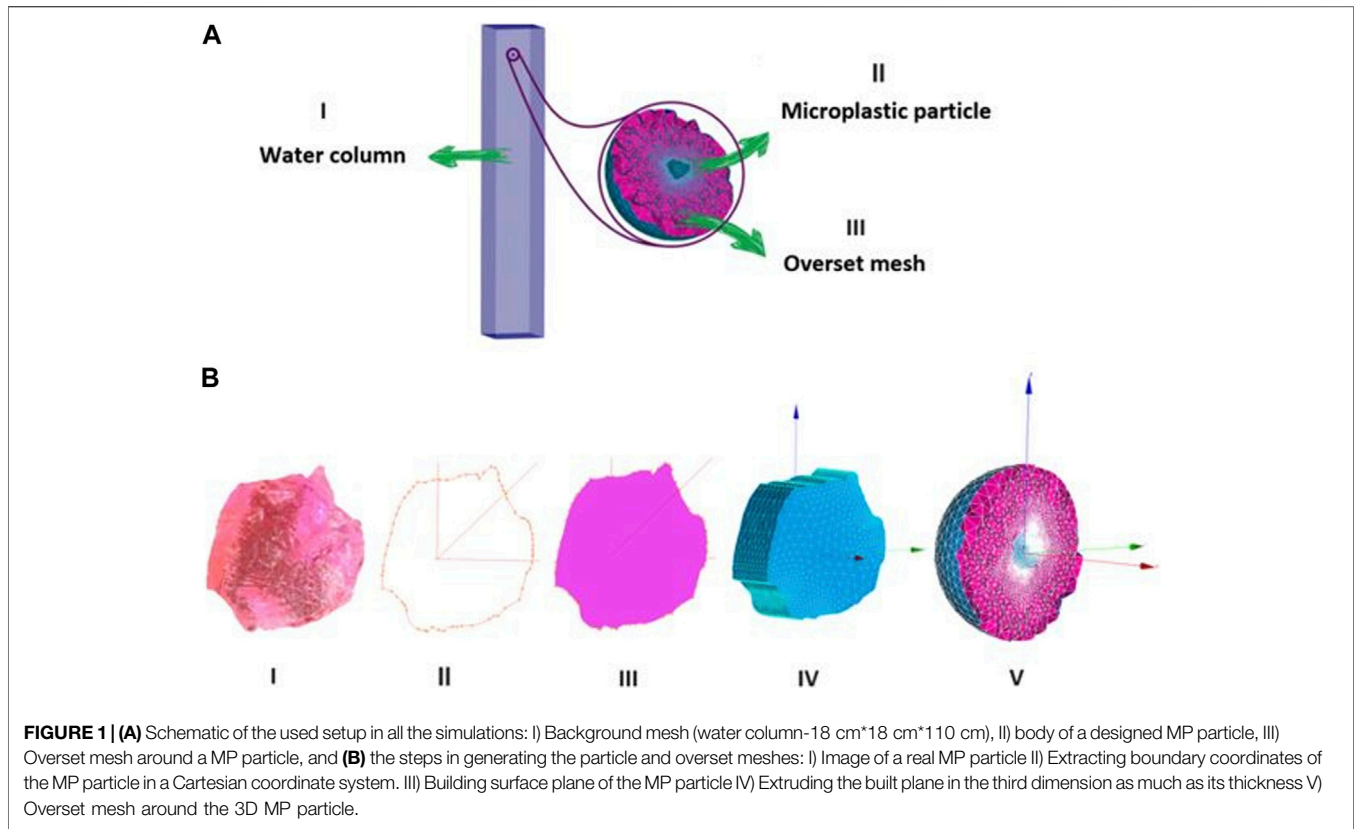
To simulate the TSV of MP particles, we use the solver `overInterDyMFoam` out of the open source C++ toolbox

`OpenFOAM v1812` (Weller et al., 1998). The used solver is for two incompressible, immiscible fluids (water and air in this application), which employs the volume-of-fluid method to capture the water-air interface. It solves the Navier-Stokes equations and supports moving meshes using the overset method. In the present study, we employed the overset method (also known as Chimera framework (Houzeaux et al., 2014)), as it allows to simulate MP settling in a deep-water column without the need for any mesh deformation.

The general simulation setup consists of two mesh domains for i) the water column (background mesh) and ii) the particle and its close surroundings (overset mesh) as shown in **Figure 1A**. As the two mesh sets are disconnected, the approach allows for a large freedom in movement (6 DOF) of the simulated object, especially compared to traditional approaches which employ mesh morphing/deformation. While the background mesh remains stationary, the overset mesh can move according to the calculated forces on the enclosed object. During each time step, the cells covered by the overset mesh are removed from the background mesh (cell type “hole”). The results are exchanged/interpolated at the boundary between the background and overset mesh using specific patch types. As the overset mesh is moving, the holes and interfacial patch cells are re-defined for each time step based on the current position of the overset mesh.

Figure 1B illustrates the design steps taken to mesh the arbitrarily shaped MP particle based on images taken from the particles in the laboratory experiments and how the overset mesh encloses the particle's body. The SALOME 9.4 (Ribes and Caremoli, 2007) software was used to generate the numerical meshes for all simulation setups. The software ParaView (Ahrens et al., 2005) was used for visualization of the conducted simulations.

Figure 2A illustrates the general setup of the simulations representing the water column dimensions and the boundary conditions in the experiments (see **Section 2.2** for more details). To implement the same condition as in the experiments, in all of the performed simulations $1 \text{ mm}^2 \text{ s}^{-1}$ and 0.9982 gcm^{-3} were considered as water kinematic viscosity and density at 20°C respectively. Moreover, the velocity boundary condition of “pressureInletOutletVelocity” was set to keep the upper side of the column open and in contact with air. In turn an air/water interfacial tension of “sigma: 0.007 kgs^{-2} ” was set for all simulations. The outer surface of the MP particle which is settling in the water (a viscous fluid), is surrounded by stationary walls of the column. Hence, to represent the velocity boundary conditions accordingly, the boundary types “movingWallVelocity” and “fixedValue” in OpenFOAM were used for the walls of the MP particle and water column, respectively. More details concerning the applied initial and boundary conditions for pressure, phase saturation and velocity have been provided in **Supplementary Table S2**. Quantities such as particle volume, mass, center of mass (COM), location, and moment of inertia (MOI) (cf. **Supplementary Material S3**), are important input parameters for the OpenFOAM solver and had to be accurately calculated beforehand.



2.2 Experiment Setup and Data

We used TSVs measured in the laboratory for a set of spherical and irregularly shaped MP particles (Elagami et al., 2022) for comparison with the CFD results. Besides that, we carried out an additional set of experiments to test our hypothesis, that the

hydrophobicity of MP particles will affect their TSV. Settling experiments were first run for pristine, untreated PLA and PS particles in the size range from 1 to 2 mm and then repeated after the particles had been treated by immersion in a surfactant (Tween-20) for 2 hours. All the experiments were conducted

using the same experimental setup as in (Elagami et al., 2022) consisting of a water column with the dimensions of 18 cm*18 cm*110 cm and a Particle Image Velocimetry (PIV) system to measure the settling velocity (**Figure 2B**). The 2D-PIV system (iLA 5,150) consists of a LED light sheet with 530 nm wave length as light source, a 40 fps high speed camera to track MP velocities during settlement, and also the hardware to synchronize the image acquisition frequency with the light source. The air conditioned laboratory and the water temperature were kept constant at 20°C and two thermometers were used to record the temperature of water during the experiments.

2.3 Comparison of Simulations to Semi-Empirical Relationships and Experimental Data

Comparison of the model with results from experiments and semi-empirical relationships was carried out in two steps: First, simulations of 120 irregular MP particles made of the polymers PS, PA66, PCL, PLLA, PLA, and PBAT from the experiments in (Elagami et al., 2022) were conducted to quantify their TSV and the findings were compared to the TSVs measured in the laboratory experiments. Images of some of these MP particles and the associated “model designed” particles for the numerical mesh in the simulations are illustrated in **Supplementary Table S3** (cf. **Supplementary Material S4**) as an example. In the second step, simulated TSVs were compared to TSVs estimated based on two existing semi-empirical relationships between TSV and particle characteristics, namely i) the relationship originally proposed by Dietrich (1982), Dietrich, (1982) for mineral particles, which has been shown to return acceptable TSVs for regular MP particles (Khatmullina and Isachenko, 2017; Kaiser et al., 2019), and ii) the relationship formulated by Waldschläger et al. (2019) (Waldschläger and Schüttrumpf, 2019) for a broad size and shape range of MP particles. TSV of spherical particles with ten different sizes (0.5, 0.6, 0.75, 1, 1.25, 1.5, 1.75, 2, 2.25, and 2.5 mm) were simulated for each polymer with densities of 1.03 (PS), 1.12 (PA66), 1.14(PCL), 1.20(PLLA), and 1.38 gcm⁻³(PVC), and then the simulation results were compared to the TSV results of the same particles returned by the two semi-empirical relationships.

2.4 Evaluating the Influence of Physical Parameters on TSV of MP Particles

After confirming adequate performance of the model in the previous stage, the impact of particle roundness, size and density as well as water temperature on TSV were systematically evaluated to assess the sensitivity of the TSV of MP particles to the variation of each of the these physical parameters.

2.4.1 Effects of Shape Characteristics

To systematically investigate the effect of different levels of roundness on TSV we used regular polygons (**Figure 3B**). Increasing the number N of sides of a regular polygon, yields

polygons with a growing number of sides of shorter length and more internal angles, which evolve towards a perfect circle when N approaches infinity. Revolving such regular polygons with identical areas around one of their symmetry axes, produces 3D shapes with equal volumes (**Figure 3A**). This procedure was followed to produce five series of regular polygons with the same areas of their 2D projections as circles with diameters of 0.5, 1, 1.5, 2, and 2.5 mm (cf. **Supplementary Material S5**, **Supplementary Figure S2**) to generate a set of “virtual particles” with increasing levels of roundness but the same volumes for a model-based assessment of the effects of roundness on TSV. To reduce the computational costs, simulations were only carried out for virtual particles with a density of 1.38 gcm⁻³ (PVC), to show the general trend of the impact of roundness on the TSV of MP particles.

The level of roundness of the irregular MP particles used in our study was classified based on the Powers scale of roundness and the Corey Shape Factor (CSF), both of which are metrics having commonly been used in other studies (Dietrich, 1982; Khatmullina and Isachenko, 2017; Kaiser et al., 2019; Waldschläger and Schüttrumpf, 2019). The Powers scale of roundness is a measure, which defines particle roundness on a scale from 1 (very angular) to 6 (well rounded) based on the average of two assessments by independent observers using a graphical chart for comparison (Powers, 1953). The CSF is a measure of the flatness of a particle and is determined based on the lengths of its shortest, intermediate and longest perpendicular axes (Corey, 1949).

The surface area to volume ratio (SA:V) is also an important physical characteristic of MP particles, derived from their shape. It determines how drag forces are exerted on a MP particle and how these forces are distributed across its surface. The larger the SA:V, the more friction forces relative to gravitational forces will be exerted on the particle and consequently the less TSV the particle will have and vice versa. The SA:V was determined based on calculations of the particle surface area and volume from the numerical mesh for all regular and irregular MP particles.

2.4.2 Impact of Particle Density and Volume

First we selected a distinct set of polygon-shaped particles from the analysis of roundness and systematically increased their densities and sizes. These peculiar shapes of the particles were intentionally chosen to be able to simultaneously evaluate the relative influence of evolving particle roundness versus the effects of increasing particles size and density. To this end, the polygons with areas identical to a sphere with 1 mm diameter and the density of $\rho_{PVC} = 1.1 \text{ gcm}^{-3}$ were selected for the analysis. By choosing this initial size, the new set of virtual particles with increased sizes approximately stays within the size range of the MP definition. To examine the size effects, generated particles corresponding to the polygons with 5, 6, 7, 8, and 12 sides as well as a sphere were chosen and their volume enlarged by 10, 20, 50, and 100%. Similarly, the same percentages were used to increase the density of the original particles, which means that the initial density of $\rho_{PVC} = 1.1 \text{ gcm}^{-3}$ was increased by 10, 20, 50, and 100% to yield particle densities of 1.21, 1.32, 1.65, and 2.2 gcm⁻³ respectively. The highest density obtained using this procedure

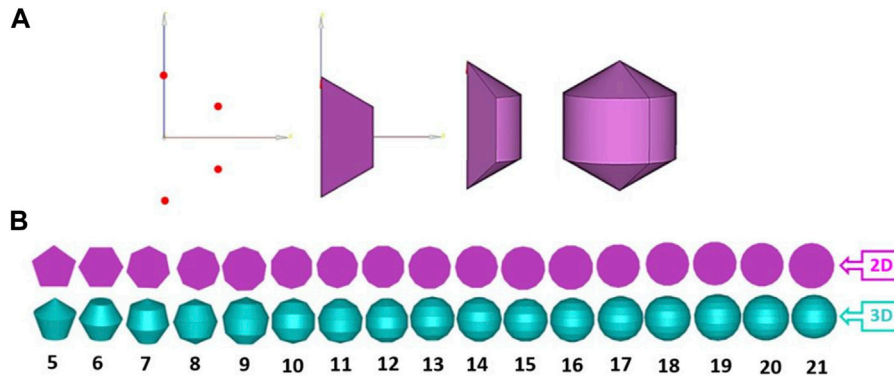


FIGURE 3 | (A) The steps of generating a 3D regular hexagon. In the first step one half of a regular polygon is defined based on the coordinates of its vertices. This half-polygon is then rotated around one of its symmetry axes to form a 3D, regular, axis-symmetric particle; **(B)** 2D regular polygons and their corresponding 3D regular particles (for side numbers ranging from 5 to 21).

is only found in very heavy polymers (e.g., polytetrafluoroethylene ($2.1\text{--}2.3\text{ gcm}^{-3}$) (Chubarenko et al., 2016)), which may be found less frequently in the environment. However, for the purpose of a systematic evaluation of density effects this was assumed to be acceptable.

In addition 10 irregular MP particles (from the particles used in **Section 2.2**) with an equivalent diameter range from 1 to 2 mm, a Powers scale of roundness (Powers, 1953) of 4 and a Corey Shape Factor (CSF), (Corey, 1949), ranging from 0.7 to 0.85, were selected as model particles to investigate the impact of an increase in size and density on TSVs. The initial density of the particles was assumed to be 1.1 gcm^{-3} , and similar scenarios with respect to increasing volume and density as performed for regular particles were repeated for the irregular ones as well.

2.4.3 Temperature

Vertical temperature gradients and the associated changes in water density result in a thermal stratification of lakes during summer with the formation of an epilimnion, metalimnion, and hypolimnion (Hersch, 2012; Singh et al., 2019). The vertical temperature variations lead to changes in the kinematic viscosity of the water and the resulting TSV of the particles as the move from the relatively warm epilimnion, via the metalimnion to the colder hypolimnion (Gorham and Boyce, 1989; Singh et al., 2019). These changes in TSV will affect the residence times of MP particles in the different compartments of a stratified lake system. To quantify the effects of temperature changes on TSV in the different compartments, TSVs were simulated for the different temperature regimes. In temperate climates water temperatures in the three main compartments typically range from 18 to 24°C , $18\text{--}7.5^\circ\text{C}$, and $7.5\text{--}4^\circ\text{C}$ in the epilimnion, metalimnion, and hypolimnion, respectively (Boehrer and Schultze, 2008). TSVs for 30 randomly selected irregular PVC particles (from the set of particles used in **Section 2.3**) were simulated for temperatures of 20, 10 and 4°C as characteristic temperatures for the epilimnion, metalimnion and hypolimnion respectively. The densities and kinematic viscosities of water at 10 and 4°C are 0.9997 gcm^{-3} , $1.3063\text{ mm}^2\text{s}^{-1}$ and 1 gcm^{-3} , $1.5674\text{ mm}^2\text{s}^{-1}$, respectively (Wagner and Kretzschmar, 2008).

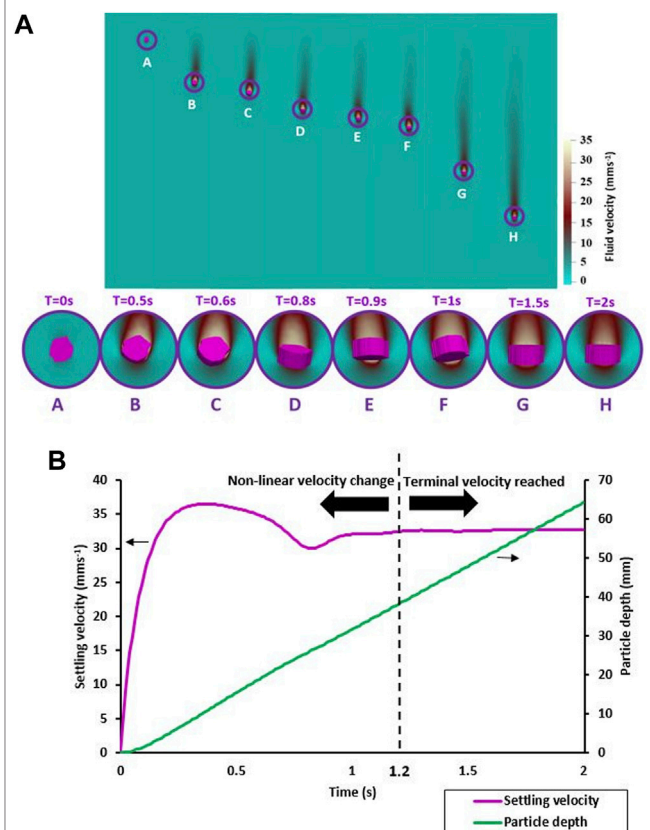


FIGURE 4 | (A) The fluid velocity field around one of the 120 irregular MP particles at different point in time. Insets A to F show stages of the transient phase of settling, while insets G and H depict the phase after the TSV has been reached. Initial water velocity is zero and once the particle starts settling, the fluid velocity field around the particle shows changes in water velocity, while the velocity of the water in immediate contact with the particle reflects the settling velocity of the particle itself. **(B)** Velocity and particle location.

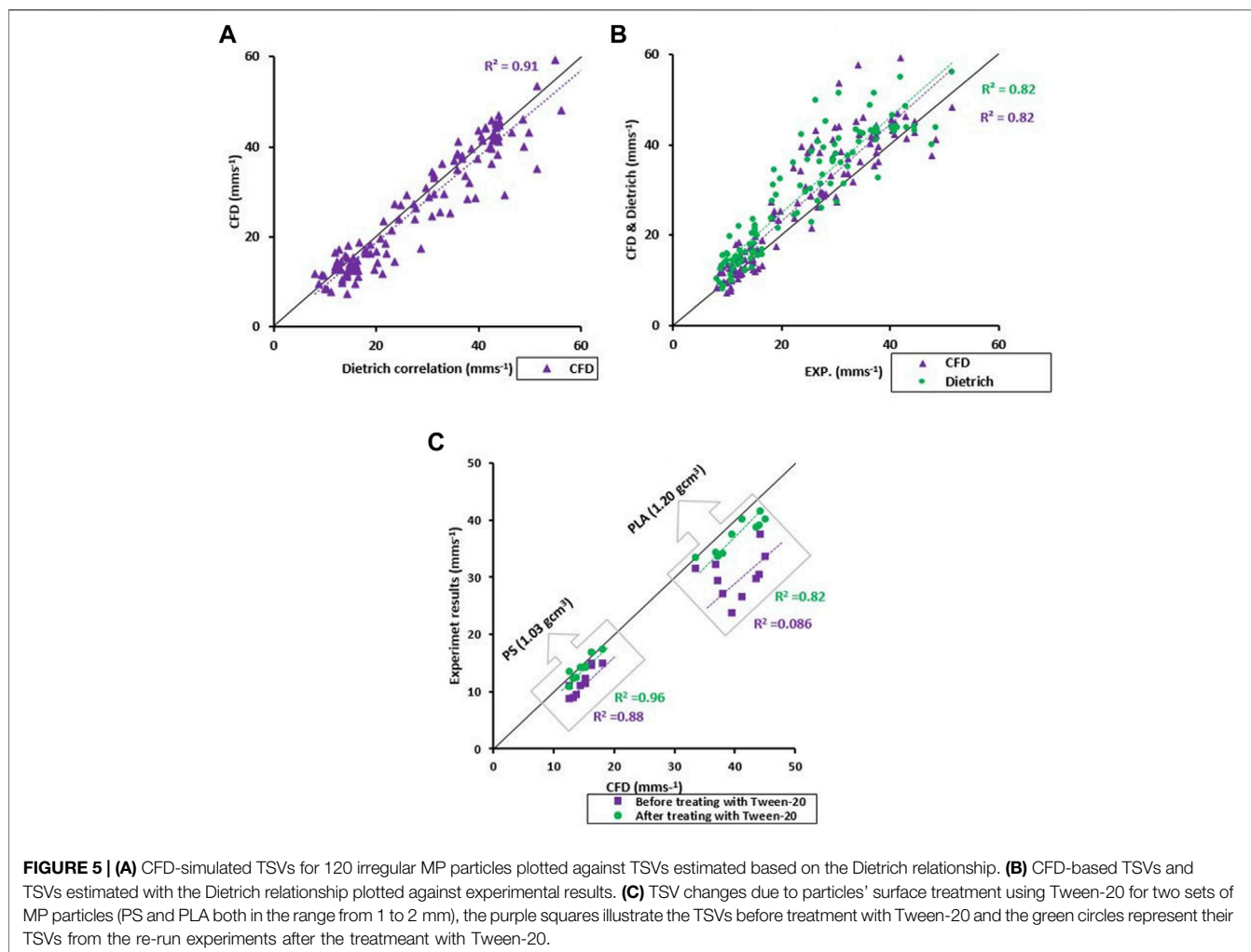


FIGURE 5 | (A) CFD-simulated TSVs for 120 irregular MP particles plotted against TSVs estimated based on the Dietrich relationship. **(B)** CFD-based TSVs and TSVs estimated with the Dietrich relationship plotted against experimental results. **(C)** TSV changes due to particles' surface treatment using Tween-20 for two sets of MP particles (PS and PLA both in the range from 1 to 2 mm), the purple squares illustrate the TSVs before treatment with Tween-20 and the green circles represent their TSVs from the re-run experiments after the treatment with Tween-20.

3 RESULTS

3.1 CFD Results for Irregular MP Particles Compared to Experimental Results and the Dietrich Relationship

The settling process for one of the 120 simulated irregular MP particles is illustrated in **Figure 4A**. In the initial phase of the settling the particle velocity dynamically changes as the particle shows secondary movements such as rotations and tumbling (**Figure 4B** at $t = 1.2$ s and **Figure 4A**, in-set A-F) before the particle reaches a stable orientation in the fluid with a constant settling velocity at $t = 1.2$ s. This initial, dynamic phase lasted around one second for all simulated particles. The second phase was characterized by a stable particle orientation (**Figure 4A**, G and H) and constant settling velocities for most particles. Some particles, however, showed small harmonic oscillations in their continuing downward movement, but with a constant average TSV.

Simulated TSVs of 120 individual MP particles are plotted against the TSVs estimated by the Dietrich relationship in

Figure 5A. CFD results are scattered along the 1:1 line with a slope of 0.95 and a coefficient of determination (R^2) of 0.91. In **Figure 5B** TSVs simulated with CFD as well as TSVs from the Dietrich semi-empirical relationship are plotted against TSVs from the settling experiments. TSVs from CFD simulations as well as estimates based on the Dietrich relationship overestimate TSVs compared to the settling experiments. The coefficients of determination still showed relatively high values at 0.82 for both correlations and both trend lines have roughly the same slope of about 1.059. The strongest deviations were found for the biodegradable polymers (i.e., PCL, PLA and PLLA). However, a deviation was observed for PS, as a non-biodegradable polymer, as well. For PLA and PS particles an additional set of settling experiments were performed, initially with pristine untreated particles and subsequently with particles being treated with a surfactant to assess the effects of hydrophobicity on the TSV. Results of these additional experiments are plotted in **Figure 5C**. While the untreated particles show significantly slower experimental TSVs compared to the TSVs obtained from the CFD model, this deviation between simulated and experimental TSVs is practically removed for the treated particles. The R^2 improved from $R^2 = 0.88$ to $R^2 = 0.96$ and from $R^2 = 0.086$ to $R^2 =$

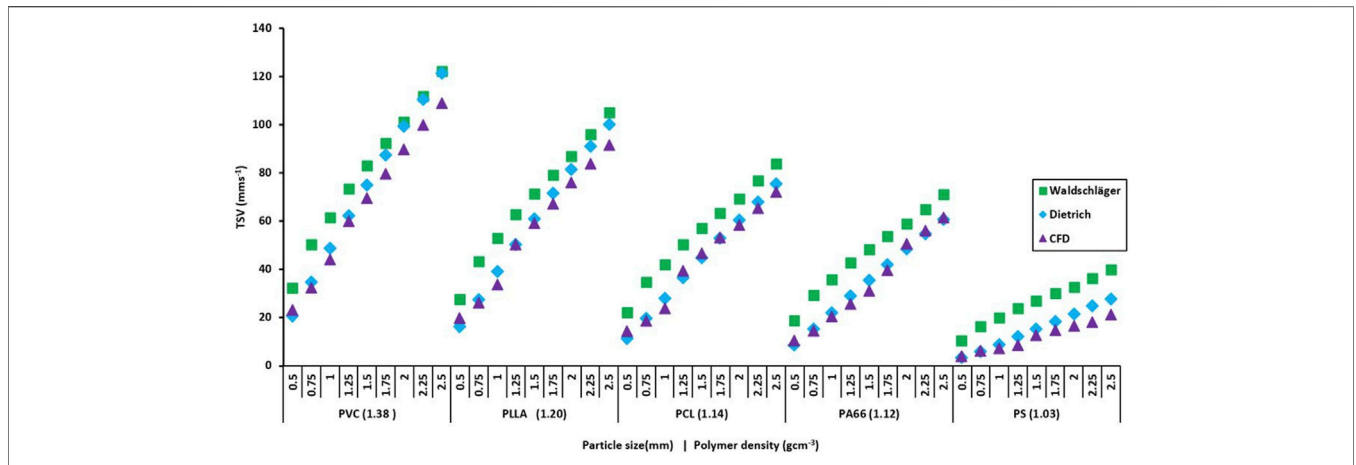


FIGURE 6 | Comparison of the CFD-simulated TSVs and the TSVs estimated using the Dietrich and Waldschläger empirical relationships. The diameters of the spheres and the polymer types (and their densities in brackets) are shown on the x-axis.

0.82 between the untreated and treated particles for the PS- and PLA-particles respectively (Figure 5C).

3.2 Evaluation of CFD Results for Spherical MP Particles Against the Semi-Empirical Relationships

In Figure 6 the CFD-simulated TSVs are plotted against particle size and density for a set of spherical particles. For comparison the TSVs estimated based on the (Waldschläger and Schüttrumpf, 2019) and (Dietrich, 1982) relationships are plotted for the same particles. For all polymers TSVs increased quasi-linearly with particle diameter. However, the slope of the quasi-linear relationship decreased with declining polymer density (density declines from left to right in Figure 6).

Overall the TSVs simulated with CFD are quite well matched by the values estimated from the Dietrich equation ($R^2 > 0.98$). This is especially the case for the smallest diameters (0.5 and 0.75 mm), for which the simulated and estimated TSVs match very closely for all polymer types and densities. For larger diameters the match slightly deteriorates. In contrast, the TSVs predicted by the Waldschläger relationship are systematically biased towards higher TSV values for all particle sizes and diameters. This bias gets slightly smaller with increasing particle size and density.

3.3 Systematic Investigation of the Relative Importance of Different Parameters on TSV

3.3.1 Roundness

Increasing the degree of roundness of the virtual particles from $N = 5$ to 9 causes a linear increase in TSVs for all the examined particle sizes (Figure 7A). Linear regressions between the degree of roundness (N) and the TSV yield coefficients of determination (R^2) larger than 0.97 for all particles. The slope of the linear regressions steadily grows from the smallest (0.5 mm) to the largest (2.5 mm) particle diameter.

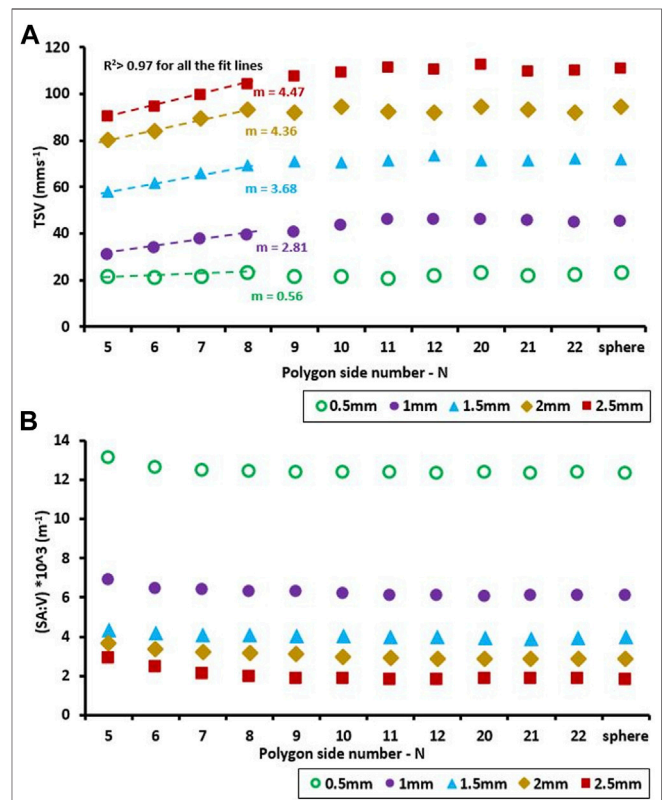
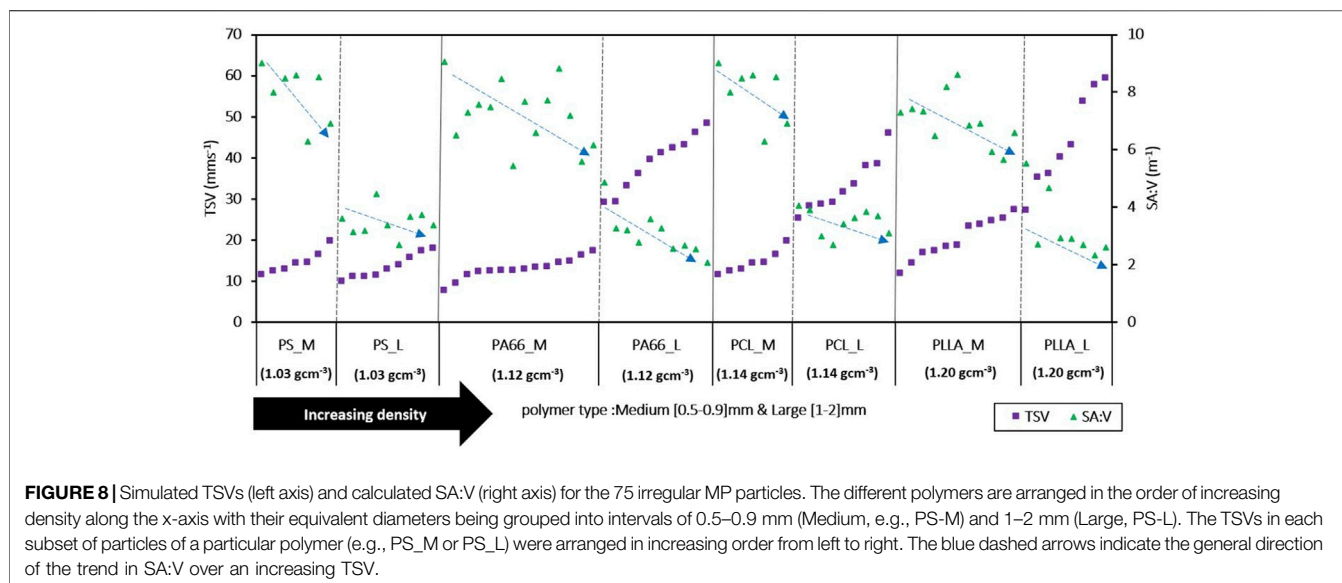


FIGURE 7 | (A) Effects of increasing roundness on TSV of MP particles for five different particle sizes. The different symbols depict the different diameters of the equivalent perfect spheres, which have the same volumes as the respective virtual particles derived from the polygons. Particles in all simulations have a density of 1.38 g cm^{-3} . (B) calculated SA:V for particles corresponding to the particles of panel A.

Comparing the changes in SA:V for increasing side numbers (Figure 7B) with the corresponding changes in TSVs (Figure 7A), shows that for a given particle diameter a



decreasing SA:V is associated with an increase in TSV. However, for all the investigated particle diameters a threshold in N emerges at the value of 8, beyond which a further increase in N does not yield further increases in TSV. Beyond this threshold changes in SA:V with increasing N become minimal and in turn show little to no effect on the simulated TSVs. In this range TSV stays quasi-constant only showing minimal, non-systematic variations (**Figure 7A**, $N > 8$). Since the magnitudes of TSV and SA:V for $N > 8$ were very similar, we removed the data for $13 \leq N \leq 19$ to improve the readability of the figure.

3.3.2 Surface Area to Volume Ratio–Particles With Irregular Shapes

The general relationship between SA:V and TSV, was also evaluated for all the 75 irregular MP particles used in the simulations in **Section 3.1** (**Figure 8**). Sorting the TSVs in ascending order for each type of polymer depicted descending trends for SA:V ratios (dashed blue arrows in **Figure 8**). This inverse relationship indicates that lower SA:V generally facilitate faster TSVs. However, this trend shows significant scatter, in particular for the lighter polymers such as PS. Spearman rank correlations between the SA:V and TSV for each of the polymer classes yielded values ranging from 0.31 to 0.9, indicating only mild correlations between the two variables. In contrast spearman rank correlations between the particle volumes and TSV showed generally higher values ranging from 0.58 to 0.99, indicating that variability in TSV for the irregular particles investigated here is predominantly driven by variability in particle volume (i.e., weight), while the effect of variability in the SA:V is secondary.

3.3.3 Effects of Increasing Particle Size and Density on TSV

3.3.3.1 MP Particles With Regular Shapes

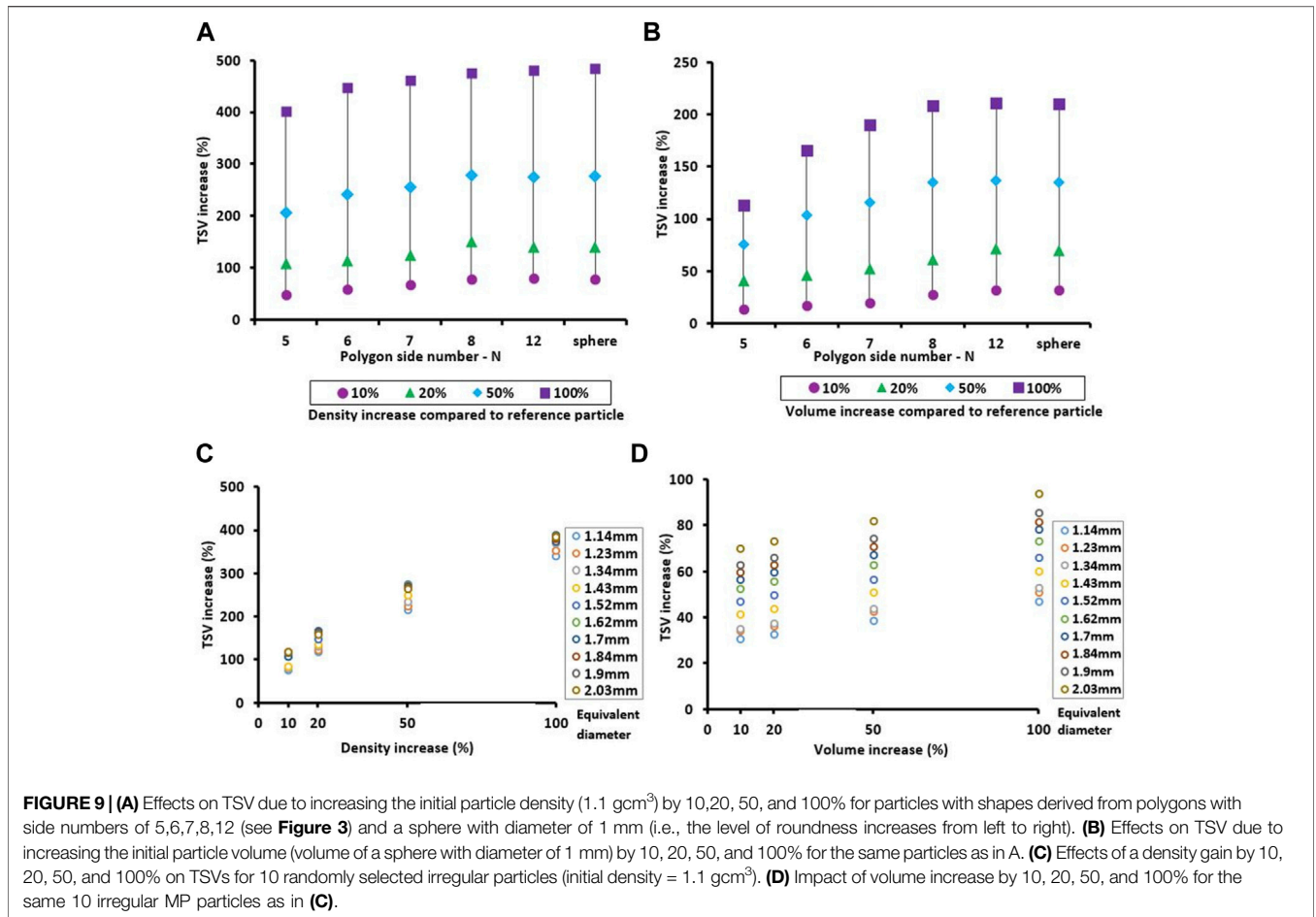
Effects of density and size (volume) on the TSV of the MP particles are depicted in **Figure 9**. For a 10% increase in density

the TSV increases from 48% for the least rounded particle ($N = 5$) to 78% for a perfect sphere with a gradual increase with the degree of roundness. For density increases of 20, 50 and 100% the associated increases in TSV range between 107 and 139%, 206 and 275% and 401 and 483% respectively. The largest effects on TSV by increasing density can generally be seen for a perfect sphere, which has the smallest SA:V. Doubling the density of a sphere increases the associated TSV by approximately 50% compared to a respective particle derived from a polygon with five sides.

Plotting the increases in TSV for the same particles used in **Figure 9A** over the same percent increases in volume (**Figure 9B**) reveals similar patterns as for the increases in density, but at significantly lower magnitude. Increases in TSV for the least rounded particles ($N = 5$) ranged from 13 to 112% when and from 32 to 223% for a perfect sphere ($N = \infty$). Similar to the effects of increasing density the largest effect on TSV can be seen for particles approaching the shape of a sphere ($N > 8$).

3.3.3.2 MP Particles With Irregular Shapes

The effect of increasing the density of the irregular MP particles on their TSVs was generally quite similar to that observed for the regular particles (**Figure 9C**). For example, doubling the density of these particles led to an increase in TSV of up to five times, only slightly less than the maximum increase for the regular particles. However, the effect of increasing volume on TSV for the irregular MP particles deviated in magnitude from that of particles with regular shapes. While doubling the volume of the regular particles with a high level of roundness (e.g. $N > 8$) led to TSV increases of 200% (**Figure 9B**), the irregular particles only reached maximum TSV increases around 90% (**Figure 9C**). However, the regular particles with the least degree of roundness ($N = 5$) generally showed significantly smaller TSV increases ($<120\%$), which are more in the range observed for the irregular particles. Interestingly, the clear sorting of the volume related TSV-increases for the irregular particles by their equivalent

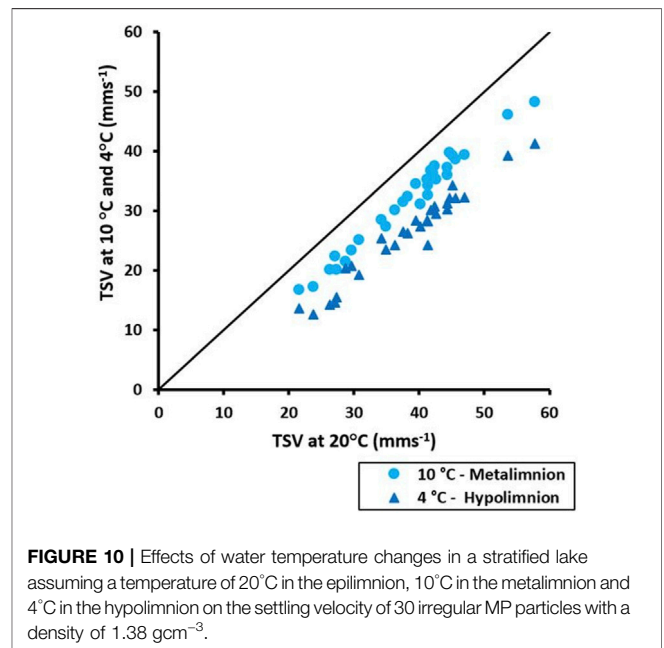


diameter (**Figure 9D**) was not seen for the effects of density-increases (**Figure 9C**). This indicates that changes in surface drag due to the increase in surface area resulting from the volume-increase is directly related to the particle’s equivalent diameter, while the equivalent diameter does not directly affect TSV changes due to an increase in density.

Calculating the coefficients of determination for the correlation between simulated TSVs, and the corresponding particles volumes and densities yielded values of $R^2 > 0.90$, and $R^2 > 0.94$, respectively. This implies that variations in particle TSV can be largely explained by variations in particle density and volume and that shape characteristics of the investigated particles play less of a role in determining the settling velocity.

3.3.4 Effects of Water Temperature on TSV

The TSVs in the epilimnion with an assumed reference temperature of 20°C are plotted against the TSVs in the metalimnion, with an assumed temperature of 10°C (light blue circles), and the hypolimnion with an assumed temperature of 4°C (dark blue triangles) for 30 MP particles (**Figure 10**). The average decrease in TSVs resulting from the temperature drop between the epilimnion and the hypolimnion is 32%. The largest temperature effects on TSVs can be seen for the smallest particles



[equivalent diameter (cf. **Supplementary Material S4**, Eq. 5) from 0.57 to ~1 mm], with a drop in TSVs from 32 to 46% compared to the reference temperature of 20°C.

4 DISCUSSION

4.1 CFD-Based Assessment of the Initial Settling Process

Although the main purpose of our simulations was to quantify the TSVs of MP particles, which defines their overall settling times in lentic water bodies such as lakes (Lambert and Wagner, 2018), the transient CFD simulations also allow to evaluate the dynamic initial behavior during settling. The settling of all particles, with regular or irregular shape, showed two distinct phases during the initial settling period. The first phase represents the time period before the particle reaches the TSV. In this phase the irregular particles often show dynamic movements including rotations and tumbling with dynamical changes in settling velocities before they finally reach a stable settling position at the TSV. This marks the beginning of the second phase, in which the particles settle with a quasi-steady TSV. However, even after a steady TSV is reached, gentle secondary particle movements are possible depending on the particle's shape. The specific time to reach the TSV needs to be considered in experimental setups (Khatmullina and Isachenko, 2017; Waldschlager and Schuttrumpf, 2019) to ensure that velocity measurements are done at a point where the forces exerted on the particle are balanced and the TSV has truly been reached. In our simulations, the initial phase of settling with transient velocities only lasted for a fraction of a second (usually $t < 0.5$ s) for symmetric particles such as spheres. In contrast for asymmetric particles with different roundness levels and stronger secondary movements, this phase could last up to one second (more details on the behavior of MP particles before reaching TSV, cf. **Supplementary Material S6**). The beginning of phase two is marked by the point when the particles reach their stable settling position at a steady TSV. However, some particles showed small oscillating secondary movements with very small harmonic velocity fluctuations around a steady average TSV during this phase. These oscillating, rotating, and tumbling secondary movements have also been reported from experimental work in the laboratory (Khatmullina and Isachenko, 2017; Waldschlager and Schuttrumpf, 2019). Given that the TSVs of the particles are reached very fast, the initial phase with transient velocities is negligible in terms of an assessment of the settling of particles in larger stagnant water bodies such as lakes.

4.2 Comparison of TSVs From CFD-Simulations, Semi-Empirical Relationships and Settling Experiments

The CFD model accounts for the exact particle shape and density and all the hydrodynamic forces that are exerted on the particle body. Therefore CFD simulations can be considered to reflect the true movement of a particle in water. As such CFD results can be used on the one hand to evaluate the accuracy of commonly used

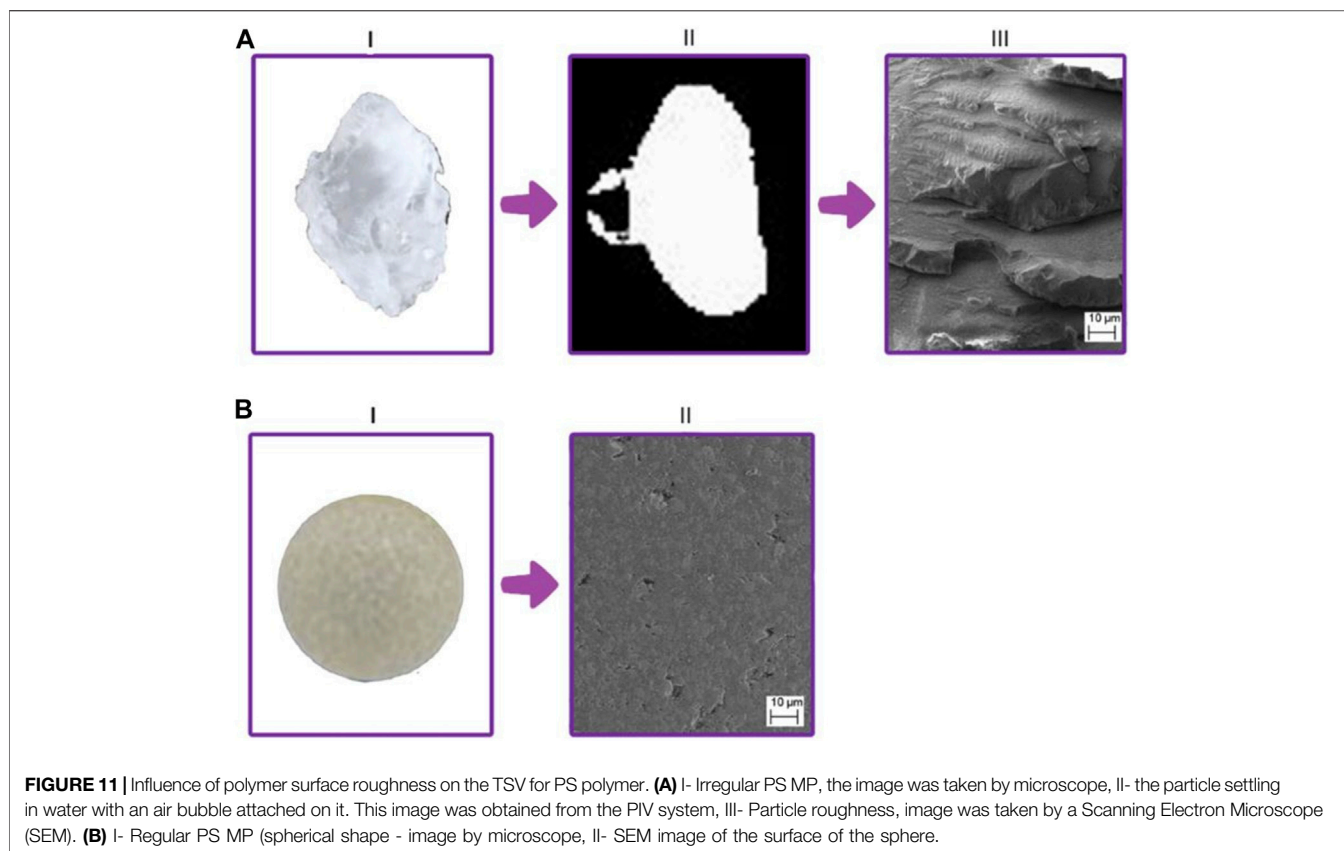
semi-empirical relationships, which make simplifications in the description of particles shapes, and on the other hand reveal additional non-hydrodynamic effects on particle TSVs by comparison with the results from settling experiments with the real MP particles of the same shapes and densities. In the following we will first briefly discuss the results from the spherical particles (**Section 3.2**) and then move to a more detailed discussion of the results from the irregular particles (**Section 3.1**).

4.2.1 Regular, Spherical Particles

For the spherical particles the CFD-simulated TSVs were generally better matched by estimates from the Dietrich relationship than by estimates obtained from the Waldschlager relationship (Waldschlager and Schuttrumpf, 2019) (**Figure 6**). The Dietrich relationship (Dietrich, 1982) had originally been developed for mineral particles of significantly higher densities (>2.2 gcm⁻³) than the polymers investigated in this study (<1.4 gcm⁻³). Surprisingly, however, it also yielded very reasonable TSV estimates for the much lower-density MP particles. This good agreement is likely due to the strong shape similarities between the mineral particles used to develop the Dietrich relationship (including smooth spheres, prolate ellipsoids, natural and crushed sediments (Dietrich, 1982)) and the MP particles we used in this study. In contrast the study by Waldschlager et al. (2019) (Waldschlager and Schuttrumpf, 2019) also included particles with significantly different shapes and also with lower densities and is in turn adapted to accommodate a broader range of particle characteristics. While we used very detailed descriptions of 3D particles shapes in our simulations, Waldschlager et al. (2019) only used the relatively coarse measures of the Powers scale of roundness and the CSF to describe particle shapes in their empirical relationships. These measures may not fully define all shape characteristics that affect the hydrodynamic forces acting on the particles during settling. This presumably explains the larger offset between the CFD-simulated TSVs and the TSV estimates based on the Waldschlager relationship.

4.2.2 Irregular Particles

Comparing the CFD-based TSVs with the TSVs obtained from the Dietrich semi-empirical relationship for the corresponding irregular MP particles yielded a strong correlation with an R^2 of 0.91 and a deviation of the slope of the regression line to the 1:1 line of only 5% (**Figure 5A**). This indicates that the Dietrich relationship generally provides a good estimate of the TSVs of the particles with their respective shapes and densities. The scatter of the data points along the 1:1 line we attribute to the fact that the Dietrich relationship uses only three principal dimensions of a particle (i.e., longest, intermediate, shortest perpendicular axes) to calculate the particle equivalent diameter and its relative flatness (CSF) (Dietrich, 1982), which does not allow to account for individual details in differences in particle shapes. Furthermore, the Powers scale of roundness, a measure used in the Dietrich relationship to define the roundness of a particle is an observational measure, which for well-rounded elliptical and



spherical particles with only small differences in their shapes will yield the same values.

Although the comparison between the CFD-simulated TSVs and the TSV estimates from the Dietrich semi-empirical relationship with the TSVs from the settling experiments overall showed a good agreement ($R^2 = 0.82$), simulated (CFD) and estimated (Dietrich relationship) TSVs were generally biased towards faster TSVs compared to the experimentally determined values (**Figure 5B**). The strongest deviations we observed for the biodegradable polymers (PLLA, PCL, PLA), however, also MP particles of PS, a non-biodegradable light polymer, showed a noticeable deviation. We suspect that the hydrophobicity of the particle surfaces may have been the reason for this deviation between simulated and observed TSVs (**Figure 5C**). Hydrophobicity is a common characteristic of the surfaces of most polymers typically found in waste (Al Harraq and Bharti, 2021) and can enhance the sorption of hydrophobic contaminants to MP particles (Kwon et al., 2017) leading to bioaccumulation of these contaminants (Ziccardi et al., 2016). It can also potentially lead to the adhesive attachment of air (Al Harraq and Bharti, 2021). The latter process will change the net density of the particles by adding an additional upward force, which will affect their movement in water. This phenomenon is in fact a commonly used method to separate MP particles from water filled sediments (Renner et al., 2020).

The fact that the treatment with the surfactant Tween-20 shifted the experimental TSVs of PLA and PS particles to the CFDs-simulated TSV values (**Figure 5C**), strongly suggests that the observed TSVs deviations are related to effects of surface hydrophobicity. This general interpretation is further corroborated by the observation of discrete, large air bubbles at surface irregularities on some of the particles during settling in PIV images (**Figure 11A-II**). We attribute the generally stronger deviation of the experimentally determined TSVs from the respective CFD-simulated TSVs for the biodegradable polymers to the fact that the surfaces of biodegradable polymers tend to have higher surface roughness to facilitate better degradation (Szewczyk et al., 2019; Moghadam and Tafreshi, 2020). Very small surface heterogeneities associated with those rougher surfaces (Al Harraq and Bharti, 2021) probably facilitate enhanced adhesive attachment of air at surface irregularities. Air-attachment, with potential effects on TSV, will also occur on the rough surface of non-biodegradable particles, but presumably to a lesser degree (**Figure 11A-III**). This could explain why we also observed a noticeable deviation of the experimental TSV from the respective CFD-estimate for the irregular particles made of PS (**Figure 5C**), a non-biodegradable polymer with a density (1.03 g cm^{-3}) very close to that of water. The low density of the PS particles makes them more susceptible to changes in TSV due to attached air than the non-biodegradable particles made of denser polymers, for which

no significant deviations between experiment and CFD had been observed.

The images of particles (taken by a light microscope, Zeiss Axioplan) and a high definition digital single lens reflex (DSLR) camera Canon EOS 5D)) and their surfaces in **Figure 11** generally illustrate the differences in the surface roughness of an irregular, non-biodegradable particle (**Figure 11A-I**) and a spherical non-biodegradable particle (**Figure 11B-I**) made from the same type of polymer (PS). The surface of the irregular particle shows larger irregularities and a generally rougher surface structure (**Figure 11A-III**) compared to the spherical particle with a relatively smooth surface (**Figure 5B-II**). The surface irregularities and the rougher surface of an irregular PS particle will better facilitate the attachment of larger air bubbles than the smoother surface of a respective spherical PS particle. This interpretation is further supported by earlier settling experiments using spherical particles with and without treatment with Tween-20, which had been conducted at the Limnological Research Station at Bayreuth University (personal communication, Hassan Elagami), which had practically shown no difference in the TSVs before and after treatment with Tween-20.

4.3 Roundness and SA:V Relationship and its Influence on TSVs of MP Particles

In previous studies the degree of roundness of a particle has commonly been considered as an important parameter for estimating the TSV of particles and it has usually been described by using the CSF and the Powers scale of roundness (Dietrich, 1982; Khatmullina and Isachenko, 2017; Waldschläger and Schüttrumpf, 2019). We examined the effect of roundness more systematically using exact 3D particle shapes obtained from revolving polygons with an increasing number of sides (see **Section 2.4.1** for more details). Increasing the level of roundness leads to a decrease in SA:V (**Figure 7B**) and thus less drag forces being exerted on the particles body resulting in a faster TSV. This general inverse relationship between SA:V and TSV can be observed for the regular, spherical particles (**Figure 7A**) as well as the irregular particles (**Figure 8**). However, it is more evident for the virtual, regular particles investigated here as they all have the same volumes and densities, isolating roundness and the associated SA:V as the only variable parameters (**Figure 7**). However, even for the irregular MP particles shown in **Figure 8**, which have variable volumes, the general descending trend in SA:V for increasing TSVs is clearly discernable.

The gradual increase of the slopes of the regression lines for increasing particle diameters (**Figure 7A**) suggests that the magnitude of the effect of increasing roundness on a particle's TSV increases with particle diameter. While the larger particles show significant increases in TSV over the initial increases in roundness, the smallest particles with a diameter of 0.5 mm practically do not show any significant change in TSV over the same increase in roundness. We attribute this to the drastic increase in SA:V when moving from particles with 1 mm diameter to the smallest particles with a diameter of

0.5 mm (**Figure 7B**). For these very small particles the SA:V is very high and in turn their TSV is driven more by the drag forces resulting from their large surface area relative to their volume than by additional hydrodynamic forces resulting from changes in their roundness.

4.4 Particle Density and Volume Effects on TSV

A comparison of the magnitudes of TSV increases associated with a density increase versus a volume increase for regular and irregular particles, respectively, showed a clear dominance of density over volume effects on TSV for the same percent increases in either parameter (**Figure 9**). By increasing the density of a MP particle, the only force that is amplified is weight, which will accelerate the downward movement of the particle. For the same percentage increase in volume in turn, the respective increase in weight and downward gravitational force is counteracted by additional upward forces resulting from an increase in drag due to the enlarged surface area and in the buoyancy of the particle, both attenuating the increase in TSV.

The relative increases in TSV in percent for the same percentage increases in density were very similar between the regular (**Figure 9A**) and irregular particles (**Figure 9C**) with values exceeding 400% for a doubling of the density. This was not the case for the same percentage increases in volume. While we observed TSV increases of up to 200% for the regular particles (**Figure 9B**) the irregular particles only showed TSV increases of less than 100% (**Figure 9D**). This illustrates the crucial role of shape irregularities in affecting the hydrodynamic forces (e.g., drag) acting on the irregular particles during settling and the resulting slow-down of their TSVs. Volume increases seem to amplify the effect of such irregularities causing a non-linear increase of the drag forces on the particles for increasing volumes. Interestingly for the irregular particles the ranking of their TSV increases relative to their equivalent particle diameter changed over the different increments in density gain (**Figure 9C**), while it stayed the same for volume increases. Likely the simultaneous increase in weight, drag and buoyancy associated with a volume increase maintains a certain balance in downward and upward forces acting on a particle of a specific shape. In contrast the more dramatic gains in weight due to the density increases seem to result in significant differences in the hydrodynamics forces (drag) that act on particles of different shapes and in turn counteract the gain in gravitational force.

4.5 Impact of Water Temperature on TSV

Our simulations on the effects of temperature on the TSV of MP particles (**Figure 10**) indicate that typical temperature differences between the compartments of a stratified lake in a temperate climate, will lead to significant differences in TSV (up to 46%). Differences in temperature and in turn density and kinematic viscosity of water in the different lake compartments have an influence on the drag forces exerted on the particles altering their TSVs. This temperature dependency of TSV can significantly affect the residence times of particles in the different lake compartments (Cole et al., 2016) and with that the exposure

time of organisms to the MP particles (Elagami et al., 2022). This implies that the seasonal temperature evolution in the different lake compartments needs to be considered when evaluating exposure. In addition to the temperature effect, however, other parameters such as water oxygen content, salinity, water pH and changes in food quality and availability have to be taken into account to assess the complex patterns of interactions between organisms and MP particles in the different lake compartments (Migwi et al., 2020; Hiltunen et al., 2021; Hoffschroer et al., 2021).

4.6 The Relative Importance of the Different Parameters Affecting Particle TSV

As highlighted by our analyses the TSV of MP particles in lakes and stagnant water bodies is affected by a range of different physical parameters such as density, volume, shape, surface roughness and hydrophobicity of the particles as well as the temperature and in turn density and viscosity of water. Evaluating the relative impact of these parameters on the TSV of MP particles quantitatively is challenging, as some of the parameters are coupled and their effects on TSV will overlap (Al Harraq and Bharti, 2021). Furthermore the settling of particles in the investigated size range (0.5–2.2 mm) is largely outside the true Stokes range of a laminar regime and hydrodynamic forces induced by turbulence will affect particle settling specifically for the larger particles. However, our rigorous, model-based evaluation of the hydrodynamic effects of the parameters listed above on particle TSVs, combined with respective laboratory settling experiments, including modifications to the particles' hydrophobicity, allowed a more systematic, qualitative assessment of the relative importance of the different parameters. In the following we will compare the relative change of TSV in percent over the parameter ranges evaluated in our analyses, which reflect the ranges typically observed for MP particles found in the environment.

Our analyses demonstrate the importance of particle density for controlling TSV. While an increase in particle density directly affects the gravitational force driving settling, it has no impact on the particle's volume and surface area, which would in turn change buoyancy and drag. A doubling of particle density led to TSV increases of up to 483 and 388% for regular and irregular particles respectively. In contrast, TSV increases of only 224% for the regular and 93% for the irregular particles could be realized for a doubling of particle volume. We attribute the significantly smaller TSV increase for the irregular particles to effects of the enlarged surface irregularities on drag and turbulence at the particle-water interface slowing down the settling velocity. The attachment of air on the surfaces of some of the biodegradable MP particles led to a reduction of the TSV by up to 58%, followed by relatively similar maximum changes in TSV of 47 and 45% due changes in water temperature and particle roundness respectively. Changes in particle roundness only significantly affected the TSVs of particles larger than 1 mm in diameter, while the smallest particles (0.5 mm diameter) were unaffected and their TSVs seemed to be controlled by their large SA:V. While

the effects of water temperature and particle roundness similarly affected particles of all shapes and polymer types, effects of air attachment were most pronounced for particles with significant shape irregularities and rough surfaces (mainly the biodegradable particles in our study), but also evident for irregular particles made of the lightest polymer PS with a density close to that of water ($= 1.03 \text{ g cm}^{-3}$). In contrast, regular, spherical particles with smooth surfaces did not show any significant effects of air attachment on TSV in our experiments.

5 SUMMARY AND CONCLUSION

In this study we systematically investigated the effects of different physical parameters on the TSV of MP particles in stagnant water bodies such as lakes. Parameters, which were varied over ranges typical for MP particles found in the environment, included particle density, volume, shape and roundness, surface hydrophobicity and water temperature. In total we conducted 683 individual CFD simulations of the settling behavior of MP particles of regular and irregular shapes and compared the simulation results to two semi-empirical equations to estimate particle TSVs as well as to laboratory settling experiments with the respective particles.

Our CFD simulations illustrated the peculiar, shape-dependent movement of irregular particles in the initial, transient phase of settling before reaching a quasi-steady TSV. This transient phase was found to be short, usually not exceeding one second, and is therefore negligible for estimating the time-scales of particle settling in larger stagnant water bodies such as lakes. The CFD-based calculations of TSV for MP particles of regular and irregular shapes were found to be in good agreement ($R^2 = 0.91$) with TSV estimates obtained from the semi-empirical Dietrich equation (Dietrich, 1982), which is based on simple shape metrics and was originally developed for mineral (sediment) particles. Deviations from the CFD results can be attributed to the simplicity of the shape metrics used, which presumably play out more significantly for the lighter MP particles than for the heavier mineral particles, for which the relationship was originally developed. Surprisingly the comparison of our CFD-based TSVs with values obtained from another semi-empirical relationship, which was specifically developed for MP fragments, pellets and spheres (Waldschläger and Schüttrumpf, 2019) yielded a poorer agreement. We suspect that this deviation is related to differences between the shapes of the particles used to derive this relationship and the particle shapes in our study.

A comparison between the CFD-based TSV values and the experimentally determined values for the irregular particles also showed a good general agreement ($R^2 = 0.82$), but with some more significant deviations for the particles made of biodegradable polymers and the very light non-biodegradable polymer PS ($=1.03 \text{ g cm}^{-3}$). Separating the data from the biodegradable particles from the other data revealed a significantly weaker correlation ($R^2 = 0.09$), which we hypothesized to be related to the attachment of air on the

particle surface due to its hydrophobicity. Our hypothesis was corroborated by the results of additional settling experiments, in which the MP particles were treated with a surfactant to reduce their surface hydrophobicity, which brought the experimental results into good agreement with the CFD results ($R^2 = 0.82$). Maximum changes in TSV related to effects of hydrophobicity were on the order of 58%. Our results further indicated that the magnitude of air attachment on the hydrophobic particle surfaces seems to be related to the presence of larger surface irregularities as well as to the generally rougher surfaces of the bio-degradable polymers. The effects observed for the irregular, non-biodegradable PS particles are presumably related to their low density, which makes them more susceptible to TSV changes even at smaller magnitudes of air attachment. Regular, spherical particles with relatively smooth surfaces in contrast, did not show any measurable effects of air attachment on their TSVs.

For an evaluation of the relative importance of the different physical parameters investigated we conclude that density is the most decisive parameter for the TSV as it predominantly affects particle weight and in turn the gravitational force controlling TSV. Increases in TSV in excess of 400% could result from a doubling of density. In contrast, gains in weight due to a doubling of particle volume are counteracted by increases in buoyancy of the larger particle and drag on the enlarged particle surface leading to comparably smaller TSV increases on the order of 100–200%. Effects of air attachment follow with TSV changes of up to 58%, but they are restricted to particles with specific shape and surface characteristics. Effects of water temperature and particle roundness were responsible for maximum TSV changes of 47 and 45% respectively. Our systematic evaluation of the effects of key physical parameters on TSV provides a framework to evaluate their relative importance in future studies on the behavior of MP particles in lakes and can help to design future experiments on MP particle settling. It is clear, however, that the settling of MP particles in real lakes will also be affected by processes such as the formation of biofilms and/or mineral crusts on particle surfaces (Kaiser et al., 2017; Chen et al., 2019; Leiser et al., 2020; Elagami et al., 2022), the sorption of metals on particle surfaces (Leiser et al., 2021), particle interactions and aggregation (Leiser et al., 2021; Elagami et al., 2022; Wu et al., 2022), particle aging (Brandon et al., 2016) or the uptake and excretion by organisms (Koelmans et al., 2022), and turbulent flows (Kumar et al., 2021). How these processes interact with the basic physical processes investigated in this study and how that

may change the settling behavior of MP particles remains to be investigated in future work.

DATA AVAILABILITY STATEMENT

The original contributions presented in the study are included in the article/**Supplementary Material**, further inquiries can be directed to the corresponding authors.

AUTHOR CONTRIBUTIONS

PA: Set up the CFD modeling framework, conducted the CFD simulations, designing the additional experiments, data interpretation and writing the manuscript. HE: Performed the laboratory experiments, assisted in data interpretation and writing the manuscript. FD: Contributed to the initial set-up of the CFD modeling framework, to data interpretation and writing of the manuscript. CS: Assisted in data interpretation and writing the manuscript. BG: Assisted in data interpretation and writing the manuscript. SF: Assisted in data interpretation and writing the manuscript. SP: Assisted in data interpretation and writing the manuscript. JF: Conceived the project, assisted in data interpretation and contributed to writing and editing of the manuscript.

FUNDING

Funded by the Deutsche Forschungsgemeinschaft (DFG, German Research Foundation)–Project Number 391977956–SFB 1357.

ACKNOWLEDGMENTS

We would like to thank Ulrich Mansfeld and Martina Heider for taking the SEM images.

SUPPLEMENTARY MATERIAL

The Supplementary Material for this article can be found online at: <https://www.frontiersin.org/articles/10.3389/fenvs.2022.875220/full#supplementary-material>

REFERENCES

- Ahrens, J., Geveci, B., and Law, C. (2005). Paraview: An End-User Tool for Large Data Visualization. *The visualization handbook*, 717–731(8). doi:10.1016/b978-012387582-2/50038-1
- Akdogan, Z., and Guven, B. (2019). Microplastics in the Environment: A Critical Review of Current Understanding and Identification of Future Research Needs. *Environ. Pollut.* 254, 113011. doi:10.1016/j.envpol.2019.113011
- Al Harraq, A., and Bharti, B. (2021). Microplastics through the Lens of Colloid Science. *ACS Environ. Au* 2 (1), 3–10. doi:10.1021/acsenvironau.1c00016

- Anderson, P. J., Warrack, S., Langen, V., Challis, J. K., Hanson, M. L., and Rennie, M. D. (2017). Microplastic Contamination in lake Winnipeg, Canada. *Environ. Pollut.* 225, 223–231. doi:10.1016/j.envpol.2017.02.072
- Arora, C., Kumar, B. P., and Narayana, A. C. (2010). Influence of Particle Shape on Drag Coefficient for Commonly Occurring sandy Particles in Coastal Areas. *Int. J. Ocean Clim. Syst.* 1 (2), 99–112. doi:10.1260/1759-3131.1.2.99
- Ballent, A., Corcoran, P. L., Madden, O., Helm, P. A., and Longstaffe, F. J. (2016). Sources and Sinks of Microplastics in Canadian Lake Ontario Nearshore, Tributary and beach Sediments. *Mar. Pollut. Bull.* 110 (1), 383–395. doi:10.1016/j.marpolbul.2016.06.037
- Barnes, D. K. A., Galgani, F., Thompson, R. C., and Barlaz, M. (2009). Accumulation and Fragmentation of Plastic Debris in Global

- Environments. *Phil. Trans. R. Soc. B* 364 (1526), 1985–1998. doi:10.1098/rstb.2008.0205
- Berlemont, A., Desjonqueres, P., and Gouesbet, G. (1990). Particle Lagrangian Simulation in Turbulent Flows. *Int. J. Multiphase Flow* 16 (1), 19–34. doi:10.1016/0301-9322(90)90034-g
- Boehrer, B., and Schultze, M. (2008). Stratification of Lakes. *Rev. Geophys.* 46 (2), RG2005. doi:10.1029/2006rg000210
- Brandon, J., Goldstein, M., and Ohman, M. D. (2016). Long-term Aging and Degradation of Microplastic Particles: Comparing *In Situ* Oceanic and Experimental Weathering Patterns. *Mar. Pollut. Bull.* 110 (1), 299–308. doi:10.1016/j.marpolbul.2016.06.048
- Browne, M. A., Crump, P., Niven, S. J., Teuten, E., Tonkin, A., Galloway, T., et al. (2011). Accumulation of Microplastic on Shorelines Worldwide: Sources and Sinks. *Environ. Sci. Technol.* 45 (21), 9175–9179. doi:10.1021/es201811s
- Chen, X., Xiong, X., Jiang, X., Shi, H., and Wu, C. (2019). Sinking of Floating Plastic Debris Caused by Biofilm Development in a Freshwater lake. *Chemosphere*. 222, 856–864. doi:10.1016/j.chemosphere.2019.02.015
- Chubarenko, I., Bagaev, A., Zobkov, M., and Esiukova, E. (2016). On Some Physical and Dynamical Properties of Microplastic Particles in marine Environment. *Mar. Pollut. Bull.* 108 (1-2), 105–112. doi:10.1016/j.marpolbul.2016.04.048
- Chubarenko, I., Esiukova, E., Bagaev, A., Isachenko, I., Demchenko, N., Zobkov, M., et al. (2018). “Behavior of Microplastics in Coastal Zones,” in *Microplastic Contamination in Aquatic Environments*. Editors E. Y. Zeng (Elsevier), 175–223. doi:10.1016/b978-0-12-813747-5.00006-0
- Claessens, M., De Meester, S., Van Landuyt, L., De Clerck, K., and Janssen, C. R. (2011). Occurrence and Distribution of Microplastics in marine Sediments along the Belgian Coast. *Mar. Pollut. Bull.* 62 (10), 2199–2204. doi:10.1016/j.marpolbul.2011.06.030
- Cole, M., Lindeque, P., Fileman, E., Halsband, C., Goodhead, R., Moger, J., et al. (2013). Microplastic Ingestion by Zooplankton. *Environ. Sci. Technol.* 47 (12), 6646–6655. doi:10.1021/es400663f
- Cole, M., Lindeque, P. K., Fileman, E., Clark, J., Lewis, C., Halsband, C., et al. (2016). Microplastics Alter the Properties and Sinking Rates of Zooplankton Faecal Pellets. *Environ. Sci. Technol.* 50 (6), 3239–3246. doi:10.1021/acs.est.5b05905
- Coppock, R. L., Galloway, T. S., Cole, M., Fileman, E. S., Queirós, A. M., and Lindeque, P. K. (2019). Microplastics Alter Feeding Selectivity and Faecal Density in the Copepod, *Calanus helgolandicus*. *Sci. total Environ.* 687, 780–789. doi:10.1016/j.scitotenv.2019.06.009
- Corey, A. T. (1949). *Influence of Shape on the Fall Velocity of Sand Grains*. Fort Collins, CO: Colorado A & M College.
- Derraik, J. G. B. (2002). The Pollution of the marine Environment by Plastic Debris: a Review. *Mar. Pollut. Bull.* 44 (9), 842–852. doi:10.1016/s0025-326x(02)00220-5
- de Souza Machado, A. A., Kloas, W., Zarfl, C., Hempel, S., and Rillig, M. C. (2018). Microplastics as an Emerging Threat to Terrestrial Ecosystems. *Glob. Change Biol.* 24 (4), 1405–1416. doi:10.1111/gcb.14020
- Dietrich, W. E. (1982). Settling Velocity of Natural Particles. *Water Resour. Res.* 18 (6), 1615–1626. doi:10.1029/wr018i006p01615
- Doyle, M. J., Watson, W., Bowlin, N. M., and Sheavly, S. B. (2011). Plastic Particles in Coastal Pelagic Ecosystems of the Northeast Pacific Ocean. *Mar. Environ. Res.* 71 (1), 41–52. doi:10.1016/j.marenvres.2010.10.001
- Elagami, H., Ahmadi, P., Fleckenstein, J. H., Frei, S., Obst, M., Agarwal, S., et al. (2022). Measurement of Microplastic Settling Velocities and Implications for Residence Times in Thermally Stratified Lakes. *Limnology & Oceanography* Ino.12046, 1–12. doi:10.1002/Ino.12046
- Fendall, L. S., and Sewell, M. A. (2009). Contributing to marine Pollution by Washing Your Face: Microplastics in Facial Cleansers. *Mar. Pollut. Bull.* 58 (8), 1225–1228. doi:10.1016/j.marpolbul.2009.04.025
- Fischer, E. K., Paglialonga, L., Czech, E., and Tamminga, M. (2016). Microplastic Pollution in Lakes and lake Shoreline Sediments - A Case Study on Lake Bolsena and Lake Chiusi (central Italy). *Environ. Pollut.* 213, 648–657. doi:10.1016/j.envpol.2016.03.012
- Frias, J. P. G. L., and Nash, R. (2019). Microplastics: Finding a Consensus on the Definition. *Mar. Pollut. Bull.* 138, 145–147. doi:10.1016/j.marpolbul.2018.11.022
- Gorham, E., and Boyce, F. M. (1989). Influence of lake Surface Area and Depth upon thermal Stratification and the Depth of the Summer Thermocline. *J. Great Lakes Res.* 15 (2), 233–245. doi:10.1016/s0380-1330(89)71479-9
- Gregory, M. R. (1983). Virgin Plastic Granules on Some Beaches of Eastern Canada and Bermuda. *Mar. Environ. Res.* 10 (2), 73–92. doi:10.1016/0141-1136(83)90011-9
- Gregory, M. R. (1996). Plastic ‘scrubbers’ in Hand Cleansers: a Further (And Minor) Source for marine Pollution Identified. *Mar. Pollut. Bull.* 32 (12), 867–871. doi:10.1016/s0025-326x(96)00047-1
- Guerrini, F., Mari, L., and Casagrandi, R. (2021). The Dynamics of Microplastics and Associated Contaminants: Data-Driven Lagrangian and Eulerian Modelling Approaches in the Mediterranean Sea. *Sci. Total Environ.* 777, 145944. doi:10.1016/j.scitotenv.2021.145944
- Hendrickson, E., Minor, E. C., and Schreiner, K. (2018). Microplastic Abundance and Composition in Western Lake Superior as Determined via Microscopy, Pyr-GC/MS, and FTIR. *Environ. Sci. Technol.* 52 (4), 1787–1796. doi:10.1021/acs.est.7b05829
- Hersch, R. W., Herschy, R. W., Wolanski, E., Andutta, F., Delhez, E., Fairbridge, R. W., et al. (2012). Ecological Threat to Lakes and Reservoirs. *Encyclopedia of Lakes and Reservoirs*, 233–234. doi:10.1007/978-1-4020-4410-6_74
- Hiltunen, M., Vehniäinen, E.-R., and Kukkonen, J. V. K. (2021). Interacting Effects of Simulated Eutrophication, Temperature Increase, and Microplastic Exposure on *Daphnia*. *Environ. Res.* 192, 110304. doi:10.1016/j.envres.2020.110304
- Hoffschroer, N., Grassl, N., Steinmetz, A., Sziegoleit, L., Koch, M., and Zeis, B. (2021). Microplastic burden in *Daphnia* Is Aggravated by Elevated Temperatures. *Zoology (Jena)*. 144, 125881. doi:10.1016/j.zool.2020.125881
- Houzeaux, G., Eguzkitza, B., Aubry, R., Owen, H., and Vázquez, M. (2014). A Chimera Method for the Incompressible Navier-Stokes Equations. *Int. J. Numer. Meth. Fluids.* 75 (3), 155–183. doi:10.1002/fld.3886
- Isachenko, I. (2020). Catching the Variety: Obtaining the Distribution of Terminal Velocities of Microplastics Particles in a Stagnant Fluid by a Stochastic Simulation. *Mar. Pollut. Bull.* 159, 111464. doi:10.1016/j.marpolbul.2020.111464
- Jalón-Rojas, I., Wang, X. H., and Fredj, E. (2019). A 3D Numerical Model to Track marine Plastic Debris (TrackMPD): Sensitivity of Microplastic Trajectories and Fates to Particle Dynamical Properties and Physical Processes. *Mar. Pollut. Bull.* 141, 256–272. doi:10.1016/j.marpolbul.2019.02.052
- Jérémy, R., Gaston, L. P., and Valyrakis, M. (2020). Coupled CFD-DEM Modelling to Assess Settlement Velocity and Drag Coefficient of Microplastics. *EGU General Assembly 2020*. doi:10.5194/egusphere-egu2020-10049
- Kaiser, D., Estelmann, A., Kowalski, N., Glockzin, M., and Waniek, J. J. (2019). Sinking Velocity of Sub-millimeter Microplastic. *Mar. Pollut. Bull.* 139, 214–220. doi:10.1016/j.marpolbul.2018.12.035
- Kaiser, D., Kowalski, N., and Waniek, J. J. (2017). Effects of Biofouling on the Sinking Behavior of Microplastics. *Environ. Res. Lett.* 12 (12), 124003. doi:10.1088/1748-9326/aa8e8b
- Khatmullina, L., and Isachenko, I. (2017). Settling Velocity of Microplastic Particles of Regular Shapes. *Mar. Pollut. Bull.* 114 (2), 871–880. doi:10.1016/j.marpolbul.2016.11.024
- Koelmans, A. A., Redondo-Hasselerharm, P. E., Nor, N. H. M., de Ruijter, V. N., Mintenig, S. M., and Kooi, M. (2022). Risk Assessment of Microplastic Particles. *Nat. Rev. Mater.*, 1–15. doi:10.1038/s41578-021-00411-y
- Kooi, M., Reisser, J., Slat, B., Ferrari, F. F., Schmid, M. S., Cunsolo, S., et al. (2016). The Effect of Particle Properties on the Depth Profile of Buoyant Plastics in the Ocean. *Sci. Rep.* 6 (1), 33882–33910. doi:10.1038/srep33882
- Kowalski, N., Reichardt, A. M., and Waniek, J. J. (2016). Sinking Rates of Microplastics and Potential Implications of Their Alteration by Physical, Biological, and Chemical Factors. *Mar. Pollut. Bull.* 109 (1), 310–319. doi:10.1016/j.marpolbul.2016.05.064
- Kumar, R., Sharma, P., Verma, A., Jha, P. K., Singh, P., Gupta, P. K., et al. (2021). Effect of Physical Characteristics and Hydrodynamic Conditions on Transport and Deposition of Microplastics in Riverine Ecosystem. *Water* 13 (19), 2710. doi:10.3390/w13192710
- Kwon, J.-H., Chang, S., Hong, S. H., and Shim, W. J. (2017). Microplastics as a Vector of Hydrophobic Contaminants: Importance of Hydrophobic Additives. *Integr. Environ. Assess. Manag.* 13 (3), 494–499. doi:10.1002/ieam.1906

- Lambert, S., and Wagner, M. (2018). Microplastics Are Contaminants of Emerging Concern in Freshwater Environments: An Overview. *Freshw. microplastics*, 1–23. doi:10.1007/978-3-319-61615-5_1
- Leiser, R., Jongsma, R., Bakenhus, I., Möckel, R., Philipp, B., Neu, T. R., et al. (2021). Interaction of Cyanobacteria with Calcium Facilitates the Sedimentation of Microplastics in a Eutrophic Reservoir. *Water Res.* 189, 116582. doi:10.1016/j.watres.2020.116582
- Leiser, R., Wu, G.-M., Neu, T. R., and Wendt-Potthoff, K. (2020). Biofouling, Metal Sorption and Aggregation Are Related to Sinking of Microplastics in a Stratified Reservoir. *Water Res.* 176, 115748. doi:10.1016/j.watres.2020.115748
- Liao, J., and Chen, Q. (2021). Biodegradable Plastics in the Air and Soil Environment: Low Degradation Rate and High Microplastics Formation. *J. Hazard. Mater.* 418, 126329. doi:10.1016/j.jhazmat.2021.126329
- Maximenko, N., Hafner, J., and Nilner, P. (2012). Pathways of marine Debris Derived from Trajectories of Lagrangian Drifters. *Mar. Pollut. Bull.* 65 (1–3), 51–62. doi:10.1016/j.marpolbul.2011.04.016
- Migwi, F. K., Ogunah, J. A., and Kiratu, J. M. (2020). Occurrence and Spatial Distribution of Microplastics in the Surface Waters of Lake Naivasha, Kenya. *Environ. Toxicol. Chem.* 39 (4), 765–774. doi:10.1002/etc.4677
- Moghadam, A., and Vahedi Tafreshi, H. (2020). On Liquid Bridge Adhesion to Fibrous Surfaces under normal and Shear Forces. *Colloids Surf. A: Physicochemical Eng. Aspects.* 589, 124473. doi:10.1016/j.colsurfa.2020.124473
- Mountford, A. S., and Morales Maqueda, M. A. (2019). Eulerian Modeling of the Three-Dimensional Distribution of Seven Popular Microplastic Types in the Global Ocean. *J. Geophys. Res. Oceans.* 124 (12), 8558–8573. doi:10.1029/2019jc015050
- Nooteboom, P. D., Delandmeter, P., van Sebille, E., Bijl, P. K., Dijkstra, H. A., and von der Heydt, A. S. (2020). Resolution Dependency of Sinking Lagrangian Particles in Ocean General Circulation Models. *PLoS one.* 15 (9), e0238650. doi:10.1371/journal.pone.0238650
- North, E. J., and Halden, R. U. (2013). Plastics and Environmental Health: the Road Ahead. *Rev. Environ. Health.* 28 (1), 1–8. doi:10.1515/reveh-2012-0030
- Powers, M. C. (1953). A New Roundness Scale for Sedimentary Particles. *J. Sediment. Res.* 23 (2), 117–119. doi:10.1306/d4269567-2b26-11d7-8648000102c1865d
- Renner, G., Nellessen, A., Schwiers, A., Wenzel, M., Schmidt, T. C., and Schram, J. (2020). Hydrophobicity-water/air-based Enrichment Cell for Microplastics Analysis within Environmental Samples: A Proof of Concept. *MethodsX.* 7, 100732. doi:10.1016/j.mex.2019.11.006
- Ribes, A., and Caremoli, C. (2007). “Salome Platform Component Model for Numerical Simulation,” in 31st annual international computer software and applications conference (COMPSAC 2007): IEEE), 553–564.
- Rocha-Santos, T., and Duarte, A. C. (2015). A Critical Overview of the Analytical Approaches to the Occurrence, the Fate and the Behavior of Microplastics in the Environment. *Trac Trends Analytical Chemistry.* 65, 47–53. doi:10.1016/j.trac.2014.10.011
- Rochman, C. M. (2018). Microplastics Research-From Sink to Source. *Science.* 360 (6384), 28–29. doi:10.1126/science.aar7734
- Sighicelli, M., Pietrelli, L., Lecce, F., Iannilli, V., Falconieri, M., Coscia, L., et al. (2018). Microplastic Pollution in the Surface Waters of Italian Subalpine Lakes. *Environ. Pollut.* 236, 645–651. doi:10.1016/j.envpol.2018.02.008
- Singh, P., Bagrania, J., and Haritash, A. (2019). Seasonal Behaviour of thermal Stratification and Trophic Status in a Sub-tropical Palustrine Water Body. *Appl. Water Sci.* 9 (5), 1–6. doi:10.1007/s13201-019-1011-z
- Szewczyk, P. K., Ura, D. P., Metwally, S., Knapczyk-Korczak, J., Gajek, M., Marzec, M. M., et al. (2019). Roughness and Fiber Fraction Dominated Wetting of Electrospun Fiber-Based Porous Meshes. *Polymers (Basel).* 11 (1), 34. doi:10.3390/polym11010034
- Trunk, R., Bretl, C., Thäter, G., Nirschl, H., Dorn, M., and Krause, M. J. (2021). A Study on Shape-dependent Settling of Single Particles with Equal Volume Using Surface Resolved Simulations. *Computation.* 9 (4), 40. doi:10.3390/computation9040040
- Van Cauwenberghe, L., Claessens, M., Vandegehuchte, M. B., Mees, J., and Janssen, C. R. (2013). Assessment of marine Debris on the Belgian Continental Shelf. *Mar. Pollut. Bull.* 73 (1), 161–169. doi:10.1016/j.marpolbul.2013.05.026
- Vaughan, R., Turner, S. D., and Rose, N. L. (2017). Microplastics in the Sediments of a UK Urban lake. *Environ. Pollut.* 229, 10–18. doi:10.1016/j.envpol.2017.05.057
- Wagner, W., and Kretzschmar, H.-J. (2008). “IAPWS Industrial Formulation 1997 for the Thermodynamic Properties of Water and Steam,” in International steam tables: properties of water and steam based on the industrial formulation IAPWS-IF97, 7–150.
- Waldschläger, K., and Schüttrumpf, H. (2019). Effects of Particle Properties on the Settling and Rise Velocities of Microplastics in Freshwater under Laboratory Conditions. *Environ. Sci. Technol.* 53, 1958–1966. doi:10.1021/acs.est.8b06794
- Webb, H., Arnott, J., Crawford, R., and Ivanova, E. (2013). Plastic Degradation and its Environmental Implications with Special Reference to Poly (Ethylene Terephthalate). *Polymers* 5, 1–18. doi:10.3390/polym5010001
- Wei, X.-F., Bohlén, M., Lindblad, C., Hedenqvist, M., and Hakonen, A. (2021). Microplastics Generated from a Biodegradable Plastic in Freshwater and Seawater. *Water Res.* 198, 117123. doi:10.1016/j.watres.2021.117123
- Weller, H. G., Tabor, G., Jasak, H., and Fureby, C. (1998). A Tensorial Approach to Computational Continuum Mechanics Using Object-Oriented Techniques. *Comput. Phys.* 12 (6), 620–631. doi:10.1063/1.168744
- Williams, A. T., and Simmons, S. L. (1996). The Degradation of Plastic Litter in Rivers: Implications for Beaches. *J. Coast Conserv.* 2 (1), 63–72. doi:10.1007/bf02743038
- Wright, S. L., Thompson, R. C., and Galloway, T. S. (2013). The Physical Impacts of Microplastics on marine Organisms: a Review. *Environ. Pollut.* 178, 483–492. doi:10.1016/j.envpol.2013.02.031
- Wright, S. L., Ulke, J., Font, A., Chan, K. L. A., and Kelly, F. J. (2020). Atmospheric Microplastic Deposition in an Urban Environment and an Evaluation of Transport. *Environ. Int.* 136, 105411. doi:10.1016/j.envint.2019.105411
- Wu, J., Ye, Q., Wu, P., Xu, S., Liu, Y., Ahmed, Z., et al. (2022). Heteroaggregation of Nanoplastics with Oppositely Charged Minerals in Aquatic Environment: Experimental and Theoretical Calculation Study. *Chem. Eng. J.* 428, 131191. doi:10.1016/j.cej.2021.131191
- Zbyszewski, M., Corcoran, P. L., and Hockin, A. (2014). Comparison of the Distribution and Degradation of Plastic Debris along Shorelines of the Great Lakes, North America. *J. Great Lakes Res.* 40 (2), 288–299. doi:10.1016/j.jglr.2014.02.012
- Zhang, H. (2017). Transport of Microplastics in Coastal Seas. *Estuarine, Coastal Shelf Sci.* 199, 74–86. doi:10.1016/j.ecss.2017.09.032
- Zhang, Y., Xie, M., Adamaki, V., Khanbareh, H., and Bowen, C. R. (2017). Control of Electro-Chemical Processes Using Energy Harvesting Materials and Devices. *Chem. Soc. Rev.* 46 (24), 7757–7786. doi:10.1039/c7cs00387k
- Ziccardi, L. M., Edgington, A., Hentz, K., Kulacki, K. J., and Kane Driscoll, S. (2016). Microplastics as Vectors for Bioaccumulation of Hydrophobic Organic Chemicals in the marine Environment: A State-Of-The-Science Review. *Environ. Toxicol. Chem.* 35 (7), 1667–1676. doi:10.1002/etc.3461

Conflict of Interest: The authors declare that the research was conducted in the absence of any commercial or financial relationships that could be construed as a potential conflict of interest.

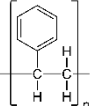
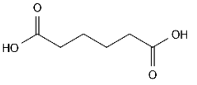
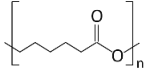
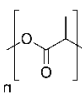
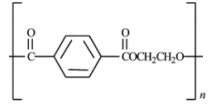
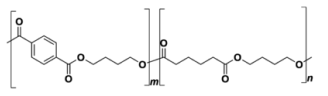
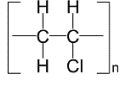
Publisher’s Note: All claims expressed in this article are solely those of the authors and do not necessarily represent those of their affiliated organizations, or those of the publisher, the editors and the reviewers. Any product that may be evaluated in this article, or claim that may be made by its manufacturer, is not guaranteed or endorsed by the publisher.

Copyright © 2022 Ahmadi, Elagami, Dichgans, Schmidt, Gilfedder, Frei, Peiffer and Fleckenstein. This is an open-access article distributed under the terms of the Creative Commons Attribution License (CC BY). The use, distribution or reproduction in other forums is permitted, provided the original author(s) and the copyright owner(s) are credited and that the original publication in this journal is cited, in accordance with accepted academic practice. No use, distribution or reproduction is permitted which does not comply with these terms.

Supplementary Material

S1: Details on the used polymers in the carried out experiments and simulations

Table S1. Properties of the seven abundant polymers used in this study.

Polymer name	Abbreviation	Structure	Density (gcm ⁻³)	Type
Polystyrene	PS		1.030	Non-biodegradable
Polyamide 66	PA66		1.12	Non-biodegradable
Polycaprolacton	PCL		1.14	Biodegradable
Polylactic acid	PLA		1.20	Biodegradable
Poly(L-lactic acid)	PLLA		1.20	Biodegradable
Polybutylenadipate terephthalate	PBAT		1.22	Non-biodegradable
Polyvinyl chloride	PVC		1.38	Non-biodegradable

S2: Adjusted initial and boundary conditions in all the conducted simulations

Table S2. The used initial and boundary conditions in the simulations conducted by OpenFOAM.

		Velocity	Pressure	Phase Saturation
Upper wall	type	inletOutlet;	fixedValue;	fixedValue;
	value	internalField	internalField	uniform 0;
MP particle	type	movingWallVelocity	fixedFluxPressure;	zeroGradient;
	value	internalField	-	-
Side walls	type	fixedValue	fixedFluxPressure;	zeroGradient;
	value	internalField	-	-
Lower wall	type	fixedValue	fixedFluxPressure;	zeroGradient;
	value	internalField	-	-

S3: Calculation of MOI for an arbitrary particle

The following equations are used to calculate mass (m) and mass moment of inertia (I_o) of particle with arbitrary shape (Ehrlich and Weinberg, 1970; Peraire and Widnall, 2008; Tang and Shangguan, 2011) (Figure S1) in which r_i is a vector that points out to the position of the i^{th} cell in the mesh of a designed particle within a Cartesian coordinate system and $\rho(r_i)$ is the particle density in the i^{th} cell:

$$m = \int_{v(r)} \rho(r_i) dV(\vec{r}) \quad (1)$$

$$I_o = \int_{v(r)} \rho(r_i) r_i^2 dV(\vec{r}) = \int \begin{bmatrix} x_i^2 + y_i^2 & -x_i y_i & -x_i z_i \\ -x_i y_i & x_i^2 + y_i^2 & -y_i z_i \\ -x_i z_i & -y_i z_i & x_i^2 + y_i^2 \end{bmatrix} \rho(r_i) dV(\vec{r}) \quad (2)$$

Origin is the rotational axis of the particle's moment of inertia which is calculated by equation 2. Having the coordinate of the particle's center of mass (\vec{c}) (equation 3) and using the parallel axes theorem, MOI of the particles around their center of gravity can be calculated using equation 4.

$$\vec{c} = \frac{1}{m} \int_{v(r)} \vec{r}_i \rho(r_i) dV(\vec{r}) \quad (3)$$

$$I_o = \int \begin{bmatrix} x_i^2 + y_i^2 & -x_i y_i & -x_i z_i \\ -x_i y_i & x_i^2 + y_i^2 & -y_i z_i \\ -x_i z_i & -y_i z_i & x_i^2 + y_i^2 \end{bmatrix} \rho(r_i) dV(\vec{r}) - \int_{v(r)} \rho(r_i) dV(\vec{r}) \begin{bmatrix} C_y^2 + C_z^2 & -C_x C_y & -C_x C_z \\ -C_x C_y & C_x^2 + C_z^2 & -C_y C_z \\ -C_x C_z & -C_y C_z & C_x^2 + C_y^2 \end{bmatrix} \quad (4)$$

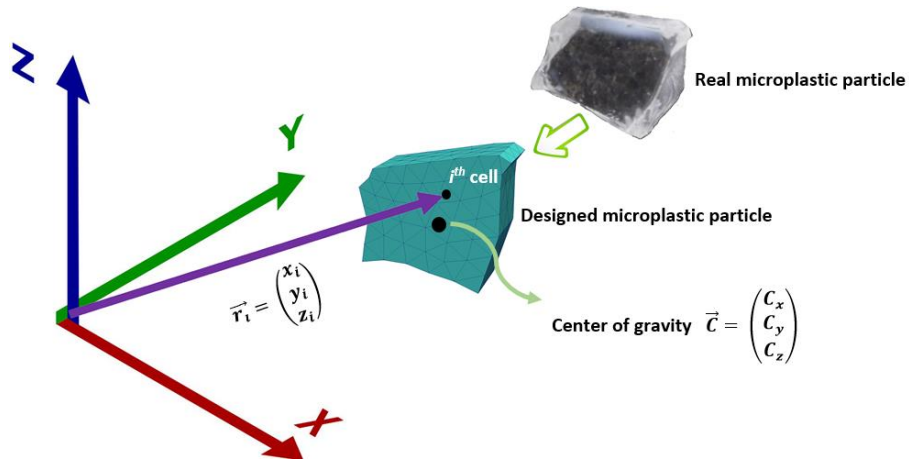











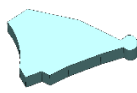







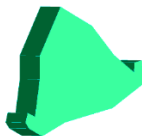



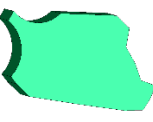








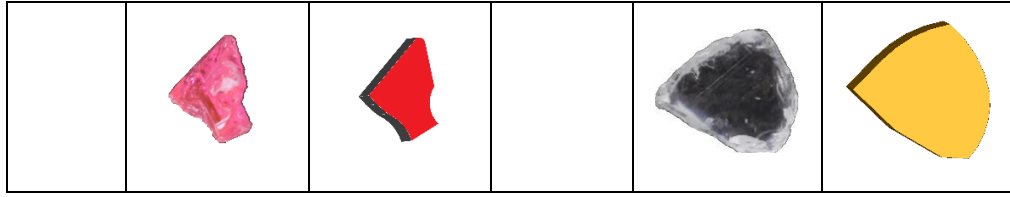


Figure S1. Position vector and center of mass location of an irregularly shaped MP particle.

S4: A number of the designed irregularly shaped MP particles and their real images

Table S3. Some of the designed particles based on the shape of real irregularly shaped MP particles.

Polymer type	Real MP particle	Simulated MP particle	Polymer type	Real MP particle	Simulated MP particle
PLLA			PA66		
					
					
PCL			PBAT		
					
					
PS			PVC		
					



In the table a selection of the real MP particles used in the experiments and their designed shapes using the meshing software SALOME 9.4 software (Ribes and Caremoli, 2007) are depicted. The simulation results for three random particles software are visualized using ParaView software (Ahrens et al., 2005) (see supplementary animation (Video 1)). In order to compare their sizes in the interpretations, equation 5 was used to calculate the diameter of spheres with volumes identical to the volumes of the MP particles.

$$D_{eq} = \sqrt[3]{ABC} \quad (5)$$

A and C are the longest and shortest lengths of each particle and B is the arithmetic average of A and C (Kooi et al., 2016; Waldschläger and Schüttrumpf, 2019).

S5: Calculating side length of the polygons with identical areas to generate particles of the same volumes

A regular polygon with N sides is a cyclic polygon which is described using two circles, an inscribed circle that forms the tangent to the middle points of all sides of a regular polygon, and a circumscribed circle which passes through all its vertices. As the number of sides of a polygon increase towards infinity, the lengths of its sides converge to zero, so that the inscribed and circumscribed circles eventually overlap. Knowing the side length and the number of sides, equation 6 returns the area of a regular polygon. Figure S2 has been drawn based on equation 6 so that considering areas equal to circles with diameters of 0.5 mm, 1mm, 1.5mm, 2mm, and 2.5mm, the side length (a) of the polygons with areas equal to their corresponding circles were calculated.

$$A = \frac{1}{4} na^2 \cot \frac{\pi}{n} \quad (6)$$

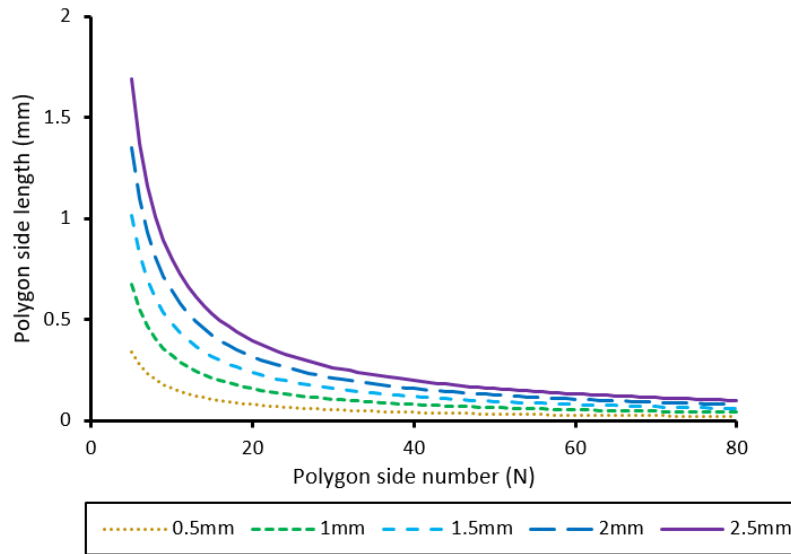


Figure S2. The side lengths of regular 2D polygons with areas identical to a circle derived from a polygon with an infinite number of sides (legend shows the diameters of the circles).

S6. Behavior of a particle before and after reaching its terminal settling velocity (TSV)

Figure S3-A illustrates the evolution of the settling velocity in the initial transient phase of settling for four particles with different shapes, which show different, shape-dependent behavior. Figure S3-B shows the velocity evolution for 5 triangular particles entering the water column with different orientations at angles of 45° , 90° , 135° , and 180° . The velocity evolution in the transient phase of settling before reaching a constant terminal settling velocity (TSV) clearly depends on the orientation of the particle when entering the water column (Figure S3-B). In this transient phase the settling velocity can fluctuate around the TSV as a result of secondary oscillating, rotating and tumbling movements of the MP particles. Those types of secondary movements were also observed in the settling experiments in the present as well as other studies (Khatmullina and Isachenko, 2017).

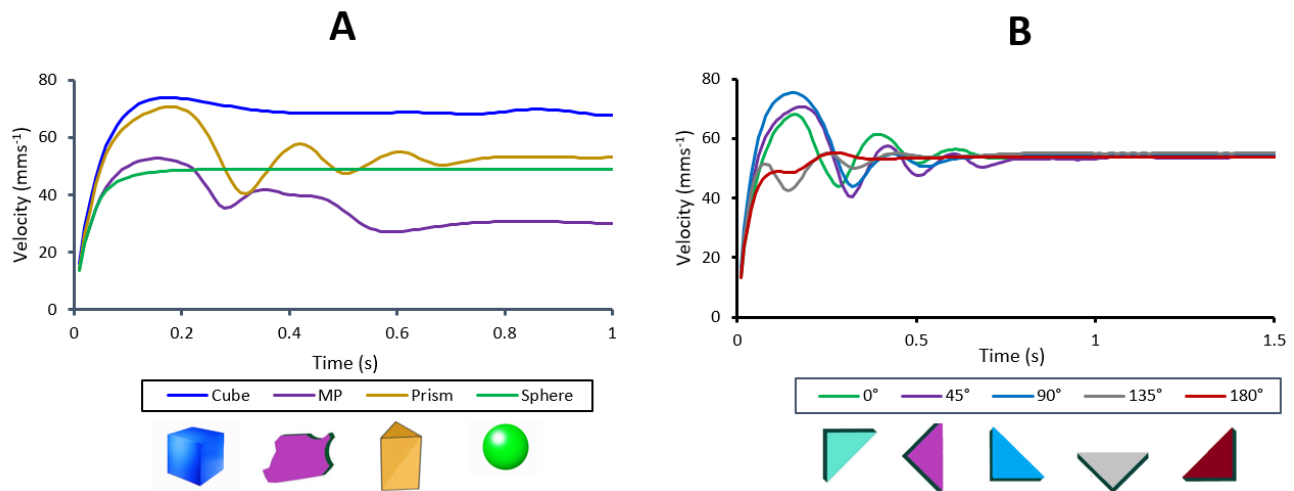


Figure S3. Velocity profile before and after reaching TSV for (A) three different regular particles (cube, prism, and sphere) and an irregular MP particle, (B) Evolution of the settling velocity of a triangular particle entering the water column with orientations at different angles (0°, 45°, 90°, 135°, 180°).

References

- Ahrens, J., Geveci, B., and Law, C. (2005). Paraview: An end-user tool for large data visualization. *The visualization handbook* 717(8).
- Ehrlich, R., and Weinberg, B. (1970). An exact method for characterization of grain shape. *Journal of sedimentary research* 40(1), 205-212.
- Khatmullina, L., and Isachenko, I. (2017). Settling velocity of microplastic particles of regular shapes. *Marine pollution bulletin* 114(2), 871-880.
- Kooi, M., Reisser, J., Slat, B., Ferrari, F.F., Schmid, M.S., Cunsolo, S., et al. (2016). The effect of particle properties on the depth profile of buoyant plastics in the ocean. *Scientific reports* 6(1), 1-10.
- Peraire, J., and Widnall, S. (2008). Lecture L26-3D Rigid Body Dynamics: The Inertia Tensor. *Dynamics*.
- Ribes, A., and Caremoli, C. (Year). "Salome platform component model for numerical simulation", in: *31st annual international computer software and applications conference (COMPSAC 2007)*: IEEE, 553-564.
- Tang, L., and Shangguan, W.-B. (2011). An improved pendulum method for the determination of the center of gravity and inertia tensor for irregular-shaped bodies. *Measurement* 44(10), 1849-1859.
- Waldschläger, K., and Schüttrumpf, H. (2019). Effects of particle properties on the settling and rise velocities of microplastics in freshwater under laboratory conditions. *Environmental science & technology* 53(4), 1958-1966.

Study 2: Measurement of microplastic settling velocities and implications for residence time in thermally stratified lakes

Hassan Elagami, **Pouyan Ahmadi**, Jan H. Fleckenstein, Sven Frei, Martin Obst, Seema Agarwal, Benjamin S. Gilfedder

Corresponding Author: Hassan Elagami

Published in Association for the Science of Limnology and Oceanography in February 2022

<https://doi.org/10.1002/lno.12046>

Own contribution:

- Concept and study design 50%
- Data acquisition 30%
- Data analyses 30%
- Figures 30%
- Discussion of results 50%
- Manuscript writing 30%

Author contribution statement:

HE performed the laboratory experiments, whole lake modeling and worked on the manuscript. PA and JHF assisted in data interpretation and writing the manuscript. SF developed the whole lake model, conducted the simulations, and contributed to writing the manuscript. MO performed the confocal laser scanning microscopy and assisted with analysis and interpretation of the biofilm data. SA provided the microplastics, and assisted in data interpretation from the settling column, especially relating to the surface chemistry of plastic polymers. BSG conceived the project, and assisted in data interpretation and writing and editing the manuscript.

Measurement of microplastic settling velocities and implications for residence times in thermally stratified lakes

Hassan Elagami^{1,2*}, Pouyan Ahmadi,³ Jan H. Fleckenstein,^{3,4} Sven Frei,² Martin Obst,⁵ Seema Agarwal,⁶ Benjamin S. Gilfedder^{1,2}

¹Limnological Research Station, Bayreuth Center of Ecology and Environmental Research, University of Bayreuth, Bayreuth, Germany

²Department of Hydrology, Bayreuth Center of Ecology and Environmental Research (BayCEER), University of Bayreuth, Bayreuth, Germany

³Department of Hydrogeology, Helmholtz Centre for Environmental Research – UFZ, Leipzig, Germany

⁴Hydrologic Modelling Unit, Bayreuth Center of Ecology and Environmental Research (BayCEER), University of Bayreuth, Bayreuth, Germany

⁵Experimental Biogeochemistry, BayCEER, University of Bayreuth, Bayreuth, Germany

⁶Macromolecular Chemistry II, University of Bayreuth, Bayreuth, Germany

Abstract

Microplastics residence times in lakes are currently poorly understood. In this work, settling experiments with pristine and biofilm-colonized microplastic particles were combined with model calculations to evaluate settling velocities, particle distributions, and residence times in the epilimnion, metalimnion, and hypolimnion of a hypothetical stratified lake broadly based on Upper Lake Constance. Settling velocities of various biodegradable and nonbiodegradable polymers of various shapes, sizes, and biofilm colonization were measured in a settling column. The settling velocities ranged between ~ 0.30 and ~ 50 mm s⁻¹. Particle sizes and polymer densities were identified as primary controls on settling rates. Microplastic particles that had been exposed to a lake environment for up to 30 weeks were colonized by a range of biofilms and associated extracellular polymeric substances; surprisingly, however, the settling velocity did not vary significantly between pristine and colonized microplastic particles. Simulated microplastic residence times in the model lake varied over a wide range of time scales (10⁻¹ to 10⁵ d) and depended mainly on the size of the particles and depth of the lake layer. Long residence times on the order of 10⁵ d (for 1- μ m microplastic particles) imply that for small microplastic particles there is a high probability that they will be taken up at some stage by lake organisms. As the lake retention time (~ 4.5 years) is considerably shorter than the residence time of small microplastics, negligible quantities of these microplastic particles should be found in the lake sediment unless some other process increases their settling velocity.

*Correspondence: hassan.elagami@uni-bayreuth.de

This is an open access article under the terms of the Creative Commons Attribution License, which permits use, distribution and reproduction in any medium, provided the original work is properly cited.

Additional Supporting Information may be found in the online version of this article.

Author Contribution Statement: H.E. performed the laboratory experiments, whole lake modeling and worked on the manuscript. P.A. and J.H.F. assisted in data interpretation and writing the manuscript. S.F. developed the whole lake model, conducted the simulations, and contributed to writing the manuscript. M.O. performed the confocal laser scanning microscopy and assisted with analysis and interpretation of the biofilm data. S.A. provided the microplastics, and assisted in data interpretation from the settling column, especially relating to the surface chemistry of plastic polymers. B.S.G. conceived the project, and assisted in data interpretation and writing and editing the manuscript.

Over the past 70 years, plastic polymers have established themselves as cost-effective and durable materials that are used ubiquitously in industry, agriculture, and domestic applications. In 2015, global annual production of plastic polymers reached ~ 322 Mt (Worm et al. 2017). Roughly 50% of the plastic volume produced is made for single-use applications, and in particular for packaging purposes (Worm et al. 2017). By 2015, ~ 6300 Mt of plastic waste had been produced, of which approximately 9% was recycled, while 79% accumulated in landfills and the environment (Geyer et al. 2017). The majority of the plastic debris found in nature are high molar mass polymers such as polyethylene and polyethylene terephthalate (Agarwal 2020).

Rivers and streams are considered the dominant transport pathway moving plastic from terrestrial sources to the marine

sink (Fischer et al. 2016). In contrast to fluvial systems, lakes and reservoirs are mostly considered as permanent or temporary sinks for plastics due to their low-energy hydrodynamic regimes. Plastics in lakes and rivers originate predominantly from terrestrial sources such as effluents from waste-water treatment plants (Sun et al. 2019), agriculture, and improper dumping of plastic waste (Bellasi et al. 2020). During the transport of plastic in freshwater systems, it is exposed to various physical, chemical, and biological degradation processes (Browne et al. 2007; Meides et al. 2021). Fragmentation and degradation processes in natural environments transform plastic fragments larger than 5 mm into microplastics < 5 mm (Arthur et al. 2009) and nanoplastics (Toussaint et al. 2019).

As the density of pristine nonbuoyant plastic polymers lies close to that of water, microplastics are expected to remain in suspension for a substantial time before sedimentation to lake sediments. Long residence times in the water column increases the probability of uptake by organisms such as zooplankton (Nguyen et al. 2020) as such organisms cannot differentiate between microplastics and natural particulate matter used as food (Aljaibachi and Callaghan 2018).

Once microplastics have entered the food chain, organisms including zooplankton and fish uptake microplastics through ingestion via predation (Nelms et al. 2018). After microplastics have been ingested, they can also be egested within fecal pellets (Cole et al. 2016). As fecal pellets are a source of food for many aquatic organisms, the ingestion of these microplastic-containing pellets facilitates the transfer of microplastics to various trophic levels (Nelms et al. 2018). Fecal pellets may also form a pathway for microplastic sedimentation, removing them from the lake water column (Cole et al. 2016), although this remains poorly understood.

Existing studies have proposed that the physical properties of microplastics such as polymer density, shape, and size control the settling velocity of pristine microplastics (Khatmullina and Isachenko 2017; Waldschläger and Schüttrumpf 2019) and the residence time in the water column (Nguyen et al. 2020). Since most of microplastics in aquatic systems are irregularly shaped, they tend to have a larger surface area compared to spherical particles. The high surface area of the irregular particles leads to increased hydrodynamical friction and drag forces, resulting in lower settling velocities compared to ideal spheres (Dietrich 1982).

Pristine microplastics are also exposed to various types of biofilm-building microorganisms over time scales that are largely dependent on residence times of the particles in the water column and polymer properties (Zettler et al. 2013; Leiser et al. 2020; Ramsperger et al. 2020). Also, the hydrophobic nature of pristine microplastics favors biofilm formation (Zettler et al. 2013; Rummel et al. 2017; Lacerda et al. 2019). Accumulation of biofilms and attachment of microorganisms on the surfaces of pristine microplastics can potentially alter their density (Rummel et al. 2017; Michels et al. 2018) and thus their settling velocities (Kaiser et al. 2017). While some

studies have suggested that the development of biofilms on microplastic surfaces increases the settling velocity (Kaiser et al. 2017), other recent studies have found no substantial changes in the settling rates (Leiser et al. 2020). However, there is still very little known about how the physical, biological, and chemical conditions in lakes (which are very different from oceans) affect the formation of biofilm on microplastics and how this affects their settling behavior (Leiser et al. 2020). For example, biofilms may make the surface of colonized particles “stickier,” facilitating the formation of aggregates with other suspended materials such as mineral sediments or organic matter (Rummel et al. 2017).

The temperature gradient in the stratified lake water column is associated with changes in the density and the viscosity of water. As a consequence, drag forces exerted on particles increase from the relatively warm epilimnion (lower viscosity) to the cold hypolimnion (higher viscosity). Microplastic transport is also influenced by turbulence occurring in the epilimnion, which is mainly driven by wind (Singh et al. 2019), and in the hypolimnion caused by internal hydrodynamic forces such as seiches, currents, and bed roughness (Kirillin et al. 2012; Nishri et al. 2015). Compared to laminar conditions in the metalimnion, turbulent mixing in the epilimnion and hypolimnion likely causes resuspension of the settling particles and increases their residence time in these zones (Reynolds 2006, pp. 70–71). Due to the largely laminar conditions in the metalimnion, the residence time of microplastics only depends on the settling velocity of the particle and the thickness of the layer.

In this work, we combine systematic laboratory experiments, lake incubations, and model calculations to understand the effect of microplastic properties on sedimentation behavior. We then estimate the residence time, accumulation in, and transfer of microplastics between, lake compartments via virtual lake simulations. The residence time is presented as a critical parameter for determining accumulation of microplastics in the water column and potential uptake and transfer within the lake ecosystem. We anticipate that the residence times of pristine microplastics are controlled by the physical properties of the particles, as well as lake properties, such as turbulent mixing and depth.

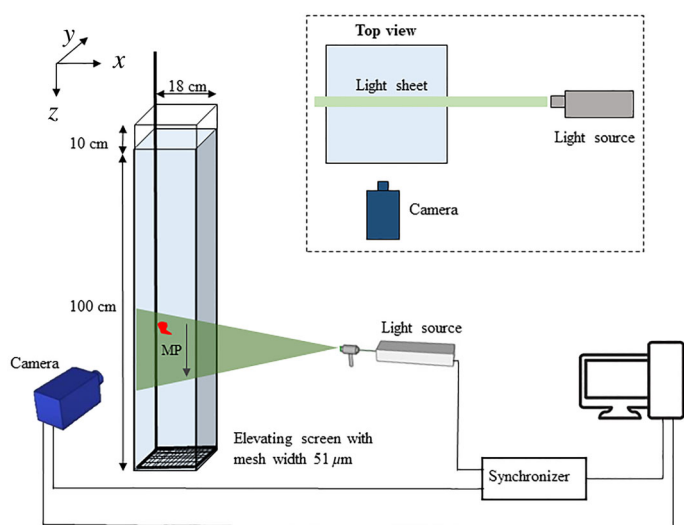
Methods

Characterization of microplastic particles

All biodegradable and nonbiodegradable fragments were provided by the Department of Macromolecular Chemistry at the University of Bayreuth, Germany. The selected polymers (Table 1) capture the dominant plastics produced by the plastic industry (Wright et al. 2013; Rocha-Santos and Duarte 2015). The size of the particles ranged between ~ 150 and ~ 2200 μm . The selection of various particles and polymer types aimed at assessing the effect of particle size, and polymer density on the settling velocity. The distinction between

Table 1. A list of all polymers used during settling velocity experiments and their measured densities.

Polymer	Abbreviation	Density (g cm ⁻³)	Type
Polystyrene	PS	1.03	Nonbiodegradable
Polyamide 66	PA66	1.12	Nonbiodegradable
Polyvinylchloride	PVC	1.38	Nonbiodegradable
Polycaprolactone	PCL	1.14	Biodegradable
Poly lactide	PLLA	1.20	Biodegradable
Polybutylenadipate terephthalate	PBAT	1.22	Biodegradable

**Fig. 1.** The water column and the setup of the two-dimensional particle image velocimetry system.

biodegradable and nonbiodegradable polymers was aimed at assessing the potential effect of polymer surface chemistry and polymer type on the settling behavior of microplastic particles in lakes. Also, several recent studies, such as Bagaev et al. (2017) and Waldschläger and Schüttrumpf (2019), focus mainly on non-biodegradable polymers. Our work extends the types of polymers assessed in sinking experiments to a potentially important class of plastics that may become more prevalent in the future as society move toward biodegradable plastics.

Particle geometries were determined in the laboratory using a light microscope and a high definition digital single-lens reflex camera (Zeiss Axioplan microscope and Cannon EOS 5D respectively). The maximum particle length A [L] and the minimum particle length C [L] in the XY -plane of each irregularly shaped particle were measured based on these images using ImageJ software (Schindelin et al. 2012) (Supporting Information Fig. S1). The XZ -plane length B [L] was estimated as the average of A and C as a necessary approximation due to only being able to acquire two-dimensional images with the microscope available. As all particles used in the experiments were irregularly shaped (Supporting Information Fig. S1, S2), the equivalent diameter of each particle was calculated based on the best-fitting ellipsoid. The equivalent spherical diameter for

each particle D_{eq} [L] was then calculated according to Eq. 1 using the value from the ellipsoid. The Corey shape factor (CSF) was also calculated as in Eq. 2. The CSF is widely used to describe the overall shape of the particles and can be calculated as the thickness of the particle divided by the geometric average of the other two dimensions. It ranges from 0 to 1.0 and it is correlated with particle flatness.

$$D_{eq} = \sqrt[3]{ABC}, \quad (1)$$

$$CSF = \frac{C}{\sqrt{A \cdot B}}. \quad (2)$$

The density of each nonbuoyant polymer was determined according to the procedure described in Waldschläger and Schüttrumpf (2019): Each particle was placed in a 50-mL glass beaker of distilled water. After the particle had sunk to the bottom, 1 μ L of zinc chloride solution was added. This procedure was repeated until the particle was in a stable suspension. One milliliter of the solution was then weighed to determine the density of the particle. This process was repeated three times for each polymer using three different particles and the average polymer density was calculated. Some of the particles initially did not sink, despite their densities exceeding that of water. This is thought to be due to the hydrophobic surface chemistry of the pristine plastic. To avoid this, the particles were pretreated for 20 min in an ultrasonic bath. The hydrophobicity effect was particularly noticeable for polystyrene as its polymer density 1.03 g cm⁻³ is very close to that of water.

Settling velocity measurements

Settling velocities of the microplastic particles were measured in a water-filled glass column with a cross-section of 18 cm \times 18 cm and a height of 1.10 m (Fig. 1) based on the design of Khatmullina and Isachenko (2017). At the bottom of the column, a filter mesh (width 51 μ m) was used to collect and retrieve the individual particles after each settling experiment. The glass column was also equipped with two thermometers to measure the water temperature during each experiment. The laboratory was air-conditioned at 20 \pm 1°C. Settling velocities were measured using tap water (density = 0.998 g cm⁻³, kinematic viscosity = 0.01 cm² s⁻¹, and oxygen content = 9.45 mg L⁻¹).

The settling velocity for each microplastic particle was determined using a two-dimensional particle image velocimetry system iLa 5150. The system consists of a high-speed camera (80 frames per second), a light source (high-power light-emitting diodes) with a wavelength = 530 nm, and hardware for synchronization (Fig. 1). The software can determine the settling velocities in two dimensions using the recorded image stream by cross-correlation of sequential pairs of images. The image pairs were used to analyze the settling path of each particle and the time elapsed. The system was tested for accuracy and precision. A reference particle (polyamide 66) with an equivalent diameter of 1.75 mm was measured seven times under identical conditions. After each measurement, the particle was collected using the mesh. The mean and relative standard deviation (RSD%) was $32 \text{ mm s}^{-1} \pm 7\%$.

Each particle was lowered slowly into the settling column using tweezers and released a few centimeters below the water surface. The settling velocity of each particle was measured after the particle had reached its estimated (Stokes) terminal velocity and a stable orientation in the water column. The particle image velocimetry setup was placed at the lowest third of the settling column. In total, between 60 and 70 settling experiments were conducted for each polymer amounting to a total of about 400 settling experiments.

Lake incubations

To measure the effects of biofilm colonization on microplastic settling behavior, polyamide 66, polystyrene, polyvinylchloride, polycaprolactone, polylactide, and polybutylenadipate terephthalate particles with a size range from 300 to 2200 μm , used previously as part of the settling experiments, were incubated in a pond close to the University of Bayreuth. All incubations started in January and the incubation periods were 6, 8, 10, and 30 weeks. Each particle was incubated in a separate glass tube that was sealed at both ends using stainless steel screens with a mesh size of 51 μm (Supporting Information Fig. S3). This design allowed microorganisms to enter the tubes and to colonize microplastic particles but did not allow the particles to be lost from the tubes. Several polystyrene particles (300 to 350 μm) were incubated in the same tube for 10 weeks to investigate potential particle–particle interactions and how this may be influenced by biofilms. The changes in size, density, and shape of each incubated particle were characterized following the same procedures as described for the pristine particles.

Colonization of microplastic particle surface with biofilm-building microorganisms was characterized by confocal laser scanning microscopy. Colonized microplastic particles were incubated in 100 μL staining solution for 20 min. All dyes and lectin-dye conjugates were used in a concentration of 1 $\mu\text{g ml}^{-1}$. DNA/RNA was stained using Syto 40. The DNA/RNA signal was used to visualize microbial cells whereas lectin-fluorophore conjugates were used to visualize the

extracellular polymeric substances (wheat germ agglutinin—Alexa Fluor 555, soybean agglutinin—Alexa Fluor 488, and peanut agglutinin—Alexa Fluor 647). After incubating the particles in the dyes, the samples were rinsed three times with tap water. Aggregates were analyzed in a Petri dish in their original hydrated condition. The images were collected with $\times 10$ and $\times 20$ water immersion lenses with numerical apertures of 0.3 and 0.6, respectively.

Finally, after incubation, the changes in the settling velocity of each particle were evaluated by comparing the settling velocity between the pristine and incubated particles. The density of the incubated particle was determined after the settling velocity measurements to keep the biofilm in its original state as the zinc chloride solution is likely to destroy the biofilm structure. In addition, the settling column was filled with filtered lake water so that changes in osmotic pressure would not disturb the delicate biofilm structure. The density and the viscosity of the filtered lake water were determined in the laboratory. The physical properties of the filtered lake water were essentially the same as tap water.

Settling velocity model

As most of the particles were irregularly shaped and relatively large ($> 0.1 \text{ mm}$) (Supporting Information Figs. S1, S2), the hydrodynamic flow conditions around the particles were likely to be at Reynolds number > 1.0 . To account for the non-spherical geometry of the particles the semiempirical model of Dietrich (1982) was used to calculate the theoretical settling velocities. Rather than expressing the results in the terms of Reynolds number and drag coefficient, Dietrich (1982) uses the terms of dimensionless particle size and dimensionless settling velocity (Supporting Information Eq. S4a–f). For small particles, Dietrich (1982) converges on Stokes' law (at about a dimensionless particle size less than 2.0). For the “large” particles, the model accounts for the progressive growth in the flow field separation which increases the drag pressure more rapidly for a given increase in the settling velocity. However, Dietrich (1982) notes that the equation should not be used for dimensionless particle size greater than 5×10^9 as the boundary layer around the particles becomes fully turbulent, reducing the flow separation and thus pressure drag. The Reynolds number and dimensionless particle size were checked for each particle to investigate the flow regime around the particles. The settling velocity formulas are presented in the Supporting information (Eq. S4a–f).

Continuum model for microplastic particles in a stratified lake

The residence times and particle number within a hypothetical lake system and the flux between lake compartments (epilimnion, metalimnion, and hypolimnion) were modeled using a generic continuum model for vertical microplastic transport. The model represents a lumped parameter approach

consisting of three interacting model sub-systems representing the epilimnion, metalimnion, and hypolimnion. For the epilimnion and hypolimnion, the model assumes fully mixed (turbulent) conditions represented by exponential transfer functions (i.e., exponential residence time distributions) as first implemented by Reynolds and Wiseman (1982) and Reynolds (1984, pp. 46–50) and summarized by Reynolds (2006, pp. 70–71) and Lampert and Sommer (2010, pp. 48–49). In this approach, rather than representing the hydrodynamic conditions of the different lake compartments explicitly using, for example, an eddy diffusion coefficient and calculating fluxes in one dimension, the effect of turbulent mixing was simplified using the transfer functions so that each sub-system could be treated as zero-dimensional. In reality, this means that the eddy diffusion coefficient is large enough that the system can be treated as well mixed on time-scales relevant for microplastic transport. For the metalimnion, the model assumes laminar flow conditions and settling behavior, where particles have a single residence time. The combination of the three lake compartments gives a set of three differential equations that are solved simultaneously (Eq. 3a–c):

$$\frac{dN_{\text{epi}}}{dt} = N_{\text{in}} - k_{\text{epi}}N_{\text{epi}}(t), \quad (3a)$$

$$\frac{dN_{\text{meta}}}{dt} = k_{\text{epi}}N_{\text{epi}}(t) - k_{\text{epi}}N_{\text{meta}}(t - \tau_{\text{meta}}), \quad (3b)$$

$$\frac{dN_{\text{hypo}}}{dt} = k_{\text{epi}}N_{\text{meta}}(t - \tau_{\text{meta}}) - k_{\text{hypo}}N_{\text{hypo}}(t). \quad (3c)$$

Equation 3a describes the dynamic change of microplastics in the epilimnion, where N_{in} [particles T^{-1}] represents a defined input flux of particles into the lake (e.g., via an inflowing river), $-k_{\text{epi}}N_{\text{epi}}(t)$ [particles T^{-1}] is the loss of particles to the metalimnion, and k_{epi} [T^{-1}] is a first-order exchange coefficient. Equation 3b calculates the microplastic particles in the metalimnion where τ_{meta} [T] is the residence time of the particles. The particle flux from the metalimnion into the hypolimnion is $-k_{\text{epi}}N_{\text{meta}}(t - \tau_{\text{meta}})$ [particles T^{-1}] while Eq. 3c represents the dynamic change of particles in the hypolimnion. The loss of particles from the lake to the sediments is $k_{\text{hypo}}N_{\text{hypo}}(t)$ [particles T^{-1}] where k_{hypo} [T^{-1}] is a first-order exchange coefficient similar to that in the epilimnion. The first-order exchange coefficients k_{epi} and k_{hypo} [T^{-1}] were calculated by $k_{\text{epi,hypo}} = \frac{1}{\tau_{\text{epi,hypo}}}$ with τ [T] being the mean residence time in each respective layer.

In the well-mixed layers, the residence times τ_{epi} [T] and τ_{hypo} [T] were defined as the time required until the particle number was reduced to $1/e \approx 0.368$ (i.e., 36%) of the initial

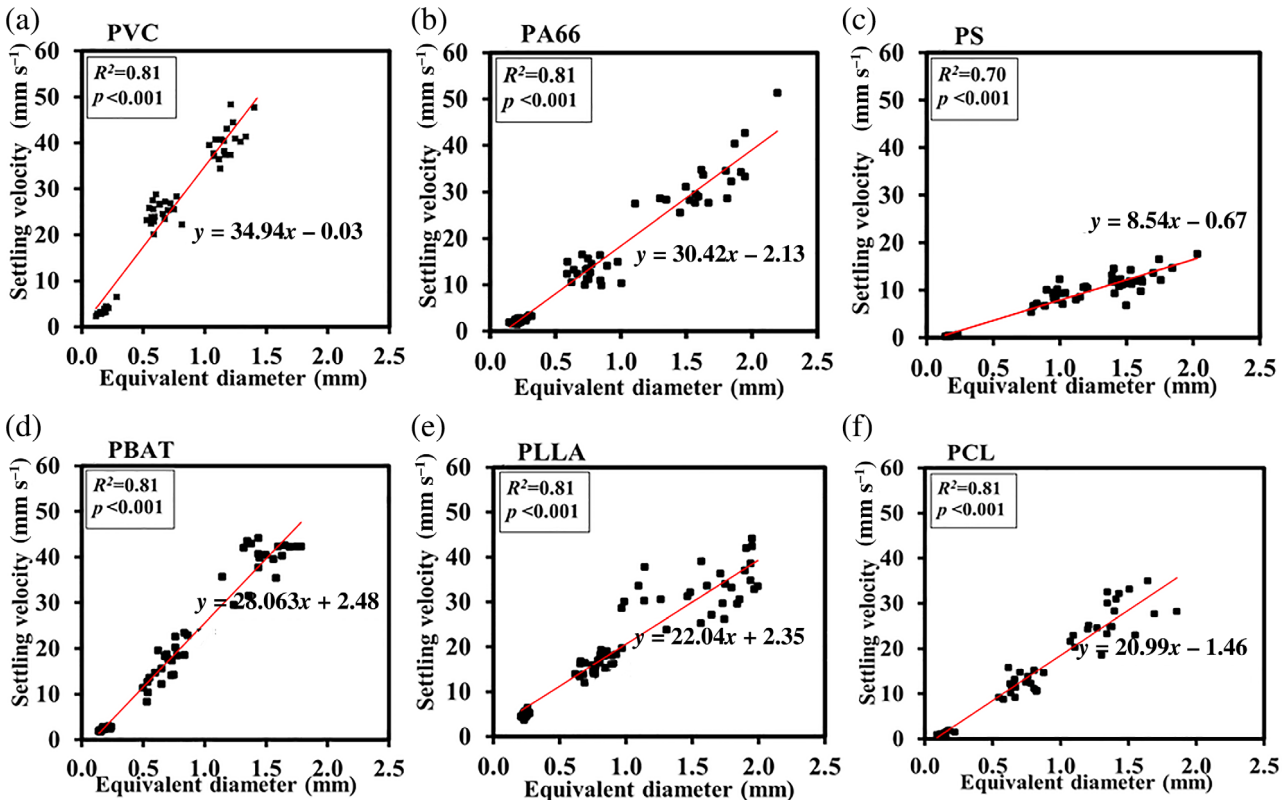


Fig. 2. Results of the experimentally measured settling velocities vs. equivalent diameter of the polyvinylchloride (PVC), polyamide 66 (PA66), polystyrene (PS), polybutylenadipate terephthalate (PBAT), polylactide (PLLA), and polycaprolactone (PCL) fragments, where p is the probability obtained from the t -test, R^2 (–) is the coefficient of determination, and the red line represents the regression line.

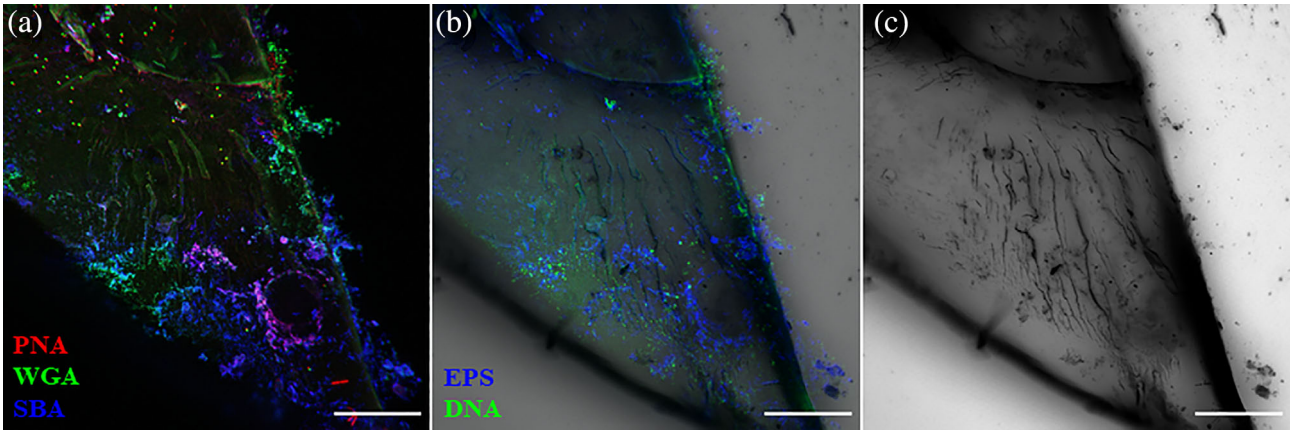


Fig. 3. Confocal laser scanning microscope images for the extracellular polymeric substances (EPS matrix) and microbial cells (DNA) colonizing the surfaces of a polyamide 66 particle after 10 weeks of incubation. (a) Peanut agglutinin (PNA), wheat germ agglutinin (WGA), and soybean agglutinin (SBA) lectins visualize the EPS matrix in a red, green, and blue overlay; (b) the EPS matrix and DNA are visible on the particle; and (c) the surface of the microplastic is shown in gray scale. The length of the scale bar is 150 μm .

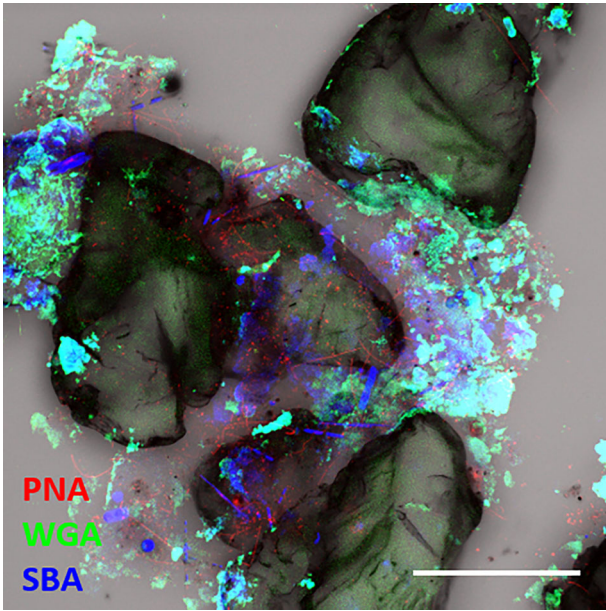


Fig. 4. A confocal laser scanning microscope image of the aggregation of polystyrene particles after 10 weeks of incubation. Peanut agglutinin (PNA), wheat germ agglutinin (WGA), and soybean agglutinin (SBA) lectins visualize the EPS matrix in a red, green, and blue overlay. The length of the scale bar is 150 μm .

particle concentrations (Reynolds 2006, pp. 70–71). The residence time in the metalimnion τ_{meta} [T] was calculated by dividing the thickness z_{meta} [L] of the layer by the laminar settling velocity of the particle. Values for the mean residence time were estimated according to Eq. 4, where v_s [LT^{-1}] represents the laminar settling velocities for microplastics in the relevant lake compartment and z [L] is the corresponding thickness of the epilimnion, metalimnion, or hypolimnion.

$$\tau_{\text{epi,meta,hypo}} = \frac{z_{\text{epi,meta,hypo}}}{v_{s_{\text{epi,meta,hypo}}}} \quad (4)$$

For simplicity, and to illustrate the effect of microplastic particle size on residence time, the model was run using settling velocity data from polystyrene spheres. The laminar settling velocities of the polystyrene spheres (1, 10, 500, and 1000 μm) were measured using the same procedures mentioned before. To account for the changes in the settling velocities of the microplastics due to the change of the water temperature in each lake compartment, the settling velocities were corrected as in Ghawi and Kris (2012) using their eq. S5. The dynamic model was constructed and solved using the Simulink toolbox included in MATLAB.

In addition to the dynamic model above, a simplified steady-state solution for Eqs. 3a–c assuming a constant particle influx $\dot{N}_{\text{in}} = \text{const}$, was derived for the particle number in each lake compartment:

$$N_{\text{epi}} = \frac{\dot{N}_{\text{in}}}{k_{\text{epi}}} = \dot{N}_{\text{in}} \tau_{\text{epi}}, \quad (5a)$$

$$N_{\text{meta}} = \frac{\dot{N}_{\text{in}}}{k_{\text{epi}}} \left[e^{(k_{\text{epi}} \tau_{\text{meta}})} - 1 \right], \quad (5b)$$

$$N_{\text{hypo}} = \frac{\dot{N}_{\text{in}}}{k_{\text{hypo}}} = \dot{N}_{\text{in}} \tau_{\text{hypo}}. \quad (5c)$$

This steady-state solution was used to quantify the relative distribution of microplastic particles in each lake compartment of thermally stratified lakes. In particular, the ratio between particles located in the epilimnion and hypolimnion ($N_{\text{epi}}/N_{\text{hypo}}$) was used as a characteristic parameter to compare lake systems. This ratio can be used to rapidly determine if most microplastic particles will be found in the epilimnion or the hypolimnion, which is important as the epilimnion is where microplastics are most likely to be taken up by organisms such as filter feeders. In this model, the ratio $N_{\text{epi}}/N_{\text{hypo}}$ only

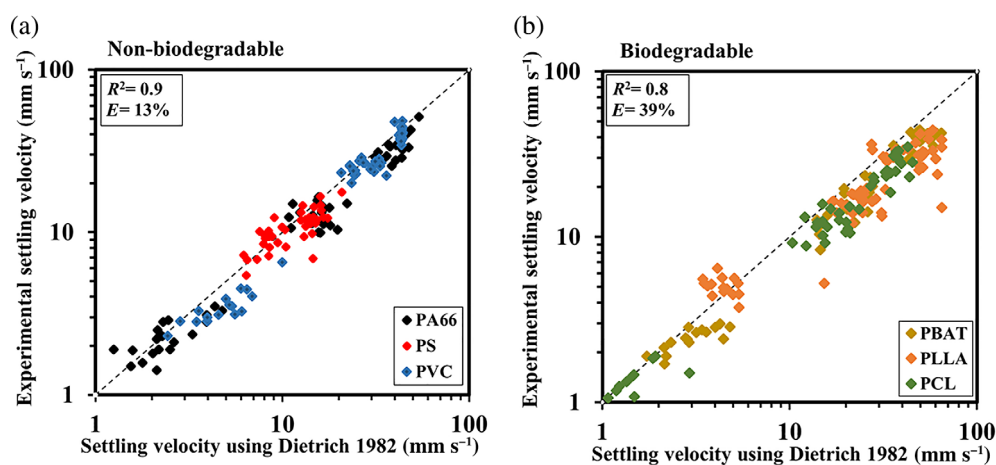


Fig. 5. A comparison between the experimental settling velocities and Dietrich model for the nonbiodegradable polyvinylchloride (PVC), polyamide 66 (PA66), polystyrene (PS), and biodegradable polybutylenadipate terephthalate (PBAT), polylactide (PLLA), and polycaprolactone (PCL) particles, where E is the relative error (%), and R^2 (–) is the coefficient of determination. The dashed line presents the 1 : 1 line.

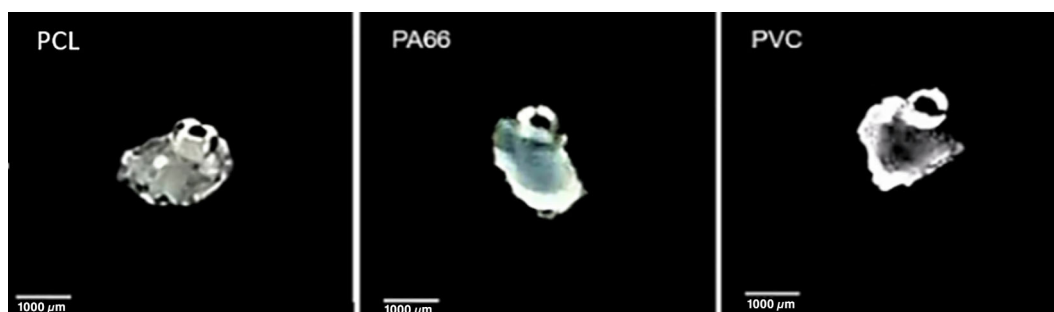


Fig. 6. Attachment of fine air bubbles on the surfaces of polycaprolactone (PCL), polyamide 66 (PA66), and polyvinylchloride (PVC) particles during the settling velocity experiments.

depends on $\tau_{\text{epi}}/\tau_{\text{hypo}}$, which can be expressed as $\frac{v_{s,\text{epi}}}{v_{s,\text{hypo}}} \cdot \frac{z_{\text{epi}}}{z_{\text{hypo}}}$. The relationship $N_{\text{epi}}/N_{\text{hypo}} = f(v_{s,\text{epi}}/v_{s,\text{hypo}}, z_{\text{epi}}/z_{\text{hypo}})$ is universally valid for all types of microplastics (independent of size, shape, and density) as long as the ratio $v_{s,\text{epi}}/v_{s,\text{hypo}}$ in a lake system is constant. This implies that $N_{\text{epi}}/N_{\text{hypo}}$ only depends on lake characteristics such as the temperature and thickness of each compartment.

Results

Settling velocities of pristine particles

The settling velocities for the six polymers ranged between ~ 0.30 and ~ 50 mm s⁻¹ (Fig. 2). Supporting Information Fig. S6 presents the distribution of the CSF of the microplastic particles. The results show a clear dependence of the settling velocities on particle size, with a coefficient of determination (R^2) between 0.70 and 0.81 and a high statistical significance ($p < 0.001$). In addition, the effect of polymer density on the settling velocity was clearly visible in the slope of the regression lines. Polymers with high density were consistently associated with a steeper slope, and thus a faster settling velocity. The calculated Reynolds number for the particles varied

between 0.05 and 130, thus being at the transition between laminar and the intermediate regimes.

Biofilm-coated particles

No significant changes were observed in the density, shape, or roundness of the incubated particles, even after 30 weeks of incubation (Supporting Information Fig. S7). However, the confocal laser scanning microscope images at 10 weeks incubation clearly showed a varying abundance of biofilms on the microplastic particle surface (Fig. 3). These were mainly composed of microbial cells and extra polymeric substances. The surfaces of the particles were only partially covered with biofilm, where it was concentrated in a few dense spots.

The potential formation of aggregates was investigated by incubating various polystyrene particles with an average equivalent diameter between 300 and 350 μm for 10 weeks in a single tube. The sample shown in Fig. 4 has a high abundance of extra polymeric substances despite the surface of the particles not being densely colonized by microbial cells. It also shows that individual polystyrene particles in combination

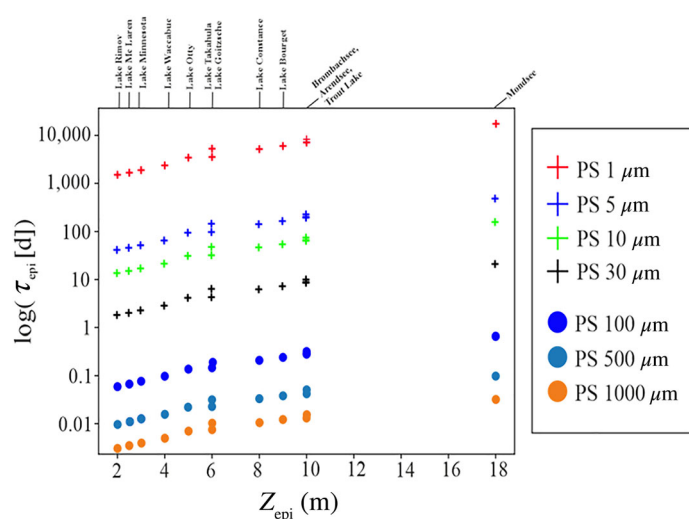


Fig. 7. Dependency of the mean residence time τ (d) on the particle size of the polystyrene (PS) particles, and depth of the epilimnion Z_{epi} (m). Note the logarithmic scale.

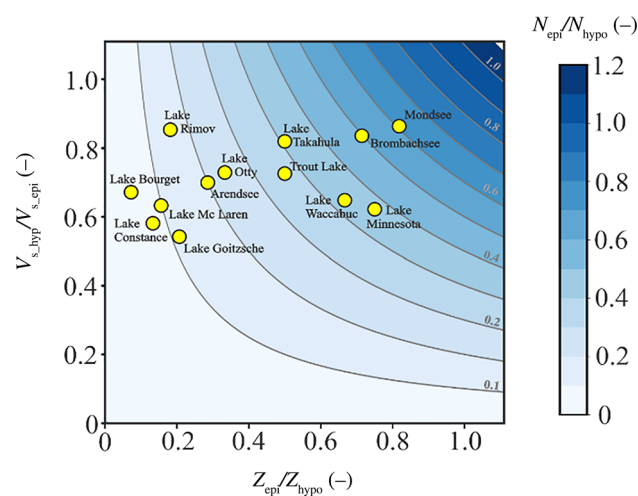


Fig. 8. Relative abundance for microplastics (N_{epi}/N_{hypo}) in the epilimnion and hypolimnion assuming steady-state conditions for different lake systems as a function of the settling velocity (v_{s_hypo}/v_{s_epi}) and depth (Z_{epi}/Z_{hypo}) ratios.

with the extra polymeric substances form a larger aggregate with the biofilm appearing to act as an “adhesive.”

After 6, 8, 10, and 30 weeks of incubation, no substantial differences in sedimentation rates between pristine and incubated microplastic particles were observed (Supporting Information Fig. S8). The maximum deviation in the mean settling velocities was $\pm 5\%$ which is within the measurement error of the particle image velocimetry system. An F -test and paired t -test confirmed that there was no significant difference ($p > 0.05$) before and after incubation in either means or variance. Both incubated and pristine particles followed much the

same settling trajectories after the incubation periods (Supporting Information Fig. S9).

Calculated settling velocity

Despite significant scatter in the data, the measured settling velocities were systematically lower than those calculated using Dietrich (1982) (Fig. 5). The nonbiodegradable particles had significantly less scatter around the 1 : 1 line than biodegradable polymers (Fig. 5). During the experiments, it was observed that fine air bubbles tend to attach to the surfaces of all polymer types and most obviously on the biodegradable microplastic particles (Fig. 6), despite all particles being pretreated in an ultrasonic bath prior to the experiments.

Residence times of microplastics in stratified lakes

The effect of particle size on the mean residence time in the epilimnion for 13 different lake systems is shown in Fig. 7. The mean depths of the epilimnion (Z_{epi}) during summer during stratified conditions ranged from 2 to 18 m. The modeled epilimnic mean residence times for the various lakes depended strongly on particle size and to a lesser extent on the polymer type. For the large microplastic particles (100–1000 μm), the modeled mean residence time was less than 1 d for all lakes. In contrast, the mean residence times for the smallest microplastic particles (1–30 μm) were orders of magnitudes higher, with residence times up to 10,000 d for 1- μm particles in the Mondsee.

Relative particle abundance (N_{epi}/N_{hypo}) for the selected lake systems during steady-state conditions is shown in Fig. 8. These lakes show a large variation in the Z_{epi}/Z_{hypo} ratios, ranging between 0.1 and 0.8. As the lake data was measured entirely during stratification in the summer months, water temperatures for the hypolimnion were consistently lower than the epilimnion, leading to $v_{s_hypo}/v_{s_epi} < 1$ (higher viscosities in the cold hypolimnion). The N_{epi}/N_{hypo} ranged between < 0.1 for the larger lakes such as Lake Constance in Germany and 0.6 for the Mondsee in Austria and shows that the proportion of microplastics found in either the epilimnion or hypolimnion scales with the Z_{epi}/Z_{hypo} . Interestingly, the Mondsee has the highest N_{epi}/N_{hypo} ratio (> 0.6), meaning the majority of microplastics will be found in the epilimnion and the highest mean epilimnic residence time ($\sim 10,000$ d for 1- μm particles). This maximizes the probability of microplastic uptake by filter feeders and other organisms at the base of the food chain that are generally found in the epilimnion. In contrast, for Lake Constance, Lake Bourget, and Lake McLaren most of the microplastics should be found in the hypolimnion ($N_{epi}/N_{hypo} < 0.1$) despite often substantial residence time in the epilimnion (Fig. 8).

As an example to demonstrate how the redistribution of particles occurs between the different lake compartments, the dynamic model was used to calculate the flux of polystyrene spheres (Supporting Information Fig. S10) with a size range of 1, 10, 500, and 1000 μm to a virtual lake loosely based on Upper Lake Constance (Fig. 9). One hundred meters of the stratified lake water column were modeled using the data from

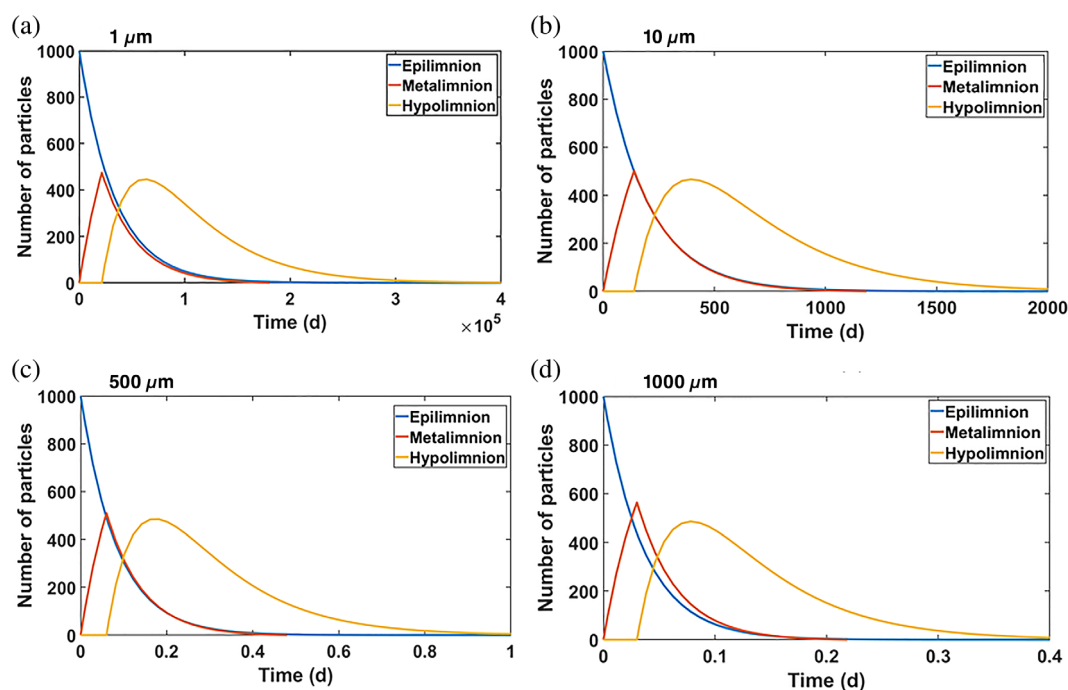


Fig. 9. Simulation results of 1-, 10-, 500-, and 1000- μm polystyrene spheres showing the modeled numbers of the accumulated microplastics in each lake compartment vs. elapsed time in Upper Lake Constance on Day 319 according to lake data from Appt et al. (2004). The simulations were initiated with a pulse of 1000 spherical polystyrene particles uniformly distributed in the well-mixed epilimnion.

Appt et al. (2004) (Supporting Information Table S11). The simulations were initiated with a pulse of 1000 spherical polystyrene particles that were uniformly distributed in the well-mixed epilimnion (Fig. 9). The microplastic numbers in the epilimnion decreased exponentially following the pulse. In contrast, in the metalimnion and the hypolimnion, the microplastic particles initially increased as they received particles from the overlying lake layer. Microplastic numbers in the metalimnion and hypolimnion started to decrease after the loss rate to the underlying layer (or sediment in the case of the hypolimnion) exceeded the input rate from the overlying layer. The modeling results showed that the residence time τ (d) in each layer was very strongly dependent on particle size, similarly to the steady-state model.

Discussions

Various factors such as particle size, polymer density, hydrophobicity of the particle surface, biofouling, water temperature, and turbulent mixing control the residence times of microplastics in lakes. These factors, combined with high or constant input of microplastics will increase the probability that microplastics will be ingested by aquatic organisms and potentially be transferred within the lake food chain (Nelms et al. 2018).

The experimentally determined settling velocities showed that the density and size of the microplastics are the most critical parameters controlling the settling velocity. Since the

microplastic settling velocity during laminar conditions depends on their weight, drag forces, and buoyancy forces, all large and dense particles have significantly higher settling velocities than the smaller and lighter microplastics.

As the CSF describes the flatness of the particle and it depends only on the ratio between the three axes of the particles rather than its size, it was experimentally difficult to isolate the effect of particle shape on the settling velocity, separating it from that of density and size. This problem was exacerbated by the fact that all particles were similar in shape, despite being irregular (having similar CSF) (Supporting Information Fig. S1, S2) and no fibers or special geometric objects such as cubes, cylinders, or discs were used in the experiments.

We originally expected rapid and somewhat uniform colonization of the particles by biofilms (Zettler et al. 2013; Rummel et al. 2017). However, the confocal laser scanning microscope images showed that the biofilm rather forms dense patches with large parts of the particles left uncolonized. The formation of biofilm and in particular the presence of a thick extra polymeric substance increased the tendency for microplastic aggregation, which is consistent with findings from Rummel et al. (2017). Such aggregates are larger and likely to have different surface properties, densities, and shapes compared to the pristine particles, which should result in different physical behavior within the water column (Leiser et al. 2020).

The literature suggests that the colonization process alters the polarity of the plastic surface, changing it from hydrophobic to hydrophilic (Michels et al. 2018; Tu et al. 2020; van

Melkebeke et al. 2020), increases the density of the particle (Rummel et al. 2017; Michels et al. 2018), and reduces the attachment of air bubbles on the surface (Renner et al. 2020). Therefore, it was anticipated that the settling velocity would increase after incubation. However, no measurable changes in the physical properties or sedimentation behavior were observed. This may be due to the “short” incubation periods of 6, 8, 10, and 30 weeks. Also, the pond was frozen for the first 3 weeks of incubation during the winter season which may explain the small volumes of biofilm accumulated on the particle surface, assuming that the metabolism of the biofilm-building organisms was affected by the low temperatures (Farhat et al. 2016).

In accordance with Waldschläger and Schüttrumpf (2019); van Melkebeke et al. (2020), the settling velocities of the microplastics were not well described using the traditional sediment settling equation of Dietrich (1982). We believe this is due to the hydrophobicity of the microplastic surfaces, which is conducive to the formation of fine air bubbles, which then increased the buoyancy force exerted on the settling particle and reduced their settling velocity. Since Dietrich (1982) was originally developed for mineral particles, the hydrophobic adhesion between microplastics and air bubbles did not play a role in the settling behavior. Whether microplastic remains hydrophobic in the environment or not likely depends on microplastic surface properties, for example, after biofilm colonization. Pristine microplastics are unlikely to be found in natural aquatic environments as they are usually rapidly colonized by biofilms or adsorb natural material such as dissolved organic carbon or mineral precipitates (e.g., iron oxides) (Leiser et al. 2020). Also, measuring the size of particles from two-dimension images may not properly capture the third dimension of the particles. This is a potential source of error in the calculations of the theoretical settling velocities. These observations suggest, however, that the settling behavior of microplastic is more complex than in simplified theoretical models and more advanced methods such as computational fluid dynamics should be used to investigate this more exactly.

In the lake model, the epilimnion and the hypolimnion were presented as well-mixed systems to mimic turbulent processes within these layers during the thermal stratification. In contrast, the metalimnion was assumed to be laminar. The residence time of microplastics in the metalimnion is relatively short compared to the epilimnion and hypolimnion due to the lack of mixing processes as well as to a limited thickness. The extremely long residence time for small microplastic particles in the epilimnion in particular forms a high uptake probability for aquatic organisms such as filter feeders. This lake model has, however, a highly simplified and theoretical representation of residence times in the three lake compartments. Real lake systems are considerably more complex than these simplified representations of lake physics. In real lakes, the residence times of the settling microplastics are likely coupled with the changes in lakes' hydrodynamics such as temperature fluctuation, waves, transient turbulence, or

lake mixing in autumn and spring as stratification destabilizes. Also, lake retention time (flushing time), which is strongly dependent on the internal physical processes and water fluxes from the catchment (Ambrosetti et al. 2003), plays a decisive role in how long the microplastics will actually reside in a lake, and thus how long organisms have the opportunity to ingest them. Calculated residence times were on the order of 10^5 d for the smallest particles, meaning that the flushing time is significantly shorter than the residence time for most lakes, and thus is not really a meaningful number for a real lake system such as Lake Constance, which has a theoretical average flushing time of 4.5 years (Wessels 2015). It does suggest, however, that there should only be a negligible amount of microplastics of this size range found in the lake sediments unless some process increases their settling velocity, for example, aggregation with existing lake particles and detritus or uptake and death of organisms or egestion via fecal pellets. In addition, the biologically driven mixing of the water column due to the vertical migration of zooplankton increase turbulence in the water column (Dean et al. 2016) which may cause resuspension and redistribution of the microplastics, which may be particularly important in the hypolimnion.

Conclusion

This research aimed to identify the primary controls and time scales of microplastic residence times in stratified lake systems. By combining laboratory experiments and modeling, it was clear that microplastic residence times in the lake water column highly depend on the size and to a less extent the density of the particle, varying over many orders of magnitude. The comparison between laboratory-measured and calculated settling velocities using Dietrich (1982) showed that hydrophobic surface properties of the pristine microplastics are a key factor that needs to be considered when estimating settling velocities. It is expected that the hydrophobic adhesion between pristine microplastics and fine air bubbles can increase the buoyancy forces exerted on the particles and increase their residence time in the lake water column.

The microplastic polymers incubated in a small lake were effectively and rapidly colonized by biofilm and included bacteria cells and extra polymeric substances. However, the settling experiments did not show any substantial differences in the sedimentation trajectories and velocities between individual (i.e., not aggregates) pristine and incubated microplastics. The presence of biofilms on the surfaces of incubated microplastics did tend to favor the formation of aggregates. These aggregates are expected to sink faster and to have shorter residence time than individual pristine microplastics because of their increase in size and changes in surface properties.

Our lumped parameter modeling approach is a simple way to estimate residence times, fluxes, and numbers of microplastics in the epilimnion, metalimnion, and hypolimnion during both steady-state and dynamic conditions. The functional relationship

$N_{\text{epi}}/N_{\text{hypso}}$ allows a rapid assessment of where most microplastics will be found in different lakes and is independent of the input influx to the lake as long as the ratio $v_{s,\text{epi}}/v_{s,\text{hypso}}$ is constant. Also, the modeling approach was capable of showing the dynamic redistribution of microplastics in the stratified lake water column. The accumulated numbers and residence times of microplastics in the three lake compartments varied over several orders of magnitude and were strongly dependent on particle size as well as physical lake properties such as depth and temperature of the hypolimnion, metalimnion, and epilimnion. This is crucial for the uptake of microplastics by, for example, filter feeders, in lake systems. The simulated residence times suggest that significant numbers of microplastics should be found in lake sediment as long as their residence time is shorter than lake flushing time. In contrast, small microplastics with residence times significantly longer than lake flushing time are unlikely to be found in large numbers in lake sediment unless some biological or physical processes increase their settling velocity to deliver them to the lake bottom.

Data availability statement

Data are archived on CRC 1357 cloud storage and available on request.

References

- Agarwal, S. 2020. Biodegradable polymers: Present opportunities and challenges in providing a microplastic-free environment. *Macromol. Chem. Phys.* **221**: 2000017. doi:10.1002/macp.202000017
- Aljaibachi, R., and A. Callaghan. 2018. Impact of polystyrene microplastics on *Daphnia magna* mortality and reproduction in relation to food availability. *PeerJ* **6**: e4601. doi:10.7717/peerj.4601
- Ambrosetti, W., L. Barbanti, and N. Sala. 2003. Residence time and physical processes in lakes. *J. Limnol.* **62**: 1. doi:10.4081/jlimnol.2003.s1.1
- Appt, J., J. Imberger, and H. Kobus. 2004. Basin-scale motion in stratified Upper Lake Constance. *Limnol. Oceanogr.* **49**: 919–933. doi:10.4319/lo.2004.49.4.0919
- Arthur, C., J. Baker, and H. Bamford. 2009. Proceedings of the International Research Workshop on the Occurrence, Effects and Fate of Microplastic Marine Debris, 9–11 September 2008. NOAA Technical Memorandum NOS-OR&R-30.
- Bagaev, A., A. Mizyuk, L. Khatmullina, I. Isachenko, and I. Chubarenko. 2017. Anthropogenic fibres in the Baltic Sea water column: Field data, laboratory and numerical testing of their motion. *Sci. Total Environ.* **599–600**: 560–571. doi:10.1016/j.scitotenv.2017.04.185
- Bellasi, A., G. Binda, A. Pozzi, S. Galafassi, P. Volta, and R. Bettinetti. 2020. Microplastic contamination in freshwater environments: A review, focusing on interactions with sediments and benthic organisms. *Environments* **7**: 30. doi:10.3390/environments7040030
- Browne, M. A., T. Galloway, and R. Thompson. 2007. Microplastic—An emerging contaminant of potential concern? *Integr. Environ. Assess. Manag.* **3**: 559–561. doi:10.1002/ieam.5630030412
- Cole, M., P. K. Lindeque, E. Fileman, J. Clark, C. Lewis, C. Halsband, and T. S. Galloway. 2016. Microplastics alter the properties and sinking rates of zooplankton faecal pellets. *Environ. Sci. Technol.* **50**: 3239–3246. doi:10.1021/acs.est.5b05905
- Dean, C., A. Soloviev, A. Hirons, T. Frank, and J. Wood. 2016. Biomixing due to diel vertical migrations of zooplankton: Comparison of computational fluid dynamics model with observations. *Ocean Model.* **98**: 51–64. doi:10.1016/j.ocemod.2015.12.002
- Dietrich, W. E. 1982. Settling velocity of natural particles. *Water Resour. Res.* **18**: 1615–1626. doi:10.1029/WR018i006p01615
- Farhat, N. M., J. S. Vrouwenvelder, M. C. M. van Loosdrecht, S. S. Bucs, and M. Staal. 2016. Effect of water temperature on biofouling development in reverse osmosis membrane systems. *Water Res.* **103**: 149–159. doi:10.1016/j.watres.2016.07.015
- Fischer, E. K., L. Paglialonga, E. Czech, and M. Tamminga. 2016. Microplastic pollution in lakes and lake shoreline sediments—a case study on Lake Bolsena and Lake Chiuse (Central Italy). *Environ. Pollut.* **213**: 648–657. doi:10.1016/j.envpol.2016.03.012
- Geyer, R., J. R. Jambeck, and K. L. Law. 2017. Production, use, and fate of all plastics ever made. *Sci. Adv.* **3**: e1700782. doi:10.1126/sciadv.1700782
- Ghawi, A. H., and J. Kris. 2012. A computational fluid dynamics model of flow and settling in sedimentation tanks. *In* H. W. Oh [ed.], *Computational fluid dynamics (CFD) and discrete element method (DEM) applied to centrifuges*. INTECH Open Access Publisher.
- Kaiser, D., N. Kowalski, and J. J. Waniek. 2017. Effects of biofouling on the sinking behavior of microplastics. *Environ. Res. Lett.* **12**: 124003. doi:10.1088/1748-9326/aa8e8b
- Khatmullina, L., and I. Isachenko. 2017. Settling velocity of microplastic particles of regular shapes. *Mar. Pollut. Bull.* **114**: 871–880. doi:10.1016/j.marpolbul.2016.11.024
- Kirillin, G., H.-P. Grossart, and K. W. Tang. 2012. Modeling sinking rate of zooplankton carcasses: Effects of stratification and mixing. *Limnol. Oceanogr.* **57**: 881–894. doi:10.4319/lo.2012.57.3.0881
- Lacerda, A. L. D. F., and others. 2019. Plastics in sea surface waters around the Antarctic Peninsula. *Sci. Rep.* **9**: 3977. doi:10.1038/s41598-019-40311-4
- Lampert, W., and U. Sommer. 2010. Limnology. *In* *The ecology of lakes and streams*, 2nd ed. Univ. Press.
- Leiser, R., G.-M. Wu, T. R. Neu, and K. Wendt-Potthoff. 2020. Biofouling, metal sorption and aggregation are related to sinking of microplastics in a stratified reservoir. *Water Res.* **176**: 115748. doi:10.1016/j.watres.2020.115748

- Meides, N., and others. 2021. Reconstructing the environmental degradation of polystyrene by accelerated weathering. *Environ. Sci. Technol.* **55**: 7930–7938. doi:10.1021/acs.est.0c07718
- Michels, J., A. Stippkugel, M. Lenz, K. Wirtz, and A. Engel. 2018. Rapid aggregation of biofilm-covered microplastics with marine biogenic particles. *Proceedings. Biological sciences* **285**: 20181203. doi:10.1098/rspb.2018.1203
- Nelms, S. E., T. S. Galloway, B. J. Godley, D. S. Jarvis, and P. K. Lindeque. 2018. Investigating microplastic trophic transfer in marine top predators. *Environ. Pollut.* **238**: 999–1007. doi:10.1016/j.envpol.2018.02.016
- Nguyen, T. H., F. H. M. Tang, and F. Maggi. 2020. Sinking of microbial-associated microplastics in natural waters. *PLoS One* **15**: e0228209. doi:10.1371/journal.pone.0228209
- Nishri, A., A. Rimmer, and Y. Lechinsky. 2015. The mechanism of hypolimnion warming induced by internal waves. *Limnol. Oceanogr.* **60**: 1462–1476. doi:10.1002/lno.10109
- Ramsperger, A. F. R. M., and others. 2020. Structural diversity in early-stage biofilm formation on microplastics depends on environmental medium and polymer properties. *Water* **12**: 3216. doi:10.3390/w12113216
- Renner, G., A. Nellesen, A. Schwieters, M. Wenzel, T. C. Schmidt, and J. Schram. 2020. Hydrophobicity-water/air-based enrichment cell for microplastics analysis within environmental samples: A proof of concept. *MethodsX* **7**: 100732. doi:10.1016/j.mex.2019.11.006
- Reynolds, C. S. 1984. *The ecology of freshwater phytoplankton*. Cambridge Univ. Press.
- Reynolds, C. S. 2006. *The ecology of phytoplankton*. Cambridge Univ. Press.
- Reynolds, C. S., and S. W. Wiseman. 1982. Sinking losses of phytoplankton in closed limnetic systems. *J. Plankton Res.* **4**: 489–522. doi:10.1093/plankt/4.3.489
- Rocha-Santos, T., and A. C. Duarte. 2015. A critical overview of the analytical approaches to the occurrence, the fate and the behavior of microplastics in the environment. *TrAC Trends Anal. Chem.* **65**: 47–53. doi:10.1016/j.trac.2014.10.011
- Rummel, C. D., A. Jahnke, E. Gorokhova, D. Kühnel, and M. Schmitt-Jansen. 2017. Impacts of biofilm formation on the fate and potential effects of microplastic in the aquatic environment. *Environ. Sci. Technol. Lett.* **4**: 258–267. doi:10.1021/acs.estlett.7b00164
- Schindelin, J., and others. 2012. Fiji: An open-source platform for biological-image analysis. *Nat. Methods* **9**: 676–682. doi:10.1038/nmeth.2019
- Singh, P., J. Bagrania, and A. K. Haritash. 2019. Seasonal behaviour of thermal stratification and trophic status in a sub-tropical Palustrine water body. *Appl. Water Sci.* **9**: 139. doi:10.1007/s13201-019-1011-z
- Sun, J., X. Dai, Q. Wang, M. C. M. van Loosdrecht, and B.-J. Ni. 2019. Microplastics in wastewater treatment plants: Detection, occurrence and removal. *Water Res.* **152**: 21–37. doi:10.1016/j.watres.2018.12.050
- Toussaint, B., and others. 2019. Review of micro- and nanoplastic contamination in the food chain. *Food Addit. Contam. Part A Chem. Anal. Control Expo. Risk Assess.* **36**: 639–673. doi:10.1080/19440049.2019.1583381
- Tu, C., T. Chen, Q. Zhou, Y. Liu, J. Wei, J. J. Waniek, and Y. Luo. 2020. Biofilm formation and its influences on the properties of microplastics as affected by exposure time and depth in the seawater. *Sci. Total Environ.* **734**: 139237. doi:10.1016/j.scitotenv.2020.139237
- van Melkebeke, M., C. Janssen, and S. de Meester. 2020. Characteristics and sinking behavior of typical microplastics including the potential effect of biofouling: Implications for remediation. *Environ. Sci. Technol.* **54**: 8668–8680. doi:10.1021/acs.est.9b07378
- Waldschläger, K., and H. Schüttrumpf. 2019. Effects of particle properties on the settling and rise velocities of microplastics in freshwater under laboratory conditions. *Environ. Sci. Technol.* **53**: 1958–1966. doi:10.1021/acs.est.8b06794
- Wessels, M. 2015. Bathymetry of Lake Constance—A high-resolution survey in a large, deep Lake. *zfv – Zeitschrift für Geodäsie, Geoinformation und Landmanagement.* **140**: 203–210. doi:10.12902/zfv-0079-2015
- Worm, B., H. K. Lotze, I. Jubinville, C. Wilcox, and J. Jambeck. 2017. Plastic as a persistent marine pollutant. *Annu. Rev. Env. Resour.* **42**: 1–26. doi:10.1146/annurev-environ-102016-060700
- Wright, S. L., R. C. Thompson, and T. S. Galloway. 2013. The physical impacts of microplastics on marine organisms: A review. *Environ. Pollut.* **178**: 483–492. doi:10.1016/j.envpol.2013.02.031
- Zettler, E. R., T. J. Mincer, and L. A. Amaral-Zettler. 2013. Life in the “plastisphere”: Microbial communities on plastic marine debris. *Environ. Sci. Technol.* **47**: 7137–7146. doi:10.1021/es401288x

Acknowledgments

Funded by the Deutsche Forschungsgemeinschaft (DFG, German Research Foundation)—Project Number 391977956—SFB 1357. The authors would like to thank Peter Strohrig for providing microplastic particles for the settling experiments, Antonia Freiburger for her support during confocal laser scanning microscope experiments, and Ulrich Mansfeld and Martina Heider for the scanning electron microscope images. Open Access funding enabled and organized by Projekt DEAL.

Conflict of interest

None declared.

Submitted 09 August 2021

Revised 16 November 2021

Accepted 06 February 2022

Associate editor: Yong Liu

Supplementary Information

Measuring of microplastics settling velocities and implications for residence times in thermally stratified lakes

Hassan Elagami^{1,3*}, Pouyan Ahmadi², Jan H. Fleckenstein^{2,6}, Sven Frei³, Martin Obst⁴,
Seema Agarwal⁵, Benjamin S. Gilfedder^{1,3}

¹Limnological Research Station, Bayreuth Center of Ecology and Environmental Research
University of Bayreuth, Bayreuth, Germany

²Department of Hydrogeology, Helmholtz Centre for Environmental Research – UFZ, Leipzig, Germany

³Department of Hydrology, Bayreuth Center of Ecology and Environmental Research (BayCEER),
University of Bayreuth, Bayreuth, Germany

⁴Experimental Biogeochemistry, BayCEER, Bayreuth, Germany

⁵Macromolecular Chemistry II, University of Bayreuth, Bayreuth, Germany

⁶Hydrologic Modelling Unit, Bayreuth Center of Ecology and Environmental Research (BayCEER),
University of Bayreuth, Bayreuth, Germany

Corresponding Author:

Hassan Elagami: Limnological Research Station, & Department of Hydrology, Bayreuth Center of Ecology and Environmental Research (BayCEER), University of Bayreuth, Bayreuth, Germany;
orcid.org/0000-0002-2919-5230; Email: hassan.elagami@uni-bayreuth.de

S1) Characterization of microplastics from various polymer types

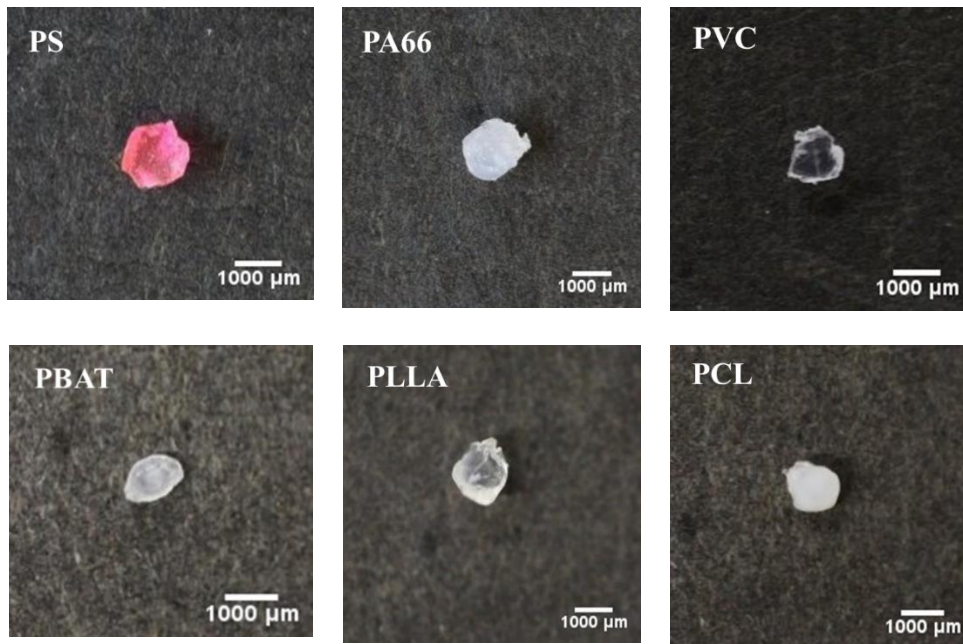


Figure S1: An example of polystyrene (PS), polyamide 66 (PA66), polyvinylchloride (PVC), polycaprolactone (PCL), polylactide (PLLA), and polybutylenadipate terephthalate (PBAT) particles investigated under the camera.

S2) Polystyrene fragments investigated under scanning electron microscope

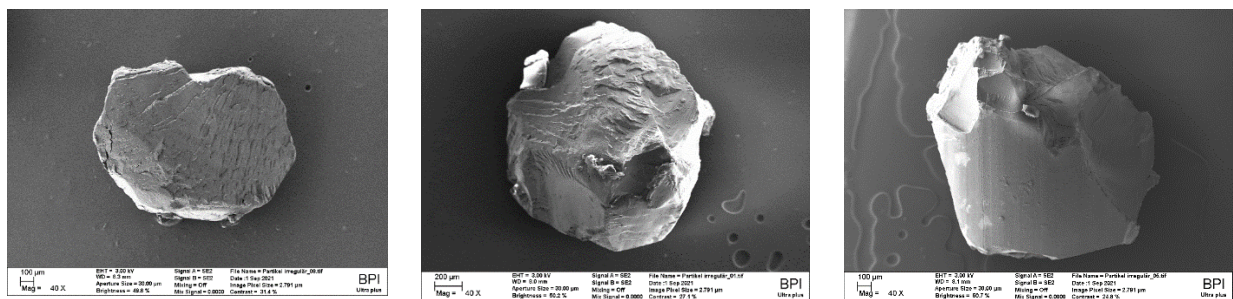


Figure S2: An example of the polystyrene fragments used in the settling velocity experiments under scanning electron microscope.

S3) The glass tubes used during the lake incubations

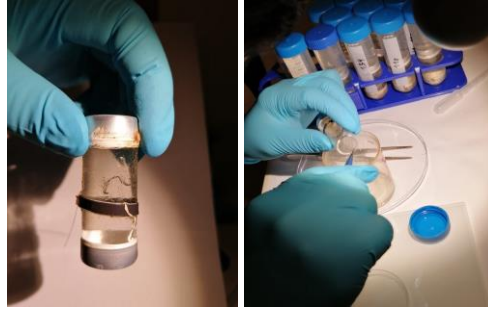


Figure S3: Example of the glass tubes used to incubate microplastic fragments in the lake.

S4) Dietrich (1928) settling velocity model

The theoretical settling velocity of each microplastic particle was calculated using the following equations:

$$W = \left(\frac{\rho_s - \rho}{\rho} g v W_* \right)^{1/3} \quad \text{a}$$

$$W_* = R^3 10^{R_1 + R_2} \quad \text{b}$$

$$R_1 = -3.76715 + 1.92944(\log D_*) - 0.09815(\log D_*)^{2.0} - 0.00575(\log D_*)^{3.0} + 0.00056(\log D_*)^{4.0} \quad \text{c}$$

$$R_2 = \left(\log \left(1 - \frac{1 - CSF}{0.85} \right) \right) - (1 - CSF)^{2.3} \tanh(\log D_* - 4.6) \quad \text{d}$$

$$+ 0.3(0.5 - CSF)(1 - CSF)^{2.0}(\log D_* - 4.6)$$

$$R_3 = \left(0.65 - \left(\frac{CSF}{2.83} \tanh(\log D_* - 4.6) \right) \right)^{\left(1 + \frac{(3.5 - P)}{2.5} \right)} \quad \text{e}$$

$$D_* = \frac{(\rho_p - \rho_w)gD_{eq}^3}{\rho_w v^2} \quad \text{f}$$

where W^* [-] is the dimensionless settling velocity, W [$L T^{-1}$] is the settling velocity of the particle, ρ_s [$M L^{-3}$] is the density of the particle, ρ [$M L^{-3}$] is the density of the fluid, ν [$L^2 T^{-1}$] is the kinematic viscosity of the fluid, R_1 [-] is a size factor, R_2 [-] is a shape factor, R_3 [-] is a roundness factor, D^* [-] is the dimensionless diameter, CSF [-] is Corey shape factor, D_{eq} [L] is the equivalent particle diameter, and P [-] is Powers roundness.

S5) Correction of settling velocity according to water temperature in each layer

The experimental settling velocities were corrected according to Ghawi and Kris (2012) using the following equation:

$$V_{ST_2} = V_{ST_1} \left(\frac{10^{\left[\frac{247.8}{T_1 + 133.15}\right]}}{10^{\left[\frac{247.8}{T_2 + 133.15}\right]}} \right)$$

where V_{ST_1} [LT^{-1}], V_{ST_2} [LT^{-1}], T_1 [$^{\circ}C$], and T_2 [$^{\circ}C$] are the settling velocity measured in the laboratory at 20 $^{\circ}C$, the corrected settling velocity in the lake compartments, water temperature in the laboratory, and the temperature of the lake compartment respectively.

S6) Spread of the Corey shape factor of the particles used in the settling velocity experiments

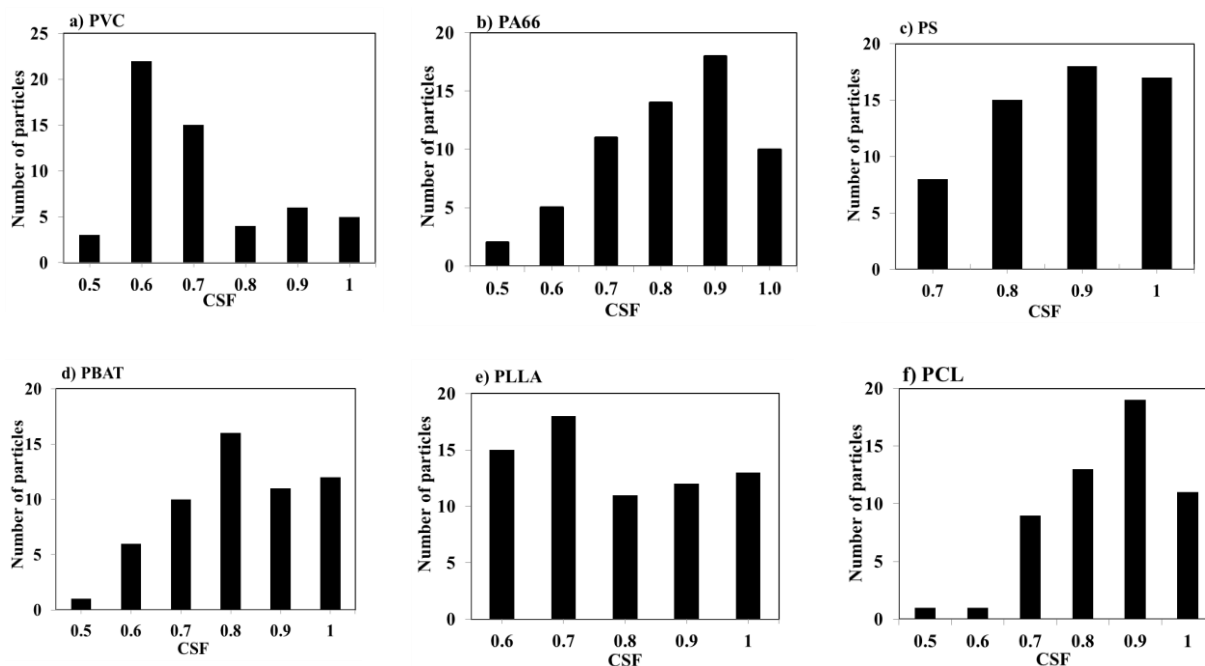


Figure S6: Distribution of Corey shape factor (CSF) of the polystyrene (PS), polyamide 66 (PA66), polyvinylchloride (PVC), polycaprolactone (PCL), polylactide (PLLA), and polybutylenadipate terephthalate (PBAT) particles across the experimental samples.

S7) Accumulation of biofilm on the surfaces of the incubated microplastics

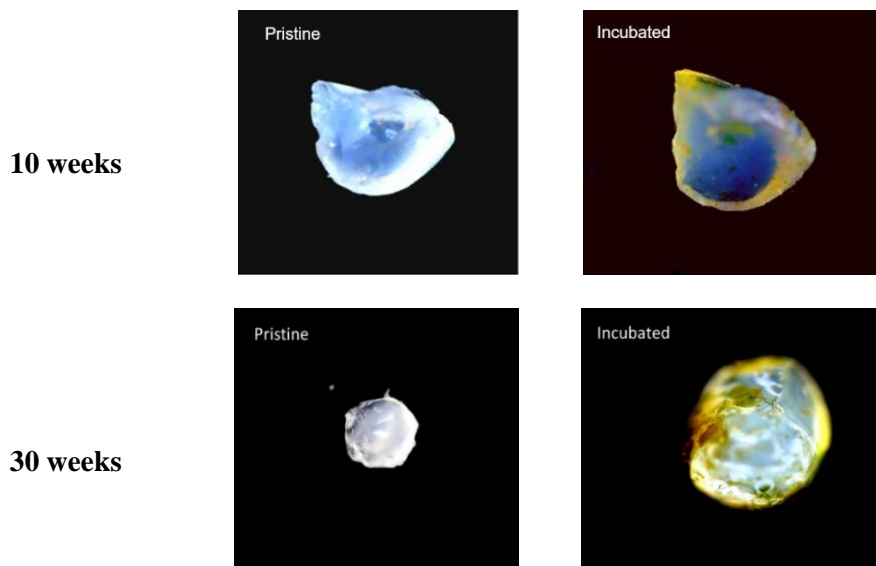


Figure S7: Comparison between pristine and biofilm-coated polyamide 66 particles after 10 and 30 weeks of incubation.

S8) Settling velocities of pristine and incubated microplastics

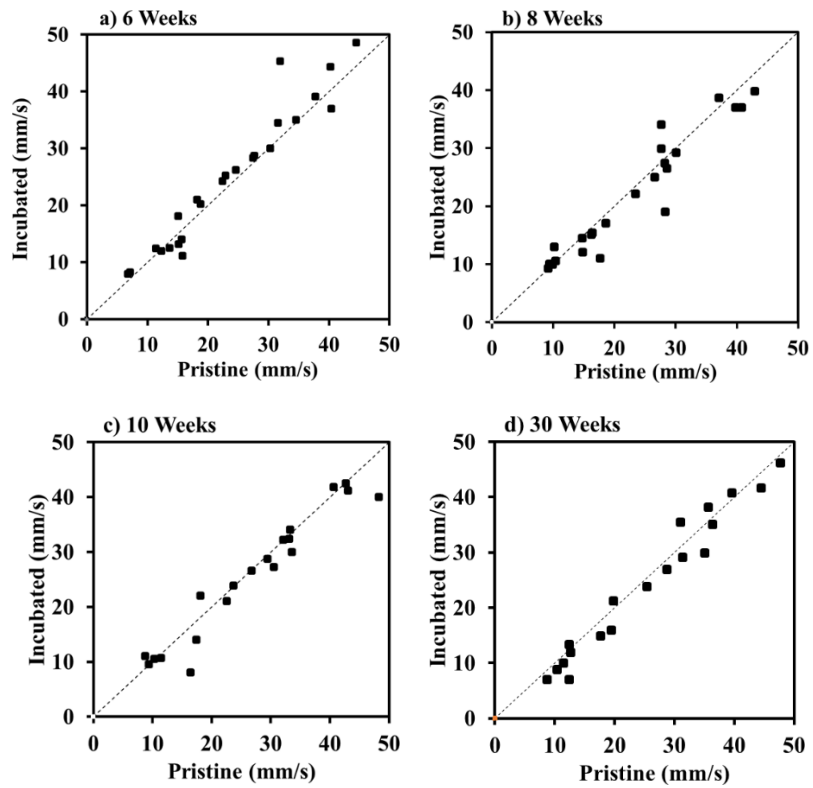


Figure S8: Comparison between experimentally determined the settling velocity of the pristine and incubated microplastics after different lake incubations. The dashed line presents the 1:1 line.

S9) Tracking the settling paths before and after incubation

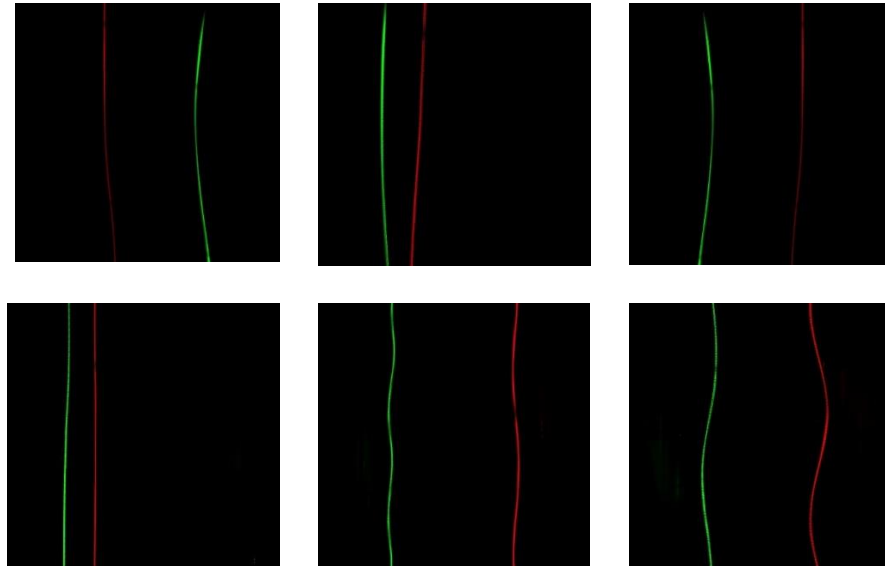


Figure S9: The sinking trajectories of 6 different particles after 30 weeks of incubation. The red trajectories and the green trajectories represent pristine and colonized microplastics respectively. The size of the frame is 30cm X 30cm.

S10) An example of the polystyrene spheres used in the lake model

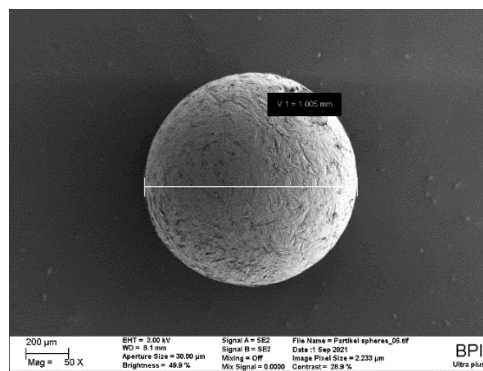


Figure S10: A scanning electron microscope image of a 1000 µm polystyrene sphere used in the lake model.

S11) Residence time the polystyrene spheres in each lake compartment

Table S11: Layer depth (m), water temperatures T ($^{\circ}\text{C}$), and the residence time τ (d) of the microplastics in the epilimnion, metalimnion, and hypolimnion of Upper lake Constance on day 319 according to Appt et al. (2004). The residence times τ (d) of the microplastics in each individual compartment were calculated according to equation 4.

Layer	Depth (m)	T ($^{\circ}\text{C}$)	$\tau_{1\mu\text{m}}$ (d)	$\tau_{10\mu\text{m}}$ (d)	$\tau_{500\mu\text{m}}$ (d)	$\tau_{1000\mu\text{m}}$ (d)
Epilimnion	30	9.0	30750	200	0.08	0.04
Metalimnion	20	7.5	21400	140	0.06	0.03
Hypolimnion	50	5.5	56695	370	0.16	0.07

Study 3: Systematic CFD-based evaluation of physical factors influencing the spatiotemporal distribution of MP particles in lakes

Pouyan Ahmadi, Franz Dichgans, Lisa Jagau, Christian Schmidt, Vadym Aizinger, Benjamin S. Gilfedder, Jan H. Fleckenstein

Corresponding Author: Pouyan Ahmadi

Published in Science of The Total Environment in January 2024.
<https://doi.org/10.1016/j.scitotenv.2024.170218>

Own contribution:

- Concept and study design 70%
- Data acquisition 90%
- Data analyses 100%
- Figures 100%
- Discussion of results 80%
- Manuscript writing 80%

Author contribution statement:

PA co-developed the research idea, designed the simulations scenarios, set up the CFD modeling framework, conducted all the CFD simulations and data interpretation and wrote the initial draft of the manuscript. FD helped in designing the simulation scenarios, assisted in data interpretation, contributed to writing and editing the manuscript. LJ helped in setting up the initial hydrodynamic simulation setup, contributed to reviewing and editing the manuscript. CS helped in designing the simulation scenarios, assisted in data interpretation, contributed to reviewing and editing the manuscript. VA contributed to reviewing and editing the manuscript. BSG contributed to reviewing and editing the manuscript. JHF conceived the project, co-developed the research idea, helped in designing the simulation scenarios, assisted in data interpretation, contributed to writing and editing the manuscript.



Systematic CFD-based evaluation of physical factors influencing the spatiotemporal distribution patterns of microplastic particles in lakes

Pouyan Ahmadi^{a,*}, Franz Dichgans^a, Lisa Jagau^b, Christian Schmidt^a, Vadym Aizinger^b, Benjamin S. Gilfedder^{c,d}, Jan H. Fleckenstein^{a,e}

^a Department of Hydrogeology, Helmholtz-Centre for Environmental Research, UFZ, 04318 Leipzig, Germany

^b Chair of Scientific Computing, University of Bayreuth, 95440 Bayreuth, Germany

^c Limnological Research Station, Bayreuth Center of Ecology and Environmental Research, University of Bayreuth, 95440 Bayreuth, Germany

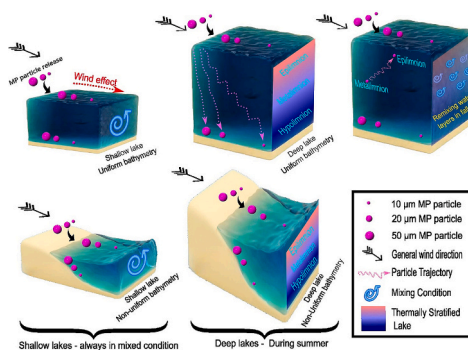
^d Department of Hydrology, Bayreuth Center of Ecology and Environmental Research (BayCEER), University of Bayreuth, 95440 Bayreuth, Germany

^e Hydrologic Modelling Unit, Bayreuth Center of Ecology and Environmental Research (BayCEER), University of Bayreuth, 95440 Bayreuth, Germany

HIGHLIGHTS

- Lake depth, bathymetry, and particle size are dominant controls of MP fate.
- Impact of wind, release location/time on MP fate grows with decreasing MP size.
- Dissipation of thermal stratification increases odds of rising for 10 μm particles.
- Assessing MP fate needs evaluation of all physical factors and their interactions.

GRAPHICAL ABSTRACT



ARTICLE INFO

Editor: Olga Pantos

Keywords:

Microplastic particles
Lake hydrodynamics
Physical factors
Thermal stratification
Lagrangian particle tracking
Computational fluid dynamics

ABSTRACT

Spatiotemporal distribution patterns of microplastic (MP) particles in lakes hinge on both the physical conditions in the lake and particle properties. Using numerical simulations, we systematically investigated the influence of lake depth and bathymetry, wind and temperature conditions, MP particle release location and timing, as well as particle diameter (10, 20, and 50 μm). Our results indicate that maximum lake depth had the greatest effect on the residence time in the water column, as it determines the settling timescale and occurrence of hydrodynamic complexity such as density-driven flows in the lake. Increasing particle size from 10 to 20 and 50 μm also significantly reduced the residence time making particle size the factor with the second strongest effect on the residence time and, in turn, on the availability of MP particles for uptake by organisms. Changing bathymetry from a uniform to a non-uniform had a less pronounced effect on particle residence time compared to maximum depth and particle size. Release location, wind conditions, and release time had comparably little effect on particle behavior but became more important as MP particle size decreased. The release of the 10 μm MP particles in the deeper lakes with uniform bathymetry during summer with stable thermal stratification, resulted in a nearly month-long turnover phase in the fall in which both settling and rising of particles occurred

* Corresponding author at: Helmholtz Centre for Environmental Research UFZ, Department Hydrogeology, Permoser Str. 15, 04318 Leipzig, Germany.

E-mail address: pouyan.ahmadi@ufz.de (P. Ahmadi).

<https://doi.org/10.1016/j.scitotenv.2024.170218>

Received 1 November 2023; Received in revised form 24 December 2023; Accepted 14 January 2024

Available online 25 January 2024

0048-9697/© 2024 The Author(s). Published by Elsevier B.V. This is an open access article under the CC BY license (<http://creativecommons.org/licenses/by/4.0/>).

simultaneously. This was caused by convective heat and water transport during this period. In these scenarios about 2.6 to 5.4 % of the released MP particles were held in or returned to the water layers near the lake surface. While acknowledging the dominant role of lake depth and MP particle size on the particle residence time, this study further emphasizes that it is ultimately a particular combination of different factors and their interactions that shape MP distribution patterns in lakes.

1. Introduction

Since the start of the industrial production of plastic in 1907 by Leo Hendrik Baekeland (Pilato, 2010), anthropogenic litter containing plastics has increased due to inadequate recycling incentives, training, and disposal infrastructure (Ahmadi et al., 2022; Burns and Boxall, 2018; Daily et al., 2022; Mcnutt, 2017; Wagner et al., 2014). Extending from the nano to macroscale, plastic debris encompasses a wide range of particle sizes, including microplastics (MP) measuring <5 mm in diameter (Falconieri et al., 2018; Lambert and Wagner, 2018). These particles originate from distinct sources: primary MP particles, commonly found in cosmetic and cleaning products, and secondary MP particles, originating from the breakdown of larger plastic fragments through chemical and mechanical forces and UV radiation (Browne et al., 2011; Williams and Simmons, 1996; Wright et al., 2020). Their slow decomposition allows MP particles to endure in the environment traveling vast distances from land to large water bodies through rivers and streams (Boos et al., 2021; Dichgans et al., 2023; Nematollahi et al., 2020; Schmidt et al., 2017). Lakes serve as potential sinks for MP particles (D'Avignon et al., 2022; Dusaucy et al., 2021; Gilfedder et al., 2023; Qian et al., 2021) introduced through atmospheric deposition or via inflows, raising significant concerns due to their detrimental effects on freshwater sources and unique aquatic ecosystems (Boos et al., 2021; Free et al., 2014; Klein et al., 2018; Yang et al., 2022). The presence of MP particles in lakes poses risks to aquatic organisms through ingestion and absorption of toxic substances, threatening ecological balance due to the particles' chemical composition and adsorption of pollutants like pesticides and heavy metals from the surrounding environment (Castro-Castellon et al., 2022; Collard et al., 2019; Gilfedder et al., 2023; Leiser et al., 2021a; Leiser et al., 2021b; Leiser et al., 2020; Wang et al., 2020).

Given the potential adverse effects of MP particles in lakes, it is important to have a quantitative understanding of the most influential factors that determine their fate in these systems (Ahmadi et al., 2022; Elagami et al., 2022; Kowalski et al., 2016). MP particles in lakes have been studied both experimentally and numerically (Ahmadi et al., 2022; Elagami et al., 2022; Khatmullina and Isachenko, 2017; Waldschläger and Schüttrumpf, 2019). Recent studies focusing on identifying the influential factors affecting the terminal settling velocity of MP particles primarily examine parameters like MP particle density, volume, shape, roundness (Ahmadi et al., 2022; Elagami et al., 2022; Khatmullina and Isachenko, 2017; Waldschläger and Schüttrumpf, 2019), and surface area to volume ratio (Ahmadi et al., 2022). However, MP particles are subject to not only gravity, but also lateral advection and dispersion processes under more complex hydrodynamic conditions (Elagami et al., 2023). These processes can cause horizontal displacement and affect vertical settling patterns (Daily and Hoffman, 2020). Thus, MP particle distribution patterns in lakes cannot be explained solely by the particle's terminal settling velocities. Larger-scale investigations are necessary for a more comprehensive understanding of their behavior (Alosairi et al., 2020; Elagami et al., 2023; Nava et al., 2023).

Over the past few years, numerous field studies have been conducted to address questions such as how MP particles are distributed across lakes and where accumulation areas are (Dean et al., 2018; Egessa et al., 2020; Eriksen et al., 2013; Fischer et al., 2016; Nava et al., 2023; Razeghi et al., 2021). But currently, there is still only poor understanding of the main mechanisms responsible for creating the distributions found in nature, making it difficult to predict how MP particles will behave in different lake systems. Just knowing where to sample may not

be enough, but knowing why MP particles are found at specific locations is where it becomes crucially important (Law, 2017). To acquire this knowledge, modeling-based studies have been proven effective in investigating the transport behavior and resulting spatiotemporal patterns of MP particles in marine systems and lakes (Cable et al., 2017; Daily et al., 2022; Hoffman and Hittinger, 2017; Lebreton et al., 2012; Maximenko et al., 2012).

Studies investigated the fate of MP particles in the ocean, sea and in lakes, each with their own unique hydrodynamic complexities (Alosairi et al., 2020; Cable et al., 2017; Elagami et al., 2023; Mountford and Morales Maqueda, 2019; Nordam et al., 2019). The hydrodynamics in such studies are typically modeled numerically using Eulerian approaches (Alosairi et al., 2020; Daily and Hoffman, 2020; Mountford and Morales Maqueda, 2019; Nordam et al., 2019). The MP particles themselves, on the other hand, can be simulated either using an Eulerian (fixed coordinate reference frame) (Mountford and Morales Maqueda, 2019) or a Lagrangian approach (moving reference frame) (Alosairi et al., 2020; Daily and Hoffman, 2020). The Eulerian-Eulerian approach is commonly used to study the fate of dissolved substances such as oxygen using the advection-diffusion equation, but also particulates such as algae and MP particles have been simulated using this approach (Gao et al., 2017; Kitazawa and Kumagai, 2005; Mountford and Morales Maqueda, 2019). In the latter case, it is generally assumed that the particles are small enough compared to the characteristic length scales of the fluid motion (Reeks, 1977) so that they behave similar to a dissolved substance (Mountford and Morales Maqueda, 2019). On the other hand, the Eulerian-Lagrangian approach is used to study the movement of individual particles within a fluid by tracking the position and velocity of each particle as it moves through the modeled domain (Alosairi et al., 2020; Daily et al., 2022). However, most of these studies have focused on specific lakes with particular geometries limiting transferability to other lakes with different characteristics. To overcome this limitation, it is important to develop scenarios that examine the sensitivity of fundamental controlling variables across a range of typical lake geometries. By doing so, we gain a better mechanistic understanding of MP particle behavior in a broader range of lake environments. This study aims to take a first step in this direction by exploring the sensitivity of MP particle transport to the key variables in elliptical lakes.

In natural lake systems, elliptical shapes are frequently observed, representing a common characteristic of a considerable percentage of lakes (O'Sullivan and Reynolds, 2008). Depending on the lake depth, bathymetry and energy input by radiation and wind, thermal stratification may develop (Woolway et al., 2020), which, in turn, can impact lake hydrodynamics and subsequently influence the fate of MP particles that enter the lake (Chevalier et al., 2023; Daily and Hoffman, 2020; Elagami et al., 2023). The joined effects of thermal stratification, lake geometry (depth and bathymetry) and other physical factors such as wind direction and speed on the fate of MP particles of different sizes and densities are still poorly understood (Ahmadi et al., 2022; Elagami et al., 2022; Elagami et al., 2023). To gain a deeper understanding of these effects on MP particle distributions in elliptical lakes, we conducted a comprehensive study using 48 simulation scenarios to shed light on the key factors which control the MP particle distribution patterns and to address the following main research questions:

- How do the lake depth and bathymetry influence the deposition patterns and settling time scales of MP particles in lakes?

- How does the distribution of MP particles in lakes depend on the particle size?
- In which way do the wind conditions affect the distribution patterns of MP particles in lakes?
- Do the release time and location have a significant impact on the spatiotemporal particle distribution patterns?
- What are the effects of thermal stratification in lakes on the behavior of MP particles?

2. Methodology

To simulate the transport of MP particles in lakes, Delft3D, a state-of-the-art Computation Fluid Dynamics (CFD) model for hydrodynamics, water quality, waves, particle tracking, and sediment transport, was utilized (Deltares, 2013). Delft3D-FLOW is the hydrodynamic modeling module that solves the system of the 3D hydrostatic equations with free surface (Deltares, 2013). Combining the Lagrangian particle tracker implemented in the Delft3D-PART module with the FLOW module can yield 3D maps of MP particle path lines affected by advection,

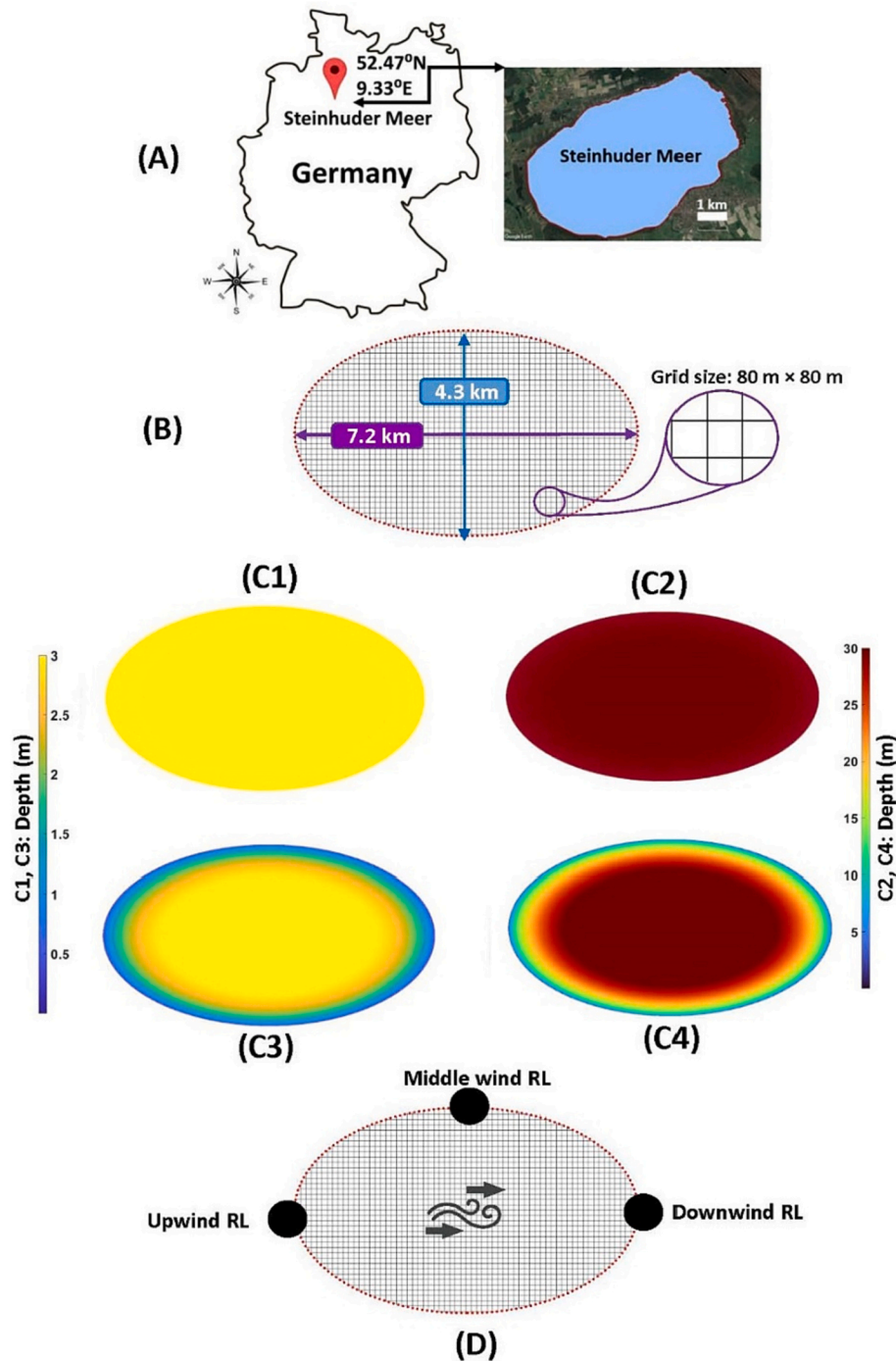


Fig. 1. Setups for particle tracking scenarios; (A) the map of Steinhuder Meer, (B) lake surface geometry and size of the used grid cells in the simulations, (C) the depicted bathymetries, C1 and C2, represent uniform depth distributions across the lake, with yellow indicating 3 m depths for shallow lakes and red indicating 30 m depths for deep lakes. In contrast, C3 and C4 illustrate non-uniform bathymetries, with the deepest points for shallow lakes (center colored in yellow) set at 3 m and for deep lakes (center colored in red) set at 30 m, (D) the positioned RLs in the direction of the general western wind.

dispersion, and settling (Deltares, 2013; Raimundo et al., 2020; Stuparu et al., 2015). Previous water quality studies have confirmed the accuracy and efficiency of the computational algorithms of the Delft3D suite of models (Alosairi et al., 2020; Nunez et al., 2021; Raimundo et al., 2020; Stuparu et al., 2015).

2.1. Hydrodynamic model configuration

2.1.1. Geometry and meshing

Elliptical lakes are a common type of lake found across the globe (O'Sullivan and Reynolds, 2008) and were chosen here as a test-case for our scenario simulations. To increase the realism of the simulations in terms of spatial dimensions, we based the model lake shape on Steinhuder Meer (52.47° N, 9.33° E), an elliptical lake in the vicinity of Hannover and the largest lake by surface area in northwest Germany (Fig. 1 A). In order to generalize the findings to lakes sharing similar geometries, we opted not to confine the boundary layer of the simulated lakes strictly to the precise shoreline curvature of Steinhuder Meer. Instead, we employed its dimensions as the measures for generating our lake surface. Therefore, the ellipse covered the shoreline of the Steinhuder Meer has a surface area of approximately 29 km² with diameters of 4.3 km and 7.2 km at its narrowest and widest dimensions, respectively (Fig. 1 B). This elliptical shape of the water surface area remained unchanged for all subsequent simulations. For hydrodynamic computations, the water surface was horizontally meshed using an 80 m × 80 m structured grid (Fig. 1 B). In order to determine an optimal numerical grid resolution, we conducted a thorough sensitivity analysis during model setup. Grid sizes coarser than 80 m × 80 m led to noticeable numerical diffusion, impacting the precision of results, while finer grid sizes did not yield significant improvements in simulation results, but incurred additional computational costs. In turn, an 80 m × 80 m grid size was chosen as an optimal grid resolution, balancing numerical stability with computational efficiency, ensuring reliable and efficient simulations.

For the fixed elliptical shape of the water surface, we used two sets of scenarios to define water depths: (1) uniform bathymetry, meaning uniform water depth across the lake (two scenarios with 3 m (Fig. 1, C1) and 30 m depth (Fig. 1, C2)), and (2) non-uniform bathymetry, referring to a lake bed that slopes downward from the shorelines to the lake's center, forming a positive concavity, which is intersected by a horizontal plane at a depth of 3 m (shallow lake scenarios, Fig. 1, C3) and 30 m (deep lake scenarios, Fig. 1, C4). These depth values were defined based on the deepest points in two reference lakes, the shallow Steinhuder Meer (max. Depth ≈ 3 m) and the relatively deep and quasi-elliptical lake "Großer Brombachsee" (max. Depth ≈ 30 m) (49.12° N, 10.92° E, Middle Franconia, Germany).

In the lakes with uniform bathymetry, the vertical discretization used ten sigma-layers, gradually refined towards the lake's water surface where the wind effect is more evident. In the lakes with non-uniform bathymetry, in addition to the effects of wind on the water surface, there is also a more complex bed layer geometry. Therefore, the number of layers was increased to fifteen sigma-layers, with gradual refinements applied both towards the lake bed layer and the water surface. Hydroclimatic boundary conditions for the model, including the Coriolis force, are based on the locality of the Steinhuder Meer.

2.1.2. Hydrodynamic modeling and boundary conditions

Turbulence and convective heat fluxes due to temperature and density differences in the water column significantly influence the settling velocity of particles in lakes, especially if they are small or their density is similar to that of the lake water (Elagami et al., 2023; Raimundo et al., 2020). The Delft3D model uses the k-ε turbulence model, which computes the mean turbulence characteristics based on simplified terms for the turbulent kinetic energy and dissipation rate to model vertical eddy viscosity and eddy diffusivity in the lake water (Deltares, 2013). The composite heat flux model in Delft3D was selected to

calculate the thermal forcing (Deltares, 2013). Air temperature (Fig. 2 A), cloudiness, and relative humidity (cf. Supplementary Material, Fig. S1) serve as inputs to the heat flux model.

In our simulations, we used 30 years of meteorological data (from year 1989 to 2018) across Germany (Cornes et al., 2018) to calculate daily average air temperature values for Germany, depicted in Fig. 2 A. The turbulence and heat flux models use the same input data for all scenarios.

MP Particle accumulation in the uppermost parts of the water column was also evaluated for their susceptibility to transport by wind-induced currents. We ran the four aforementioned lake geometry scenarios (Fig. 1, from C1 to C4) once with time series of wind magnitudes and directions (variable wind) (Fig. 2 B), and once with constant wind with the average wind magnitude (3.2 m s⁻¹) and direction (216°) calculated from the data used in the variable wind scenario.

2.2. Particle transport configuration

2.2.1. Particle tracking model

The Delft3D-PART module uses an advective particle tracking scheme with a random walk routine for particle dispersion (Deltares, 2013; Raimundo et al., 2020; Stuparu et al., 2015). The dispersion process in the x, y and z directions follows a white noise process distribution with a uniform probability density function, having a zero mean and ranging between -1 and +1. In the vertical direction, the model incorporates particle displacement resulting from settling, in addition to advection- and dispersion-induced vertical displacement (Deltares, 2013; Raimundo et al., 2020; Stuparu et al., 2015). The dispersion component is resolved using an explicit Euler numerical scheme. Moreover, the numerical scheme also accounts for additional advection caused by wind in the horizontal direction. The model is able to track the distribution patterns of settled MP particles at the lake bed (Raimundo et al., 2020; Stuparu et al., 2015). In our simulations, we assumed that once a particle reaches the lake bed layer it is immobilized.

2.2.2. Implemented scenarios

MP particle release locations (RLs) were placed at the western, upwind, and eastern, downwind ends as well as in the northern, middle section of the upper arc of the elliptical shoreline (Fig. 1 D). These RLs will subsequently be referred to as upwind RL, middle RL, and downwind RL throughout this study. We did not include another middle RL at the southern shore, as results for this location would not differ significantly from the results from the northern middle RL. In each individual scenario, a total of 90,000 particles (30,000 particles per RL) were instantaneously released. This type of release is thought to mimic an instantaneous release of MP particles into a lake via a stream or river during an unplanned release event, such as from a wastewater treatment plant. In this case, the effluent contains elevated MP concentrations, which are released into the receiving waters (Daily and Hoffman, 2020). In our scenarios, we strategically chose a larger number of 30,000 MP particles per RL, to maximize the precision of the simulation results. This number of released MP particles, significantly higher than the quantities used in similar, previous studies with substantially larger study areas (<3000 particles) (Alosairi et al., 2020; Raimundo et al., 2020; Stuparu et al., 2015), was motivated by our aim to obtain robust probability distributions of particle locations from the used advective particle tracking plus random walk transport model (Lagrangian particle tracking).

Delft3D-PART allows particles to be specified based on their settling velocities (Raimundo et al., 2020; Stuparu et al., 2015). To calculate the settling velocity of the investigated MP particles, Stokes' law was utilized (Lamb, 1932) (cf. Supplementary Material, S2). Polystyrene particles with sizes of 10, 20, and 50 μm were selected for this study as it is a polymer that is commonly found in lake environments (Hale et al., 2020) and has a density (1030 kg m⁻³) that is close to that of fresh water. Clear differences were observed in the spatial and temporal

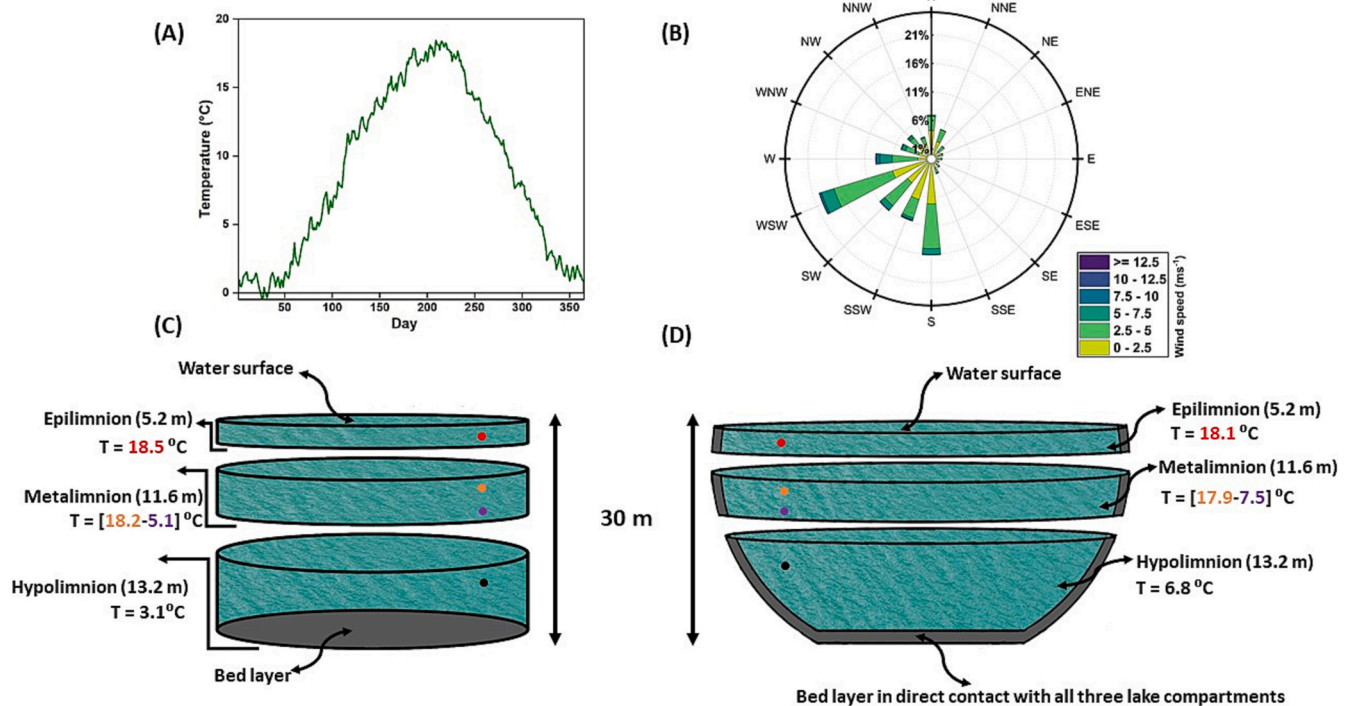


Fig. 2. (A) the daily average air temperature used in the simulations, (B) frequency of wind directions and magnitudes showing the predominant wind direction from West to East, (C) lake compartments during thermal stratification in the deep lake with uniform bathymetry, numbers in brackets are layer thickness, colored dots refer to the temperature range in each of the compartments during maximum stratification, (D) lake compartments during thermal stratification in the deep lake with non-uniform bathymetry, numbers in bracket and colored dots as in (C).

distribution patterns of 10, 20, and 50 μm MP particles. In contrast, particle sizes exceeding 50 μm demonstrated negligible disparities compared to the spatiotemporal distribution patterns associated with 50 μm particles. Consequently, particle sizes larger than 50 μm were excluded from our investigations. The chosen particle sizes are large enough to render the effect of Brownian motion on settling velocity negligible. Under these conditions, it can be assumed that the flow around the particle during sinking is laminar (Elagami et al., 2023). Further details about each MP particle size are provided in Table 1 for the different lake geometries. Moreover, the above-stated scenarios were implemented in the PART module for two different particle release times, at the beginning (1st of January) and in the middle of the year (1st of July) in order to represent a release during the typical time for thermal stratification (summer) and during a non-stratified period (winter). In each individual scenario, the simulation was run until a quasi-steady state was reached in terms of the percentage of suspended and deposited particles. Table 2 shows an overview of the scenarios conducted in this study.

The scenarios conducted in this study are designed to reflect general characteristics of quasi-elliptical natural lakes. The two lake depths of 3 and 30 m were derived from two quasi-elliptical lakes in Germany (Steinhuder Meer, Großer Brombachsee) and cover the depth range of a large fraction of lakes in Germany and elsewhere. The base bathymetry

Table 1

Particle size and deposition time correspond to the chosen settling velocities calculated based on Stokes' equations (Lamb, 1932).

Particle size (μm)	Settling velocity (m d ⁻¹)	Deposition time (d)	
		Shallow lake (3 m)	Deep lake (30 m)
10	0.14	22	213
20	0.56	6	54
50	3.52	<1	8.5

(non-uniform) reflects a typical bathymetry pattern, where sediment from surrounding watersheds accumulates in shallow littoral zones, while the lake center features deep profundal zones. The magnitude and direction of the variable wind patterns were derived from meteorological records from the region of the Großer Brombachsee.

Starting from this near-natural base scenario, different permutations have been implemented to systematically investigate the influence of the different model parameters on MP particle transport in elliptical lakes. For this, uniform bathymetry, constant wind conditions, and a range of different MP particle release locations and timings have been implemented. These permutations intentionally deviate from natural conditions at a specific locale to highlight the generic impacts of the different parameters on the spatiotemporal distribution patterns of MP particles in lakes.

2.3. Particle fate analysis

A 3D trajectory analysis of the released particles yielded spatiotemporal concentration maps for suspended as well as deposited particles in the 48 defined scenarios. As illustrated in Fig. 2C and D, we compartmentalized the water column of all 30 m deep lakes based on the thermal stratification, which evolved for the deep lakes with uniform bathymetry during summer (Fig. 3 A, B), from 0 to 5.2 m (Epilimnion), 5.2 to 16.8 m (Metalimnion), and 16.8 to 30 m (Hypolimnion). This allowed us to: (1) monitor the number of suspended particles in the epilimnion during fall when the thermal stratification becomes less stable, (2) use the same depth intervals to compare the duration it takes for MP particles to travel through the lake water column and settle (i.e., residence time) in all the scenarios. There was no thermal stratification evolving in the scenarios featuring 3 m shallow lakes. For these lakes we only distinguished between MP particles that were suspended in the water column and those that had settled on the lake bed. The lakes' thermal stratification is elaborated in more detail in Section 3.1.

Table 2
Overview of the investigated physical factors throughout the 48 scenarios.

Bathymetry shape	Depth/ deepest point (m)	Injection time	Wind state	Particle size (μm)	Number of scenarios
Uniform bathymetry	3, 30	January, July	Constant wind, Variable wind	10, 20, 50	24
Non-uniform bathymetry	3, 30	January, July	Constant wind, Variable wind	10, 20, 50	24

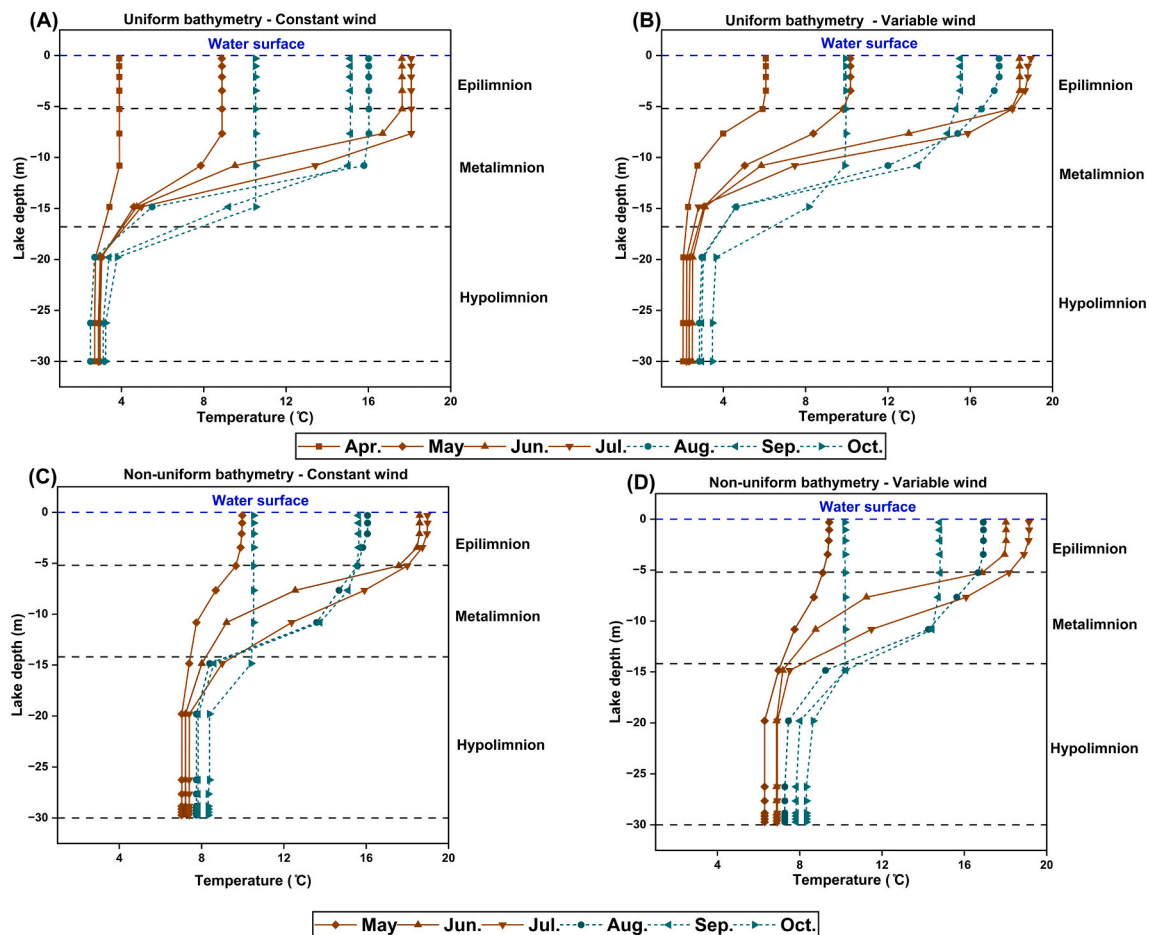


Fig. 3. Vertical temperature profiles for: (A) uniform bathymetry lake with 30 m depth and wind of constant magnitude and direction, (B) uniform bathymetry lake with 30 m depth and wind of variable magnitude and direction, (C) non-uniform bathymetry lake with 30 m maximum depth and wind of constant magnitude and direction, (D) non-uniform bathymetry lake with 30 m maximum depth and wind of variable magnitude and direction; vertical temperature profiles are only shown for the months over which the thermal stratification evolves and then dissipates. The symbols on the lines refer to the respective months in the figure legend.

2.4. Settling distance and time for 50 % of the particles to settle

Depending on the particle settling velocities, reaching 100 % deposited particles demands time-consuming simulations and consequently excessive numerical costs. The analysis of 50 % of the released particles was sufficient to produce patterns describing the impact of the examined variables. We, therefore, allowed the simulations to run until either all particles were settled within a reasonable period of simulation time (50 μm took about 3 months) or a quasi-steady state is reached with >75 % of the MP particles deposited (10 μm = 18 months, 20 μm = 12 months). Hence, after reaching the quasi-steady state of particle deposition, the distance from the release point, over which the first 50 % of the deposited particles were found, was defined as D_{50%} (i.e., median of the particle travel distance values from the injection point). This was calculated using cumulative frequency curves by counting deposited particles in equal distance intervals. Additionally, we extracted the time T_{50%} (the median settling time) taken for the first half of the released particles to settle in all scenarios. The MP particle distributions were then compared for all scenarios to elucidate how these variables affected

the D_{50%} and T_{50%}.

2.5. The ratio between mixing and settling timescales

The fate of particles is mainly influenced by two factors: turbulent mixing and settling velocity. Turbulent mixing facilitates a more even horizontal distribution of particles throughout the upper layers of a lake. On the other hand, the settling velocity enables particles to pass through the pycnocline in the metalimnion and then the hypolimnion (Boehrer and Schultze, 2008).

The time required to homogenize the concentration of particles in a water column can be estimated using typical values of the mixed layer thickness, H (m), and the vertical eddy diffusivity, K (m² s⁻¹). This homogenization time, T_m, is approximately calculated as T_m = H²/K. The timescale for settling of sinking material is T_s = H/W, with the downward migration velocity, W (m s⁻¹). This timescale represents the duration for the sinking particles to enter the pycnocline, assuming that turbulent diffusion is negligible. The Péclet number (Pe) is a dimensionless parameter that indicates the ratio of the mixing timescale to the

settling timescale, and it can be calculated as (Deleersnijder et al., 2006):

$$Pe = T_m/T_s = WH/K \tag{1}$$

In a layer with $Pe \gg 1$ the advective/ settling force dominates, leading to variable particle concentration within the layer. For $Pe \ll 1$, the particle cloud is expected to be more uniformly distributed in the respective layers, as dispersion dominates (Deleersnijder et al., 2006).

3. Numerical results

3.1. Thermal stratification and mixing in the simulated lakes

Vertical temperature profiles evolving in the simulations differed significantly between lakes with depths and bathymetry. Regardless of the type of bathymetry, the shallow lakes (water depth 3 m) exhibited minimal (<0.17 °C) or no vertical temperature variation. In contrast, the deeper lakes (water depths 30 m) were deep enough to develop a pronounced thermal stratification (Fig. 3). The lakes with uniform bathymetry had a stronger thermocline in the metalimnion than those with a non-uniform bathymetry. In the lakes with uniform bathymetry, regardless of wind conditions, thermal stratification began to develop around April (Fig. 3 A, B). Their thermal stratification then evolved to the maximum temperature difference between the epilimnion and hypolimnion of 16.7 °C in July (Fig. 3 A, B). The onset of thermal stratification in the lakes with non-uniform bathymetry occurred approximately one month later (i.e., May) and evolved to maximum temperature difference of only 12.2 °C, but also lasted until the end of July (Fig. 3 C, D) (cf. Supplementary Material, S3, for validation of the modeled temperature profiles in Fig. 3 D using empirical functions (Rimmer, 2006) developed for thermally stratified lakes).

For the uniform bathymetry with constant and variable wind, the epilimnion (0 to 5.2 m) had a relatively uniform temperature of 18.5 °C, within the metalimnion (5.2–16.8 m) temperature decreasing with depth from 18.2 to 5.1 °C, and the hypolimnion (16.8 to 30 m) again had a relatively uniform temperature of 3.1 °C (Figs. 2C and 3 A, B). Fig. 2 D and Fig. 3 C, D indicate that the lakes with non-uniform bathymetry have slightly less pronounced temperature variations between compartments compared to the lakes with uniform bathymetry.

Around the beginning of August, the daily air temperatures began to drop (Fig. 2 A) resulting in the onset of mixing between compartments in

all four cases as the weather turned colder. Dashed lines in plots A, B, C, and D in Fig. 3 provide a visual representation for the extent of the epilimnion, the metalimnion, and the hypolimnion.

In the following section, we use the compartment boundaries, emerging in the lakes with uniform bathymetry due to thermal stratification (Fig. 3 A, B) to delineate distinct depth intervals, over which we could compare the quantity of suspended MP particles between the 30 m deep lake scenarios.

3.2. Evolving spatiotemporal MP particle patterns

To analyze the MP deposition patterns at the end of the simulation, the 48 scenarios were binned in 4 groups based on MP release time (January/ July) and wind conditions (constant/ variable). The comparison between the groups demonstrated that the deposition patterns are consistently affected by MP particle size, lake depth and bathymetry. Fig. 4 illustrates the deposition patterns for one of these groups with January as the release time and constant wind conditions. Fig. 5 provides an example demonstrating the calculation of $D_{50\%}$ for the upwind, middle, and downwind RLs in one of the scenarios depicted in Fig. 4 (B1.3). In Fig. 6, the resulting $D_{50\%}$ values for the three RLs in each of the 48 scenarios are depicted separately for both the 3 m (panel A) and 30 m (panel B) lakes.

In the case of shallow lakes, regardless of bathymetry type and particle size, all released particles (i.e. 90,000 MP particles) settled within a maximum of three months after their release (Fig. 4 A1, B1). Full deposition similarly occurred in less than one month for 50 µm MP particles released in the deep lakes with both types of bathymetry (Fig. 4 A2.3, B2.3). However, the 10 µm and 20 µm MP particles released in the deep lakes with uniform (Fig. 4 A2.1, A2.2) and non-uniform bathymetries (Fig. 4 B2.1, B2.2) were not fully deposited even one year after their release. The settling of these particles continued at a low, quasi steady-state deposition rate. Fig. 7 illustrates the normalized count of MP particles over simulation time for these scenarios with the same labels as in Fig. 4 (A2.1 and A2.2 for the lakes with uniform bathymetries, B2.1 and B2.2 for the lakes with non-uniform bathymetries).

$T_{50\%}$ was evaluated for the three RLs (Fig. 1 D) in the 48 scenarios. The box plots in Fig. 8 illustrate the calculated differences in $T_{50\%}$ values, when altering each examined factor (represented on the x-axis of Fig. 8 A and C) while keeping the other factors constant. Fig. 8 A shows the results for the deep lake scenarios, while the results for the shallow lakes are shown in Fig. 8C. Fig. 8 B breaks up the results from varying RL

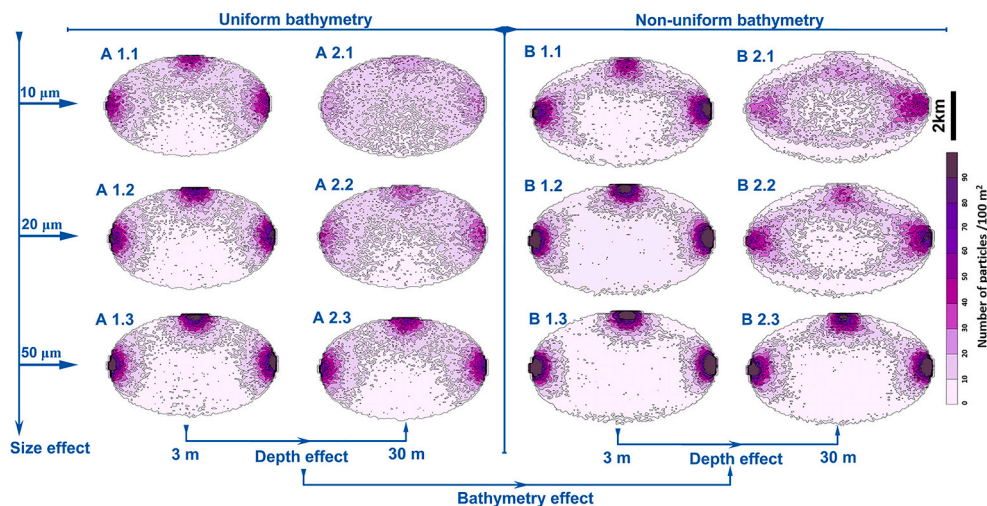


Fig. 4. The deposition patterns of MP particles after reaching a quasi-steady state. The results are shown for two types of bathymetries: uniform (denoted by ‘A’) and non-uniform (denoted by ‘B’). Panels A1 and B1 illustrate the deposition patterns in 3 m shallow lakes for particle sizes of 10 µm, 20 µm, and 50 µm (indexed as 1.1, 1.2, and 1.3, respectively). Similarly, Panels A2 and B2 represent the results for 30 m deep lakes (indexed as 2.1, 2.2, and 2.3) while maintaining the same particle size order. Wind speed was constant in this group of simulations.

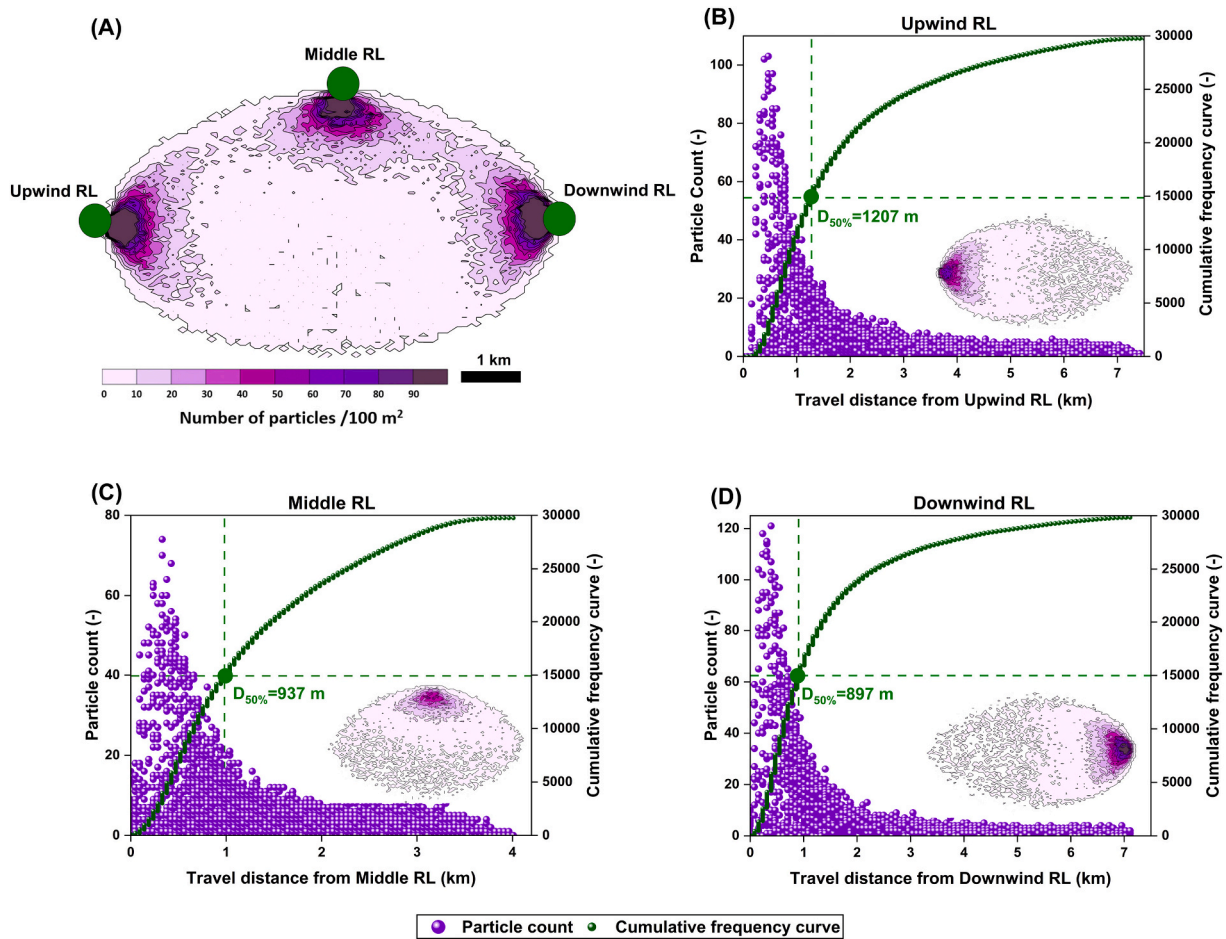


Fig. 5. (A) Simulated particle deposition patterns for a non-uniform bathymetry lake with 3 m depth when 90,000 MP particles of 50 μm are released at the beginning of January from the upwind, middle, and downwind RLs; Particle count (purple circles) vs. distance from the injection sites and calculating $D_{50\%}$ out of cumulative frequency curves (green lines) for: (B) upwind RL, (C) middle RL, (D) downwind RL.

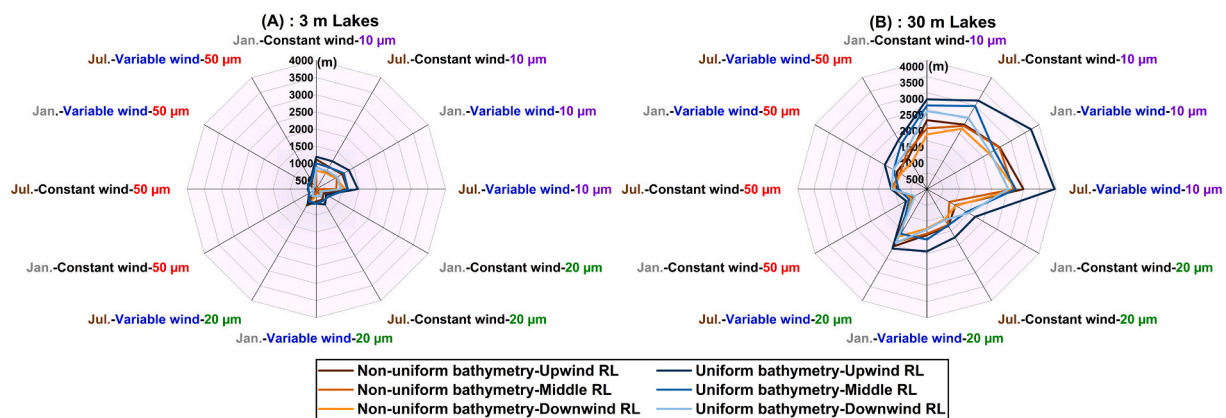


Fig. 6. The calculated $D_{50\%}$ at the end of the simulations for the 3 m lakes (panel A) and the 30 m lakes (panel B); the injection time, wind conditions, and MP particle sizes are labeled with different colors around each panel; different blue and red color tones represent the $D_{50\%}$ separately sorted for RLs in the lakes with uniform and non-uniform bathymetries.

in Fig. 8 A into the different particle sizes.

Based on the computed metrics, which were displayed in Figs. 4 to 8 in the previous section, the following subsections will provide a more detailed, comparative analysis of the relative impact of the investigated physical factors on MP particle distribution and settling patterns in the investigated virtual lakes.

3.2.1. Lake depth and bathymetry

Regardless of the injection location and lake bathymetry, a decrease in lake depth always significantly reduced the distance that MP particles traveled before settling and resulted in a more locally concentrated deposition pattern around the RL (Fig. 4). The strong impact of lake depth on the travel distance of MP particles was further reflected in the quantitative $D_{50\%}$ metric derived from the simulations of shallow (Fig. 6

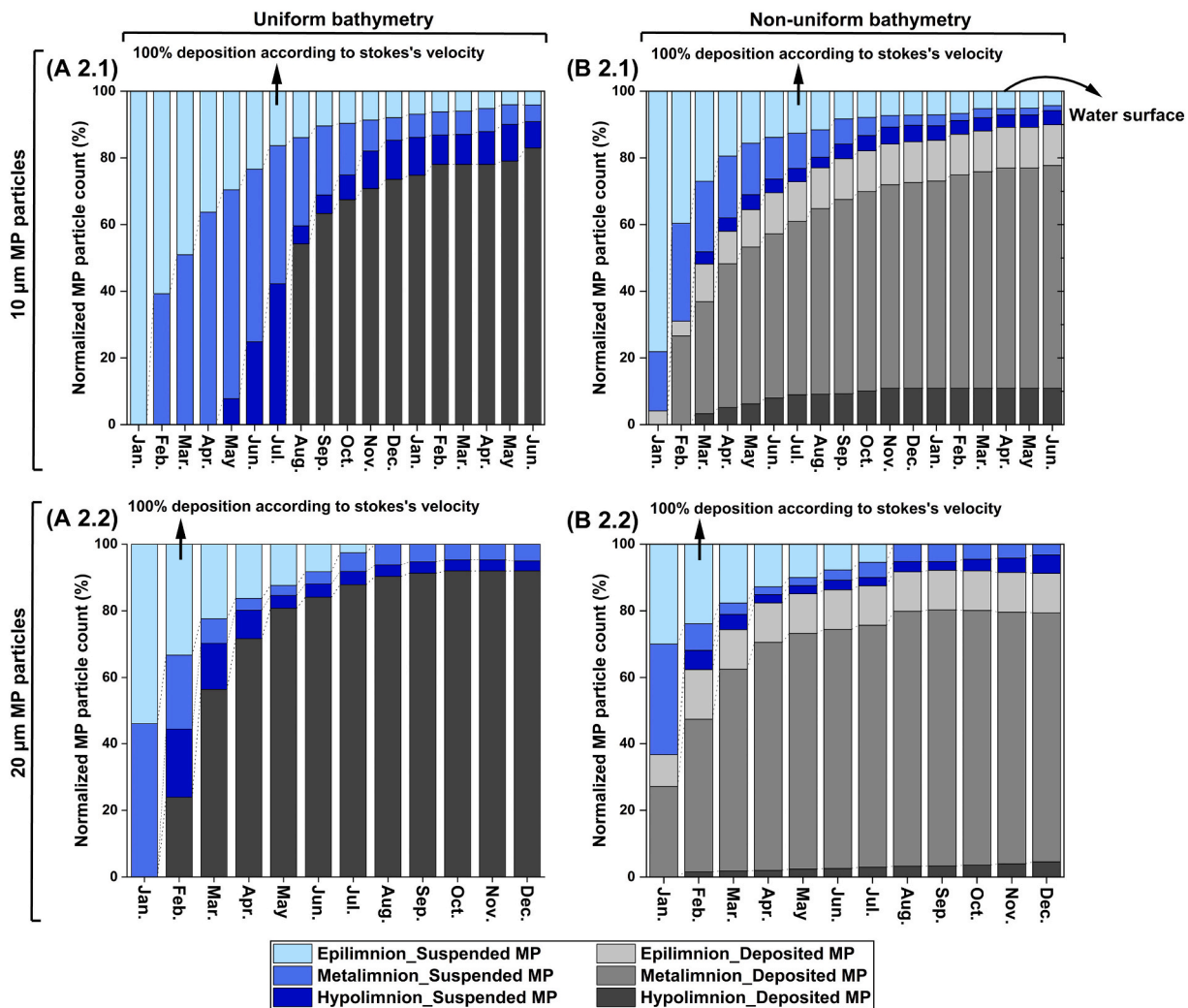


Fig. 7. The suspended and deposited MP particles vs. time for 90,000 MP particles released at the beginning of January for: (A2.1) 10 μm MP particles in the 30 m lake with uniform bathymetry, (B2.1) 10 μm MP particles in the 30 m lake with non-uniform bathymetry, (A2.2) 20 μm MP particles in the 30 m lake with uniform bathymetry, (B2.2) 20 μm MP particles in the 30 m lake with non-uniform bathymetry; the suspended particles are shown in different blue color tones for the intervals of 0–5.2 m (Epilimnion), 5.2–16.8 m (Metalimnion), 16.8–30 m (Hypolimnion), sorted in downward order for all the plots; the gray colors depict the deposited MP particles at the lake bottom for the different lake compartments.

A) and deep lakes (Fig. 6 B). The change from a lake depth of 3 m to 30 m resulted in a significant change in the D_{50%} range of particle deposition, extending from 678 to 2026 m from the release locations within the lake. There was also a significant increase in the variation of the T_{50%} values (up to 16 times) when the lake depth was changed from 3 m to 30 m (Fig. 8 A, C).

The bathymetry of the lake had a significant effect on MP particle transport and, in turn, the deposition patterns (Fig. 4). In the lakes with non-uniform bathymetry, where water depth gradually increases from the shore towards the central area of the lake, a large number of MP particles already settled in the regions near the shoreline. This is also reflected in a decrease in D_{50%} when altering lake bathymetry from uniform to non-uniform of up to 346 m for the 3 m shallow lake (Fig. 6 A) and 834 m for the 30 m deep lake (Fig. 6 B). Furthermore, the impact of bathymetry type is also reflected in a significant variation of T_{50%} with an Inter-Quartile Range (IQR) of 11–89 d for the 30 m deep lakes, while the IQR was 4.7–7 d for 3 m lakes.

3.2.2. MP particle size

In scenarios with the same lake geometry and hydrodynamics settings, particle size was consistently an important factor influencing the MP particle deposition patterns on the lake bed. As the MP particle sizes

increased from 10 to 20 and 50 μm, the deposition patterns of MP particles became more concentrated around the RLs (Fig. 4). The simulations yielded D_{50%} values of 2909, 1678, and 998 m in the lake with 30 m depth and 986, 479, and 302 m in the lake with 3 m depth for 10, 20, and 50 μm MP particles, respectively (Fig. 6 A, B). Moreover, the T_{50%} values also indicated a significant difference in the range of settling time scales when altering the MP particle size from 10 to 20 and 50 μm in the 3 m lakes (IQR: 9–13 d) and 30 m lakes (IQR: 102–178 d), as depicted in Fig. 8.

MP particles stayed in the water column much longer than Stoke's settling velocity would predict for pure gravitational settling (Fig. 7). The fraction of the released 10 μm MP particles remaining in the epilimnion after 18 months of simulation was 4.6 %, with the deposition rate at the lake bed reaching a quasi-steady state (Fig. 7 A2.1, B2.1, Nov.). The 20 μm MP particles attained their quasi-steady state deposition rate within 7 to 8 months after starting the simulations, with no particles found in the epilimnion and 4.1 % of the released particles still suspended at a lower depth in the metalimnion (Fig. 7 A2.2, B2.2, Aug.). When comparing the corresponding individual months, scenarios with 10 μm particles consistently exhibited a significantly greater proportion of suspended MP particles compared to scenarios with 20 μm particles with all other scenario parameters being the same (Fig. 7 A2.1, A2.2 and

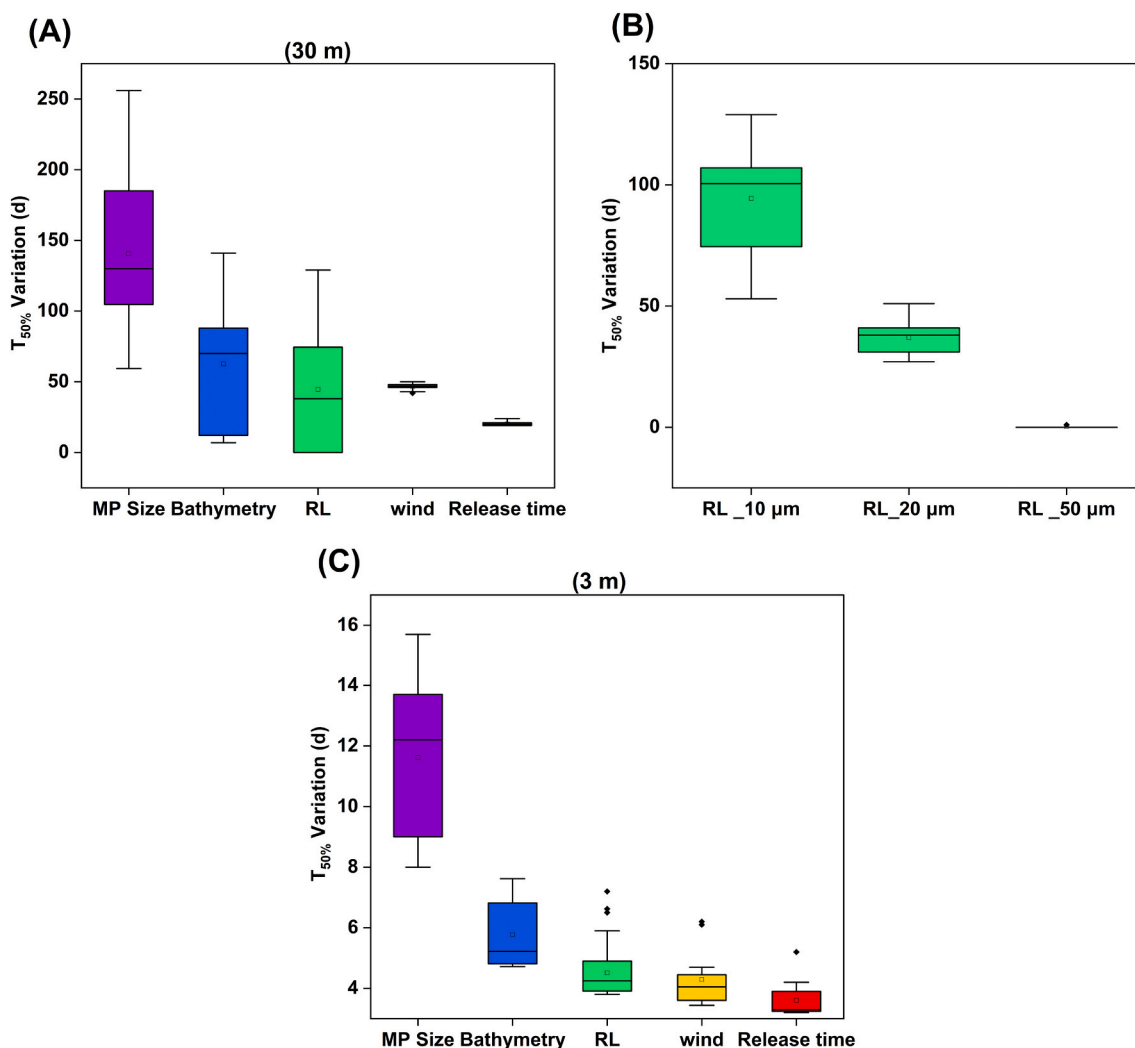


Fig. 8. (A) the T_{50%} variation in the lakes with 30 m depth under the effect of investigated factors listed on the x-axis, (B) the effect of the RL for the different particle sizes (breakdown of the “RL” box in panel A), (C) the same as panel A for the lakes with 3 m depth.

B2.1, B2.2).

In the scenarios for 10 and 20 μm MP particles, particle number in the depth intervals from 5.2 to 16.8 m (Metalimnion) and 16.8 to 30 m (Hypolimnion) did not show a gradual decline with time as in the shallowest depth range (Epilimnion). Instead, the number of suspended particles did show increases and decreases over time due to variable particle inflows and outflows into and out of the respective compartments (Fig. 7).

3.2.3. Wind effects

Fig. 9 depicts the MP particle count in the epilimnion one month after the release of 10 μm and 20 μm MP particles, both under constant and variable wind conditions. 50 μm MP particles exhibited negligible sensitivity to wind conditions and had entirely passed this compartment within one month, regardless of the varying lake characteristics in different scenarios. On the contrary, due to the very small settling velocities, 10 μm MP particles (Table 1) were all still suspended in the epilimnion in the deep lakes with uniform bathymetry one month after starting the simulation (Fig. 9).

With the exception of the 10 μm MP particles released in 30 m lakes with uniform bathymetry, all scenarios involving 10 and 20 μm MP particles generally showed a slightly larger particle count in the epilimnion when subjected to variable wind conditions compared to constant wind (Fig. 9). Also, for these scenarios, the MP particle count in

the epilimnion was slightly lower (by ≈ 3.9 %) when the particles were released in July compared to a release in January (Fig. 9).

The test for significance revealed a nearly zero likelihood that the observed relationship between particle size and its concentration in the epilimnion is a result of chance alone (*p*-value < 6.9 × 10⁻¹⁰). Furthermore, employing Spearman’s Rank correlation coefficient yielded a high value of -0.97, signifying a strong negative correlation between the size of MP particles and their residence time in the epilimnion.

For different wind conditions (constant or variable) over all scenarios, differences in T_{50%} values showed an IQR of 47–51 d for the 30 m lakes (Fig. 8 A), while for the 3 m lakes, the IQR was 2.2–4.7 d (Fig. 8C).

3.2.4. Release location and time

Simulated D_{50%} values for upwind, middle, and downwind RLs in Fig. 5 (D_{50%}_upwind RL > D_{50%}_middle RL > D_{50%}_downwind RL) were similar between the scenarios performed with 20 and 50 μm MP particles for the 30 m deep lakes (Fig. 6 B). For upwind, middle, and downwind RLs, D_{50%} for 20 μm MP particles was calculated as 1899, 1656, and 1512 m in the lakes with uniform bathymetry, and 1567, 1422, and 1339 m in those with non-uniform bathymetry, respectively. For 50 μm MP particles in the 30 m deep lakes, the difference in the D_{50%} values between the RLs was rather insignificant (< 87 m). The D_{50%} values for the 10 μm MP particles did not exhibit a clear trend for the three RLs and were considerably larger than those for the 20 μm and 50

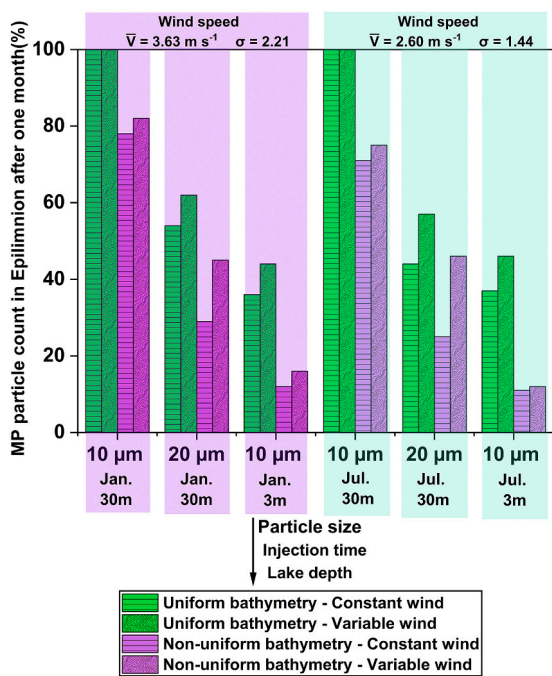


Fig. 9. The percentage of MP particles residing in the epilimnion (0 to 5.2 m); the columns with the purple background represent the scenarios where the particles were released in January, and the columns with the green background represent the scenarios with a release in July. The mean and standard deviation of the wind speed at the top plot are calculated over the month of the particle release.

µm particle sizes. For upwind, middle, and downwind RLs, the $D_{50\%}$ values were 3447, 2549, and 2628 m in the uniform bathymetry lakes, and 2678, 2303, and 2397 m in the non-uniform bathymetry lakes, respectively (Fig. 6 B).

In the lakes with 3 m depth, the evolving MP particle deposition patterns for 20 µm and 50 µm particles did not display significant differences between the different RLs (Fig. 4, 20 µm and 50 µm). However, the 10 µm MP particles showed notably wider deposition patterns (Fig. 4, 10 µm). The difference in $D_{50\%}$ values between the RLs for 20 µm and 50 µm MP sizes did not exceed 97 m and 58 m, respectively, for both types of bathymetry (Fig. 6 A). In contrast, for the 10 µm MP particle size, the maximum differences in $D_{50\%}$ values between the three RLs, were 478 m and 369 m for uniform and non-uniform bathymetries, respectively (Fig. 6 A).

Changing particle release time from January to July increased the $D_{50\%}$ values by 15, 9, and 4 % for 10, 20, and 50 µm MP particles released in 30 m lakes scenarios, respectively (Fig. 6 B). The values of $D_{50\%}$ for 20 and 50 µm MP particles within the 3 m lakes were almost unaffected by the release time change. Only $D_{50\%}$ of 10 µm MP particles increased by 42 m.

The $T_{50\%}$ values in the 3 m shallow lakes showed minimal variation for different RLs (IQR: 2.2–4.6 d, Fig. 8 C), while the variation in 30 m lakes was significantly higher (IQR: 3–78 d, Fig. 8 A). For the 30 m deep lakes, the simulation results indicate a significant impact of the RL on the $T_{50\%}$ of 10 µm MP particles, which had an IQR of 71–119 d across the different RLs. The impact of the RL was found to be significantly lower for 20 µm MP particles (IQR: 37–43 d), while there was hardly any impact of the RL on the $T_{50\%}$ of the 50 µm MP particles (Fig. 8 B). The different particle release times (January and July), showed effects on $T_{50\%}$ for both deep and shallow lakes. In 30 m deep lakes, the IQR for the difference in $T_{50\%}$ values was 25–27 d, while in 3 m shallow lakes, the IQR was 0.3–4.1 d (Fig. 8 A, C).

3.3. Impact of water layering instability on MP particle behavior

Fig. 10 A, B depicts the evolution of particle distributions in the different lake compartments for the deep lake with uniform bathymetry for a July release of 10 µm particles for constant and variable wind conditions. For this scenario, the 10 µm particles showed a temporary increase of MP particle numbers in the epilimnion of approximately 2.6 % for the constant wind scenario and 5.5 % for the variable wind scenario about 2 months after the July release (Fig. 10A, B). Such a behavior was neither evident in the simulation results for the 20 and 50 µm particles for the July release (data not shown) nor in any of the January release scenarios (Fig. 7). As no additional MP particles were released after the initial July release, this increasing number of 10 µm particles in the epilimnion indicates an upward movement of particles from the metalimnion.

During the first quarter of the year (January to March), when the vertical temperature profile in the water column was nearly uniform, water densities in the epilimnion and metalimnion were the same (Fig. 10 C). During this period, the simulated velocity vectors of 10 µm MP particles consistently pointed downward, ranging in magnitude from 0.041 to 0.151 $m\ d^{-1}$. As the air temperature began to rise, thermal stratification started to develop during the second quarter with water density being lower near the lake’s surface and density gradually increasing towards the lake bed layer (Fig. 10 C). Towards the end of the second quarter, the most pronounced thermal stratification was established (Fig. 3 B) and the Péclet number (Eq. (1)) reached its highest value (Fig. 10 D), indicating a stronger dominance of particle settling over particle dispersion for the 10 µm MP particles. This was, in turn, also reflected in a slight increase in MP particle downward velocities during this period (0.047 to 0.163 $m\ d^{-1}$) compared to the other quarters of the year.

At the beginning of the third quarter (beginning of July) the particles were released. During the third quarter air temperatures begin to cool down, causing an increase in water density near the water surface (Epilimnion) and a subsequent reversal in the vertical density profile across the lake (Fig. 10 C, Q3). This altered density gradient led to an unstable stratification inducing convective vertical mixing, which resulted in the simultaneous presence of downward as well as upward particle velocities ranging from -0.032 to $0.092\ m\ d^{-1}$ during this time. This was also reflected in the lower Péclet number indicating a shift towards increasing particle dispersion. These changes in the vertical density gradients were most pronounced around the middle RL followed by the upwind and downwind RLs (Fig. 10 C, D). In the last quarter of the year (October to December), after complete dissipation of the thermal stratification, MP particles velocity vectors again predominantly pointed downward with the velocities ranging from 0.035 to 0.142 $m\ d^{-1}$ (Fig. 10 C).

4. Discussion

The following discussion of our results is organized around the investigated factors and their potential importance for defining MP particle fate in lakes. We further evaluate the relative importance of the different factors in the light of the specific interplay between the factors defining transport mechanisms (i.e. lake depth, bathymetry, wind conditions, and release time and location) and MP particle size and how this interplay can shape particle distribution patterns in the different lake types investigated in this study.

4.1. Depth

The depth of the lake was found to be the most influential factor affecting the settling time scales of MP particles (Fig. 8 A, C) as well as their travel distance (Fig. 6 A, B). In the shallow lakes, the settling of MP particles happens over a relatively short time scale. In addition, particles in these lakes are exposed to constant turbulent mixing conditions (Dean

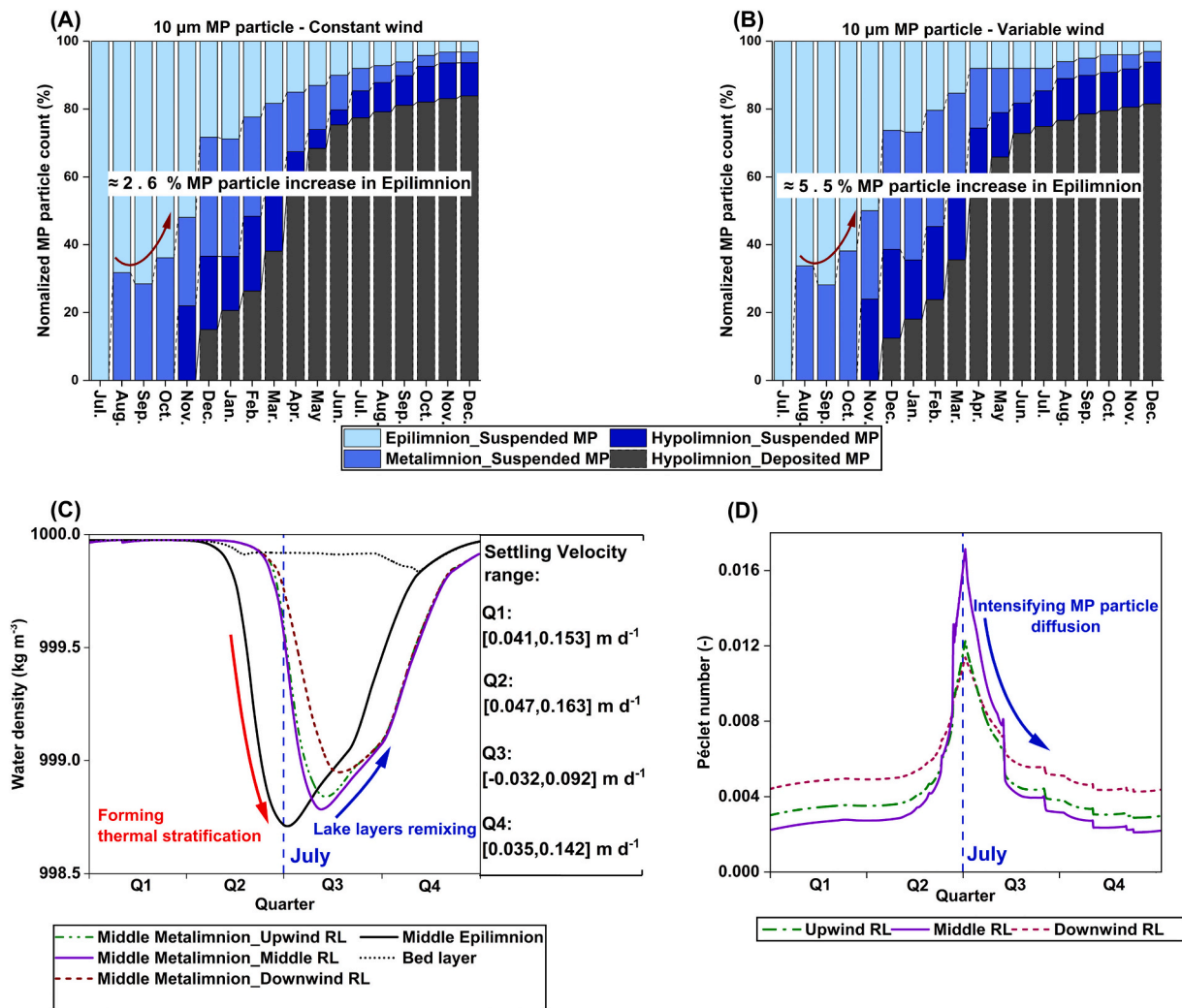


Fig. 10. (A) MP particle counts for the suspended and deposited 10 µm particles over 18 months of simulation for the lake with uniform bathymetry and 30 m depth under constant wind, (B) same scenario as in panel A but under variable wind, (C) density comparison between the water depth in the middle-epilimnion and middle-metalimnion around the upwind, middle, and downwind RLs, for the lakes in panel B, (D) the calculated Péclet number for the MP particles released at upwind, middle, and downwind RLs for the lake presented in panel B.

et al., 2018; Elagami et al., 2023) due to the combined effects of wind-induced velocity and bed layer (Lorke et al., 2003; Umlauf and Lemmin, 2005). This increases the probability of accelerated particle settling. On the other hand, in deep lakes, MP particles face a longer travel distance from the lake surface to the lake bottom, leading to an extended settling time. Also, in these lakes, due to the increased water volume and depth (Cannon et al., 2021), a strong thermal stratification develops (Fig. 3). Subsequent remixing of the lake water layers in the fall leads to the formation of density-driven flows (Fig. 10 D). Hence, this could reduce the likelihood of pure gravity-driven settling of MP particles, yielding an increased residence time within the deep lakes.

4.2. Particle size

In the lakes with equal depths, the size of MP particles dictated their deposition patterns and residence time. The resulting variation in $D_{50\%}$ (Fig. 6) in conjunction with a qualitative visual analysis of the deposition patterns (Fig. 4) clearly suggested more dispersed deposition patterns as the MP particle size decreased. The particle residence time in the water column is dominantly controlled by their effective settling velocity, which is, in turn, affected by particle characteristics and lake properties. The settling behavior in conjunction with hydrodynamic forces causing lateral flows shape distinct deposition patterns in

different lake types.

The simulated settling velocities for the 10 µm particles were much lower than the settling velocities of the larger particles, which made them susceptible to being transported laterally over larger distances by the wind-induced currents in the shallower water layers, regardless of whether the lake was 3 m or 30 m deep (Fig. 4, row of 10 µm scenarios, and Fig. 6). This, in turn, resulted in an increased spread over the lake water surface and contributed to building wider simulated deposition patterns compared to the other MP sizes (Fig. 4 A1.1, A2.1 and B1.1, B2.1). The fate of the MP particles was predominantly influenced by the settling process, as the increase in particle size reduced the time that the particles spent near the water surface where they could be affected by wind-induced currents. For larger MP particles, the dominant settling velocity component governs the orientation of the resultant velocity vector, minimizing horizontal displacement arising from advective and dispersive transport. Consequently, these larger particles exhibit a swifter settling process within the water column, contributing to shorter residence time.

Dispersion, along with wind-induced currents, plays a significant role in horizontal displacement of small MP particles (Daily and Hoffman, 2020). However, consistent with studies in deep water bodies such as the ocean (Chevalier et al., 2023; Daily and Hoffman, 2020; Daily et al., 2022), this effect only became apparent in our simulations when

the particles had settled a significant vertical distance through the 30 m lakes, exposing them to density-driven currents and turbulence over prolonged periods. In the shallow lake scenarios, the long-term influence of dispersion within the water column was less pronounced due to the particles reaching the lake bed layer more quickly (Fig. 4 A1.1, A2.1 (uniform bathymetry), and B1.1, B2.1 (non-uniform bathymetry)). Consequently, the $D_{50\%}$ for the 10 μm MP particles decreased. As the settling velocity of MP particles increased, the spatial extent of the deposition patterns decreased for 20 μm particles, leading to fewer particles being deposited towards the center of the lake. In the deep lakes with non-uniform bathymetry, for instance, in comparison to 10 μm particles, fewer 20 μm MP particles were found in the segment of the bed layer in contact with the hypolimnion (Fig. 7 B2.1, B2.2). For 50 μm MP particles, high settling velocities made the particles less susceptible to lateral displacement by the surrounding lateral flow components, thereby allowing them to move through the water column with less interference. It thus reduced the likelihood of these MP particles reaching the central lake basin through dispersive processes, leading to nearly identical deposition patterns across lakes with different depths but similar bathymetry shapes (Fig. 4 A1.3, A2.3 (uniform bathymetry) and B1.3, B2.3 (non-uniform bathymetry)).

4.3. Bathymetry

The effect of lake bathymetry on the residence time and deposition patterns of MP particles was less significant than the influence of lake depth and particle size ranking it lower in importance. When particle size and lake depth were kept constant, it was observed that particles took significantly longer to settle in the bed layer of deep lakes with uniform bathymetry, compared to the ones with non-uniform bathymetry (Fig. 7 A (uniform bathymetry), B (non-uniform bathymetry)). The observed variations in settling times between scenarios (Fig. 7) can be attributed to the specific geometry of the latter, characterized by significant shallow near-shore areas. In the 30 m deep uniform bathymetry scenario, where the water column height is 30 m, particles uniformly experience longer (30 m) settling paths. In contrast, the non-uniform scenarios, with an average water column height of only 22.3 m, include a significant fraction of much shorter settling path lengths, leading to overall shorter settling times.

In the deep lakes with uniform bathymetry, the complex hydrodynamic processes in the 30 m lake scenarios, specifically the increased mixing intensity, which is commonly found in deeper lakes (Boehrer and Schultze, 2008; Woolway et al., 2020), kept MP particles suspended for longer before they could reach the bed layer. These processes especially affected the smaller particles. After 18 and 12 months of simulation time for the 10 μm and 20 μm MP particles, there were still some particles remaining suspended in the water columns of the lakes of both types of bathymetry, despite the fact that according to their calculated Stokes' settling velocity, they should ideally have completely settled by that time (Fig. 7).

4.4. Release location, wind, and release time

Compared to the lake depth and bathymetry and MP particle size, altering the RL, wind conditions or shifting the release time from January to July had less impact on the deposition patterns and residence time of the MP particles. While for 50 μm particles those factors did not alter the results significantly, their impact increased with decreasing particle size.

In both shallow and deep lakes, the distribution of MP particles showed distinct patterns depending on the RL. MP particles were slightly pushed away from an upwind RL, remained nearly unaffected when released from the middle RL, and showed a slightly more concentrated deposition pattern, when released from the downwind RL (Fig. 6). These variations could be attributed to an increased lateral transport component due to the predominantly western wind and the resulting

horizontal displacement. However, this influence diminished as the size of the MP particles increased due to their larger terminal settling velocity, resulting in less time spent in the upper water layers. Additionally, wind-induced currents had a further impact on MP particles, leading to an extended residence time in the upper layers of the water column, thereby affecting their $T_{50\%}$ value (Fig. 8 B). This effect also decreased with increasing MP particle size. The MP particle count in the epilimnion was slightly elevated when particles were released in January compared to corresponding scenarios where the release occurred in July. This difference is likely due to a larger standard deviation (σ) of wind speed in January than that in July (Fig. 9).

The settling velocity of 10 μm MP particles was found to be impacted by unstable stratification when the MP particles were released at a time closer to the dissipation of thermal stratification (i.e., July release, Fig. 10 A, B). With the release of 10 μm MP particles in July, there was a higher likelihood of MP particles being present in regions where and at times when convective water movement occurred. This probability further increased when the wind conditions were variable, making the MP particles stay longer in the water column due to the unstable water layering and increasing the number of MP particles moving upward from the metalimnion to the epilimnion by approximately 3 % (Fig. 10 A, B). Due to the shallow bed layer near the shorelines in the deep lakes with non-uniform bathymetry, the particles had a higher probability to settle near the RLs. Therefore, the chance for the MP particles to be exposed to the density-driven currents caused by the dissolving thermal stratification was reduced.

The Péclet number calculated using the simulation results for the vicinity of each RL indicated a decreased probability of MP particle settling and a higher chance of horizontal dispersion, particularly around the middle and upwind RLs for 10 μm MP particles (Fig. 10 D, Q3). The varying time scales for delaying the deposition of the MP particles at each RL emphasized the significance of the RLs for the smallest MP particles (Fig. 8 B) and were in line with the Péclet number results, indicating that the MP particles released in proximity to the middle and upwind RLs were more prone to stay suspended during the convective mixing period.

The behavior of MP particles is largely influenced by the drag force acting on them (Ahmadi et al., 2022). As the particles become smaller, their surface area to volume ratio increases, increasing the drag force relative to their size (Ahmadi et al., 2022). While the dissipation of thermal stratification in fall slowed down settling of the 10 μm particles, the evolution of the thermal stratification in spring and early summer had an opposite effect. Therefore, the gradual reduction in water temperature from the lake surface to the bottom led to a corresponding decrease in lake water density and kinematic viscosity, leading to lower drag force exerted on the particles in the upper layers of the lake. As a result, the settling of the MP particles was slightly accelerated (Fig. 10 C, D).

4.5. Complex interplay of influential physical factors on MP particle behavior

Evaluating the relative importance of each individual factor for MP fate is a challenging task, due to their interdependencies and interactions. The relative importance of an individual factor may vary depending on the values of the other factors and their combination. For example, when the particle size is reduced from 50 μm to 10 μm , the influence of wind on the residence time becomes more prominent. This effect arises from the longer exposure of small particles to the influence of wind-induced currents and turbulence, due to their slower settling velocities.

In certain cases, the influence of a specific physical factor on the fate of MP particles may only be detectable under certain configurations of other factors. For example, the influence of the RLs on the behavior of 10 μm particles is only visible when the particles are released in July. This timing increases the probability of their presence in areas of the

lake where they can be influenced by the lake turnover.

4.6. Potential impact of MP particles on lake ecosystems

Lakes provide a diverse habitat for organisms across various trophic levels, presenting opportunities for direct uptake of MP particles for instance through filter-feeding (Scherer et al., 2017), accidental ingestion, or by consuming prey-carrying MP particles (Chae et al., 2018), allowing their introduction into the aquatic food chain (Yıldız et al., 2022). The results show an inverse relationship between particle size and residence time within the water column (Spearman's Rank correlation coefficient = -0.97), particularly within the epilimnion (Fig. 7). The small size of MP particles allows them to stay in shallower water layers for extended periods (Gilfedder et al., 2023). Furthermore, MP particles might migrate from the metalimnion back into the epilimnion during the fall, further increasing the overall MP particle concentration in this lake compartment (Fig. 10 A, B). As the epilimnion is a common feeding ground for many limnic species such as fish and small crustaceans (Estlander et al., 2009) as well as filter-feeding organisms like *Daphnia* (Gilfedder et al., 2023), increased concentrations of smaller, easily ingestible MP particles, significantly increase the risk of MP uptake (Ahmadi et al., 2022; Elagami et al., 2023; Gilfedder et al., 2023).

Moreover, with a decrease in the size of MP particles, the increased potential for widespread distribution (Figs. 4, 7, 9, 10) threatens the quality of freshwater resources (Eerkes-Medrano et al., 2015). Managing and mitigating the effects of MP particles require strategic approaches in water resource management. Implementing advanced filtration systems designed to capture and remove MP particles from water sources becomes imperative to safeguard drinking water reservoirs and supplies (Krishnan et al., 2023; Senathirajah and Palanisami, 2023; Xue et al., 2022).

Alongside the physical factors found to be influential in determining the fate of MP particles, it is important to acknowledge additional factors stemming from the MP particles' unique characteristics and the presence of other substances within the lake. These factors can exert additional influence on the behavior of MP particles. For instance, factors such as the surface area to volume ratio, polymer type, and particle surface charge can play a crucial role in determining the terminal settling velocity of MP particles, alongside their density and size (Ahmadi et al., 2022; Elagami et al., 2022; Khatmullina and Isachenko, 2017; Waldschläger and Schüttrumpf, 2019). Our earlier research (Ahmadi et al., 2022) has demonstrated that irregularly shaped MP particles with higher surface area-to-volume ratios tend to have longer residence time due to increased drag forces. Furthermore, the processes of aggregation with particulate matter and agglomeration may add additional complexity to particle behavior (Schmidtmann et al., 2022). To gain a more comprehensive understanding of MP particle fate, future studies should incorporate these additional factors that can influence particle transport velocities in lakes, also including the effects of lake inlets and outlets, to account for more complex lake hydrodynamics. By carrying out further comprehensive simulations in continuation of this research, an improved mechanistic understanding of the complex interplay between different factors affecting the transport and fate of MP particles in lakes could be reached. This understanding can help to develop strategies to mitigate detrimental effects on ecosystems and humans posed by MP particles.

5. Conclusion

The investigated physical factors all have an influence on the behavior of MP particles in lakes but with varying levels of importance. Overall, lake depth emerged as the most important factor, exerting control on hydrodynamic complexity and, in turn, defining the settling time scale, over which other physical factors can act on the settling particles. Following in importance is particle size, which is decisive for the settling velocity and for the exposure time of MP particles to

hydrodynamic conditions in various lake compartments. Bathymetry (uniform or non-uniform) additionally affects MP particle settling times as do the locally varying hydrodynamic conditions that evolve during the dissipation of the thermal stratification in the deeper lakes, leading to spatial differences in density-driven flows and associated mixing in nearshore areas. A more subordinate factor is the release location, which only has a pronounced effect when the MP particles are small enough to be significantly impacted by the specific hydrodynamics in the vicinity of the RL (e.g. during the dissipation of thermal stratification). Wind conditions are also a lower-ranked factor, generally showing a comparatively small influence on the particle movement within the investigated lakes. Only for sufficiently small particles, which stay suspended near the water surface, wind patterns showed a significant effect on the lateral spread of particles. Release time exhibited the weakest impact on the spatial patterns of particle deposition. However, particles released when the thermal stratification of the lake dissolves may have an increased likelihood of being uplifted from the metalimnion to the epilimnion due to convective water movement occurring in the upper layers of the lake.

Despite the strong impact of individual factors on MP particle movement in the virtual lakes, it is ultimately the complex interplay between all factors that eventually controls the transport and fate of MP particles in lakes. For example, the effects of wind conditions, release location, or release time may only become important when coinciding with specific combinations of other factors, such as lake depth, bathymetry, and the size of the released MP particles. Thus, evaluating MP particle transport and fate in lakes based on single factors or a subset of factors alone may be misleading, and a thorough assessment and evaluation of all relevant factors and their interactions is needed. 3D numerical models are tools well suited to elucidate these complex interactions. This study has taken the first steps in this direction and can provide a starting point for further investigations.

Funding

This research was funded by the Deutsche Forschungsgemeinschaft (DFG, German Research Foundation), CRC Microplastic, project Number 391977956-SFB 1357, additional funding was provided by the Helmholtz Research Program (POF, phase IV, Topic 5, Subtopic 5.2) as well as by Deutscher Akademischer Austauschdienst (DAAD), funding program 57709211.

CRediT authorship contribution statement

Pouyan Ahmadi: Formal analysis, Methodology, Software, Validation, Writing – original draft, Conceptualization, Investigation, Visualization. **Franz Dichgans:** Methodology, Writing – review & editing. **Lisa Jagau:** Software, Writing – review & editing. **Christian Schmidt:** Methodology, Writing – review & editing. **Vadym Aizinger:** Writing – review & editing. **Benjamin S. Gilfedder:** Writing – review & editing. **Jan H. Fleckenstein:** Conceptualization, Methodology, Supervision, Writing – review & editing.

Declaration of competing interest

The authors declare that they have no known competing financial interests or personal relationships that could have appeared to influence the work reported in this paper.

Data availability

Data will be made available on request.

Acknowledgment

We acknowledge the E-OBS dataset from the EU-FP6 project UERRA

(<http://www.uerra.eu>) and the data providers in the ECA&D project (<https://www.ecad.eu>). We would also like to express our gratitude to Pia Ebeling for her support in conducting statistical analyses and preparing the temperature data employed in this study.

Appendix A. Supplementary data

Supplementary data to this article can be found online at <https://doi.org/10.1016/j.scitotenv.2024.170218>.

References

- Ahmadi, P., Elagami, H., Dichgans, F., Schmidt, C., Gilfedder, B.S., Frei, S., Peiffer, S., Fleckenstein, J.H., 2022. Systematic evaluation of physical parameters affecting the terminal settling velocity of microplastic particles in lakes using CFD. *Front. Environ. Sci.* 389.
- Alosairi, Y., Al-Salem, S., Al Ragum, A., 2020. Three-dimensional numerical modelling of transport, fate and distribution of microplastics in the northwestern Arabian/Persian gulf. *Mar. Pollut. Bull.* 161, 111723.
- Boehrer, B., Schultze, M., 2008. Stratification of lakes. *Rev. Geophys.* 46 (2).
- Boos, J.P., Gilfedder, B.S., Frei, S., 2021. Tracking microplastics across the streambed interface: using laser-induced-fluorescence to quantitatively analyze microplastic transport in an experimental flume. *Water Resour. Res.* 57 (12), e2021WR031064.
- Browne, M.A., Crump, P., Niven, S.J., Teuten, E., Tonkin, A., Galloway, T., Thompson, R., 2011. Accumulation of microplastic on shorelines worldwide: sources and sinks. *Environ. Sci. Technol.* 45 (21), 9175–9179.
- Burns, E.E., Boxall, A.B., 2018. Microplastics in the aquatic environment: evidence for or against adverse impacts and major knowledge gaps. *Environ. Toxicol. Chem.* 37 (11), 2776–2796.
- Cable, R.N., Beletsky, D., Beletsky, R., Wigginton, K., Locke, B.W., Duhaime, M.B., 2017. Distribution and modeled transport of plastic pollution in the Great Lakes, the world's largest freshwater resource. *Front. Environ. Sci.* 5, 45.
- Cannon, D.J., Troy, C., Bootsma, H., Liao, Q., MacLellan-Hurd, R.A., 2021. Characterizing the seasonal variability of hypolimnetic mixing in a large, deep lake. *J. Geophys. Res. Oceans* 126 (11), e2021JC017533.
- Castro-Castellon, A.T., Horton, A.A., Hughes, J.M., Rampley, C., Jeffers, E.S., Bussi, G., Whitehead, P., 2022. Ecotoxicity of microplastics to freshwater biota: considering exposure and hazard across trophic levels. *Sci. Total Environ.* 816, 151638.
- Chae, Y., Kim, D., Kim, S.W., An, Y.-J., 2018. Trophic transfer and individual impact of nano-sized polystyrene in a four-species freshwater food chain. *Sci. Rep.* 8 (1), 284.
- Chevalier, C., Vandenberghe, M., Pagano, M., Pellet, I., Pinazo, C., Onrubia, J.A.T., Guilloux, L., Carlotti, F., 2023. Investigation of dynamic change in microplastics vertical distribution patterns: the seasonal effect on vertical distribution. *Mar. Pollut. Bull.* 189, 114674.
- Collard, F., Gasperi, J., Gabrielsen, G.W., Tassin, B., 2019. Plastic particle ingestion by wild freshwater fish: a critical review. *Environ. Sci. Technol.* 53 (22), 12974–12988.
- Cornes, R.C., van der Schrier, G., van den Besselaar, E.J., Jones, P.D., 2018. An ensemble version of the E-OBS temperature and precipitation data sets. *J. Geophys. Res. Atmos.* 123 (17), 9391–9409.
- Daily, J., Hoffman, M.J., 2020. Modeling the three-dimensional transport and distribution of multiple microplastic polymer types in Lake Erie. *Mar. Pollut. Bull.* 154, 111024.
- Daily, J., Tyler, A.C., Hoffman, M.J., 2022. Modeling three-dimensional transport of microplastics and impacts of biofouling in Lake Erie and Lake Ontario. *J. Great Lakes Res.* 48 (5), 1180–1190.
- D'Avignon, G., Gregory-Eaves, I., Ricciardi, A., 2022. Microplastics in lakes and rivers: an issue of emerging significance to limnology. *Environ. Rev.* 30 (2), 228–244.
- Dean, B.Y., Corcoran, P.L., Helm, P.A., 2018. Factors influencing microplastic abundances in nearshore, tributary and beach sediments along the Ontario shoreline of Lake Erie. *J. Great Lakes Res.* 44 (5), 1002–1009.
- Deleersnijder, E., Beckers, J.-M., Delhez, E.J., 2006. The residence time of settling particles in the surface mixed layer. *Environ. Fluid Mech.* 6, 25–42.
- Deltares, D., 2013. *Delft3D-FLOW User Manual*. Deltares Delft, The Netherlands, p. 330.
- Dichgans, F., Boos, J.-P., Ahmadi, P., Frei, S., Fleckenstein, J.H., 2023. Integrated numerical modeling to quantify transport and fate of microplastics in the hyporheic zone. *Water Res.* 120349.
- Dusaucy, J., Gateuille, D., Perrette, Y., Naffrechoux, E., 2021. Microplastic pollution of worldwide lakes. *Environ. Pollut.* 284, 117075.
- Eerkes-Medrano, D., Thompson, R.C., Aldridge, D.C., 2015. Microplastics in freshwater systems: a review of the emerging threats, identification of knowledge gaps and prioritisation of research needs. *Water Res.* 75, 63–82.
- Egessa, R., Nankabirwa, A., Ocaya, H., Pabire, W.G., 2020. Microplastic pollution in surface water of Lake Victoria. *Sci. Total Environ.* 741, 140201.
- Elagami, H., Ahmadi, P., Fleckenstein, J.H., Frei, S., Obst, M., Agarwal, S., Gilfedder, B. S., 2022. Measurement of microplastic settling velocities and implications for residence times in thermally stratified lakes. *Limnol. Oceanogr.* 67 (4), 934–945.
- Elagami, H., Frei, S., Boos, J.-P., Trommer, G., Gilfedder, B.S., 2023. Quantifying microplastic residence times in lakes using mesocosm experiments and transport modelling. *Water Res.* 229, 119463.
- Eriksen, M., Mason, S., Wilson, S., Box, C., Zellers, A., Edwards, W., Farley, H., Amato, S., 2013. Microplastic pollution in the surface waters of the Laurentian Great Lakes. *Mar. Pollut. Bull.* 77 (1–2), 177–182.
- Estlander, S., Nurminen, L., Olin, M., Vinni, M., Horppila, J., 2009. Seasonal fluctuations in macrophyte cover and water transparency of four brown-water lakes: implications for crustacean zooplankton in littoral and pelagic habitats. *Hydrobiologia* 620, 109–120.
- Falconieri, M., Iannilli, V., Lecce, F., Pietrelli, L., Sighicelli, M., 2018. Microplastic pollution in the surface waters of Italian Subalpine Lakes. *Environ. Pollut.* 236.
- Fischer, E.K., Paglialonga, L., Czech, E., Tamminga, M., 2016. Microplastic pollution in lakes and Lake shoreline sediments—a case study on Lake Bolsena and Lake Chiusi (Central Italy). *Environ. Pollut.* 213, 648–657.
- Free, C.M., Jensen, O.P., Mason, S.A., Eriksen, M., Williamson, N.J., Boldgiv, B., 2014. High-levels of microplastic pollution in a large, remote, mountain lake. *Mar. Pollut. Bull.* 85 (1), 156–163.
- Gao, X., Kong, B., Vigil, R.D., 2017. Comprehensive computational model for combining fluid hydrodynamics, light transport and biomass growth in a Taylor vortex algal photobioreactor: Eulerian approach. *Algal Res.* 24, 1–8.
- Gilfedder, B., Elagami, H., Boos, J., Brehm, J., Schott, M., Witt, L., Laforsch, C., Frei, S., 2023. Filter feeders are key to small microplastic residence times in stratified lakes: a virtual experiment. *Sci. Total Environ.* 164293.
- Hale, R.C., Seeley, M.E., La Guardia, M.J., Mai, L., Zeng, E.Y., 2020. A global perspective on microplastics. *J. Geophys. Eng. Oceans* 125 (1), e2018JC014719.
- Hoffman, M.J., Hittinger, E., 2017. Inventory and transport of plastic debris in the Laurentian Great Lakes. *Mar. Pollut. Bull.* 115 (1–2), 273–281.
- Khatmullina, L., Isachenko, I., 2017. Settling velocity of microplastic particles of regular shapes. *Mar. Pollut. Bull.* 114 (2), 871–880.
- Kitazawa, D., Kumagai, M., 2005. Numerical Simulation on Seasonal Variation in Dissolved Oxygen Tension in Lake Biwa, pp. 21–22.
- Klein, S., Dimzon, I.K., Eubeler, J. and Knepper, T.P. 2018. Analysis, occurrence, and degradation of microplastics in the aqueous environment. *Freshwater Microplastics: Emerging Environmental Contaminants?*, 51–67.
- Kowalski, N., Reichardt, A.M., Waniek, J.J., 2016. Sinking rates of microplastics and potential implications of their alteration by physical, biological, and chemical factors. *Mar. Pollut. Bull.* 109 (1), 310–319.
- Krishnan, R.Y., Manikandan, S., Subbaya, R., Karmegam, N., Kim, W., Govarthanan, M., 2023. Recent approaches and advanced wastewater treatment technologies for mitigating emerging microplastics contamination—a critical review. *Sci. Total Environ.* 858, 159681.
- Lamb, H., 1932. *Hydrodynamics*, 6th edition. C.U.P.
- Lambert, S., Wagner, M., 2018. *Microplastics Are Contaminants of Emerging Concern in Freshwater Environments: An Overview*. Springer International Publishing.
- Law, K.L., 2017. Plastics in the marine environment. *Annu. Rev. Mar. Sci.* 9, 205–229.
- Lebreton, L.-M., Greer, S., Borrero, J.C., 2012. Numerical modelling of floating debris in the world's oceans. *Mar. Pollut. Bull.* 64 (3), 653–661.
- Leiser, R., Wu, G.-M., Neu, T.R., Wendt-Potthoff, K., 2020. Biofouling, metal sorption and aggregation are related to sinking of microplastics in a stratified reservoir. *Water Res.* 176, 115748.
- Leiser, R., Jongsma, R., Bakenhus, I., Möckel, R., Philipp, B., Neu, T.R., Wendt-Potthoff, K., 2021a. Interaction of cyanobacteria with calcium facilitates the sedimentation of microplastics in a eutrophic reservoir. *Water Res.* 189, 116582.
- Leiser, R., Schumann, M., Dadi, T., Wendt-Potthoff, K., 2021b. Burial of microplastics in freshwater sediments facilitated by iron-organos flocs. *Sci. Rep.* 11 (1), 1–12.
- Lorke, A., Müller, B., Maerki, M., Wüest, A., 2003. Breathing sediments: the control of diffusive transport across the sediment—water interface by periodic boundary-layer turbulence. *Limnol. Oceanogr.* 48 (6), 2077–2085.
- Maximenko, N., Hafner, J., Nilner, P., 2012. Pathways of marine debris derived from trajectories of Lagrangian drifters. *Mar. Pollut. Bull.* 65 (1–3), 51–62.
- Mcnutt, M., 2017. Production, use, and fate of all plastics ever made. *Sci. Adv.* 19.
- Mountford, A., Morales Maqueda, M., 2019. Eulerian modeling of the three-dimensional distribution of seven popular microplastic types in the global ocean. *J. Geophys. Res. Oceans* 124 (12), 8558–8573.
- Nava, V., Chandra, S., Aherne, J., Alfonso, M.B., Antão-Geraldes, A.M., Attermeyer, K., Bao, R., Bartrons, M., Berger, S.A., Biernaczyk, M., 2023. Plastic debris in lakes and reservoirs. *Nature* 619 (7969), 317–322.
- Nematollahi, M.J., Moore, F., Keshavarzi, B., Vogt, R.D., Saravi, H.N., Busquets, R., 2020. Microplastic particles in sediments and waters, south of Caspian Sea: frequency, distribution, characteristics, and chemical composition. *Ecotoxicol. Environ. Saf.* 206, 111137.
- Nordam, T., Kristiansen, R., Nepstad, R., Röhrs, J., 2019. Numerical analysis of boundary conditions in a Lagrangian particle model for vertical mixing, transport and surfacing of buoyant particles in the water column. *Ocean Model* 136, 107–119.
- Nunez, P., Castanedo, S., Medina, R., 2021. Role of ocean tidal asymmetry and estuarine geometry in the fate of plastic debris from ocean sources within tidal estuaries. *Estuar. Coast. Shelf Sci.* 259, 107470.
- O'Sullivan, P., Reynolds, C.S., 2008. *The Lakes Handbook, Volume 1: Limnology and Limnetic Ecology*. John Wiley & Sons.
- Pilato, L., 2010. *Phenolic Resins: A Century of Progress*. Springer.
- Qian, J., Tang, S., Wang, P., Lu, B., Li, K., Jin, W., He, X., 2021. From source to sink: review and prospects of microplastics in wetland ecosystems. *Sci. Total Environ.* 758, 143633.
- Raimundo, G.I., Sousa, M.C., Dias, J.M., 2020. Numerical modelling of plastic debris transport and accumulation throughout Portuguese coast. *J. Coast. Res.* 95 (SI), 1252–1257.
- Razeghi, N., Hamidian, A.H., Wu, C., Zhang, Y., Yang, M., 2021. Microplastic sampling techniques in freshwaters and sediments: a review. *Environ. Chem. Lett.* 19 (6), 4225–4252.
- Reeks, M., 1977. On the dispersion of small particles suspended in an isotropic turbulent fluid. *J. Fluid Mech.* 83 (3), 529–546.

- Rimmer, A., 2006. Empirical classification of stratification patterns in warm monomictic lakes. *Verh. - Int. Ver. Theor. Angew. Limnol.* 29 (4), 1773–1776.
- Scherer, C., Brennholt, N., Reifferscheid, G., Wagner, M., 2017. Feeding type and development drive the ingestion of microplastics by freshwater invertebrates. *Sci. Rep.* 7 (1), 17006.
- Schmidt, C., Krauth, T., Wagner, S., 2017. Export of plastic debris by Rivers into the sea. *Environ. Sci. Technol.* 51 (21), 12246–12253.
- Schmidtman, J., Elagami, H., Gilfedder, B.S., Fleckenstein, J.H., Papastavrou, G., Mansfeld, U., Peiffer, S., 2022. Heteroaggregation of PS microplastic with ferrihydrite leads to rapid removal of microplastic particles from the water column. *Environ Sci Process Impacts* 24 (10), 1782–1789.
- Senathirajah, K., Palanisami, T., 2023. Strategies to reduce risk and mitigate impacts of disaster: increasing water quality resilience from microplastics in the water supply system. *ACS ES&T Water* 3 (9), 2816–2834.
- Stuparu, D., van der Meulen, M., Kleissen, F., Vethaak, D. and El Serafy, G. 2015 **Developing a transport model for plastic distribution in the North Sea.**
- Umlauf, L., Lemmin, U., 2005. Interbasin exchange and mixing in the hypolimnion of a large lake: the role of long internal waves. *Limnol. Oceanogr.* 50 (5), 1601–1611.
- Wagner, M., Scherer, C., Alvarez-Muñoz, D., Brennholt, N., Bourrain, X., Buchinger, S., Fries, E., Grosbois, C., Klasmeier, J., Marti, T., 2014. Microplastics in freshwater ecosystems: what we know and what we need to know. *Environ. Sci. Eur.* 26 (1), 1–9.
- Waldschläger, K., Schüttrumpf, H., 2019. Effects of particle properties on the settling and rise velocities of microplastics in freshwater under laboratory conditions. *Environ. Sci. Technol.* 53 (4), 1958–1966.
- Wang, T., Yu, C., Chu, Q., Wang, F., Lan, T., Wang, J., 2020. Adsorption behavior and mechanism of five pesticides on microplastics from agricultural polyethylene films. *Chemosphere* 244, 125491.
- Williams, A., Simmons, S., 1996. The degradation of plastic litter in rivers: implications for beaches. *J. Coast. Conserv.* 2, 63–72.
- Woolway, R.I., Kraemer, B.M., Lenters, J.D., Merchant, C.J., O'Reilly, C.M., Sharma, S., 2020. Global lake responses to climate change. *Nat. Rev. Earth Environ.* 1 (8), 388–403.
- Wright, S.L., Ulke, J., Font, A., Chan, K.L.A., Kelly, F.J., 2020. Atmospheric microplastic deposition in an urban environment and an evaluation of transport. *Environ. Int.* 136, 105411.
- Xue, J., Samaei, S.H.-A., Chen, J., Doucet, A., Ng, K.T.W., 2022. What have we known so far about microplastics in drinking water treatment? A timely review. *Front. Environ. Sci. Eng.* 16, 1–18.
- Yang, S., Zhou, M., Chen, X., Hu, L., Xu, Y., Fu, W., Li, C., 2022. A comparative review of microplastics in lake systems from different countries and regions. *Chemosphere* 286, 131806.
- Yıldız, D., Yalçın, G., Jovanović, B., Boukal, D.S., Vebrová, L., Riha, D., Stanković, J., Savić-Zdraković, D., Metin, M., Akyürek, Y.N., 2022. Effects of a microplastic mixture differ across trophic levels and taxa in a freshwater food web: in situ mesocosm experiment. *Sci. Total Environ.* 836, 155407.

Supplementary Material on:

Systematic CFD-based evaluation of physical factors influencing the spatiotemporal distribution of microplastic particles in lakes

Pouyan Ahmadi^{1*}, Franz Dichgans¹, Lisa Jagau², Christian Schmidt¹, Vadym Aizinger², Benjamin S. Gilfedder^{3,4}, Jan H. Fleckenstein^{1,5}

¹Department of Hydrogeology, Helmholtz-Centre for Environmental Research, UFZ, 04318 Leipzig, Germany

²Chair of Scientific Computing, University of Bayreuth, 95440 Bayreuth, Germany

³Limnological Research Station, Bayreuth Center of Ecology and Environmental Research, University of Bayreuth, 95440 Bayreuth, Germany

⁴Department of Hydrology, Bayreuth Center of Ecology and Environmental Research (BayCEER), University of Bayreuth, 95440 Bayreuth, Germany

⁵Hydrologic Modelling Unit, Bayreuth Center of Ecology and Environmental Research (BayCEER), University of Bayreuth, 95440 Bayreuth, Germany

***Corresponding author:**

Pouyan Ahmadi at Helmholtz Centre for Environmental Research - UFZ, Department Hydrogeology, Permoserstr. 15, 04318 Leipzig, Germany. Email address: pouyan.ahmadi@ufz.de.

S1. Meteorological data used in the hydrodynamics model configuration

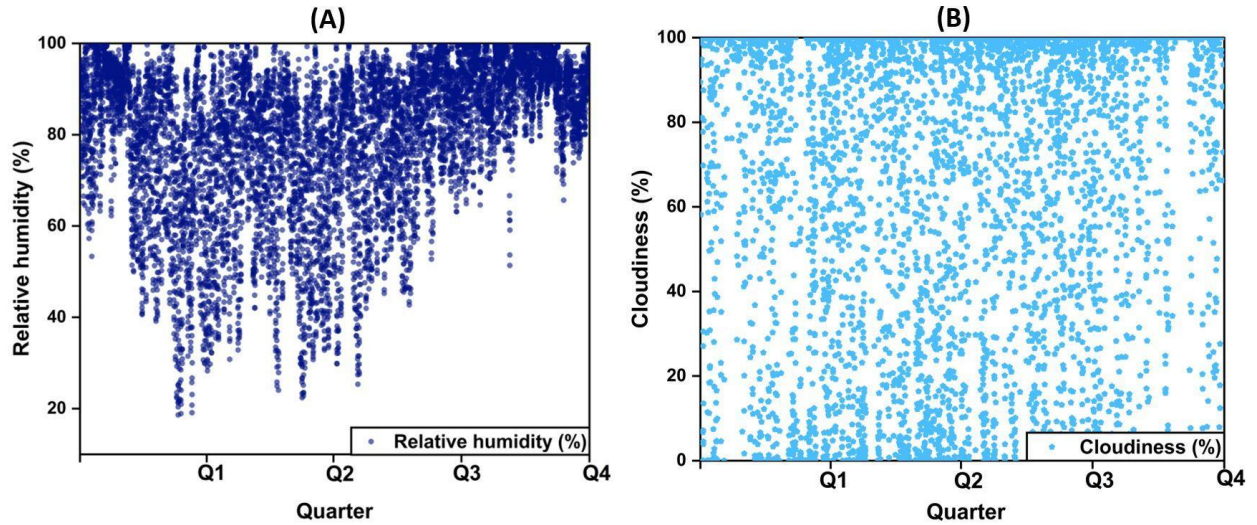


Figure S1: (A) Relative humidity at Brombachsee (49.12° N, 10.92° E, Middle Franconia, Germany), (B) Cloudiness at Brombachsee (49.12° N, 10.92° E, Middle Franconia, Germany).

S2. Utilizing Stoke's law for calculating the terminal settling velocity of MP particles

The Delft3D model dynamically computes the trajectory of particles over time, providing a detailed spatial and temporal representation of their paths. The individual position of each particle is subject to factors such as advection (transport by water flow), dispersion (random component), and settling. In the model, each particle represents real-world particles, where its mass signifies the amount of substance attached to it (Stuparu et al., 2015). The settling velocity of each particle at a specific time is determined using Stokes' law.

$$\mathbf{V}_p = \frac{9(\rho_p - \rho_w)}{2\mu} \mathbf{g}R^2 \quad \text{S1}$$

Where ρ_p [M L^{-3}] is the density of the particle, ρ_w [M L^{-3}] is the density of the lake water, R [L] is the radius of the particle, g [LT^{-2}] is the acceleration due to gravity, and μ [$\text{M L}^{-1} \text{T}^{-1}$] is the dynamic viscosity of the water (Elagami et al., 2023; Stuparu et al., 2015).

S3. Validating the simulated temperature profiles using an empirical function for thermally stratified lakes

The temperature profiles presented in Figure 3D in the manuscript are derived from our hydrodynamic model, representing a scenario closely aligned with real-world conditions since the simulated lake is characterized by non-uniform bathymetry and variable wind patterns. Given that our study involves synthetic scenarios, the model outcomes lack direct validation through field measurements. To address this, we applied the empirical approach introduced by Rimmer (Rimmer, 2006) to compute temperature profiles based on our specified boundary conditions. The comparison, depicted in Figure S2 for months featuring thermal stratification, reveals a robust correspondence between these independently generated profiles and our model results, affirming the validity and accuracy of the simulated temperature profiles.

The empirical function (S2), $T(b)$, representing the temperature at any depth b (considered positive in the downward direction), is described by the following general equation:

$$\frac{T(b) - T_h}{T_e - T_h} = \left[\frac{1}{1 + (b\alpha)^n} \right]^m ; m = 1 - \frac{1}{n} \quad \text{S2}$$

where T_h is the minimal temperature at the bottom of the hypolimnion [$^{\circ}\text{C}$]; T_e is the temperature of the water at the lake surface [$^{\circ}\text{C}$], and α and n are empirical, unitless parameters (Rimmer, 2006).

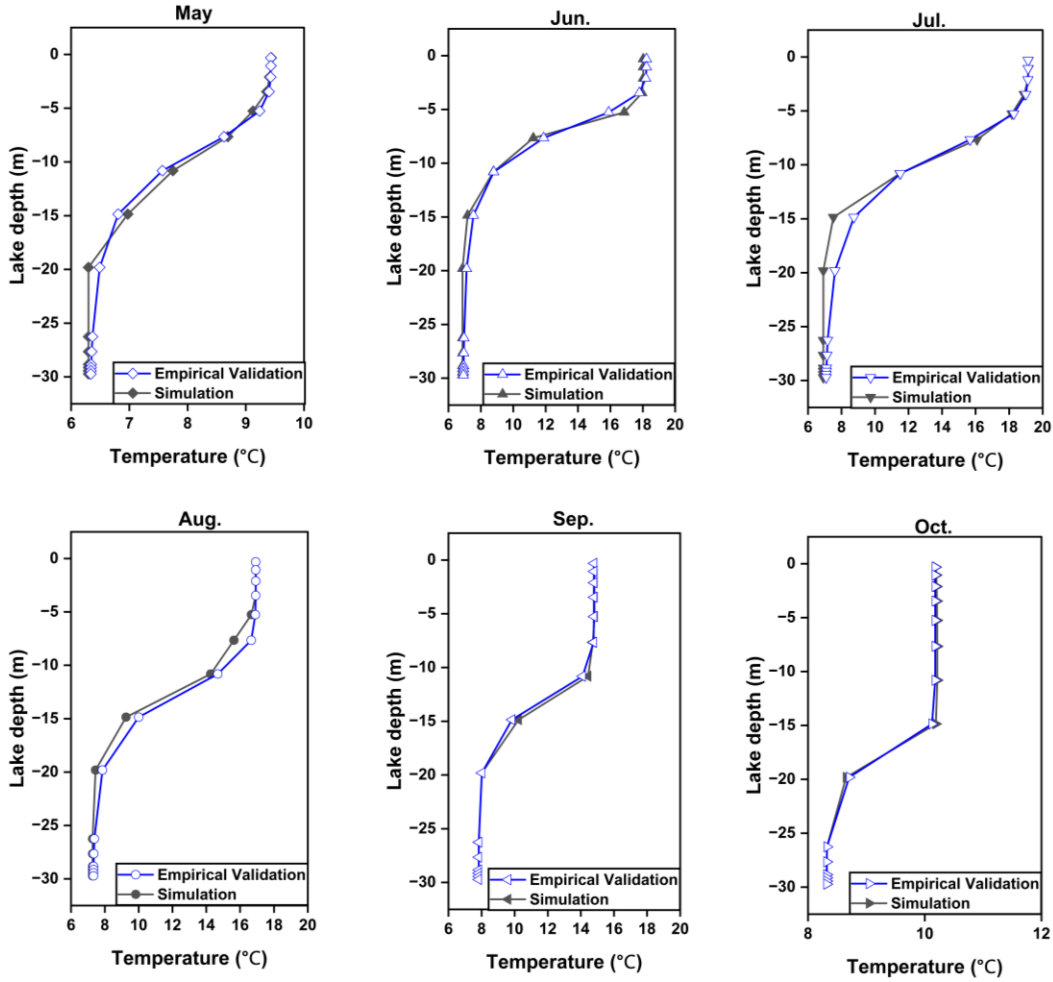


Figure S2: Comparison between temperature profiles modeled for a lake characterized by non-uniform bathymetry and variable wind conditions and the corresponding computed temperature profiles utilizing an empirical function introduced for thermally stratified lakes.

Table S1: The parameters used to calculate the empirical temperature profiles shown in Figure S2.

Month	T_e (°C)	T_h (°C)	n	alpha
May	9.43	6.29	4.5	0.11
Jun.	6.87	18.23	4.5	0.15
Jul.	6.91	19.14	4.5	0.113
Aug.	7.27	16.92	7	0.08
Sep.	7.82	14.79	10	0.075
Oct.	8.32	10.18	17	0.055

References

- Elagami H, Frei S, Boos J-P, Trommer G, Gilfedder BS. Quantifying microplastic residence times in lakes using mesocosm experiments and transport modelling. *Water Research* 2023; 229: 119463.
- Rimmer A. Empirical classification of stratification patterns in warm monomictic lakes. *Internationale Vereinigung für Theoretische und Angewandte Limnologie Verhandlungen* 2006; 29: 1773-1776.
- Stuparu D, van der Meulen M, Kleissen F, Vethaak D, El Serafy G. Developing a transport model for plastic distribution in the North Sea. *E-proceedings of the 36th IAHR World Congress*. 28, 2015.

List of publications

Publications included in this thesis

Ahmadi, P., Elagami, H., Dichgans, F., Schmidt, C., Gilfedder, B.S., Frei, S., Peiffer, S. and Fleckenstein, J.H., 2022. Systematic evaluation of physical parameters affecting the terminal settling velocity of microplastic particles in lakes using CFD. *Frontiers in Environmental Science*, 10, p.875220.

Elagami, H., **Ahmadi, P.**, Fleckenstein, J.H., Frei, S., Obst, M., Agarwal, S. and Gilfedder, B.S., 2022. Measurement of microplastic settling velocities and implications for residence times in thermally stratified lakes. *Limnology and Oceanography*, 67(4), pp.934-945.

Ahmadi, P., Dichgans, F., Jagau, L., Schmidt, C., Aizinger, V., Gilfedder, B.S., and Fleckenstein, J.H., 2022. Systematic CFD-based evaluation of physical factors influencing the spatiotemporal distribution of MP particles in lakes. *Science of The Total Environment*, 917, p.170218.

Publications not included in this thesis

Dichgans F, Boos JP, **Ahmadi P**, Frei S, Fleckenstein JH. Integrated numerical modeling to quantify transport and fate of microplastics in the hyporheic zone. *Water Research*. 2023 Sep 1;243:120349.

(Eidesstattliche) Versicherungen und Erklärungen

(§ 9 Satz 2 Nr. 3 PromO BayNAT)

Hiermit versichere ich eidesstattlich, dass ich die Arbeit selbstständig verfasst und keine anderen als die von mir angegebenen Quellen und Hilfsmittel benutzt habe (vgl. Art. 97 Abs. 1 Satz 8 BayHIG).

(§ 9 Satz 2 Nr. 3 PromO BayNAT)

Hiermit erkläre ich, dass ich die Dissertation nicht bereits zur Erlangung eines akademischen Grades eingereicht habe und dass ich nicht bereits diese oder eine gleichartige Doktorprüfung endgültig nicht bestanden habe.

(§ 9 Satz 2 Nr. 4 PromO BayNAT)

Hiermit erkläre ich, dass ich Hilfe von gewerblichen Promotionsberatern bzw. -vermittlern oder ähnlichen Dienstleistern weder bisher in Anspruch genommen habe noch künftig in Anspruch nehmen werde.

(§ 9 Satz 2 Nr. 7 PromO BayNAT)

Hiermit erkläre ich mein Einverständnis, dass die elektronische Fassung meiner Dissertation unter Wahrung meiner Urheberrechte und des Datenschutzes einer gesonderten Überprüfung unterzogen werden kann.

(§ 9 Satz 2 Nr. 8 PromO BayNAT)

Hiermit erkläre ich mein Einverständnis, dass bei Verdacht wissenschaftlichen Fehlverhaltens Ermittlungen durch universitätsinterne Organe der wissenschaftlichen Selbstkontrolle stattfinden können.

.....
Ort, Datum, Unterschrift